

UNITED STATES
DEPARTMENT OF THE INTERIOR
GEOLOGICAL SURVEY

DEEP OCEAN MINING ENVIRONMENTAL STUDY,
NE PACIFIC NODULE PROVINCE, SITE C,
GEOLOGY AND GEOCHEMISTRY



OPEN-FILE REPORT 76-548

This report is preliminary and has not
been edited or reviewed for conformity
with Geological Survey standards and
nomenclature

Menlo Park, California

July 1976

UNITED STATES
DEPARTMENT OF THE INTERIOR
GEOLOGICAL SURVEY

DEEP OCEAN MINING ENVIRONMENTAL STUDY,
NE PACIFIC NODULE PROVINCE, SITE C,
GEOLOGY AND GEOCHEMISTRY

By

James L. Bischoff and others

OPEN-FILE REPORT 76-548

**This report is preliminary and has not
been edited or reviewed for conformity
with Geological Survey standards and
nomenclature**

Menlo Park, California

July 1976

Table of Contents

Geological Studies of DOMES Site C: Introduction and Summary of Investigations	
J.L. Bischoff, Principal Investigator.....	pg. 1
Physiographic Characteristics of the Equatorial North Pacific and of DOMES Site C	
D.Z. Piper	pg. 16
DOMES Area C: General Statement About Mineralogy, Diagenesis and Sediment Classification	
J.R. Hein, C. Gutmacher and J. Miller	pg. 63
Preliminary Geotechnical Properties Northeast Central Pacific Nodule Mining Area	
A.F. Richards, T.J. Hirst and J.M. Parks.....	pg. 81
Analysis of Strength Characteristics of Deep Sea Sediments From Potential Manganese Nodule Mining Areas in the North Central Pacific	
F. Simpson	pg. 95
Micropaleontological Dating of Sediments of DOMES PROJECT Box Cores, Test Area "C", Tropical Pacific Ocean	
F. Theyer	pg. 106
Chemical Composition of Marine Sediments of DOMES Site C	
J.L. Bischoff and D.Z. Piper	pg. 113
Interstitial Water Chemistry in DOMES Site C Sediments	
E. Callender and J.L. Bischoff	pg. 131
Recent Metalliferous Sediment in the Pacific Manganese Nodule Area	
J.L. Bischoff and R.J. Rosenbauer	pg. 145

Microfeatures of Typical Manganese Nodules From Six Box Cores From NOAA Cruise RP6-0C-75	
R.K. Sorem and D.L. Banningpg. 167
Origin of the Surface Textures of Some Manganese Nodules from the Equitorial North Pacific	
C.C. Woopg. 217
Chemical Changes in Surface Sea Water Caused by Suspension of Marine Sediments	
J.L. Bischoff and R.J. Rosenbauerpg. 233
Settling Velocities of the Sediment in Seawater and X-Radiography of the Box Cores: Site C Preliminary Data Report	
A.H. Sallenger, Jr. and G. Luepkepg. 257

Geological Studies of DOMES Site C:
Introduction and Summary of Investigations

James L. Bischoff
U.S. Geological Survey
Menlo Park, California

I Objectives and Philosophy

Probably the single most obvious and important environmental effect during deep-sea mining operations will be the re-suspension and discharge of large amounts of sea floor sediment into the water column. The objectives of the geological program, therefore, were two-fold. The first was to provide baseline information on the sediment system by defining the nature of the sediment, its contained pore fluids and associated nodules. The second was to carry out laboratory studies to help predict how the resuspended sediment might interact chemically with surface sea water and how rapidly the sediment might settle out.

II Baseline Parameters

In that the specific parameters of environmental importance are largely identified only by hindsight, our philosophy was to study the sediment, its associated nodules, and contained pore water in a reasonably thorough manner, using established procedures and techniques, and taking samples in sufficient detail to resolve local variation and heterogeneity.

We therefore set out to determine the composition of the sediment, both chemical and mineralogical, the physical properties, the size distribution of the sediment particles, and the age of

the sediment. These studies were subdivided into seven separate projects each with an independent principle investigator as follows:

- 1) Regional Geology--concerned with defining tectonic environment, seismicity, bathymetry, regional stratigraphy and present environment of sedimentation; largely a literature review (D. Piper, Principal Investigator, U.S.G.S.).
- 2) Sedimentary Petrography--description of core samples in terms of major components and mineralogy (J. Hein, Principal Investigator, U.S.G.S.).
- 3) Geotechnical and Physical Properties of Sediments--study of water content, size distribution, bulk density, and strength properties of core samples (A. Richards, Principal Investigator, Lehigh Univ.).
- 4) Biostratigraphy--age determination and estimate of accumulation rate based on microfossils in core samples (F. Theyer, Principal Investigator, Univ. of Hawaii).
- 5) Chemical Composition of Sediment--analysis of major and minor elemental composition of core samples (J. Bischoff, Principal Investigator, U.S.G.S.).
- 6) Interstitial Water Chemistry--major and minor elemental composition of pore fluids extracted from core samples (E. Callender, Principal Investigator, U.S.G.S.).
- 7) Nodule Studies--physical and petrographic characterization of nodules from cores (R. Sorem, Principal Investigator, Washington State Univ.). Nodule mineralogy (C.C. Woo, Principal Investigator, U.S.G.S.).

III Predictive Experiments

Aliquots of sediments collected and analyzed as part of the baseline studies were used to conduct the following laboratory experiments:

- 1) Resuspension Experiments--designed to test whether sediment and nodules suspended into surface water release or remove chemical components of biologic importance (J. Bischoff, Principal Investigator, U.S.G.S.).
- 2) Settling Experiments--designed to estimate actual settling velocities of resuspended sediment in sea water in order to assist predictive modeling of the sediment plume (A. Sallenger, Principal Investigator, U.S.G.S.).

IV Cruise Activities and Sampling

During April through June 1975 field work was carried out in Site C by R/V Oceanographer, cruise RP-6-0C-75. Fourteen stations for boxcoreing and 8 stations for bottom photos were occupied (Table 1, Figure 1). During traverses between stations bathymetric (12 KHz) and magnetic profiling were undertaken (see Piper's report, this volume for track chart and bathymetry). As of this writing, however, the magnetic data had not yet been made available.

Table 1
 Box Core and Camera Station Locations Within Area C, Cruise
 RP-6-0C-75

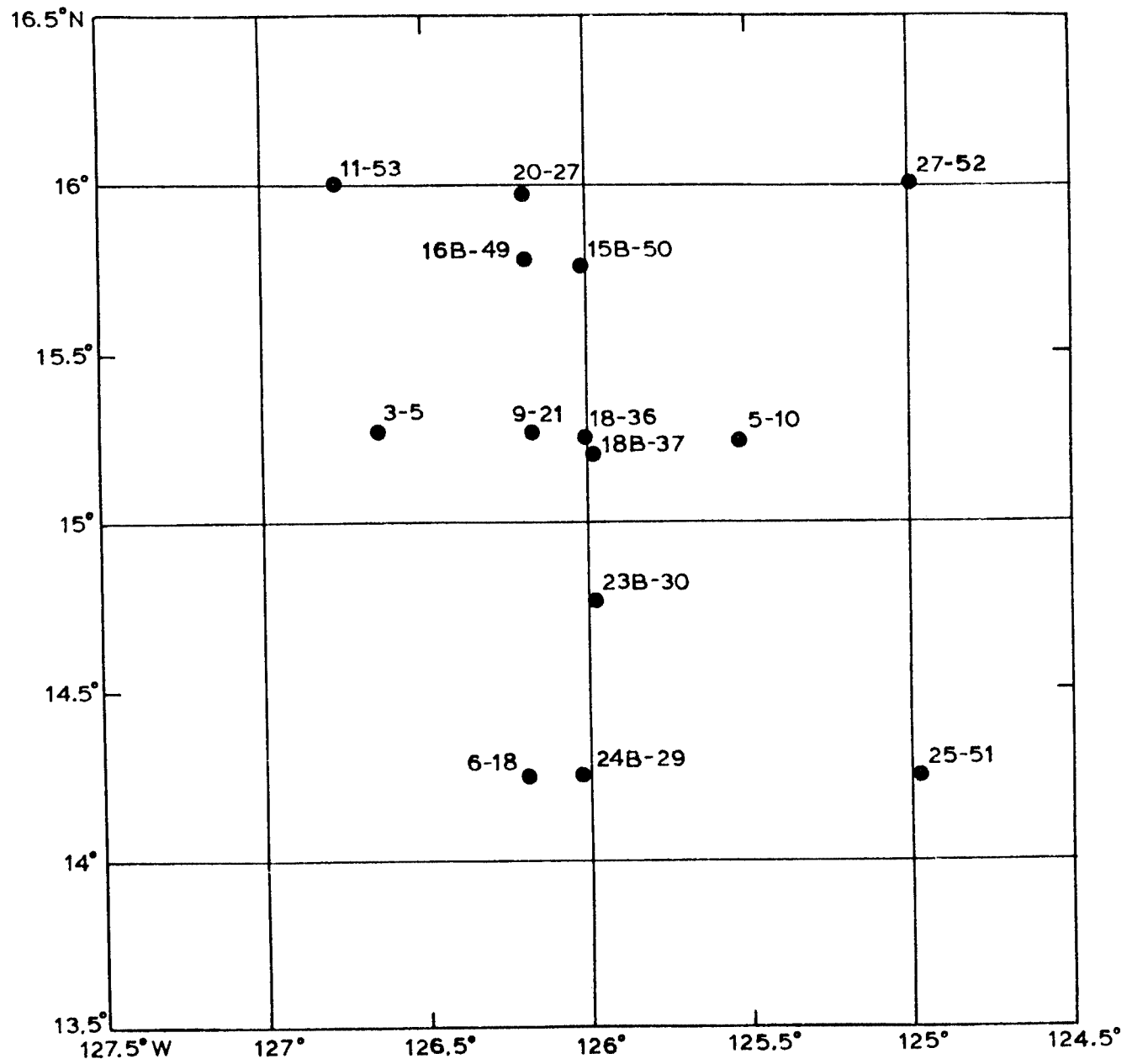
Ship's Station-Box Core number	number	Lat N	Long W	Depth, m
	3-5	15 ⁰ 15.9	126 ⁰ 38.4'	4675
	5-10	15 ⁰ 14.7'	126 ⁰ 32.1'	4493
	6-18	14 ⁰ 15.0'	126 ⁰ 11.5'	4430
	9-21	15 ⁰ 16.4'	126 ⁰ 9.6'	4630
	11-53	16 ⁰ 00.7'	126 ⁰ 46.3'	4603
	15B-50	15 ⁰ 45.6'	126 ⁰ 00.5'	4552
	16B-49	15 ⁰ 46.7'	126 ⁰ 11.2'	4552
	18A-36	15 ⁰ 15.7'	126 ⁰ 00.0'	4339
	18B-37	15 ⁰ 12.2'	125 ⁰ 58.6'	4406
	20-27	15 ⁰ 59.3'	126 ⁰ 11.6'	4672
	23B-30	14 ⁰ 45.9'	125 ⁰ 58.6'	4667
	24B-29	14 ⁰ 15.4'	126 ⁰ 01.4'	4468
	25-51	14 ⁰ 14.5'	124 ⁰ 58.5'	4561
	27-52	16 ⁰ 00.5'	124 ⁰ 59.6'	4406

Ship's Station numbers
 with bottom photos

1	16 ⁰ 01.5'	126 ⁰ 40.3'
2	15 ⁰ 45.5'	126 ⁰ 10.0'
4	15 ⁰ 15.1'	125 ⁰ 59.2'
5	15 ⁰ 16.5'	125 ⁰ 31.4'
6	14 ⁰ 17.5'	126 ⁰ 15.4'
8	15 ⁰ 16.4'	126 ⁰ 52.0'
9	15 ⁰ 16.6'	126 ⁰ 09.2'
10	15 ⁰ 15.3'	125 ⁰ 01.5'

Figure 1

DOMES Site C, showing location of box cores used in geological baseline studies. Cruise no. RP-6-0C-75, R/V Oceanographer, Spring 1975.



The box core measured 50 x 50 cm and routinely penetrated between 20 and 45 centimeters of sediment. Immediately after retrieval, subsamples of the box cores were taken by inserting cylindrical plastic tubes (6.7 cm. i.d.) vertically through the sediment using a stationary piston at the sediment surface to prevent compaction. These subcores were then sealed and stored upright at 5⁰C on the ship. Usually several such subcores were taken from each box. One subcore was preserved for archive, and another devoted entirely for physical and geotechnical studies at Lehigh University. An additional subcore was divided into 2 cm intervals on board for pore water extraction. In some cases, 2 or 3 such subcores from the same box core were processed to determine pore water variability within one core. After extraction of pore water, the remaining sediment intervals, or "squeeze cakes" were sealed in evacuated plastic bags and stored at 5⁰C. The squeeze cakes were then opened at the shore-based laboratory and each interval was carefully subdivided with separate aliquots for petrography-mineralogy, biostratigraphy, chemical analysis, resuspension studies, and settling velocity measurement.

Additionally, 5 of the large box cores (stations 11, 15B, 16B, 23B, and 25) were subsampled using a smaller box shaped device made of sheet stainless steel measuring 25 cm on a side. These were taken primarily for nodule studies, and were transferred and sealed in wax-lined wooden boxes and stored at 5⁰C. These were also subdivided in the shore laboratory into 2 cm intervals for several, but not all, of the above studies.

Our philosophy was to carry out as many studies as possible on aliquots of the same sample in order to maximize intercorrelation and calibration of results. Each core, however, was not subdivided in exactly the same way and Table 2 is presented to show the exact distribution of samples and aliquots.

In that several of the reports refer to interval numbers, and others to actual depth in sediment for their respective samples, Table 3 is presented as a key for cross-referencing sample numbers among the various reports.

Summary of Findings

The remainder of this volume is a collection of reports from each of the individual groups participating in the geological program for Site C. A brief integrated summary is presented here.

DOMES Site C is situated in a region of gentle abyssal hills with relief of 50-200 m, displaying N-S trends. Although the area lacks significant seismic activity, active high angle faults with several meters apparent vertical displacement commonly bound the abyssal hills, and cut through recent-most sediments. Apparently, movement along such faults is taking place at a greater rate than sedimentation can cover them. Acoustic surveys indicate total sediment thickness above basement of 150 to 200 meters. Surface sediment belongs to the Clipperton Oceanic Formation and is apparently of Quaternary age.

Table 2
Distribution of samples from DOMES Site C box cores among various sub-groups.

Station- boxcore no.	Physical and Geotechnical	Petrography and mineralogy	Biostratgraphy	Chemical composition	Pore water	Nodule Studies	Resuspension experiments	Settling experiments
3-5	10 intervals	--	--	--	--	--	--	--
5-10	6 intervals	--	--	--	--	--	--	--
6-18	8 intervals	--	--	--	--	--	--	--
9-21	10 intervals	--	--	--	--	--	--	--
11-53	24 intervals 2 subcores	5 intervals	8 intervals	--	--	4 nodules	composite	2 composites
15B-50	--	5 intervals	8 intervals	--	--	7 nodules	composite	2 composites
16B-49	--	10 intervals	9 intervals	10 intervals	27 intervals 3 subcores	9 nodules	3 intervals	--
18A-36	14 intervals 2 subcores	5 intervals	8 intervals	5 intervals	8 intervals	--	3 intervals	--
18B-37	11 intervals	9 intervals	9 intervals	9 intervals	18 intervals 2 subcores	--	5 intervals	2 composites
20-27	19 intervals 2 subcores	8 intervals	8 intervals	8 intervals	16 intervals 2 subcores	--	3 intervals	--
23B-30	--	5 intervals	8 intervals	--	--	2 nodules	composite	2 composites
24B-29	18 intervals 2 subcores	10 intervals 2 subcores	8 intervals	10 intervals 2 subcores	17 intervals 2 subcores	--	6 intervals 2 subcores	--
25-51	--	3 intervals	8 intervals	--	--	3 nodules	composite	composite
27-52	--	5 intervals	8 intervals	--	--	--	composite	2 composites

Table 3
Sediment samples from DOMES, Site C, box cores showing sediment depths
with corresponding interval designations.

Station-core number	Interval number	Depth in core (cm)	Station-core number	Interval number	Depth in core (cm)	Station-core number	Interval number	Depth in core (cm)
11-53	1	0-2	15B-50	1	0-2	23B-30	1	0-2
	2	2-4		2	2-4		2	2-4
	3	4-6		3	4-6		3	4-6
	4	6-8		4	6-8		4	6-8
	5	8-10		5	8-10		5	8-10
	6	10-12		6	10-12		6	10-12
	7	12-14		7	12-14		7	12-14
	8	14-18		8	14-18		8	14-18
	9	18-22		9	18-22		9	18-22
	10	22-26		10	22-26		10	22-26
	11	26-30		11	26-30		11	26-30
	12	30-34		12	30-35		12	30-34
	13	34-37		13	bottom		13	34-38
	14	37-41					14	38-41
				15	41-44			
16B-49 subcore I	1	0-2	16B-49 subcore III	1	0-2	16B-49 subcore IV	1	2-4
	2	2-4		2	2-4		2	6-8
	3	4-6		3	4-6		3	10-12
	4	8-10		4	8-10		4	14-16
	5	12-14		5	12-14		5	18-20
	6	16-18		6	16-18		6	22-24
	7	20-22		7	20-22		7	26-28
	8	24-26		8	24-26		8	30-32
	9	28-30		9	28-30		9	34-36
	10	32-34						

Table 3
Con't

Station-core number	Interval number	Depth in core (cm)	Station-core number	Interval number	Depth in core (cm)	Station-core number	Interval number	Depth in core (cm)
18A-36	1	0-2.7	18B-37 Subcore II	1	0-2.2	18B-37 Subcore I	1	2-4
	2	2.7-4.7		2	2.2-4.2		2	4-6
	3	4.7-6.7		3	6.2-8.2		3	6-8
	4	6.7-8.7		4	10.2-12.2		4	10-12
	5	8.7-10.7		5	14.2-16.2		5	14-16
	6	10.7-12.7		6	18.2-20.2		6	18-20
	7	12.7-14.7		7	22.2-24.2		7	22-24
	8	14.7-16.7		8	26.2-28.2		8	26-28
			9	30.2-32.2	9	30-32		
20-27 Subcore I	1	2-4	20-27 Subcore II	1	2-4.3	27-52	1	0-2
	2	4.2-6.3		2	4.3-6.5		2	2-4
	3	6.3-8.5		3	6.5-8.5		3	4-6
	4	8.5-10.7		4	10.5-12.5		4	6-8
	5	10.7-12.9		5	14.5-16.5		5	8-10
	6	12.9-17.9		6	18.5-20.5		6	10-12
	7	17.9-22.9		7	22.5-24.5		7	12-14
	8	22.9-27.9		8	26.5-28.5		8	14-16
				9	16-20			
				10	20-23			
				11	23-26			
				12	bottom			
24B-29 Subcore I	1	0-2	24B-29 Subcore IV	1	0-1.6	25-51	1	0-2
	2	2-4		2	1.6-3.6		2	12-14
	3	4-6		3	3.6-5.6		3	25-27
	4	6-8		4	5.6-7.6			
	5	8-10		5	7.6-9.6			
	6	12-14		6	9.6-11.6			
	7	16-18		7	11.6-13.6			
	8	20.5-22.5		8	13.6-15.7			
			9	15.7-17.7				

Sediments sampled during the Spring 1975 cruise of the R/V Oceanographer are classified, in general, as brown siliceous muds, composed primarily of clay minerals and secondarily of siliceous microfossils. Minor components include volcanic debris, Fe-Mn globules, and zeolite, with large variations in relative importance both within and between cores.

The sediments are massive and lack discernable bedding. X-radiographs reveal evidence of significant bioturbation with abundant filled burrows averaging 5 mm in diameter. Abundant micronodules are also apparent throughout the cores, but large nodules are found only at the surface.

Bulk density averages 1.32 g/cc, interstitial water content 178% dry weight (64% wet weight), liquid limit 137%, plastic limit 82%, and vane shear strength 5kPa, values typical for Pacific pelagic clay and siliceous ooze. Median diameter of sediment particles averages 8.3 phi (3.2 microns), with approximately 65% of the particles smaller than 4 microns and less than 1 % greater than 64 microns.

The upper 10 to 20 cm of the cores are generally of Quaternary age as determined by siliceous microfossils, indicating that sediment accumulation is presently active. Although the microfossil fauna does not allow an accurate estimate of the accumulation rate, a lower limit of $0.1 \text{ cm}/10^3 \text{ yrs}$ is established. In many cores, the sediment below 20 cm is barren of microfossils,

but in others, such barren zones are underlain by Quaternary fossiliferous zones, suggesting that the entire sequence of 40 cm or so represented by the box cores is a continuous Quaternary sequence.

Averaged chemical composition of the sediment compares closely with Pacific pelagic clay. Exceptions include relative enrichments in Na, Ca, Ba, Cu, and Ni. Na and Ca contents in excess of interstitial salts and CaCO_3 are due to unaltered volcanic debris, which is calculated to constitute about 10% of the bulk sediment. Local variations in sediment chemistry within and between cores are generally small. Core 18B, however, displayed significantly different chemistry in the lower 20 cm, due to the presence of metalliferous mud. This material constitutes 40% of the sediment of the horizon, and is almost identical to hydrothermal metalliferous muds of the East Pacific Rise. Such mud is essentially a hydrated gel of Si, Fe, and Mn, with several hundred ppm of Cu and Ni. Al is significantly depleted, precluding the possibility of its in-situ formation as an alteration of volcanic debris.

Interstitial waters of these sediments differ little in their element chemistry from bottom waters, indicating that the sediment is not undergoing significant diagenesis, and is, therefore, stable with respect to sea water. NH_4^+ , in contrast, is greatly enriched over bottom water values by a factor of 13, indicating metabolic activity is taking place on the small concentration of solid organic matter (organic carbon in the sediment

averages 0.24%). Dissolved SiO_2 is likewise enriched by about 73%, but PO_4^{-3} is about the same concentration as the bottom water.

Based on bottom photos, nodules commonly cover approximately 30% of the sea floor at Site C, but locally cover as much as 75%. Nuclei are predominantly older nodule fragments, and in general, the mineralogical composition is dominated by todorokite, with minor occurrences of birnessite. The nodules are quite fragile and likely will be considerably abraded and fragmented during mining operations.

Resuspension experiments carried out with sediment and with crushed nodules in surface sea water (10% suspensions) resulted in measurable changes in a number of sea water components. Most changes, if not all, were complete within a few days, and can be ascribed to changing surface absorption characteristics with changing temperatures. Neither heavy metals nor toxic elements were released, however. In contrast, observed changes in the nutrients, particularly SiO_2 and NH_4^+ might stimulate photosynthesis, and provide an explanation for earlier observations that resuspended sediment stimulates biologic productivity in excess of that produced by simple bottom water enrichments.

Settling characteristics of this sediment in sea water cannot be accurately predicted from measured particle size distributions because such particles will likely flocculate and behave as aggregates. The degree to which this will happen depends on the actual concentration of sediment during mining discharge. Experiments of DOMES Site C sediment suspended in

surface sea water at a concentration of 10^{-4} g/l indicates the sediment settles as if it had a mean particle size between 4 and 5 microns, a value close to that measured for the completely dispersed and unflocculated sediment in distilled water. However, at concentrations of 10^{-3} g/l mean median settling diameter was 10-15 microns, so the 4-5 micron figure can safely be used as a lower limit for settling characteristics in mathematical modeling of surface plume behavior.

Physiographic Characteristics of the Equatorial North
Pacific and of DOMES Site C

David Z. Piper
U.S. Geological Survey
Menlo Park, California

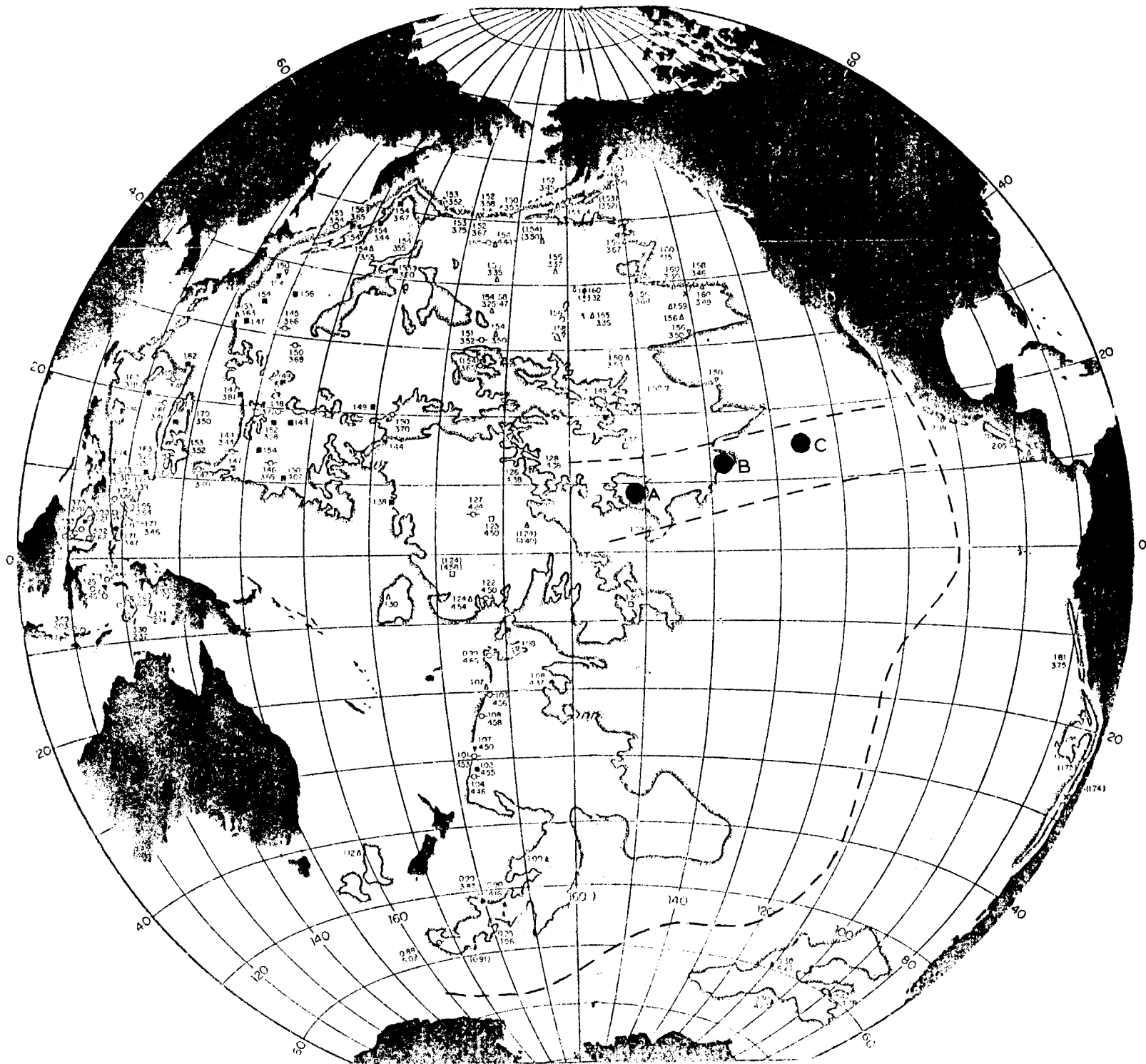
Introduction

The area of the sea floor currently under consideration for deep-ocean mining of ferromanganese nodules lies within the eastern basin of the Pacific (Fig. 1), as defined by the 5000 m isobath (Wooster and Volkman, 1960), and roughly between the Clarion and Clipperton fracture zones of the Pacific Plate. It coincides with the transition zone between the equatorial belt of high primary productivity, associated with upwelling, and the central gyre of the north Pacific that exhibits extremely low productivity. This area, however, is within the region of greatest exploitation of tuna (Calkins, 1975) in the north Pacific (Fig. 2).

The objective of this study was "to obtain sufficient baseline data"... of the geology of the area..." to determine the range of natural variability of selected environmental parameters in the mining region" (Anon. 1975). This preliminary report represents (1) a review of the geology of the central equatorial Pacific, (2) a description of the bottom water, which may contribute significantly to sculpturing of the sea floor and to the distribution and composition of surface sediments, and (3) a description of the bathymetry and sediment distribution, based on data collected during Phase 1 of the project, of one of three areas considered by industry to be representative of the spectrum of seafloor environments with high mining potential. This site, Site C, is centered at 15°N and 126°W (Fig. 1) and is 2° on a side.

This report does not represent the complete analysis of area C. A three week cruise is planned for the Fall of 1976 to collect additional bottom samples, photographs of the sea floor, bathymetric data, and 3.5 KHz seismic reflection profiles from this area. Analysis of data collected for areas A and B is also continuing.

Figure 1. The four major basins in the Pacific Ocean, southern, central, northern, and eastern, as defined by the 5000 m isobath. The numbers at each station are in situ temperature ($^{\circ}\text{C}$, upper number) and O_2 (ml/l, lower number when given). The figure is from Wooster and Volkmann (1960) who give sources of data. Dashed lines give approximate locations of the East Pacific Rise and the Clarion and Clipperton fracture zones. Sites A, B, and C are shown by large dots.



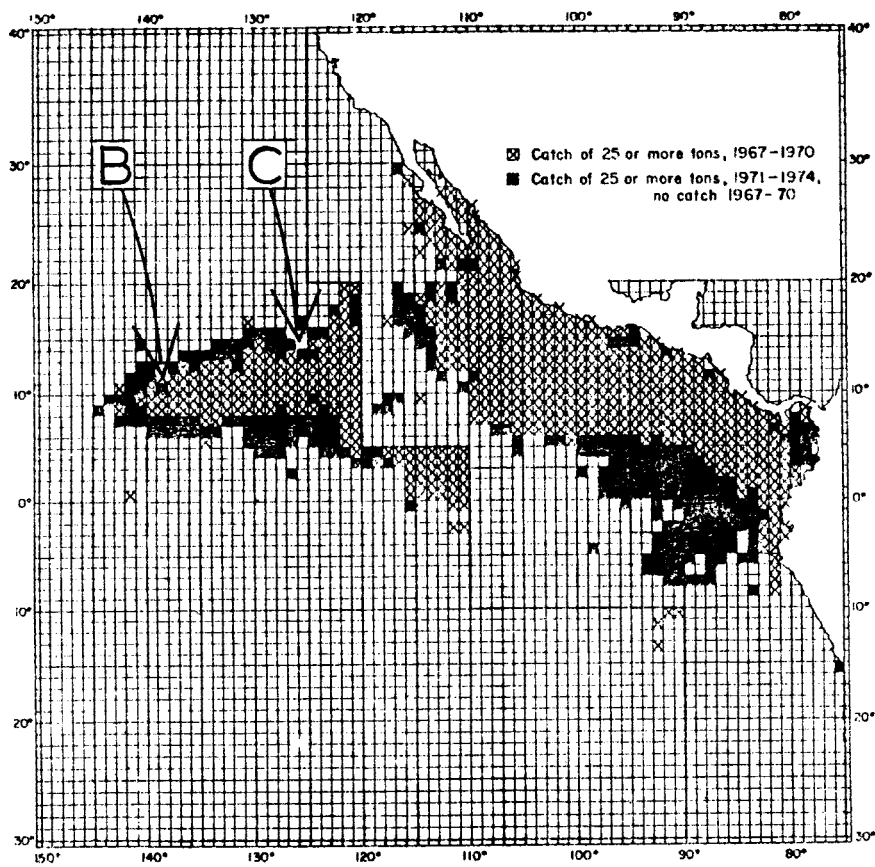


Figure 2. Catch of yellowfin tuna for the eastern Pacific. Figure is from Calkins (1975).

Bottom Water

In considering bottom water of the Pacific, Wooster and Volkmann (1960) divided the Pacific into four basins using the 5000 m isobath (Fig. 1). They showed that sills between the basins were sites of discontinuity in water properties, apparently owing to mixing with overlying Deep Water. Although the approximate temperature of Bottom Water is 1.0 to 1.5°C (Reid, 1965), the potential temperature of Bottom Water from each basin exhibits a unique distribution. Water within the eastern basin extends as a tongue of cold water (Fig. 3) originating in the central basin and increasing in temperature toward the east. The source of this water is the western boundary current, first deduced by Stommel (1958) and observed in the area of the Somoan Passage by Reid (1969) and Reid and Lonsdale (1974). This passage represents the main sill between the southern and central basins. The ultimate source of this water is Antarctic Water.

The Hawaiian Ridge, mid-Pacific Mountains, and Line Island Ridge place a severe constraint on the northward and eastward flow of this water. The major flow is to the north, between the mid-Pacific Mountains and the Marshall Islands. Eastward flow, into the eastern basin, is largely through two passes in the Line Island Ridge: Horizon Passage at 18°08'N and Clarion Passage at 12°40'N (Gordon and Gerard, 1971; Edmond et al., 1971).

In addition to its potential temperature, the O₂ and nutrient concentrations of Bottom Water within the eastern basin distinguish it from the above Deep Water. Its concentration of O₂ is higher and its concentration of the nutrients, phosphate and silicate, is lower; concentrations in Bottom Water are approximately 4 ml/l, 2.5µg-at/l, and 125 µg-at/l respectively.

The former decreases and the later two increase in an easterly and northerly direction. This trend is strongly developed in the area immediately to the south and east of Hawaii (Edmond et al., 1971).

Current measurements within the eastern basin have been made only at a few stations. The observed velocities are within the range usually observed in the deep ocean. They are less than 10 cm/sec (Isaacs, et al., 1966; Johnson, 1972) and usually less than 5 cm/sec. This value is much less than those within the Somoan Passage, where velocities as great as 15 cm/sec have been observed (Reid and Lonsdale, 1974). Although the observed direction of flow in the western area of the basin is eastward (Johnson, 1972), the direction of flow is apparently variable at stations elsewhere in the basin where flow direction has been measured.

Bathymetry

Abyssal hills represent the principal topographic feature over approximately 80% of the sea floor in the Pacific (Menard, 1964), including the area between the Clarion and Clipperton fraction zones. Hills are usually elongate, in the range of 5 x 50 km, with a relief of 50 to 300 m. The long dimension is often oriented in a north-south direction (Zenkevitch, 1961; Sysoyev, 1961; Arrhenius, 1963; Menard, 1964; Moore and Heath, 1967; Luyendyk, 1970, Johnson, 1972).

Within area C the relief falls within this range and a north-south trend in the "grain" of the sea floor is also strongly developed. East-west trending cruise tracks (Fig. 4) tend to exhibit a much higher frequency of change in slope than north-south trending tracks (Fig. 5). At a vertical exaggeration of 20 x, the length of sea floor per unit distance

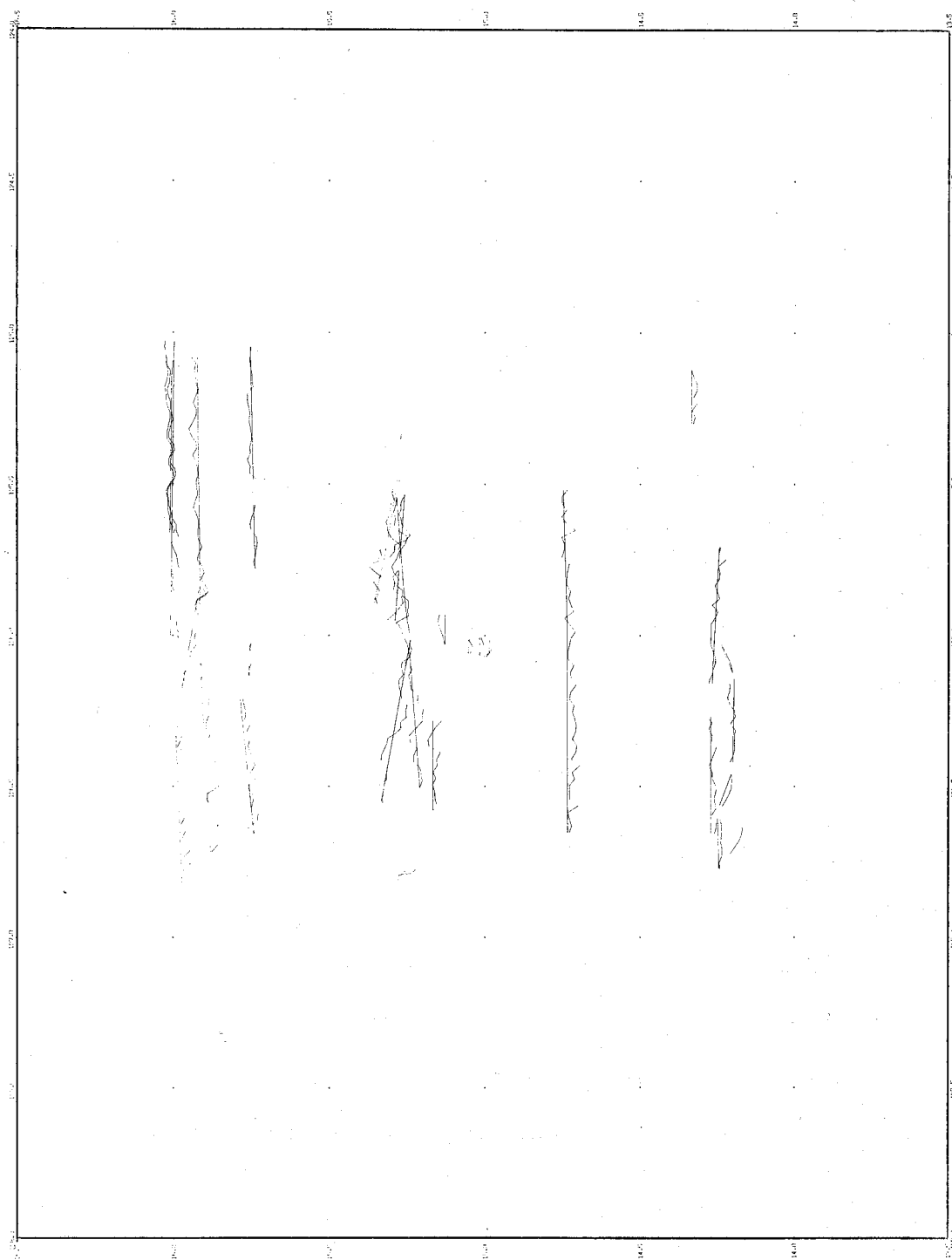


Figure 4. Bathymetric profiles within area C. All track lines are within 21° of east-west. Vertical exaggeration is 20X.

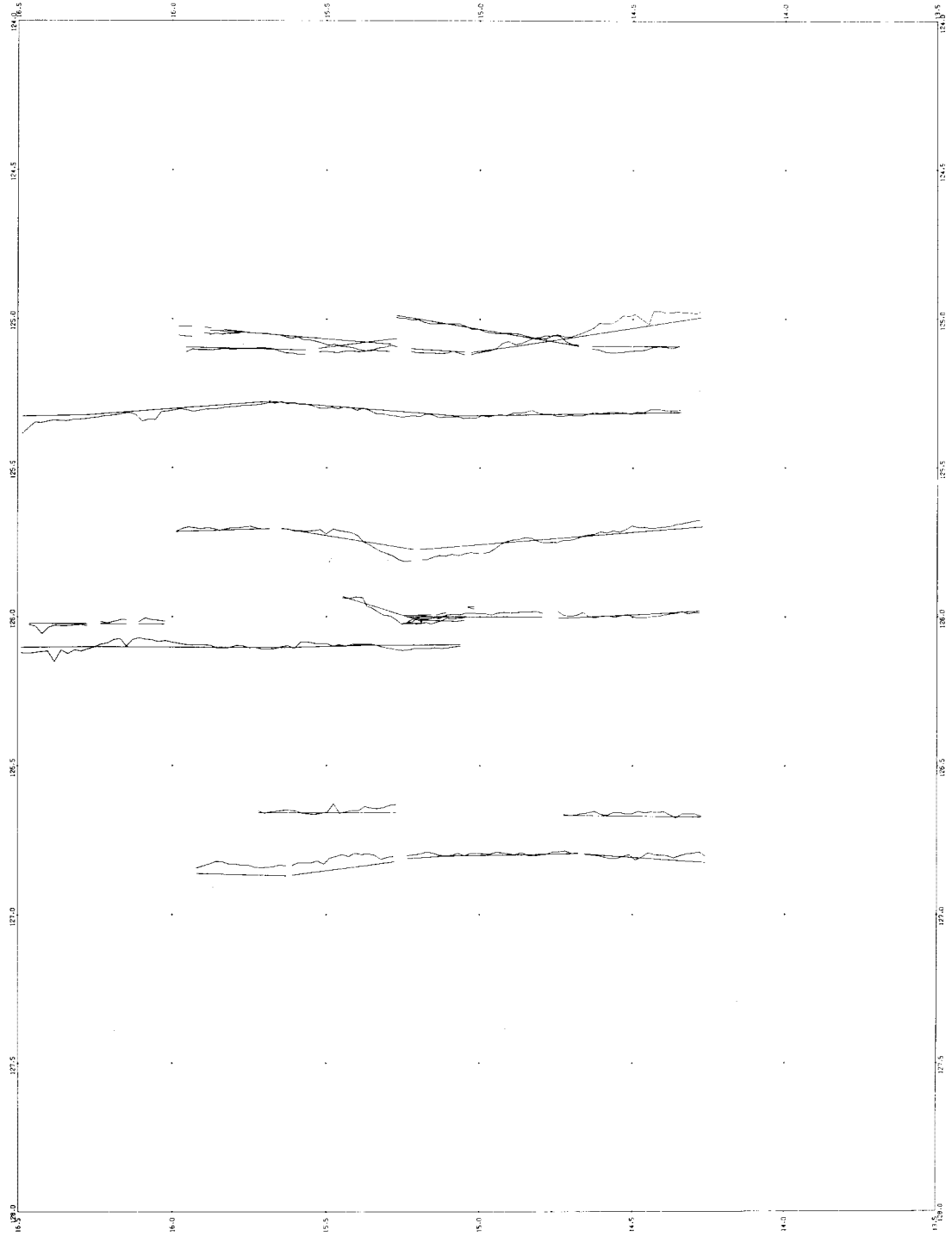


Figure 5. Bathymetric profiles within area C. All track lines are within 18° of north-south. Vertical exaggeration is 20X.

was 1.04 in the north-south direction, 1.13 in the east-west direction, and 1.11 for oblique track lines (between 20°N and 70°N).

Unfortunately it has been possible to contour only the area within the very center of C (Fig. 6), because of the low relief, relatively large distance between track lines (Fig. 7), and uncertainty in navigation. Within this small area, however, a north-south trend of bathymetry is apparent and is similar to an area 2° to the south, which was investigated by deep-tow (Johnson, 1972a).

Abyssal hill topography has usually been depicted as continuous gentle slopes of 2 to 3° and seldom exceeding 15° . The large angular dimension of the sound cone generated by a ship-mounted transducer precludes, however, the detection of small topographic features. When examined using a deep-towed system (Spiess et al., 1966), the slopes of abyssal hills often exhibit escarpments a few meters high with slopes that may be as great as 60° (Johnson, 1972a; Luyendyk, 1970). Such escarpments have also been observed in the mining area (the exact location is not known) by TV cameras that have been towed a few meters off the bottom by VALDIVIA (Williamson, personal communication). Such relief probably occurs in area C as well, although the maximum slope that has been measured from 12 KHz records, collected by OCEANOGRAPHER, is approximately 10° . Escarpments of a few cm (Fig. 8b), however, have been seen in bottom photos taken thus far.

The north-south orientation of abyssal hills within the eastern Pacific is roughly parallel to that of inferred magnetic anomalies, which have been estimated from Pitman et al. (1974). In the area of the Gorda Ridge Menard and Mammerickx (1967) noted that the two deviate from the trend of the ridge, yet maintain their parallel orientation relative to each other. The sign of anomalies, however, appeared to be randomly distributed relative to that of the hills. At low latitude this parallelism is lost owing to a thick

Figure 6. Contour map of small area at site C. See Figure 7 for exact location.

Figure 7. Cruise tracks within area C by NOAA (solid lines) and by Scripps (dashed lines). The area blocked out in the centre of the map has been contoured in Figure 6.

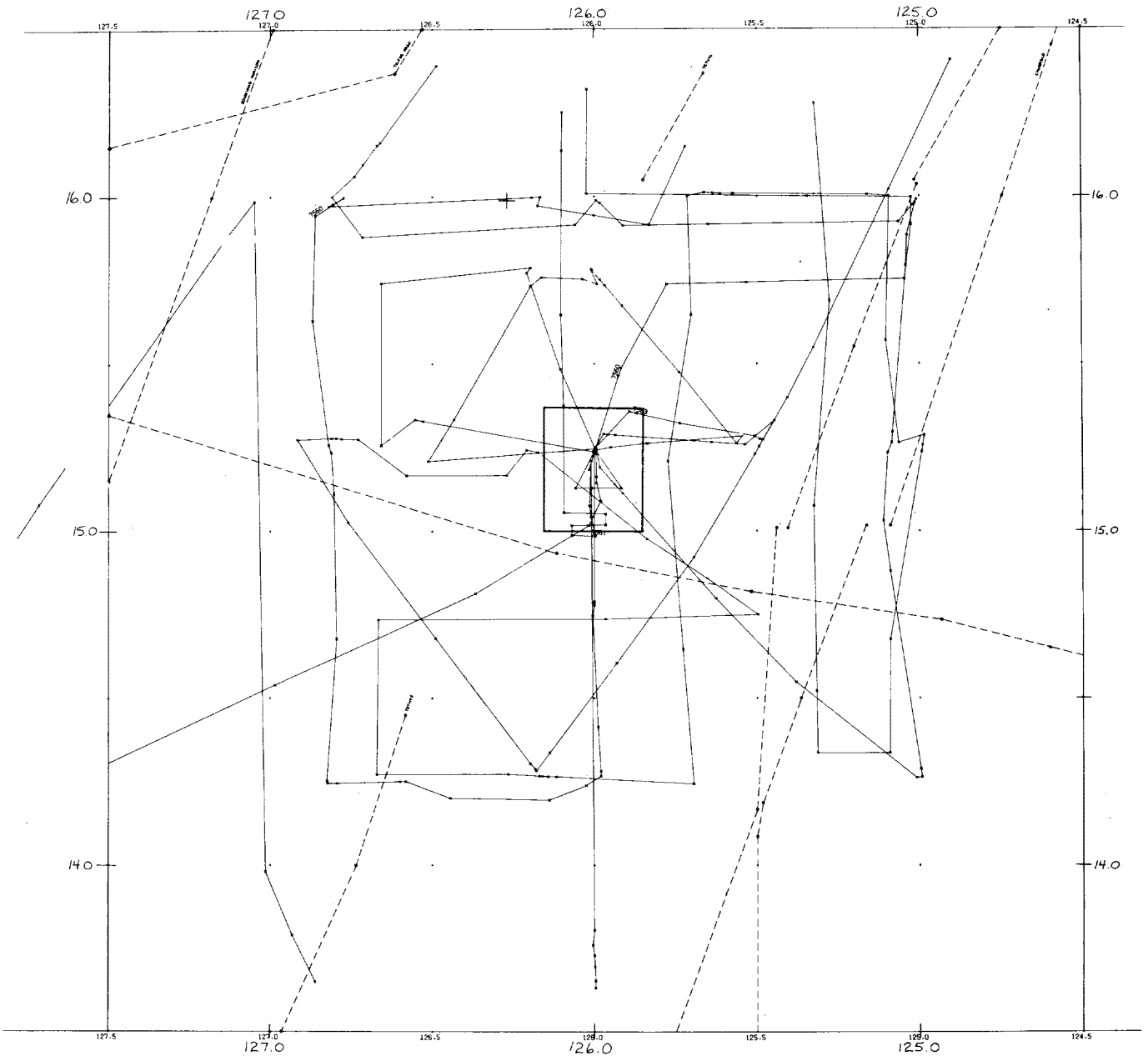
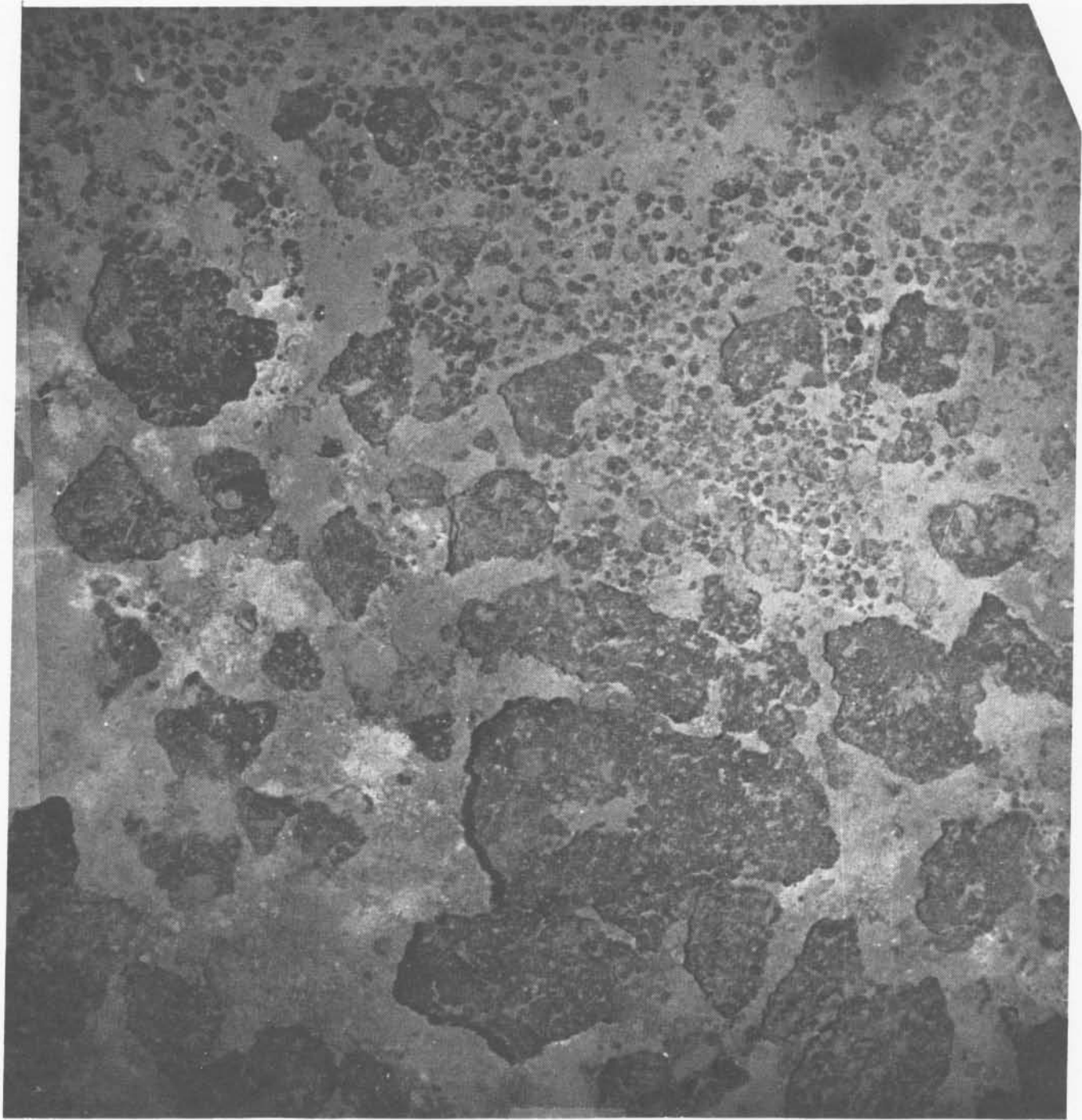
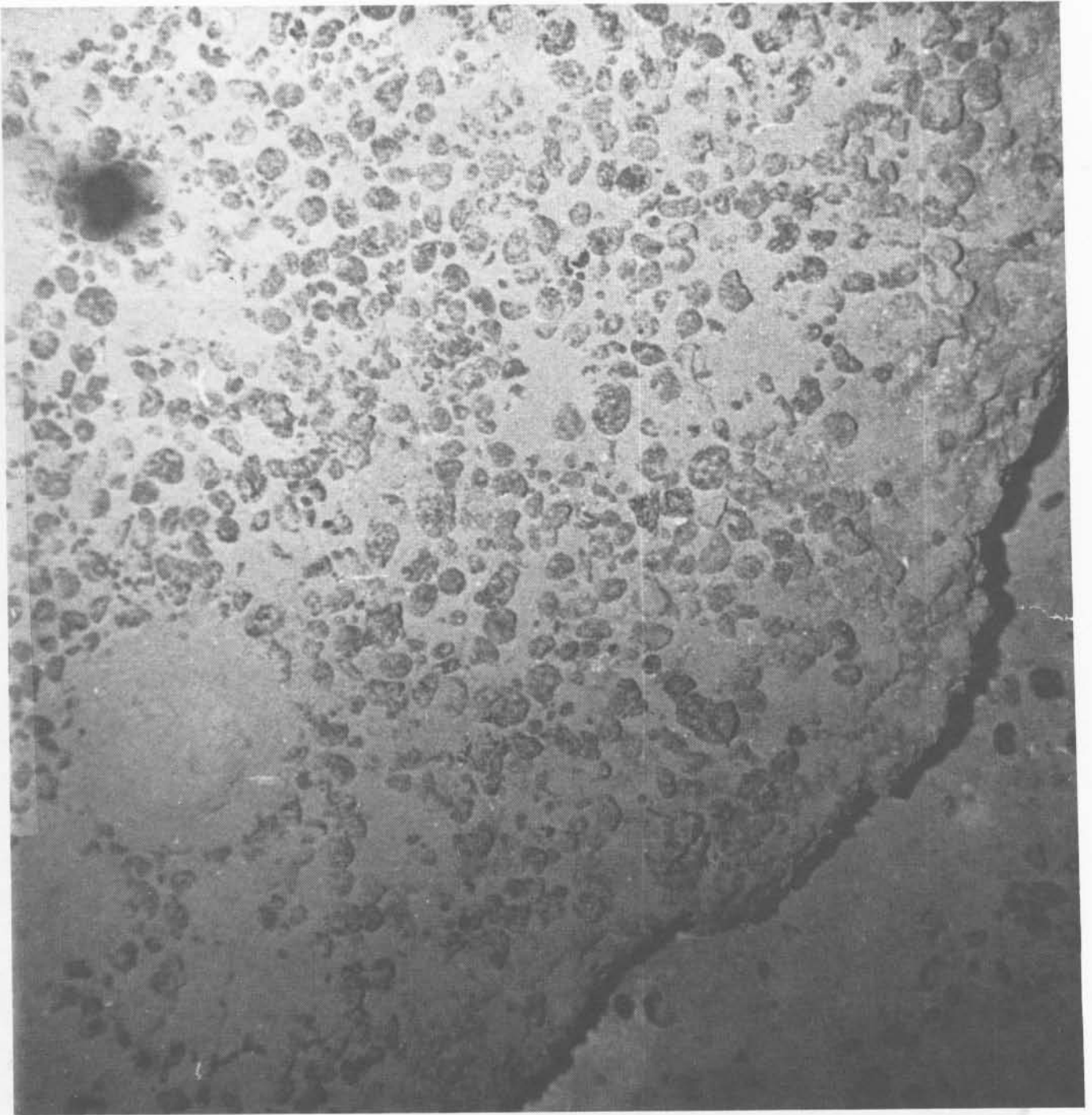


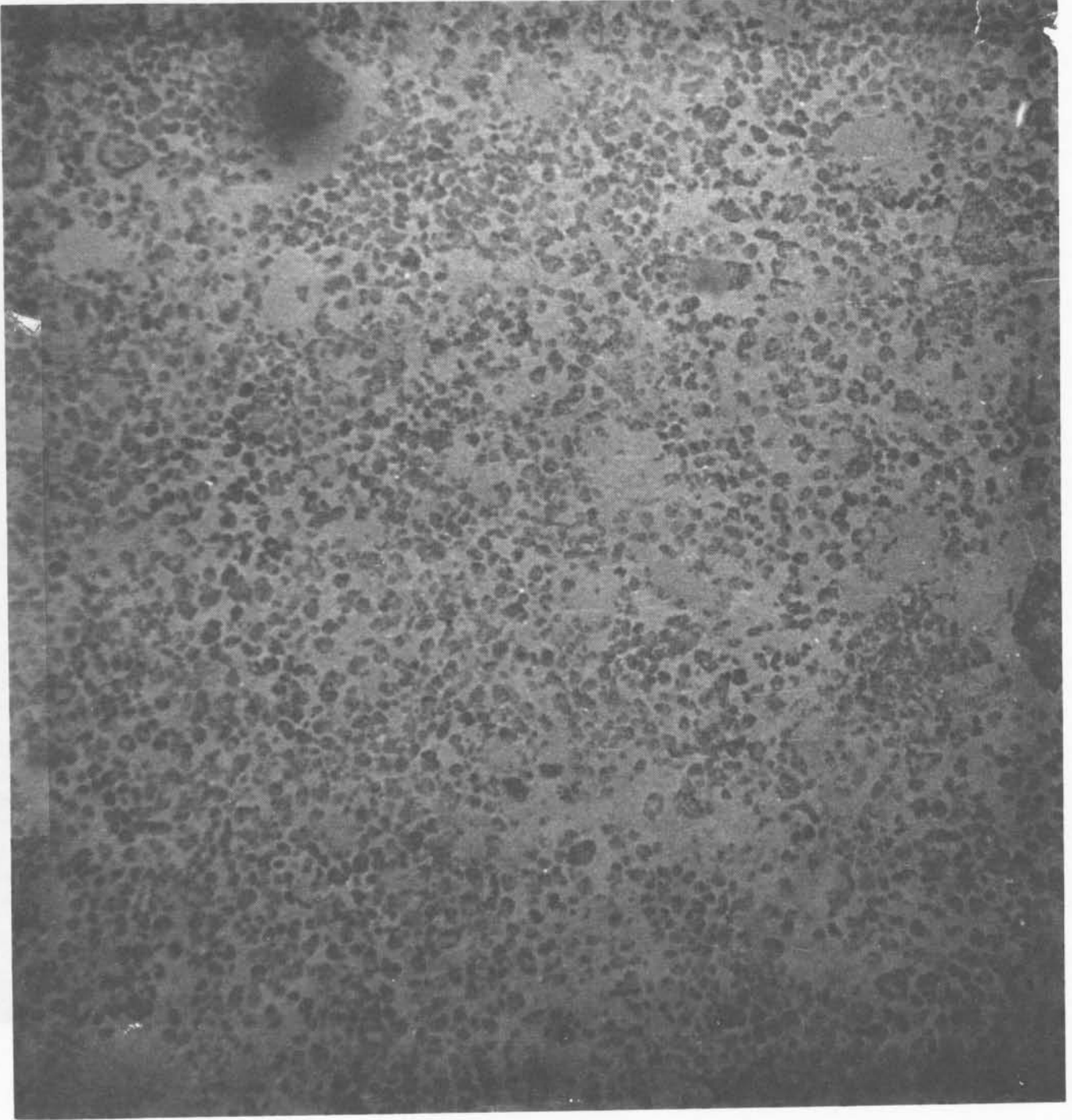
Figure 8. Bottom photographs at station 1 (photograph A) and station 9 (photographs B and C). See Figure 14 for their location. The average nodule diameter in each photograph is approximately 4 cm, as determined by measurement of nodules collected in near-by box cores. (A) Large slab may be either volcanic rock or nodule pavement. (B) Note the small escarpment in the lower right corner. Nodule coverage appears to be much less at base of ledge than above ledge. (C) The photograph shows a rather uniform nodule coverage of approximately 50%. Some nodules appear to be partially covered suggesting that nodule abundance may be greater than indicated by mere point count of the photograph.

(A)





(c)



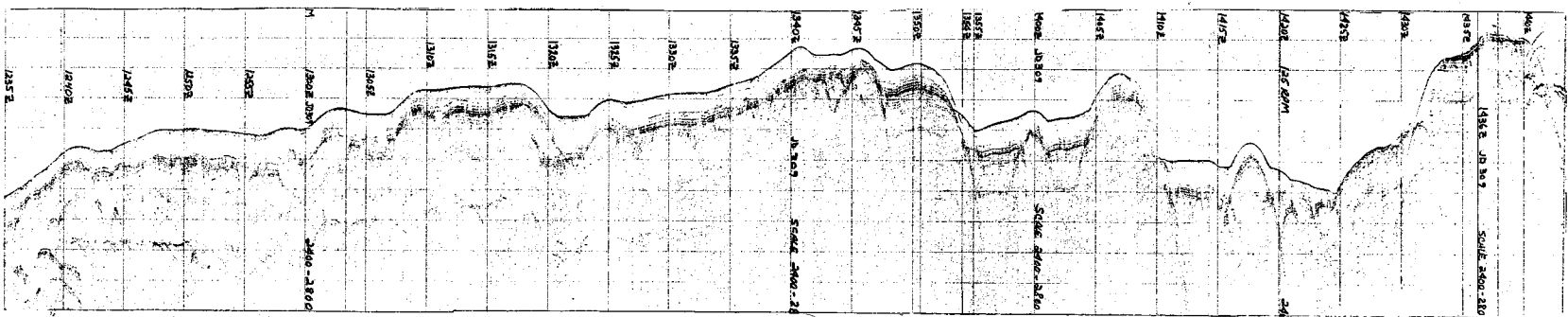
cover of sediment, which obscures topographic lineations, and difficulty in identifying magnetic lineations (Atwater and Menard, 1970). The relationship between the two in area C has not been determined. Magnetic data collected by the OCEANOGRAPHER are not yet available for comparison with bathymetry.

Thickness of sediment in abyssal hill areas exhibits a strong relation with bathymetry. It apparently varies rather markedly over distances of only a few kilometers. Assuming isochroniety for a reflector that was conformable with the sea floor and that may correspond to the base of Raitts' (1956) "first layer", Moore and Heath (1967) observed that sediment was thickest in valleys and thinnest on tops of abyssal hills. Although their assumption may not be valid when extrapolating over several 100 kilometers, it may be valid for relatively small distances of a few 10's of kilometers. Over distances of only 5 to 10 kilometers the thickness varied by as much as a factor of four. Similar observations have been made by Shor (1959) elsewhere in the equatorial North Pacific.

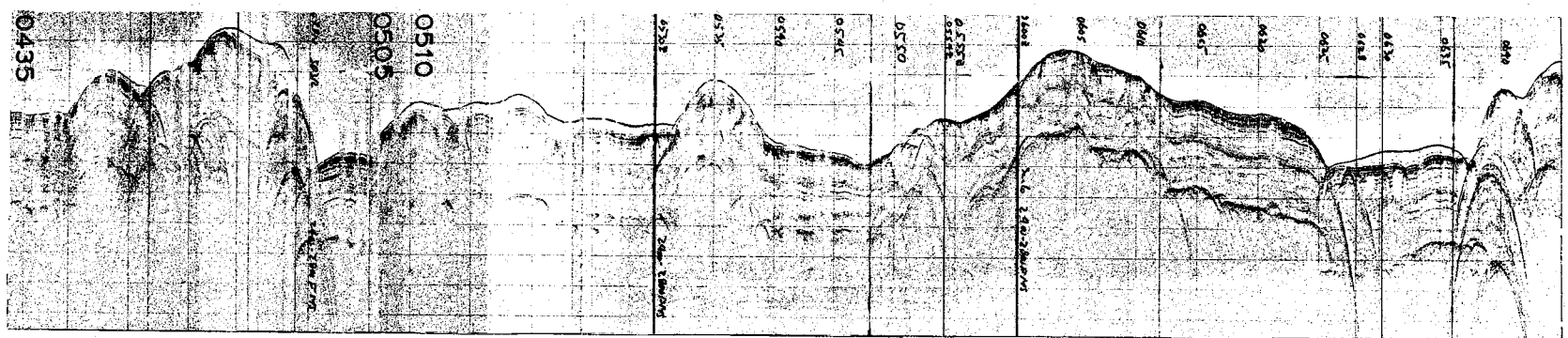
Age of surface sediment also occasionally varies with bathymetry. Using a 3.5 KHz system towed a few meters off the bottom, Johnson (1972a) observed outcrops of sub-bottom reflectors along slopes of abyssal hills. When dated using assemblages of radiolaria, the older sedimentary layers tended to occur at the base of slopes and became progressively younger up slope.

No 3.5 KHz records are yet available for area C. Records collected in areas A and B (Fig. 9) by the OCEANOGRAPHER (Fig. 1) however are similar to profile records of studies by others. The most striking feature of records from areas A and B (Fig. 9) is the occurrence of a transparent layer at the surface throughout most of the area. Its most frequently occurring thickness is approximately 40 m. However, it tends to be thickest in low

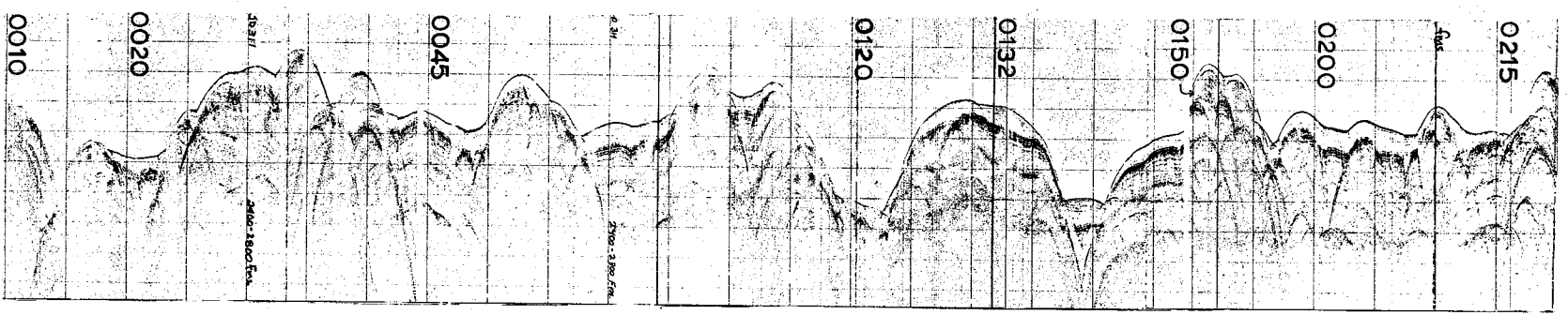
Figure 9. Profiler records (3.5 KHz) from area B. Horizontal lines represent 20 fathoms in water. The top of the record is at 2520 f in A and at 2580 f in B and C. (A) Approximate length of record is 33 n. mi. Position at the beginning of the record (left side) was $11^{\circ} 31'N$ and $139^{\circ} 11'W$. Course and course changes are as follows: o/c 157° at 1235Z, c/c 255° at 1340Z, c/c 165° at 1436Z. (B) Approximate length of record is 29 n mi. Position at the beginning of the record was $12^{\circ} 04'N$ and $137^{\circ} 52'W$. Course and course changes are as follows: o/c 054° at 0435Z, c/c 059° at 0447Z, c/c 329° at 0545Z, c/c 243° at 0554Z. (C) Approximate length of record is 31 n mi. Position at the beginning of the record was $11^{\circ} 37'N$ and $138^{\circ} 28'W$. Course and course changes are as follows: o/c 058° at 0010Z, c/c 148° at 0125Z, c/c 238° at 0132Z.



A



B



C

areas and thinnest on slopes. Its thickness on the tops of abyssal hills shows great variability; it may be absent or as thick as in adjoining valleys. Underlying reflectors, which usually are conformable with the seafloor, occasionally crop out along slopes, often where acoustic basement appears to be offset in a step-like manner (Fig. 9B between 0600Z and 0639Z), suggesting faulting.

The origin of abyssal hill topography appears to be a result of (1) volcanism and faulting and (2) sedimentation and erosion. Luyendyk (1970) and Menard and Mamerickx (1967) suggest that this type of topography is initially developed along the East Pacific Rise by a combination of volcanism and faulting. The occurrence of similar topographic features along the mid-Atlantic Ridge on Iceland (Thorarinsson, 1965) would tend to support this interpretation. Active faulting, also, apparently continues distant from the ridge axis. Although no earthquakes have been documented for the equatorial Pacific west of 120°W (NOAA Data Center, 1976), as far west as 140°W , north-south trending ridges and troughs are often bordered by small normal faults that extend to the surface, occasionally giving rise to minor relief of 10 to 20 m (van Andel, Heath et al., 1973).

Sedimentation and erosion tend to subdue relief. The thick layer of transparent sediment often observed on topographic highs (Fig. 9) and the distribution of faults described above (see profile B, Fig. 9, for records collected in this study) would suggest that sedimentation and erosion are of secondary importance.

The few measurements of bottom currents in the equatorial North Pacific further support this interpretation. Values that have been recorded are less than 10 cm/sec and usually less than 5 cm/sec (Johnson, 1972b). Such

velocities seem inadequate to move surface sediment that frequently consists of a thin layer of Quaternary and Holocene sediment (Johnson, 1972a). In the area between the Clarion and Clipperton fracture zones this sediment may be as thin as a few centimeters and rest unconformably on sediment of Miocene Age (Moore, 1968; Johnson, 1972a).

Little is known about the influence of topography on the distribution of ferromanganese nodules. A series of bottom photographs, taken by the OCEANOGRAPHER in area C show that nodule coverage may vary from 20% to 80% over a distance of less than a kilometer, but coverage is usually in the range of 25% (Fig. 8). Moore and Heath (1968) noted that nodules appear to be more common on slopes of abyssal hills than on the tops or intervening valleys. This distribution may be expected if, as the 3.5 records suggest (Fig. 9), the slope is an area of slower deposition, perhaps even erosion, of fine material. Mizuno et al. (1976) observed that, within a small area of the central Pacific basin, where abyssal hills are prominent, nodules are largely restricted to areas where the transparent layer is less than 20 m (Fig. 10). In areas where the transparent layer is less than 10 m thick, however, they observed nodular pavement and usually less nodule coverage. These possible relationships between bathymetry, sediment ages and nodule distribution suggest that mining operations may focus on the slopes of abyssal hills and that, a fraction of older sediment, usually covered by Quaternary and Holocene sediment, may be resuspended in the water column in an amount disproportionate to its surface distribution.

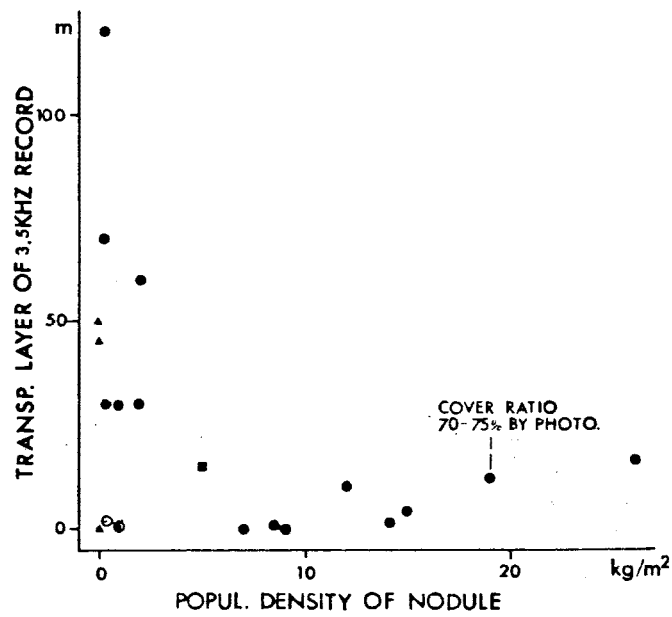


Figure 10. Correlation between coverage of nodules and thickness of transparent layer for the for the Central Basin of the Pacific. Figure is from Mizuno et al. (1976).

Currently the central equatorial Pacific is one of the most biologically productive areas in the open ocean (Fig. 11). Deep water, which has a high concentration of the essential nutrients NO_3^{-1} , PO_4^{3-} , and SiO_4^{-4} upwells along the equatorial divergence (Reid, 1962). As a result, within the photic zone primary productivity attains a value of approximately $73 \text{ gC/m}^2/\text{yr}$ (Menzel, 1974). At mid-latitudes, in the oligotrophic water of the central gyres, productivity is less by roughly $1/3$. Calcareous and, to a lesser degree, siliceous tests of planktonic organisms, that accumulate on the sea floor under this zone of high productivity, form a west trending tongue of biogenic surface sediment along the equator. Within approximately 7° of the equator the sediment consists largely of CaCO_3 . This grades into a somewhat irregular west-trending tongue of siliceous ooze. At a latitude of 10 to 15° N siliceous sediment grades into lithogenic sediment largely barren of remains of micro organisms. The boundary of calcareous ooze roughly coincides with that of highest sediment accumulation for the central Pacific (Fig. 12), demonstrating the dominant role of CaCO_3 in the accumulation of pelagic sediment of the central Pacific.

Planktonic foraminifera and coccolithophorids are quantitatively the most important contributors of CaCO_3 to pelagic sediment (Arrhenius, 1963). Their distribution is controlled by productivity, as noted above, but also by dissolution of CaCO_3 in the water column. Below a few 100 meters depth, seawater is undersaturated with respect to both calcite and aragonite (Bernier, 1976; Li et al., 1969). Peterson (1966) and Berger (1968) noted that calcite spheres and planktonic foraminifera, when suspended in the water column of the central Pacific for several months, partially dissolve below approximately 500 m and that the rate of dissolution increases sharply below

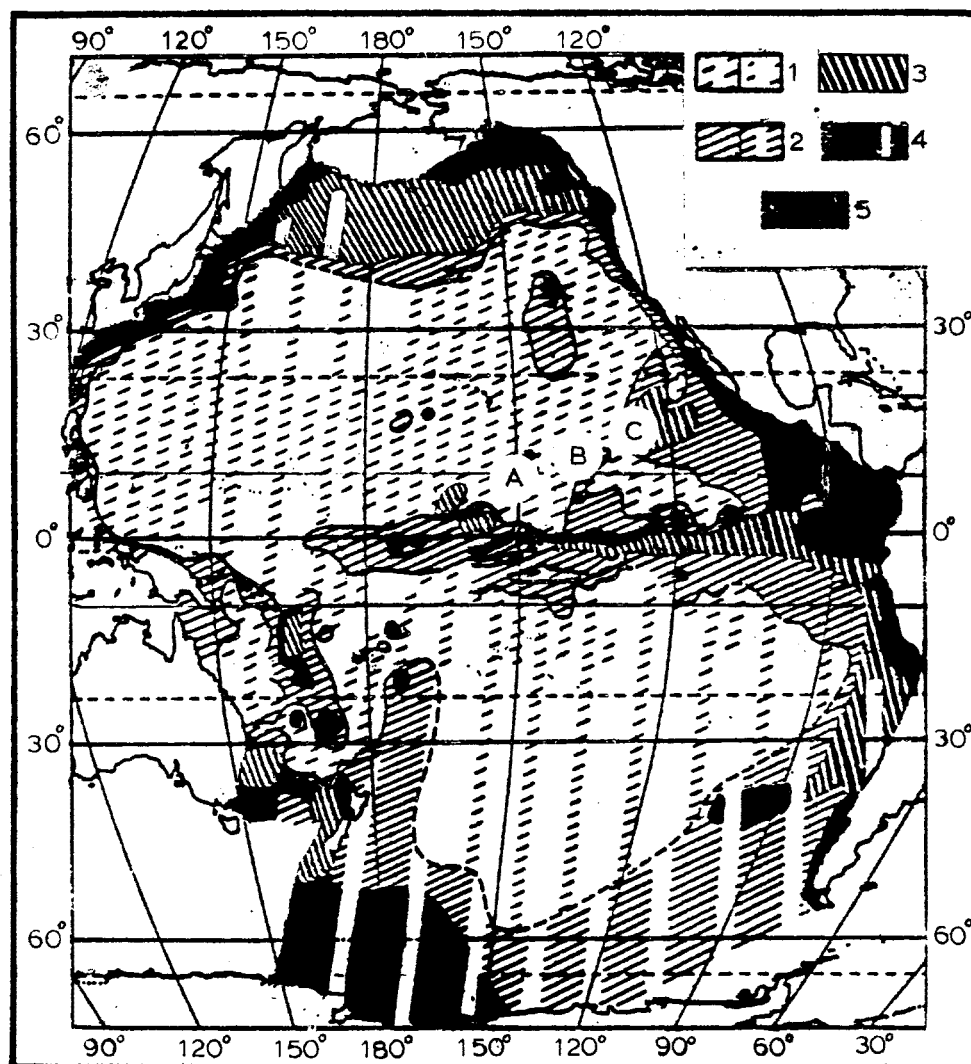


Figure 11. Primary productivity in the Pacific Ocean, in $\text{mg}/\text{m}^3/\text{day}$. Area 1 0-2; area 2 2-5; area 3 5-10; area 4 10-20; area 5 greater than 20. Figure has been taken from Bogorov (1969).

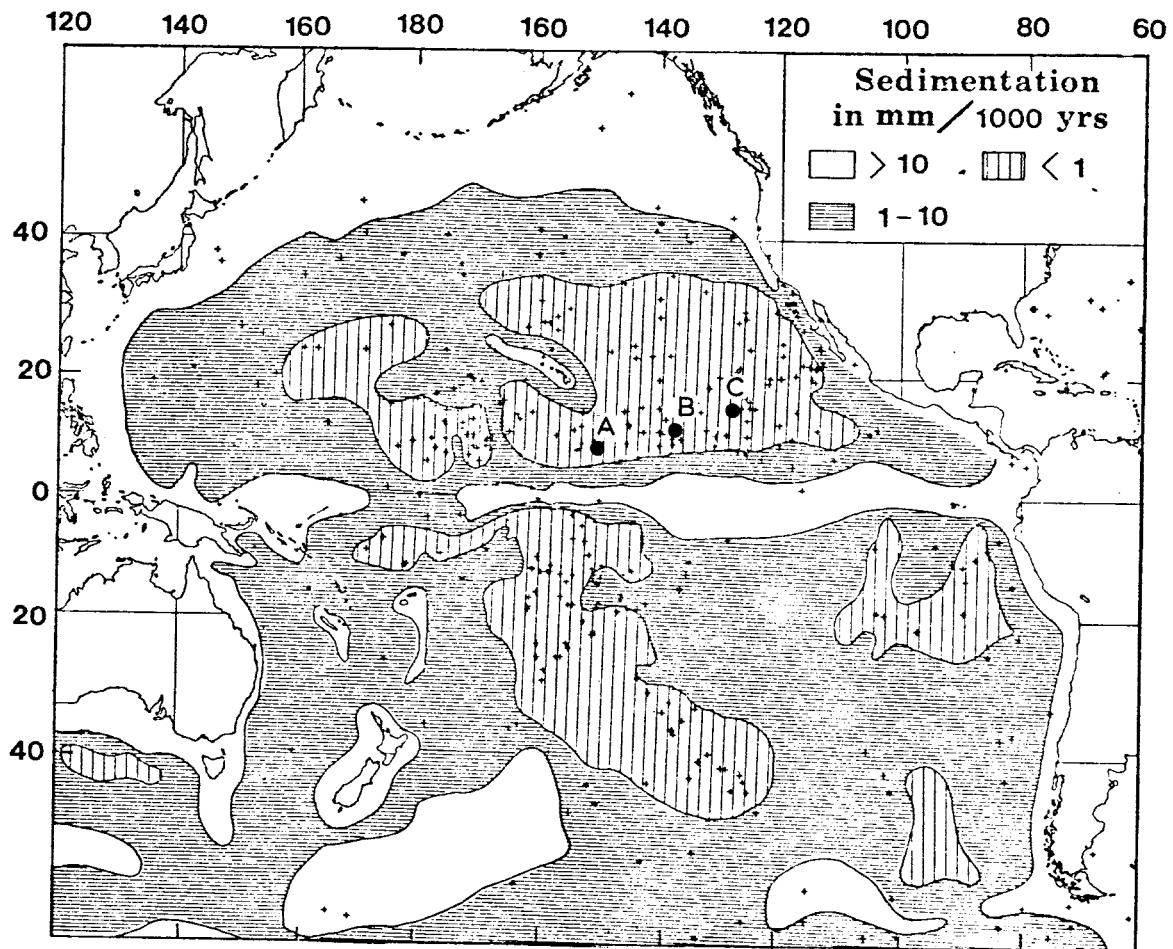


Figure 12. Sedimentation rates of the Pacific Ocean (Lisitzin, 1972).

3700 to 4000 m. This depth of increased rate of dissolution has been termed by Berger (1968) as the lysocline. It is characterized, within the sediment, as the depth at which 50 to 80% dissolution of foram fauna occurs.

van Andel et al., (1976) have shown that the lysocline may influence only slightly the total concentration of CaCO_3 in sediment from immediately above and below this depth. Above the lysocline in areas of high productivity sediment may contain greater than 95% CaCO_3 . A 50% reduction of CaCO_3 , thus, would still give a sediment with >91% CaCO_3 .

Bramlette (1961) showed that, within the central Pacific, sediment from greater than approximately 4500 m is essentially free of CaCO_3 . This depth, below which the rate of dissolution exceeds the rate of supply of CaCO_3 remains of organisms that settle through the water column, is termed the calcite compensation depth (CCD). As the depth of the CCD is a function both of CaCO_3 dissolution throughout the deep water and productivity largely within the photic zone, its depth exhibits a strong latitudinal variation. It is deepest (~ 5000 m) along the equator, where primary productivity is high, and it shoals away from the equator as productivity decreases (Heath and Culbertson, 1970).

Within the north Pacific, the sea floor is above the CCD from the equator to approximately 7°N and east of the East Pacific Rise and west of the Line Island Ridge. As noted above, this sediment consists almost exclusively of CaCO_3 ooze (Frazer, et al., 1972). North of this latitude the sea floor is below the CCD, except for bathymetric highs such as oceanic ridges. Calcium carbonate is absent, or nearly so, in this surface sediment and opaline silica becomes the dominant biogenic component of the sediment.

The distribution of biogenic silica is somewhat less complex than that of CaCO_3 . Although seawater is undersaturated with respect to opaline silica, its rate of dissolution is apparently less dependent upon depth. Its distribution in pelagic sediment exhibits no horizon similar to the CCD for calcite (Heath, 1974). Thus, its distribution is controlled almost exclusively by productivity, as is shown by its distribution when measured in sediment on a carbonate-free basis (Fig.13). Within the total sediment, its concentration north of about 15°N is limited by surface productivity. Its concentration in sediment south of 7°N is limited by a high accumulation rate of CaCO_3 . As a result, only between approximately 7°N and 15°N an irregular tongue of siliceous ooze occurs, composed largely of radiolaria and diatoms. This area lies largely within the region of low sediment-accumulation rates, i.e. in the area where the sedimentation rate is less than $1 \text{ mm}/10^3 \text{ yr}$ (Fig. 12).

North of approximately 10 to 15°N lithogenic material makes up almost the entire sediment. Its accumulation rate is also low, less than $1 \text{ mm}/1000 \text{ yr}$ (Fig. 12). It is not possible to ascertain its accumulation rate along the equator where biogenic material represents the dominant component of sediment. It is unlikely, however, to be greater than that at higher latitudes.

Ferromanganese nodules are present on the surface of the seafloor throughout the Pacific. In the area roughly between the Clarion and Clipperton Fracture zones, the area in which sites A, B, and C are located (Fig.1), nodules exhibit consistently high surface concentrations in bottom photographs (Mero, 1965; Menard, 1964). At 8 camera stations in area C (Fig. 14) the bottom coverage is usually 25 to 30% (Fig. 8). In many photographs this value may increase to 50 to 75% (Fig. 8c). It is seldom less than 20%.

At station 1, large angular fragments were observed associated with

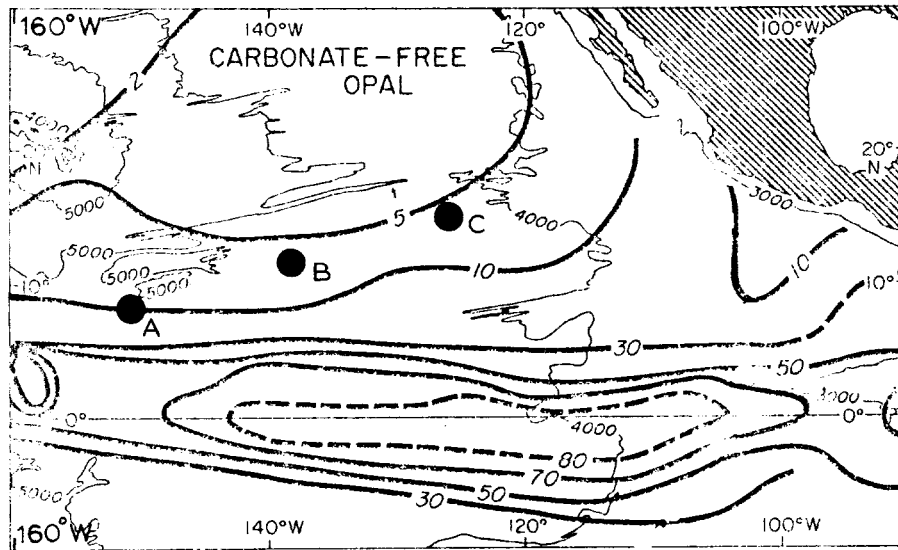
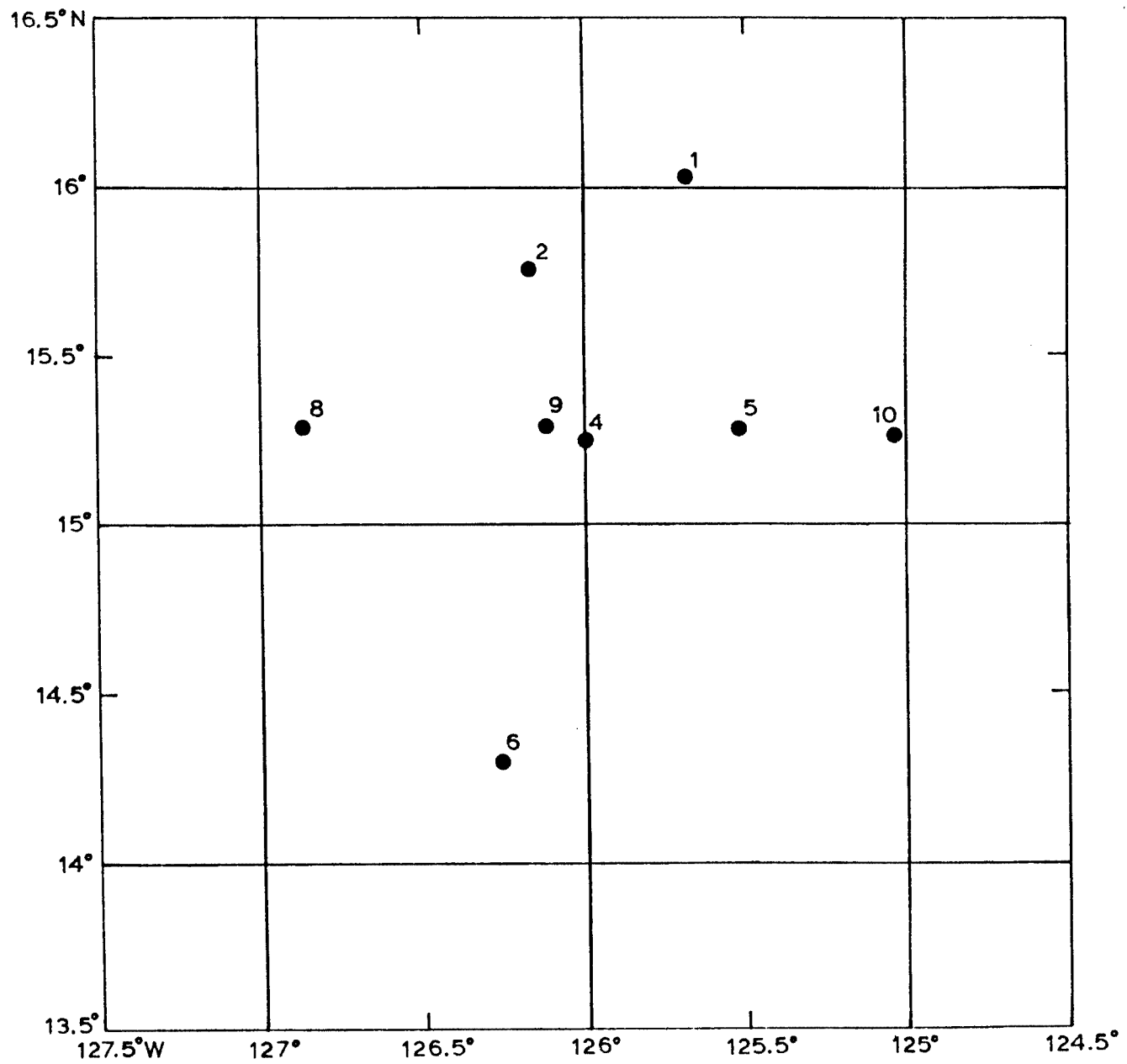


Figure 13. Distribution of opal in Recent sediment of the east-central Pacific (Heath et al., 1975). Contours are percentage of opal on a carbonate-free basis.

Figure 14. Camera stations in area C for cruise RP 6-0C-75.



nodules (Fig. 8a). These may represent fragments of volcanic rock or of a nodular pavement. The occurrence of either at the surface suggests active erosion or a period of non-deposition. The latter would suggest the presence of a thin (<10 m) transparent layer.

The bulk concentrations of Fe, Mn, Cu, and Ni have been measured in nodules collected from box-cores from site C (Table 1). Their composition is similar to that of nodules from this area (Table 1) that have been reported in the literature (Horn et al., 1973). Nodules from this area have high Ni, Cu, and Mn/Fe values relative to that of nodules from near the equator (3°S to 3°N) and to that of nodules from mid-latitudes 17° to 38° (Piper and Williamson, 1976; Fig. 15).

With the exception of nodule Amph-3 PG, variation in bulk composition of nodules is quite small. Ni plus Cu values vary between 1.82 and 2.30% and are approximately equal to the variation observed between subsamples of a single nodule (e.g. 15B; Table 1). Certainly more nodules need to be analyzed from this area to confirm this low variability. If confirmed by subsequent analyses, however, it would suggest that, for an area of such size in the this part of the Pacific, mining operations may be based more on bathymetric relief and surface coverage of nodules.

One factor that may contribute significantly to this low variability is the extreme uniformity in composition of associated sediment. With the exception of subsurface sediment in core 18B, sediment samples analyzed from this area have a rather uniform elemental and clay-mineral composition (see accompanying reports). Within areas A and B this may not be the case and both nodule and sediment compositions may exhibit large variability.

Cores collected by the Deep-Sea Drilling Project (DSDP) have provided an extensive record of Cenozoic sediment from the central Pacific. Based

Table 1. Bulk Composition of Nodules from Site "C"

Station No.	Sample Description	Mn	Fe	Cu	Ni	Zn
15 B	Interior	23.9	7.88	0.83	0.99	.122
15 B	Equatorial edge, surface	25.1	4.82	0.87	1.08	.138
15 B	Smooth surface	25.3	8.56	0.79	1.00	.114
15 B	Rough surface	24.1	5.00	1.01	1.21	.114
15 B	Bulk	26.5	5.60	1.08	1.19	.110
25	Bulk	27.3	5.86	1.05	1.25	.116
11	Bulk-a	24.7	6.72	0.72	1.13	.098
11	Bulk-b	25.5	7.12	0.83	1.27	.106

		Mn	Fe	Cu	Ni	Zn
Amph-3PG*	(Scripps)	23.2	5.95	1.24	1.91	--
Cb-3*	(Scripps)	22.2	9.7	0.82	1.00	--
		24.0	8.3	0.95	1.23	--
Cb-5*	(Scripps)	22.2	6.3	1.06	1.06	--
		27.8	2.4	1.0	0.9	--
RC12-50*	(LDGO)	22.0	8.6	0.72	1.16	--

* See Horn et al. (1973) for source of data. Station numbers are abbreviations of sample numbers in collections at Scripps and Lamont-Doherty. These samples are all within 2° of Site C.

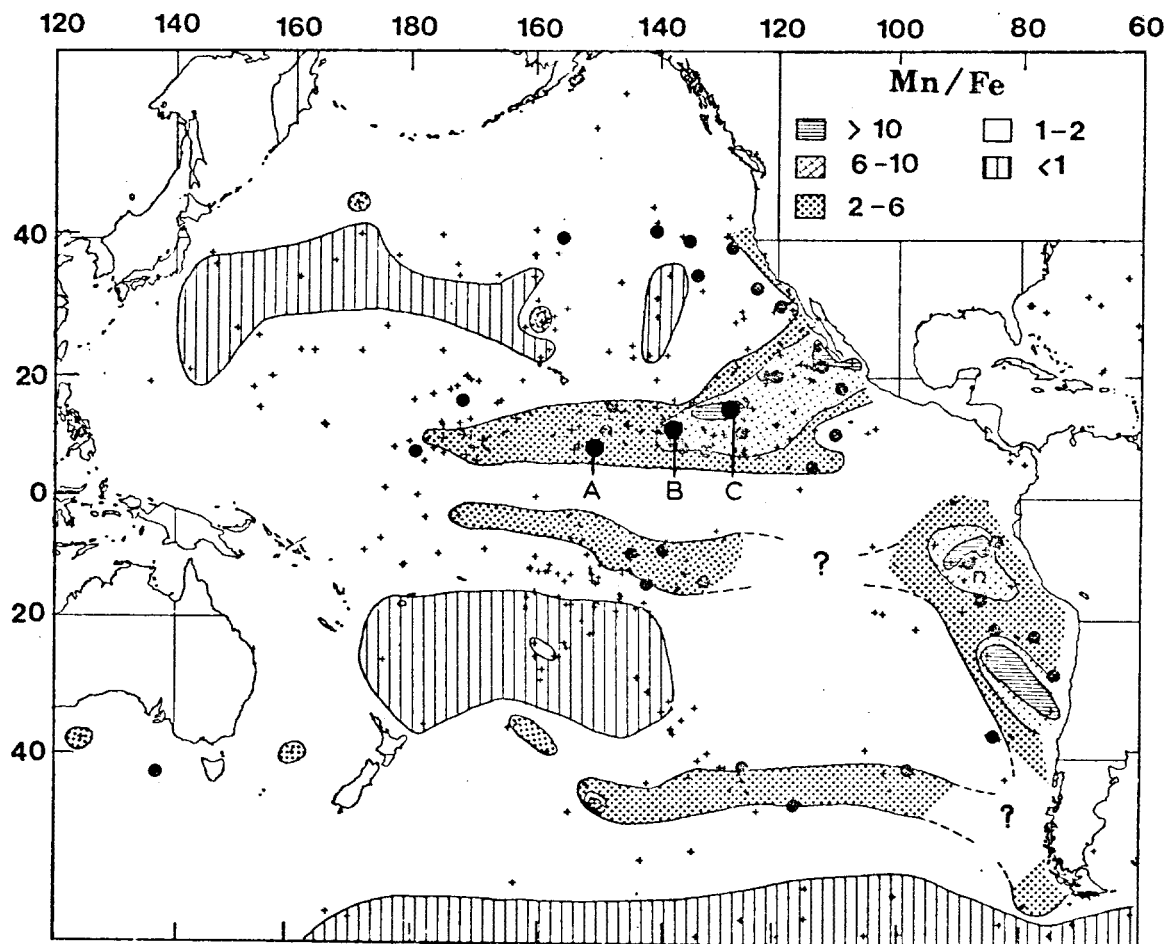


Figure 15. The Mn/Fe ratios of nodules from the Pacific Ocean. The elemental data are from Horn et al. (1973) and Piper and Williamson (1976).

on cores from DSDP legs 8, 9, and 16, van Andel et al., (1976) have attempted to decipher the sedimentary history. They have shown that sedimentation during the Cenozoic has been similar, although far from identical, to the current sedimentary environment. Sediment along the equator, and a few degrees to either side, consists largely of biogenic debris, mostly CaCO_3 . This sediment has accumulated more rapidly along the equator than to the north and south. To the north the sediment grades into non fossiliferous "red clay", that accumulates at a relatively slow rate. For example, at $19^\circ 47.57'N$ (DSDP station 40) the total amount of sediment younger than Eocene is represented by 10 m of "barren" red clay (McManus et al., 1970).

Several properties of the environment have changed significantly throughout this period to complicate the interpretation of DSDP cores far beyond this simple explanation. The summary of these changes, as given by van Andel et al., (1976), is shown in Figure 16. The more important changes are as follows:

1. Change in the depth of the CCD. The most striking fluctuation was a sharp increase of its depth at the close of Eocene. It apparently is near its greatest depth currently.
2. Dissolution rate of CaCO_3 . This rate was lowest during Oligocene and has increased since that time, more or less continuously, except for a reverse in the trend during the last 5 my.
3. Width of the zone of carbonate accumulation. It was extremely broad during Oligocene, possibly as wide as the zone of high productivity itself. Prior to and since that time it has been much more narrow.
4. Frequency of occurrence of hiatuses. This was greatest during Eocene and Late Miocene. The occurrence of hiatuses has been most pronounced in the area between approximately 5 and $15^\circ N$, the area of greatest nodule coverage. Sediment of Middle Miocene age, and older, has often been encountered in this area at the surface or within a few centimeters of the surface. At Site C, however, only a small amount of the sedimentary column corresponding to the last 5 my may be missing. DSDP cores at sites 159 and 160, the two DSDP cores closest to Site C and some 3° to the south, contain several meters of Quaternary sediment.

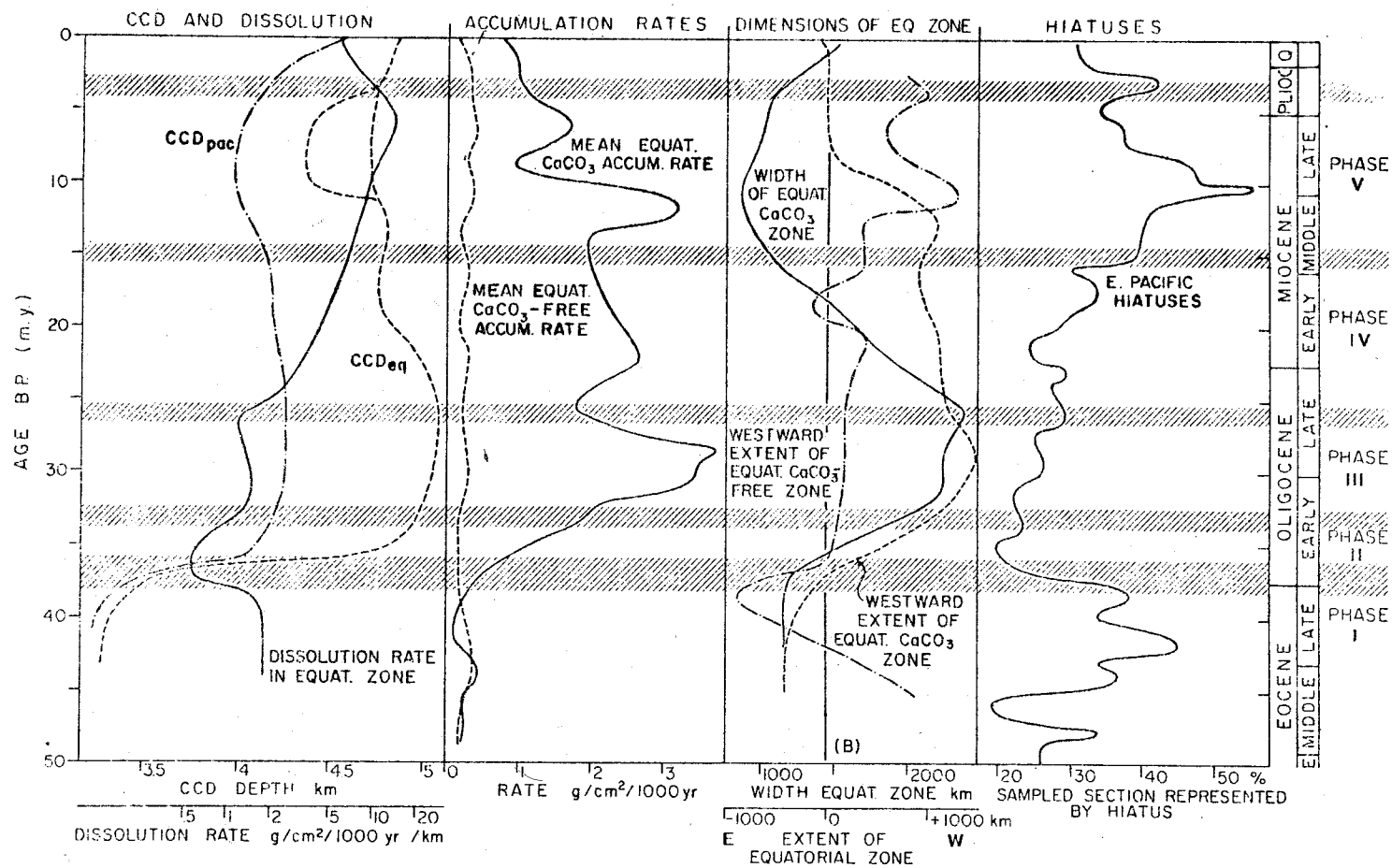


Figure 16. Variations with time of principal paleoceanographic indicators in the central equatorial Pacific during the past 50 m.y. Figure is from van Andel et. al. (1976). For complete description of figure see their paper.

5. Sea floor spreading. The Pacific plate has been moving in a north to northwest direction. A slight change occurred in this direction sometime between 20 and 50 my B.P., as a result of a change in the location of the pole of notation and in the rate of rotation. One result of these changes is that the northward component of movement has been less since this change than during prior time. A strong expression of this movement is the offset of the axis of the wedge of biogenic sediment a few degrees to the north of the equator (Ewing et al., 1968; Winterer, 1973). The present northward component of movement is approximately 2.7 cm/yr.

These factors, plus possible variations in productivity (Arrhenius, 1952), have largely controlled the accumulation and current distribution of sediment in the central Pacific.

Tertiary and Quaternary sediment of the central Pacific has been divided into four "oceanic" formations (Tracy, et al., 1971; Hayes, et al., 1971; Cook, 1975) that differ in their lithologic character (Fig. 17) such that they can be mapped within defined limits. Their surface distribution for several epochs of the Tertiary and Quaternary has been determined by Cook (1975). As an example his interpretation of Early Miocene surface sediment is shown in Figure 18.

Since the Clipperton "Oceanic" formation is accumulating at the surface throughout the equatorial Pacific at the present time and is the formation in which almost all nodules are located (i.e., it is the sediment that will be resuspended in the water column), it will be considered in some detail. It consists of two units (Fig. 17). The cyclic unit is characterized by thin interbedding of dark brown and white-to-pale yellow beds. The dark beds consist mainly of opaline silica, with a relatively high metal oxide content. The lighter colored beds have a higher concentration of CaCO_3 . The varicolored unit is characterized by a high CaCO_3 content, a somewhat lower silica concentration, and pastel shades of blue, purple, and green. This formation is distinguished from the Marquesas Oceanic formation, which is composed dominantly of CaCO_3 , has relatively less silica,

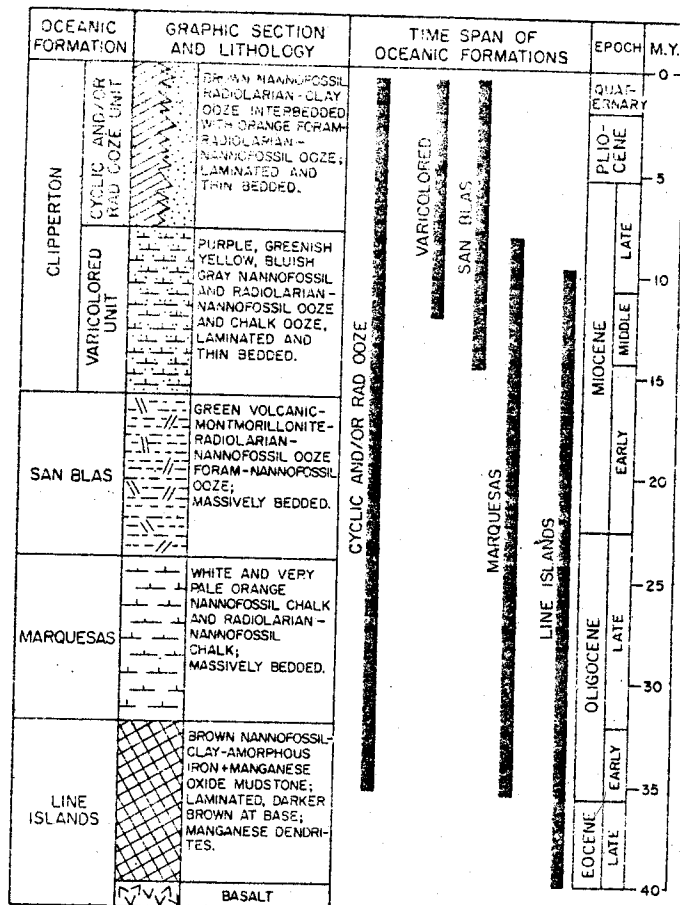


Figure 17. Composite stratigraphic section for oceanic formations and their time span, equatorial Pacific (Cook, 1975).

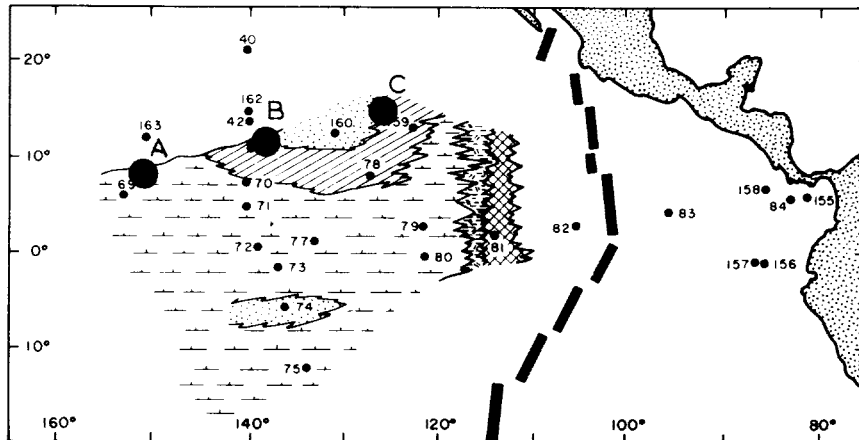


Figure 18. Early Miocene paleogeologic facies for the eastern equatorial Pacific. See figure 17 for explanation of symbols. Figure is from Cook (1975).

and has massive bedding. These formations are diachronous; at the equator the base of the Clipperton is Pleistocene. It increases in age at higher latitude where, at 15°N , it is Early Oligocene (Cook, 1975).

During Oligocene and Early Miocene time the Marquesas had its greatest extent, accumulating under conditions favorable to maximum extent of the CaCO_3 zone, extremely deep CCD at the equator, and few hiatuses (Fig. 16). The Clipperton was restricted during most of this time to latitudes greater than approximately $10\text{-}15^{\circ}$. During Miocene its areal distribution increased (Fig. 18) along the equator and by Late Miocene the varicolored unit had largely replaced the Marquesas at the surface along the equator (Cook, 1975). This change represented an increase in the silica and metal oxide components of equatorial sediment. During Pliocene and Quaternary this trend continued as the distribution of the cyclic unit of the Clipperton increased to the point of largely replacing the varicolored unit.

This trend is apparently reflected most strongly in van Andel et al's (1976) interpretation of DSDP cores by the general decrease in mean CaCO_3 accumulation rate along the equator from Oligocene to Recent (Fig. 16), which has allowed for a relative increase in the non-carbonate components of sediment in the Central Pacific.

Conclusions

In summary, the area in the north Pacific, that has high mineral potential, is characterized by the following:

1. abyssal hills of low relief (50-200 m) that have a strong north-south orientation. High angle faults, with a few meters of vertical offset and extending to the surface, were observed in the 3.5 KHz records from sites A and B and have been reported by others as being present in the vicinity of site C. Such faulting appears to have a greater influence on the bathymetry than erosion and sedimentation.

2. a sediment cover, based on 3.5 KHz records from area B, typical of other areas in the equatorial north Pacific, as reported by others. A transparent layer of approximately 40 to 60 m thickness is present at the surface throughout much of the area. Beneath this layer is a series of highly opaque layers. They are usually conformable with the bottom, but occasionally crop out along slopes of abyssal hills. Resolution of layers beneath this series of reflectors is usually very poor. The sediment column appears to be approximately 150-200 m thick, based on the depth of a reflector that was occasionally present and interpreted as acoustic basement.
3. a central location of the area on the Pacific Plate, approximately between the Clarion and Clipperton Fracture zones. No major seismic activity has been recorded for this area. The occurrence of faults that extend to the surface, however, would suggest some activity distant from the East Pacific Rise.
4. occurrence of the Clipperton "Oceanic" Formation at the surface throughout the area. Within the area of Site C the Clipperton consists of Quaternary sediments at the surface, that should rest unconformably on Miocene and older sediment. This is based on DSDP cores collected to the south of site C, as sediment older than Quaternary has not been identified in box cores collected in this study. Whether the series of beds beneath the transparent layer corresponds to these older sediments may be ascertained from gravity cores that will be collected during the next cruise.

- Anon., 1974. Deepsea Ventures files Pacific Ocean mining claim. *Ocean Industry*, 9:68.
- Arrhenius, G., 1952. Sediment cores from the east Pacific. *Reps. Swed. Deep-sea Exped.*, 5: pt.3, 189-201.
- Arrhenius, G., 1963. Pelagic sediments. In: *The Sea*, ed. M. N. Hill, 3:655-718.
- Atwater, T., and Menard, H.W., 1970. Magnetic lineations in the northeast Pacific. *Earth Planet. Sci. Letter*, 7:445-450.
- Berger, W.H., 1968. Planktonic foraminifera: selective solution and paleoclimatic interpretation, *Deep-Sea Res.*, 15:31-43.
- Berger, W.H., and Winterer, E.L., 1974. Plate stratigraphy and the fluctuating carbonate line. In: *Pelagic Sediments on Land and under the Sea*, eds., K.J. Hsü and H.C. Jenkins, *Int. Assoc. Sed. Spec. Pub.*, 1:11-48.
- Berner, R.A., 1965. Activity coefficients of bicarbonate, carbonate, and calcium ions in seawater. *Geochim. Cosmochim. Acta.*, 29:947-965.
- Bogorov, V.G., 1969. *The Pacific Ocean, biology of the Pacific Ocean, Part I-Plankton (English Translation)*. U.S. Ocean. Office, Washington, 435pp.
- Bramlette, M.N., 1961. Pelagic sediments. In: *Oceanography*: Washington, D.C., Am. Assoc. Adv. Sci., 345-366.
- Calkins, T.P., 1975. Geographical distribution of yellow fin and skipjack tuna catches in the eastern Pacific Ocean, and fleet and total catch statistics, 1971-1974. *Intra-American Tropical Tuna Commission Bull.*, 17:1-116.
- Cook, H.E., 1975. North American stratigraphic principles as applied to deep sediments. *Am. Assoc. Petrol. Geol. Bull.*, 59:817-837.
- Edmond, J.M., Chung, Y., and Sclater, J.G., 1971. Pacific Bottom Water: penetration east of Hawaii. *Jour. Geophys. Res.*, 76:8089-8097.

- Ewing J., Ewing, M., Aitken, T., and Ludwig, W.J., 1968. North Pacific sediment layers measured by seismic profiling. In: The Crust and Upper Mantle of the Pacific Area, ed. L. Knopoff, C.L. Drake, and P.J. Hart, Am. Geophys. Union Mon., 12:147-173.
- Frazer, J.Z., Hawkins, D.L., Arrhenius, G., Chase, T.E., Menard, H.W., and Mammerick, J., 1972, Surface sediments and topography of the North Pacific. Inst. Mar. Res., TR-35.
- Gordon, A.L., and Gerard, R.D., 1970, North Pacific bottom potential temperature. In: Geological Investigations of the North Pacific, ed. J.D. Hayes, Geol. Soc. Am. Mem., 126: 23-39.
- Hayes, J.D., et al., 1971. Initial reports of the Deep-Sea Drilling Project, Vol. 9, Washington (U.S. Gov't. Printing Office), 1205p.
- Heath, G.R., 1974, Dissolved silica and deep-sea sediments. In: Studies in paleo-oceanography, ed. W.W. Hay, Soc. Econ. Paleo. Min. Spec. Pub., 20:77-93.
- Heath, G.R., and Culberson, C., 1970. Calcite: degree of saturation, rate of dissolution, and the compensation depth in the deep ocean. Geol. Soc. Am. Bull., 81:3157-3160.
- Horn, D.R., Delach, M.N., and Horn, B.M., 1973, Metal content of ferromanganese deposits of the oceans, IDOE Tech. Rpt., 3:1-51 (unpublished).
- Isaacs, J.D., Reid, J.L., Jr., Schick, G.B., and Schwartzlose, R.A., 1966. Near-bottom currents measured in 4 km. depth off the Baja California coast. Jour. Geophys. Res., 71: 4297-4303.
- Johnson, D.A., and Johnson, T.C., 1970. Sediment redistribution by bottom currents in the central Pacific. Deep-Sea Res., 17:157-170.
- Johnson, D.A., 1972a. Ocean floor erosion in the equatorial Pacific. Geol. Soc. Am. Bull., 83:3121-3144.
- Johnson, D.A., 1972b, Eastward flowing bottom currents along the Clipperton Fracture Zone. Deep-Sea Res., 19:253-258;
- Krishnaswami, S., and Lal, D., 1971. Manganese nodules and budget of trace solubles in the ocean. Proceedings of the Nobel Symposium, 20:307-320.

- Li, T.H., Takahashi, T., and Broecker, W.S., 1969. The degree of saturation of CaCO_3 in the oceans. *Jour. Geophys. Res.*, 74:5507-5525.
- Lisitzin, A.P., 1972. Sedimentation in the world Ocean (English Translation). *Soc. Econ. Paleo. and Min. Sp. Publ.*, 17:218pp.
- Luyendyk, B.P., 1970. Origin and history of abyssal hills in the northeast Pacific Ocean. *Geol. Soc. Am. Bull.*, 81:2237-2260.
- McManus, D.A., et al., 1970. Initial reports of the Deep Sea Drilling Project. Vol. 5, Washington (U.S. Gov't. Printing Office), 827pp.
- Menard, H.W., 1964. Marine geology of the Pacific. M^CGraw-Hill, New York, 271pp.
- Menard, H.W., and Mammereckx, J., 1967. Abyssal hills, magnetic anomalies, and the East Pacific Rise. *Earth Planet. Sci. Lett.*, 2:465-472.
- Menzel, D.W., 1974. Primary productivity, dissolved and particulate organic matter, and the sites of oxidation of organic matter. In: *The Sea*, ed. E.D. Goldberg, 5:659-678.
- Mero, J.L., 1965. The mineral resources of the sea. Elsevier, 312pp.
- Mizuno, A., Chujo, J., and Yamakade, N., 1976. Preprospecting of manganese deposits of the eastern central Pacific basin. 3rd Internat. Devel. Conf., Tokyo, 5: 322-335.
- Moore, T.C., Jr., 1968. Deep-Sea sedimentation and Cenozoic stratigraphy in the central equatorial Pacific. PhD Thesis, Scripps Inst. Oceano., 166pp.
- Moore, T.C., Jr., and Heath, G.R., 1967. Abyssal hills in the central equatorial Pacific: detail structure of the sea floor and subbottom reflectors. *Mar. Geol.*, 5:161-180.
- Moore, T.C., Jr., and Heath, G.R., 1966. Manganese nodules, topography, and thickness of Quaternary sediments in the central Pacific. *Nature*, 212:983-985.
- NOAA Earthquake Data File for the Area 0-30°N, 120-160°W, 1965-1974, 1976, Nat. Geophys. Solar-Terrest. Data Center.
- Peterson, M.N.A., 1966. Calcite rates of dissolution in a vertical profile in the central Pacific. *Sci.*, 154:1542-1544.
- Piper, D.Z., and Williamson, M., 1976. Composition of Pacific Ocean ferromanganese nodules. *Mar. Geol.* (In Press).

- Pitman, W.C., III, Larson, R.L., and Herron, E.M., 1974. Magnetic lineations of the oceans. Geol. Soc. Am., Printing Office.
- Raitt, R.W., 1956. Seismic-refraction studies of the Pacific Ocean Basin, 1. crustal thickness of the central equatorial Pacific. Geol. Soc. Am. Bull., 67:1623-1640.
- Reid, J.L., Jr., 1965. Intermediate waters of the Pacific Ocean. John Hopkins Oceano. St., No.2, 85pp.
- Reid, J.L., Jr., 1962. On the circulation, phosphate-phosphorus content and zooplankton volumes in the upper part of the Pacific Ocean. Limnol. Oceano., 7:287-306.
- Reid, J.L., Jr. and Lonsdale, P.F., 1974. On the flow of water through the Samoan passage. Jour. Phy. Oceano., 4:58-73.
- Reid, J.L., Jr., 1969. Preliminary results of measurements of deep currents in the Pacific Ocean. Nature, 221:848.
- Shor, G.G., 1959. Reflexion studies in the eastern equatorial Pacific. Deep-Sea Res., 5:283-289.
- Somayajulu, B.L.K., 1967. Beryllium -10 in a manganese nodule. Science, 156: 1219-1220.
- Somayajulu, B.L.K., Heath, G.R., Moore, T.C., Jr. and Cronan, D.S., 1971. Rates of accumulation of Manganese nodules and associated sediment from the equatorial Pacific. Geochem. Cosmochim. Acta., 35:621-624.
- Speiss, F.N., Loughridge, M.S., McGrehec, M.N. and Boegeman, D.E., 1966. An acoustic transponder system. Navig., 13:154-161.
- Stommel, H., 1958. The abyssal circulation. Deep-Sea Res., 5:80.
- Sysoyev, N.N., 1961. Study of the bottom zone of the ocean. Transl. Oceano., 1961-1962:17-19.
- Thorarinsson, S., 1965. The median zone of Iceland. In: The world rift system, ed. T.N. Irvine, Can. Geol. Sur. Pub., 66-14:187-211.
- Tracey, J.I., et al., 1971. Initial report of the Deep Sea Drilling Project. vol. 8 Washington (U.S Gov't. Printing Office), 1037p.
- van Andel, Tj. H., Heath, G.R., et al., 1973. Initial report of the Deep Sea Drilling Project. vol. 16 Washington (U.S. Gov't. Printing Office), 949p.
- van Andel, Tj. H., Heath, G.R. and Moore, T.C., Jr., 1976. Cenozoic history and paleoceanography of the central equatorial Pacific. Geol. Soc. Am. Memoir, 143:134p.

- Winterer, E.L., 1973. Sedimentary facies and plate tectonics of the equatorial Pacific. *Am. Assoc. Pet. Geol. Bull.*, 57:265-282.
- Wooster, W.S. and Volkmann, G.H., 1960. Indications of deep Pacific circulation from the distribution of properties at five kilometers. *Jour. Geophy. Res.*, 65:1239-1250.
- Zenkevitch, N.L., 1961. New data on the bottom topography of the northeast Pacific Ocean. *Tr. Inst. Okeano., Akad. Nauk S.S.S.R.*, 45:5-21.

DOMES AREA C: GENERAL STATEMENT ABOUT
MINERALOGY, DIAGENESIS AND SEDIMENT CLASSIFICATION

BY

James R. Hein

Christina Gutmacher

and

Jacquelyn Miller

U.S. Geological Survey

Menlo Park, California

INTRODUCTION

Sediment from DOMES area C is classified according to DSDP (Deep Sea Drilling Project) standards:

<u>Term</u>	<u>Abundance</u>
Trace	<1%
Bearing	2-10%
Rich	10-25%
Major	>25%

The major sediment component is listed farthest to the right in the classification of each individual sediment sample (Table 3).

The brown siliceous muds of DOMES area C are probably part of the Clipperton Oceanic Formation (defined by Tracey et.al., 1971). However, the possibility that these samples are part of the San Blas Oceanic Formation (defined by Cook, 1972) can not be ruled out. Both vertical and lateral sample density is too low at the eastern equatorial Pacific DSDP sites to allow any further comparisons with DOMES area C samples. The same lithologies and mineralogies can be found in both of these oceanic formations.

SEDIMENT CLASSIFICATION

DOMES area C sediment is quite heterogeneous, but most commonly is classified as mud (clay minerals, quartz, and feldspar) or siliceous ooze. However, in several samples Fe-Mn globules and aggregates are the major sediment components (Table 3). Calcareous nannofossil ooze characterized only one sample, core 18A-1-8 and calcite (reworked limestone?) is present in several other cores, but never as a major com-

ponent. Volcanic ash (glassy mud) is the major sediment type in several cores (for example, 23B-1-15; Table 3).

MINERALOGY

The most common sediment particles are siliceous microfossils (radiolarians, diatoms, sponge spicules), clay minerals (illite, montmorillonite, kaolinite, chlorite), volcanic glass, quartz, and feldspar. Other grains, locally important are Fe-Mn globules and aggregates, micronodules, opaque minerals (hematite, magnetite, ilmenite, goethite), and fish debris (Tables 1, 2, 3). Minor sediment components include mica, clay aggregates (maybe fecal pellets in some samples), chert, volcanic rock fragments, pyribole (undifferentiated pyroxene and amphibole), zeolites, apatite, and calcite. Barite, ubiquitous in DSDP samples from this area (Cook and Zemmels, 1971 and 1972; Zemmels, 1973) was not positively identified in sediment from DOMES area C.

The most common coarse size fraction (greater than 44μ) particles are quartz + feldspar, volcanic glass, and siliceous microfossils. Locally, Fe-Mn grains are important (Table 2). We do not know the identity of the "flat plates" listed in Table 2. They are translucent, brown in color, have a sugary texture and can be bent or curved mica-like plates. We tentatively suggest that they are part of a siliceous organism. Techniques used in the identification of clay minerals are described by Hein et al. 1976. In general, illite is the most abundant clay mineral (40-50%) in the less than 2μ size fraction (Table 1). Locally, in the lower parts of most cores, smectite is the dominant clay mineral. Illite and smectite abundances vary inversely. Abundances of kaolinite and chlorite remain relatively uniform in all cores, most commonly 10-15% each (Table 1).

DIAGENESIS

Three diagenetic reactions are evident: 1) some of the volcanic glass is devitrified and thus, tridymite-cristobalite (?) and clay minerals are formed; 2) volcanic rock fragments have altered to clays and iron oxides; 3) siliceous microfossils undergo fragmentation and dissolution with increasing depth of burial and time. Samples that contain more than 50% smectite in the less than 2μ size fraction (Table 1) are, in part, formed from the in situ breakdown of volcanic debris. This authigenic smectite is characterized by fewer intermixed illite layers in contrast to strictly detrital smectite (Hein and Scholl, 1976). The detrital clay mineral suite consists typically of 46% illite, 30% smectite, 10% kaolinite and 14% chlorite.

References Cited

- Cook, H.E., 1972, Stratigraphy and Sedimentation: Initial Reports of the Deep Sea Drilling Project, v. 9, p. 933-944.
- Cook, H.E. and Zemmels, I., 1971, X-ray Mineralogy Studies, Leg 8: Initial Reports of the Deep Sea Drilling Project, v. 8, p. 901-950.
- Cook, H.E. and Zemmels, I., 1972, X-ray Mineralogy Studies, Leg 9, Deep Sea Drilling Project: Initial Reports of the Deep Sea Drilling Project, v. 9, p. 707-778.
- Hein, J.R., Scholl, D.W., and Gutmacher, C.E., 1976, Neogene Clay Minerals of the Far NW Pacific and Southern Bering Sea: Sedimentation and Diagenesis: Proceedings of the 1975 International Clay Conference in Mexico City, Applied Publishing LTD., Illinois, p. 71-80.
- Hein, J.R. and Scholl, D.W., 1976, Diagenesis and distribution of Late Cenozoic volcanogenic sediments in the far northwest Pacific and southern Bering Sea: Geol. Soc. Amer. Bull., (submitted).
- Tracey, J.I., et. al., 1971. Leg 8 Summary: Initial Reports of the Deep Sea Drilling Project, v. 8, p. 17-44.
- Zemmels, I., 1973, X-ray Mineralogy Studies, Leg 16: Initial Reports of the Deep Sea Drilling Project, v. 16, p. 529-572.

Table 1. Semiquantitative Clay Mineralogy of Samples From DOMES Area C
 Percentages represent the relative amount of each clay mineral in the less than 2 μ size fraction and for each sample are set to equal 100%.

Sample Number	Kaolinite+Chlorite	Kaolinite	Chlorite	Illite	Smectite
11 1-1	23	10	13	50	27
11 1-8	22	9	13	45	32
11 1-9	23	10	13	47	30
11 1-10	23	10	13	42	35
11 1-14	21	9	12	42	38
15B 1-1	26	11	15	44	30
15B 1-8	25	11	14	44	31
15B 1-9	23	10	13	45	32
15B 1-10	25	11	14	41	34
15B 1-13	23	10	13	44	34
16B 1-1	25	11	15	47	27
16B 1-2	26	11	15	43	31
16B 1-3	28	12	17	41	31
16B 1-4	25	11	15	41	34
16B 1-5	24	11	13	39	37
16B 1-6	22	10	12	38	40
16B 1-7	21	9	12	27	52
16B 1-8	19	8	11	25	57
16B 1-9	18	8	9	26	57
16B 1-10	19	9	10	27	54
18A 1-1	26	11	15	51	23
18A 1-3	24	11	14	45	31
18A 1-4	27	11	15	48	25
18A 1-6	25	10	15	39	36
18A 1-8	20	9	11	22	58
18B 1-1	26	11	16	48	26
18B 1-2	25	11	14	46	29
18B 1-3	25	11	14	43	32
18B 1-4	25	10	15	46	28
18B 1-5	22	10	12	38	40
18B 1-6	22	9	13	41	37
18B 1-7	18	8	11	30	51
18B 1-8	7	3	4	16	77
18B 1-9	13	6	7	26	61

(continued) Table 1. Semiquantitative Clay Mineralogy of Samples From DOMES Area C

Sample Number	Kaolinite+Chlorite	Kaolinite	Chlorite	Illite	Smectite
20 1-1	23	10	13	47	30
20 1-2	24	11	13	56	20
20 1-3	27	10	17	49	24
20 1-4	22	9	13	48	29
20 1-5	22	9	13	52	26
20 1-6	22	10	13	40	38
20 1-7	28	11	16	42	30
20 1-8	26	11	15	41	33
23B 1-1	24	10	14	44	32
23B 1-8	35	14	21	35	29
23B 1-9	25	11	15	45	30
23B 1-10	24	10	13	44	32
23B 1-15	20	9	10	34	46
24B 1-1	27	12	15	43	31
24B 1-3	25	11	14	46	29
24B 1-5	22	9	13	51	27
24B 1-6	25	11	14	47	28
24B 1-8	22	10	12	38	40
24B 4-1	28	12	16	46	26
24B 4-3	25	9	16	37	38
24B 4-5	26	11	15	42	32
24B 4-7	23	10	13	45	32
24B 4-9	26	11	16	39	35
25 1-1	33	14	19	53	14
25 1-2	33	15	18	48	19
25 1-3	?	?	?	?	?
27 1-1	28	13	16	50	22
27 1-8	27	13	14	49	24
27 1-9	26	12	14	48	26
27 1-10	26	12	13	48	26
27 1-12	25	11	14	44	31

Table 2. Grain Mounts, >44 μ Size Fraction, From DOMES Area C

Sample	Siliceous Microfossils	Spicules	Flat Plates	Fish Debris	Volcanic Glass	Quartz & Feldspar	Opagues	Mica	Fecal Pellets	Ferromangan- ese Grains	Others
11 1-1	XXX*	XX	X	Tr	XXX	XXX	Tr	Tr	Tr		
11 1-8	XX	XX	Tr	Tr	XXX	XXX	Tr	Tr	Tr		
11 1-9	X	XX		Tr	XXX	XXX	Tr	Tr	X		Ter. plant frag?
11 1-10	X	X		X	XXX	XXX	Tr	Tr	X		unknown bl. gr.
11 1-14	Tr	X		X	XXX	XXX		Tr	X	Tr	Pyribole
15B 1-1	XXX	XX			XXX	XX	Tr				
15B 1-8	X	XX			XXX	XX	Tr				
15B 1-9	X	X			XXX	X					
15B 1-10	Tr	XX			XXX	XX					
15B 1-13	Tr	X		Tr	XXX	X			Tr		
16B 1-1	X	XXX	XX		X	XX			XX	Tr	
16B 1-2	XXX	XX	X		X	XX	Tr	Tr			Pyribole
16B 1-3	XXX	XXX		Tr	X	XX		Tr			
16B 1-4	XXX	X		Tr	XXX	XX	X	Tr		X	Pyribole
16B 1-5	Tr	X		Tr	XXX	XXX	Tr?	Tr		Tr?	
16B 1-6	X	X		X	XXX	XXX		Tr			
16B 1-7	Tr		X	X	X	XXX	Tr	Tr	X	Tr	Zeol? Pyribole
16B 1-8	X	X		Tr	X	XXX		Tr			Zeol? Pyribole
16B 1-9	X	X	X	X	X	XXX	Tr	Tr	X		
16B 1-10	X	X	X	X	X	XXX	Tr	Tr	X	Tr	
18A 1-1	X	X	XXX	X	X	X		Tr		XXX	
18A 1-3	X	X			X	XXX		Tr		Tr	Zeolites
18A 1-4	X	X	XXX	X	X	X		Tr		XXX	
18A 1-6	XX	XX	XX	X	XX	XX		Tr		X	
18A 1-8	X	Tr	X	X	XXX	XX		Tr		Tr	

(continued) Table 2. Grain Mounts, >44 μ Size Fraction, From DOMES Area C

Sample	Siliceous Microfossils	Spicules	Flat Plates	Fish Debris	Volcanic Glass	Quartz & Feldspar	Opaques	Mica	Fecal Pellets	Ferromangan- ese Grains	Others
18B 1-1	XXX	X		X	X	XX	Tr	Tr			
18B 1-2	XXX	XX	XXX	X	X	X		Tr		X	
18B 1-3	XXX	X	X	X	X	XX		Tr	X	X	rx. frag. chert?
18B 1-4	X	X	X	XX	XX	XXX		Tr			
18B 1-5	X	X	Tr	X	XX	XXX	Tr	Tr	Tr		cht. frag. pyt. zeol.
18B 1-6	X	X	X		X	XXX			XX		
18B 1-7	X	X		X	XX	XXX	Tr	Tr	Tr		rx. frag? zeol?
18B 1-8				X	XXX	XX	Tr?		X	Tr?	zeolites?
18B 1-9	X	XX	X	X	XX	XXX	Tr	Tr			zeolites?
20 1-1	XXX	X			X	X	Tr	Tr		Tr	
20 1-2	XXX	XX		XX	X	XX	X	Tr			
20 1-3	XXX	XX			X	XX	Tr	Tr			
20 1-4	XX	X	X	X	XX	XX	Tr	Tr			
20 1-5	XXX	XX		X	XX	XX	Tr	Tr			
20 1-6	XX	XX	Tr	Tr	XXX	XXX	X	Tr			
20 1-7	X	XX		Tr	XXX	XXX	Tr	Tr			
20 1-8	X	XX	Tr	Tr	XX	XXX	X	Tr			rock fragment
23B 1-1	XXX	XX			Tr	Tr	Tr				
23B 1-8	XXX	XX			Tr	Tr	Tr				
23B 1-9	XXX	XX		Tr	XX	X					
23B 1-10	XXX	X	Tr	X	XXX	X					
23B 1-15	Tr	X		Tr	XXX	XX	Tr				Ter. plant fiber?
24B 1-1	XXX	XX			Tr	Tr	Tr				rock fragment
24B 1-3	XXX	XX			Tr	Tr	Tr	Tr			rock fragment
24B 1-5	XXX	XX		Tr	Tr	Tr	Tr				rock fragment

(continued) Table 2. Grain Mounts, >44μ Size Fraction, From DOMES Area C

Sample	Siliceous Microfossils	Spicules	Flat Plates	Fish Debris	Volcanic Glass	Quartz & Feldspar	Opaques	Mica	Fecal Pellets	Ferromangan- ese Grains	Others
24B 1-6	XXX	XX		Tr	Tr	Tr	Tr	Tr			rock fragment
24B 1-8	XXX	XX		Tr	Tr	Tr	Tr				rock fragment
24B 4-1	XXX	XX		Tr	Tr	Tr	Tr				rock fragment
24B 4-3	XXX	XX		Tr	Tr	Tr	Tr				rock fragment
24B 4-5	XXX	XX		Tr	Tr	Tr	Tr				rock fragment
24B 4-7	XXX	XX		Tr	Tr	Tr	Tr				rock fragment
24B 4-9	XXX			Tr	X	Tr	Tr	Tr			
25 1-1	X	XX	XXX	X	XX	X		Tr			unknown red gr.
25 1-2	Tr	XX	XXX	X	XXX	X		Tr			
25 1-3	Tr			Tr	XXX	Tr	Tr				
27 1-1	Tr	XX		XX	XX	XX	Tr	Tr			rock fragment
27 1-8	Tr	X		X	XXX	X	Tr				
27 1-9	Tr	X	Tr	X	XXX	XXX	Tr	Tr			
27 1-10		X		X	XXX	XX	Tr	Tr			
27 1-13		X		X	XX	XXX	Tr	Tr			

* Abundant XXX
Common XX
Present X
Trace Tr

Table 3. Smear Slides Bulk Sample From DOMES Area C

The two or three major sediment components are listed in the Sediment Classification column; mud designates fine-grained quartz, feldspar and clay minerals. Other grain types listed as primary constituents are, most commonly, each less than 2% of the sediment.

Sample	Sediment Classification	Primary Constituents
CORE 11	Detrital-Volcanic-Biogenic	
1-8	Siliceous fossil bearing glass rich mud	clay minerals, volcanic glass, siliceous microfossils, quartz, feldspar, opaque minerals, fish debris, chert
1-9	Siliceous fossil bearing glass rich mud	clay minerals, volcanic glass, quartz, feldspar, siliceous microfossils, opaque minerals, fish debris, chert, amorphous globules, volcanic rock fragments
1-10	Glass bearing mud	clay minerals, volcanic glass, quartz, feldspar, mica, pyribole, opaque minerals, siliceous microfossils, fish debris, chert, zeolites?, volcanic rock fragments
1-14	Spicule bearing glass rich mud	clay minerals, volcanic glass, quartz, feldspar, mica, pyribole, opaque minerals, fish debris, Fe globules, chert, volcanic rock fragments, zeolites?
CORE 15B	Detrital-Volcanic-Biogenic	
1-1	Glass and siliceous fossil rich mud	clay minerals, siliceous fossils, volcanic glass, fecal pellets, quartz, feldspar, mica
1-8	Siliceous fossil bearing glass rich mud	clay minerals, volcanic glass, quartz, feldspar, siliceous microfossils, fecal pellets, opaque minerals, fish debris,
1-9	Siliceous fossil bearing glass rich mud	clay minerals, volcanic glass, quartz, feldspar, siliceous microfossils, opaque minerals, mica, fish debris, chert, volcanic rock fragments, clay aggregates
1-10	Glass bearing mud	clay minerals, quartz, feldspar, volcanic glass, pyribole, siliceous microfossils, opaque minerals, fish debris, clay aggregates, volcanic rock fragments, chert

(continued) Table 3. Smear Slides Bulk Sample From DOMES Area C

Sample	Sediment Classification	Primary Constituents
1-13	Glassy mud	Clay minerals, volcanic glass, opaque minerals, volcanic rock fragments, fish debris, pyribole, chert
CORE 16B	Detrital-Volcanic-Biogenic	
1-1	Glass bearing siliceous fossil rich mud	siliceous microfossils, volc. glass, clay minerals, qtz., felds., opaque minerals, fish debris, pyribole, micronodules, volc. rx. frags.
1-2	Glass bearing siliceous mud	clay minerals, qtz., felds., siliceous microfossils, volc. glass, opaque minerals, fish debris, clay aggregates, volc. rx. fragments
1-3	Glass and siliceous fossil rich mud	clay minerals, qtz., felds., siliceous microfossils, volc. glass, opaque minerals, clay aggregates, chert
1-4	Opaque bearing glass and siliceous fossil rich mud	clay minerals, qtz., felds., volc. glass, siliceous microfossils, opaque minerals, fish debris, clay aggregates, volc. rx. fragments
1-5	Glass bearing mud	clay minerals, qtz., felds., volc. glass, opaque minerals, siliceous microfossils, pyribole, clay aggregates, volc. rx. fragments
1-6	Opaque and glass bearing mud	clay minerals, qtz., felds., volc. glass, opaque minerals, Fe-Mn micronodules, fish debris, zeolites?, apatite, chert, clay aggregates
1-7	Glass and opaque bearing amorphous globule and aggregate rich mud	clay minerals, qtz., felds., volc. glass, Fe-Mn amorphous globules and aggregates, opaque minerals, fish debris, siliceous microfossils, clay aggregates, zeolites?
1-8	Glass bearing Fe-Mn amorphous globule and aggregate rich mud	clay minerals, qtz., felds., Fe-Mn amorphous globules and aggregates, volc. glass, opaque mins., fish debris, siliceous microfossils, micronodules, mica, chert, clay aggregates, volc. rx. frags., pyribole

(continued) Table 3. Smear Slides Bulk Sample From DOMES Area C

Sample	Sediment Classification	Primary Constituents
1-9	Spicule and Fe-Mn amorphous globule and aggregate bearing mud	clay mins., qtz., felds., Fe-Mn amorphous globules and aggregates, spicules, opaque mins., mica, clay aggregates, fish debris, volc. glass, chert, volc. rx. frags., micronodules?, apatite, barite?
1-10	Spicule and Fe-Mn amorphous globule and aggregate bearing mud	clay mins., qtz., felds., Fe-Mn globules and aggregates, spicules, opaque mins., volc. rx. frags., mica, chert, volc. glass, fish debris, micronodules
CORE 18A	Biogenic-Detrital-Fe-Mn-Volcanic	
1-1	Calcite bearing clay and glass rich siliceous amorphous globule-micronodule sediment	siliceous fossils, clay mins., qtz., felds., Fe-Mn globules and aggregates, micronodules, volc. glass, calcite, opaque mins., mica, fish debris, apatite, chert
1-3	Glass and calcite rich siliceous mud	clay mins., qtz., felds., siliceous microfossils, volc. glass, calcite, fish debris, opaque minerals, Fe-Mn globules, volc. rx. frags., chert, clay aggregates
1-4	Fe-Mn amorphous globule bearing calcite rich siliceous mud	clay mins., qtz., felds., siliceous microfossils, calcite, volc. glass, Fe-Mn globules and aggregates, micronodules, fish debris, chert
1-6	Glass and siliceous fossil bearing carbonate mud	clay mins., qtz., felds., calcite, siliceous microfossils, volc. glass, Fe-Mn globules
1-8	Fe-Mn globule bearing nannofossil ooze	calcite, clay mins., qtz., Fe-Mn oxide globules, apatite?
CORE 18B	Detrital-Biogenic-Fe-Mn-Volcanic	
1-1	Glass rich, Fe-Mn globule-siliceous mud	clay mins., siliceous fossil debris, Fe-Mn globules and aggregates, volc. glass, opaque mins., chert, fish debris

(continued) Table 3. Smear Slides Bulk Sample From DOMES Area C

Sample	Sediment Classification	Primary Constituents
1-2	Glass bearing, Fe-Mn globule rich, muddy siliceous ooze	clay mins., Qtz., felds., siliceous fossil debris, Fe-Mn globules, aggregates + micronodules, volc. glass, opaque mins., fish debris, chert, volc. rx. frags., calcite?
1-3	Glass and Fe-Mn globule rich siliceous mud	clay mins., Qtz., felds., siliceous fossil debris, Fe-Mn globules, aggregates, and micronodules, volc. glass, opaque mins., chert, calcite
1-4	Fe-Mn globule and glass rich mud	clay mins., Qtz., felds., volc. glass, Fe-Mn globules, aggregates, and micronodules, opaque mins., siliceous microfossils, chert, zeolites? calcite, mica?
1-5	Fe-Mn globule bearing glass rich mud	clay mins., Qtz., felds., volc. glass, Fe-Mn globules and aggregates, opaque mins., siliceous microfossils, chert, calcite, micronodules?
1-6	Glass bearing, Fe-Mn globule rich mud	clay minerals, Qtz., felds., Fe-Mn globules, volc. glass, opaque mins., apatite, chert, micronods, fish debris, calcite
1-7	Opaque bearing glass and Fe-Mn globule rich mud	clay mins., Qtz., felds., Fe-Mn globules, glass, opaque mins., fish debris, volc. rx. frags., chert, siliceous microfossils, zeolites?
1-8	Opaque bearing glass and Fe-Mn globule rich mud	clay mins., Qtz., felds., Fe-Mn globules and aggregates, opaque mins., fish debris, glass, spicules, chert, zeolite? Tr calcite
1-9	Glass and clay rich opaque and Fe-Mn globule sediment	clay mins., Qtz., felds., opaques, Fe-Mn globules and aggregates, micronodules, fish debris, chert, glass, calcite, zeolites?
<u>CORE 20</u>	<u>Volcanic-Fe-Mn-Biogenic-Detrital</u>	
1-1	Glass rich siliceous mud	clay mins., Qtz., felds., siliceous microfossils, glass, opaques, chert, fish debris, silica and Fe-Mn globules, calcite, micronodules?

(continued) Table 3. Smear Slides Bulk Sample From DOMFS Area C

Sample	Sediment Classification	Primary Constituents
1-2	Glass, Fe-Mn globule, and siliceous microfossil rich mud	clay mins., Qtz., felds., siliceous microfossils, Fe-Mn globules and aggregates, glass, opaque mins, fish debris, chert, calcite, micronods.?
1-3	Glass, Fe-Mn globule, and siliceous microfossil rich mud	clay mins., Qtz., felds., siliceous microfossils, Fe-Mn globules, glass, opaque mins., fish debris, chert, tr. calcite, zeolites?
1-4	Siliceous fossil and Fe-Mn globule bearing glass rich mud	clay mins., Qtz., felds., glass, siliceous microfossils, Fe-Mn globs. , chert, zeolites?, opaque mins.
1-5	Siliceous fossil and Fe-Mn globule bearing glass rich mud	clay mins., Qtz., felds., glass, siliceous microfossils, Fe-Mn globs., volc. rx. frags., chert, fish debris, opaque mins., calcite, zeolites?
1-6	Glass and Fe-Mn globule rich mud	clay mins., Qtz., felds., Fe-Mn globs. and micronods., glass, volc. rx. frags., siliceous microfossils, opaque mins., chert, zeolites?
1-7	Fe-Mn globule bearing glass rich mud	clay mins., Qtz., felds., glass, Fe-Mn globs., siliceous microfossils, opaque mins., volc. rx. frags., chert, calcite
1-8	Fe-Mn globule bearing glass rich mud	clay mins., Qtz., felds., glass, Fe-Mn globs., siliceous fossil frags., opaque mins., volc. rx. frags., chert, fish debris
CORE 23B	Biogenic-Detrital-Volcanic	
1-1	Clay rich siliceous ooze	Siliceous microfossils, clay mins., Qtz., felds., glass, opaques, calcite, chert, volc., rx. frags.
1-8	Clay rich siliceous ooze	Siliceous microfossils, clay mins., Qtz., felds., glass, volc. rx. frags., opaques, chert, fish debris, calcite, Fe-Mn globules
1-9	Glass bearing clay rich siliceous ooze	siliceous microfossils, clay mins., Qtz., felds., glass, opaques, volc. rx. frags., fish debris, chert, Tr. Fe-Mn globules & aggregates

(continued) Table 3. Smear Slides Bulk Sample From DOMES Area C

Sample	Sediment Classification	Primary Constituents
1-10	Glass bearing siliceous mud	siliceous microfossils, Qtz., felds., clay mins., glass, volc. rx. frags., opaques, Fe-Mn globules
1-15	Glassy mud	glass, Qtz., felds., clay mins., fish debris, opaques, volc. rx. frags., chert, Fe-Mn globules
CORE 24B1	Biogenic-Detrital-Fe-Mn-Volcanic	
1-1	Clay rich siliceous ooze	siliceous microfossils, clay mins., Qtz., felds., glass, chert, opaques, Fe-Mn globs., volc. rx. frags., fish debris, calcite
1-3	Calcite, glass, and Fe-Mn globule bearing clay rich siliceous ooze	siliceous microfossils, clay mins., Qtz., felds., glass, Fe-Mn globules, calcite, opaques, volc. rx. frags.
1-5	Glass and calcite bearing clay rich siliceous ooze	siliceous microfossils, clay mins., Qtz., felds., calcite, glass Fe-Mn globs. and aggregates, volc. rx. frags., chert
1-6	Glass bearing clay rich siliceous ooze	siliceous microfossils, clay mins., Qtz., felds., glass, chlorite, chert, opaques, Fe-Mn globs., altered volc. rx. frags.
1-8	Glass and Fe-Mn globule bearing siliceous mud	Clay mins., Qtz., felds., siliceous microfossils, Fe-Mn globules, glass, altered volc. rx. frags., opaques, apatite, fish debris
CORE 24B4	Biogenic-Detrital-Fe-Mn-Volcanic	
4-1	Clay rich siliceous ooze	siliceous microfossils, clay mins., Qtz., felds., opaques, glass, chert, Fe-Mn globs. and micronodules, volc. rx. frags., calcite

(continued) Table 3. Smear Slides Bulk Sample From DOMES Area C

Sample	Sediment Classification	Primary Constituents
4-3	Calcite, glass and Fe-Mn globule bearing clay rich siliceous ooze	siliceous microfossils, clay mins., Qtz., felds., Fe-Mn globs., glass, calcite, opaques, chert, volc. rx. frags.
4-5	Glass and calcite bearing clay rich siliceous ooze	siliceous microfossils, clay mins., Qtz., felds., calcite, glass, Fe-Mn globs., chert, altered volc. rx. frags., opaques
4-7	Glass and Fe-Mn globule bearing clay rich siliceous ooze	siliceous microfossils, clay mins., Qtz., felds., Fe-Mn globules, glass, altered volc. rx. frags., chert, opaques, calcite
4-9	Glass and Fe-Mn globule bearing siliceous mud	clay mins., siliceous microfossils, Qtz., felds., Fe-Mn globules, glass, altered volc. rx. frags., chert, opaques, fish debris
CORE 25	Detrital-Fe-Mn-Bioogenic-Volcanic	
1-1	Glass bearing Fe-Mn globule rich siliceous mud	clay mins., siliceous microfossils, Qtz., felds., Fe-Mn globules, glass, opaque mins.
1-2	Glass and siliceous microfossil rich Fe-Mn globule mud	clay mins., Qtz., felds., Fe-Mn globs., siliceous microfossils, glass, fish debris, opaques, trace calcite
1-3	Glass and Fe-Mn globule rich mud	clay mins., Qtz., felds., Fe-Mn globules and aggregates, glass, opaques, fish debris
CORE 27	Detrital-Volcanic-Fe-Mn-Bioogenic	
1-1	Fe-Mn globule and micronodule bearing glass and siliceous microfossil rich mud	clay mins., Qtz., felds., siliceous microfossils, glass, Fe-Mn globs. and micronodules, fish debris, trace calcite, opaques

(continued) Table 3. Smear Slides Bulk Sample From DOMES Area C

Sample	Sediment Classification	Primary Constituents
1-8	Fe-Mn globule bearing glass rich mud	clay mins., qtz., felds., glass, Fe-Mn globules and micronodules, chert, altered volc. rx. frags., siliceous microfossils, opaques
1-9	Fe-Mn globule and glass bearing mud	clay mins., qtz., felds., glass, Fe-Mn globs. and micronodules, opaques, chert, fish debris, trace calcite
1-10	Fe-Mn globule bearing glass rich mud	clay mins., qtz., felds., glass, Fe-Mn globs. and micronodules, altered volc. rx. frags., opaques, chert, chlorite
1-12	Glass bearing Fe-Mn globule rich mud	clay mins., qtz., felds., Fe-Mn globs. and micronodules, glass, altered volc. rx. frags., opaques, chert, tr. calcite, zeolite?

PRELIMINARY GEOTECHNICAL PROPERTIES
NORTHEAST CENTRAL PACIFIC NODULE MINING AREA*

A. F. Richards, T. J. Hirst, and J. M. Parks
Marine Geotechnical Laboratory
Lehigh University, Building 17
Bethlehem, Pennsylvania 18015

Abstract

Thirteen short cores raised from water depths of 4.2 to 4.5 km in the Deepsea Ventures, Inc., mining claim area during Phase 1 of the NOAA Deep Ocean Mining Environmental Study (DOMES) were geotechnically analyzed at Lehigh University in 1975-76. The sediments are predominantly fine-grained, cohesive siliceous pelagic clays having average specific gravities of about 2.3. Selected geotechnical properties, measured and averaged over the 188 to 438 mm length of the cores, are: bulk density, 1.32 Mg/m³; water content, 178% dry weight; liquid limit, 137%; plastic limit, 82%; vane shear strength, 5 kPa; and sensitivity, 3.6. Reported shear strength and sensitivity values may be slightly lower because of sample disturbance. The data reported in this investigation are similar in magnitude to data for pelagic clay and siliceous ooze previously reported in the literature.

1. Introduction

A number of box cores were collected from the National Oceanographic and Atmospheric Administration (NOAA) vessel Oceanographer within the Deepsea Ventures, Inc., pelagic nodule mining claim area in April and May 1975. This paper is a preliminary report on the geotechnical properties of cylindrical cores subsampled from 13 of the box cores raised from water depths of 4.2 to 4.5 km within the area bounded by 14 to 16° north latitude and 126 to 127° west longitude.[#] This area is in the western part of Deepsea's claim. One core was analyzed at Lehigh University in November 1975 and the other 12 in January 1976. All cores were kept under refrigeration between the time they were collected and analyzed. The cores ranged in length from 188 to 438 mm.

This geotechnical investigation is a portion of a general geological study performed by the U. S. Geological Survey in Menlo Park, California, under contract to NOAA. It is a part of the Deep Ocean Mining Environmental Study (DOMES), Phase 1, at Site C. We decided to publish the preliminary data presented in this paper before it was fully analyzed and interpreted (1) because of the close time proximity of several mining companies starting to mine experimentally northeast central

* This report, without appendices, was submitted to the MTS for publication in the proceedings of OCEAN 76.

Core locations are given in Appendix I.

° Geotechnical data for each core are listed in Appendix II.

Pacific nodules for their copper, nickel, cobalt, and possibly manganese content, and (2) to place in the public domain these baseline data that will help to characterize the deposits of DOMES Site C; for example, the trafficability of the epifauna and the ability of the infauna to burrow is controlled by the sedimentary geotechnical properties, which have been previously discussed (6, 7).

2. Test Methods

The grain-size analyses, specific gravity, water content, and Atterberg limit tests were performed according to American Society for Testing and Materials standards, modified where necessary (5).^{*} Bulk density was determined by a weight/volume method (4). Shear strength was measured within the core barrel using a motorized laboratory vane, 13 x 25 mm in size, rotated at 23 m·rad/s (79°/min). [Remolding was accomplished by manually rotating the laboratory vane back and forth in the sediment prior to making the remolded strength measurement.]

The averaged data, presented in the next section, are based on 21 measurements of grain size, 11 of specific gravity, 33 of bulk density, 121 of water content, 13 of Atterberg limits, and 38 of shear strength.

3. Results

Average, minimum, and maximum geotechnical values have been tabulated for all data measured or calculated from two arbitrarily-selected depth intervals below the top of the core, which should closely correspond to the seafloor surface, in Table 1. The top 125 mm approximately represents the depth interval of maximum interest to nodule miners because it is in this interval that the nodules are founded. In both intervals, the measured shear strength exhibited considerable scatter with depth, probably as a result of variable disturbance caused by the manner in which the box cores were understood to be removed from the coring box to a storage box. Such disturbance will normally cause a reduction in strength. The cylindrical cores tested were, for the most part, collected from the storage boxes.

The cores may be characterized as siliceous brown clay. Their low average specific gravity indicates that silica fragments may be common in the pelagic clay matrix. Fragments of diatoms and radiolaria have specific gravities as low as 2.3, according to Hamilton (1) and Keller and Bennett (3). Calcium carbonate content has not yet been determined on the cores. The average salinity of the pore water throughout the cores was 33‰.

^{*} Pore water was expressed from the sediment under low pressure using a Manheim-type press. Salinity was measured using a hand-held refractometer.

Averaged data below 125 mm are perturbed for measures of water content and shear strength because one core, 18B, was mineralized below 200 mm. In this unusual core, the maximum measured values are as follows: bulk density, 1.14 Mg/m³; water content, 476 percent dry weight; liquid limit, 275%; plastic limit, 134%; and shear strength, 10 kPa.

The data from both intervals have been averaged together and compared in Table 2 to a previously published range of geotechnical properties from the northeast central Pacific. The agreement between the data reported in this paper and the general range of value for pelagic clay and siliceous ooze is good. It is to be recalled that the shear strength and the sensitivity reported in this investigation is considered to be somewhat lower because of sample disturbance.

4. Conclusions

The siliceous pelagic clay studied in this investigation is fine-grained and cohesive. Water contents are substantially greater than the liquid limit at all depths, as evidenced by a liquidity index of 1.8 for the averaged data shown in Table 2. The 5 kPa average shear strength and a sensitivity of 3.6 are believed to be different to in situ values because of known shipboard sample disturbance. Nevertheless, the averaged data show generally good agreement with published values for pelagic clay and siliceous ooze.

5. Acknowledgements

This investigation was supported by the U.S. Geological Survey Grant 14-08-001-G-257. We thank James Bischoff, Geological Survey Project Coordinator, for his assistance. Barry Erickson's, NOAA Pacific Marine and Environmental Laboratory, help in core preparation and shipment is gratefully acknowledged. Core analyses in the Marine Geotechnical Laboratory were made under the supervision of Steven Helfrich. Doreen Volk assisted in the data reduction.

References

1. Hamilton, E. L., "Sound velocity and related properties of marine sediments, North Pacific," Jour. Geophy. Res., Vol. 75, 1970, pp. 4423-4446.
2. Hirst, T. J. and A. F. Richards, "Analysis of deep-sea nodule mining-seafloor interaction," Offshore Tech. Conf., Vol. 1, 1975, pp. 923-932.

3. Keller, G. H. and R. H. Bennett, "Sediment mass physical properties-- Panama Basin and northeastern equatorial Atlantic," in van Andel, T. H. and G. R. Heath et al., Initial reports of the deep sea drilling project, vol. 16, Washington, U. S. Government Printing Office, 1975, pp. 499-512.
4. Richards, A. F., "Geotechnical properties of submarine soils, Oslofjorden and vicinity, Norway," Norwegian Geotech. Inst. Tech. Rept. 13, 1973, 107 pp.
5. Richards, A. F., "Standardization of marine geotechnics symbols, definitions, units, and test procedures," in Inderbitzen, A. L. (editor) Deep-sea sediments, physical and mechanical properties, New York, Plenum Press, 1974, pp. 271-292.
6. Richards, A. F. and J. M. Parks, "Marine geotechnology: average sediment properties, selected literatures and review of consolidation, stability, and bioturbation-geotechnical interactions in the benthic boundary layer," in McCave, I. N. (editor) The benthic boundary layer, New York, Plenum Press, 1976, pp. 157-181.
7. Rowe, G. T., "The effects of the benthic fauna on the physical properties of deep-sea sediments," in Inderbitzen, A. L. (editor) Deep-sea sediments physical and mechanical properties, New York, Plenum Press, 1974, pp. 381-400.

Table 1. Geotechnical Properties

Property	0 to 125 mm Depth			125 to 438 mm Depth		
	Average	Minimum	Maximum	Average	Minimum	Maximum
<4 μm , %	65	25	87	60	20	88
>64 μm , %	1.6	0	8	0.8	0	5
Median Diam., ϕ	8.4	9.7	7.8	8.1	7.7	8.8
Specific Gravity	-	-	-	2.31	2.06	2.64
Bulk Density, Mg/m^3	1.32	1.26	1.36	1.32	1.14	1.38
Water Content, % dry wt.	185	135	234	172	122	476
Liquid Limit, %	131	104	195	143	107	275
Plastic Limit, %	76	58	111	89	53	183
Plasticity Index, %*	55	46	84	54	49	92
Liquidity Index *	2.0	-	-	1.5	-	-
Vane Shear Strength, kPa	3.1	1.0	6.2	5.9	2.7	21.6
Remolded Vane Strength, kPa	0.9	0.4	1.9	1.6	0.2	7.3
Sensitivity *	3.4	2.5	3.3	3.7	13.5	3.0

* Calculated from the listed data and may not be representative of individual data sets.

Table 2. Generalized Range of Cohesive Sediment Geotechnical Properties *

Sediment Type	Water Content, % dry weight	Liquid Limit, %	Plastic Limit,%	Plasticity Index	Bulk Density Mg/m ³	Shear Strength kPa	Sensitivity
Pelagic Clay	50-200	70-150	35-70	35-80	1.2-1.7	2-7	5-6
Calcareous Ooze	50-200	probably lower than above			1.2-1.6	5-10	6-11
Siliceous Coze	50-200	unknown			1.2-1.7	10-19	5-10(?)
Siliceous Pelagic Clay ^o	178	137	82	55	1.32	5	3.6

* From Hirst and Richards (2), primarily for the surface 1 to 2 m.

^o This investigation; all data from 13 cores averaged, for the surface 0.4 m.

Appendix I. Locations of DOMES Cores.

Core No.	N. Lat.	W. Long.	Water Depth, m corrected	Date Collected	Date Analyzed
3-5	15° 16.0'	126° 38.5'	4675 (?)	April 26, 1975	Jan. 7, 1976
5-10	15° 14.8'	125° 32.1'	4493 (?)	April 27, 1975	Jan. 6, 1976
6-18	14° 15.0'	126° 11.6'	4430 (?)	April 29, 1975	Jan. 5, 1976
9-21	15° 16.3'	126° 10.0'	4630 (?)	April 30, 1975	Jan. 8, 1976
11-53a	16° 0.7'	126° 46.3'	4603	May 29, 1975	Jan. 15, 1976
11-53b	16° 0.7'	126° 46.3'	4603	May 29, 1975	Jan. 8, 1976
18A-36a	15° 15.7'	126° 0.0'	4339	May 21, 1975	Jan. 14, 1976
18A-36b	15° 15.7'	126° 0.0'	4339	May 21, 1975	Jan. 9, 1976
18B-37	15° 12.2'	125° 58.6'	4406	May 22, 1975	Nov. 28, 1975
20-27a	15° 59.3'	126° 11.6'	4672	May 16, 1975	Jan. 15, 1976
20-27b	15° 59.3'	126° 11.6'	4672	May 16, 1975	Jan. 14, 1976
24B-29a	14° 15.4'	126° 1.4'	4468	May 19, 1975	Jan. 15, 1976
24B-29b	14° 15.4'	126° 1.4'	4468	May 19, 1975	Jan. 9, 1976

Appendix II. Geotechnical Data

Core 3-5

15° 15.9' N 126° 38.4' W 4675 m Collected 4/26/75 Tested 1/7/76

Depth, mm	%<2µm	%>60µm	Median diam., φ	Specific gravity	Bulk density, Mg/m ³	Water content, % dry wt.	Liquid limit, %	Plastic limit, %	Plasticity index, %	Shear strength, "undist.," kPa	Shear strength, remolded, kPa	Sensitivity	Salinity, ‰
10													
33													
50	14	3	8		1.32		136	85	51				34
58										2.90	0.70	4.1	
73													
125													
150				2.28									
163													
188										4.06	0.23	17.6	
225					1.34								
263													
268	11	0	8				123	78	45				24
288										2.67	0.58	4.6	
318					1.33								

Core 5-10

15° 15.9' N 126° 38.4' W 4675 m 4/26/75 1/7/76

17													
47													
50	13	5	7.7				155	89	66				
73										1.97	0.35	5.6	
80													
125					1.33								
150				2.06									
163													
173	25	2	8.1				130	111	19				36
188										13.46	2.09	6.4	

DOMES PROJECT-USGS

Core 6-18

14° 15' N 126° 11.5' W 4430 m 4/29/75 1/5/76

Depth, mm	%<2µm φ	%>60µm φ	Median diam., φ	Specific gravity	Bulk density, Mg/m ³	Water content, % dry wt.	Liquid limit, %	Plastic limit, %	Plasti- city index,%	Shear strength, "undist.," kPa	Shear strength, remolded, kPa	Sensitivity	Salinity, ‰
13						192							
38						193				1.74	1.74	1.0	
50	28	0	8.5				136	100	36				
75					1.30	179							
125						186							
138										5.34	1.51	3.5	
150				2.64									37
175					1.29	182							
225						185							
238													
260	10	4	8				141	84	57	6.73	2.09	3.2	
275					1.28	198							35
310						185							

Core 9-21

15° 16.4' N 126° 9.6' W 4630 m 4/30/75 1/8/76

10						201							
35						213							
50	45	0	8.5				110	76	34				33
58										1.51	0.35	4.3	
75					1.31	188							
125						181							
150				2.37									
163						171							
188						171				2.90	0.35	8.3	
225					1.33	160							
260	17	0	8.2				129	71	58				32
263						155							
288						157				2.67	0.35	7.6	
310						152							

DOMES PROJECT-USGS

Core 11-53a

16° 0.7' N 126° 46.3' W 4603m 5/29/75 1/15/76

Depth, mm	%<2µm φ	%>60µm	Median diam., φ	Specific gravity	Bulk density, Mg/m ³	Water content, % dry wt.	Liquid limit, %	Plastic limit, %	Plasti- city index,%	Shear strength, "undist.," kPa	Shear strength, remolded, kPa	Sensitivity	Salinity, ‰
23						180							
58						170							
75	15	0	8.4				125	65	60				32
83										4.81	1.16	4.1	
85						161							
125					1.36	145							
163						134							
188						138				5.34	1.51	3.5	
225				2.32	1.37	135							
263						137							
283						138				4.41	1.74	2.5	
325					1.38	139							
363						145							
375	10	0	7.8				121	63	58				33
388						143				4.52	3.60	1.3	
413						129							
425					1.37								
438						138							

Core 11-53b

16° 07' N 126° 46.3' W 4603 m 5/29/75 1/8/76

20						187							
50	20	0	8.4				104	58	46				34
53						178				1.39	0.35	4.0	
83						170							
125					1.35	152							
163				2.20		139							
188						135				3.36	0.70	4.8	
225					1.38	133							
263						134							
268	18	0	8.0				113	58	55				32
288						133				2.67	1.16	2.3	
318					1.37	136							

DOMES PROJECT-USGS

Core 18A-36a

15° 15.1' N 126° 0.0' W 4339 m 5/21/75 1/14/76

Depth, mm	%<2µm	%>60µm	Median diam., φ	Specific gravity	Bulk density, Mg/m ³	Water content, % dry wt.	Liquid limit, %	Plastic limit, %	Plasticity index, %	Shear strength, "undist.," kPa	Shear strength, remolded, kPa	Sensitivity	Salinity, ‰
25						215							
50	15	0	8.1	2.45			126	83	43				32
63						197							
88						205				4.87	1.16	4.2	
125					1.26	222							
163						190							
173							178	114	64				
188	7	0	8.0			184				21.58	7.31	3.0	33
223						192							
225					1.28								

Core 18A-36b

15° 15.1' N 126° 0.0' W 4339 m 5/21/75 1/9/76

13						207							
38						209							
50	1	8	8.0				195	68	127	1.04	0.70	1.5	35
75						211							
113						234							
138						205				6.15	1.97	3.1	
170				2.38			170	139	31				
175						183							35
220					1.29	202							

DOMES PROJECT-USGS

Core 18B-37

15° 12.2' N 125° 59.3' W 4406 m 5/22/75 11/28/75

Depth, mm	%<2µm φ	%>60µm	Median diam., φ	Specific gravity	Bulk density, Mg/m ³	Water content, % dry wt.	Liquid limit, %	Plastic limit %	Plasti- city index,%	Shear strength, "undist.," kPa	Shear strength, remolded, kPa	Sensitivity	Salinity, ‰
20						209							
38						193							
50	20	0	7.9	2.29									
58						192				3.66	1.10	3.3	
75							114	95	19				
85						202							
125					1.32	161							
185	12	0	7.7										
188										5.52	1.37	4.0	
190						188							
225					1.25	213							
288						345				6.44	1.34	4.8	
325					1.14	392							
388													
390	12	0	8.0			476	275	134		10.04	1.97	5.1	
420						415							

Core 20-27a

15° 58.4' N 126° 11.6' W 4672 m 5/16/75 1/15/76

13						175							
38						168							
50							122	62	60				34
63						157				3.94	0.87	4.5	
75	25	0	8.5										
88						151							
125					1.36	135							
163				2.46									
188										5.45	1.74	3.1	
233						135							
240					1.38								
325					1.38	134							
353	8	0	8.2				107	69	38				34
363						127							
388										4.99	1.28	3.9	
390						126							

DOMES PROJECT-USGS

Core 20-27b

15° 58.4' N 126° 11.6' W 4672 m 5/16/75 1/14/76

Depth, mm	%<2µm	%>60µm	Median diam., φ	Specific gravity	Bulk density, Mg/m ³	Water content, % dry wt.	Liquid limit, %	Plastic limit %	Plasti- city index,%	Shear strength, "undist.," kPa	Shear strength, remolded, kPa	Sensitivity	Salinity, ‰
13						182							
38						176							
50							117	70	47				32
63										4.18	1.10	3.8	
75						152							
125					1.36	147							
150	4	0	8.1	2.24									
163						137							
188						140				5.10	1.74	2.9	
225					1.38	132							
258							107	67	40				33
263						129							
288						123							
308						122							

Core 24B-29a

14° 15.4' N 126° 01.4' W 4468 m 5/19/75 1/15/76

13						201							
38						178				6.15	1.86	3.3	
50							139	71	68				34
75					1.30	182							
138						191				5.22	1.62	3.2	
150	17	0	8.3	2.15									
175					1.29	189							
213						178							
238						177				7.89	1.51	5.2	
268							143	58	85				34
270					1.30								
275						178							
318						180				5.57	0.70	8.0	

DOMES PROJECT-USGS

Core 24B-29b

14° 15.4' N 126° 01.4' W 4468 m 5/19/75 1/9/76

Depth, mm	%<2µm φ	%>60µm	Median diam., φ	Specific gravity	Bulk density, Mg/m ³	Water content, % dry wt.	Liquid limit, %	Plastic limit, %	Plasti- city index,%	Shear strength, "undist.," kPa	Shear strength, remolded, kPa	Sensitivity	Salinity, ‰
13						201							
38						189				2.55	0.93	2.7	
50							131	63	68				34
75					1.29	187							
113						187							
138						192				3.02	1.04	2.9	
150	18	0	8.8	2.29									
175					1.30	183							
213						184							
230							121	63	58				34
238						178				3.02	0.70	4.3	
255						178							

ANALYSIS OF STRENGTH CHARACTERISTICS OF DEEP SEA SEDIMENTS FROM POTENTIAL
MANGANESE NODULE MINING AREAS IN THE NORTH CENTRAL PACIFIC

Frank Simpson

Lockheed Ocean Laboratory

San Diego, Calif.

ABSTRACT

A very extensive vane shear testing program of sediments from potential manganese nodule mining areas was conducted in 1975 during Leg III of NOAA's DOMES program. This effort was performed in conjunction with planned USGS studies. Replicate vane shear tests were made on 51 large box cores recovered from the three DOMES study sites A, B, and C. The statistically designed coring program (nested type), combined with efforts to sample major topographical features provided an ideal opportunity to more accurately assess the strength characteristics of nodule area sediments, including the macro- and micro- variability of this parameter.

Test results demonstrated that the original vane shear strengths for the majority of cores tested from all three sites agree very closely. Average original strength profiles for each site increase from approximately 0.5 to 1.0 psi in the first 3-6 inches of sediment depth, thereafter values remain nearly constant or increase to about 1.4 psi in the rest of the depths examined. Average sensitivity values (ratios of original to remolded strength) however, were higher for Site C than Sites A and B.

Analysis of the vane shear strength lateral variability showed that the largest percent of the variability is contributed by differences between cores from the same station, and the next largest percent by differences between tests conducted in the same core. At all test depths, strength differences between different stations and different sites were found to be less significant. These results clearly indicate the need for more detailed sediment sampling within relatively small seafloor areas.

INTRODUCTION

This report summarizes the results of shipboard vane shear measurements performed by the author on 51 box cores collected during the October-November 1975 Deep Ocean Mining Environmental Study (DOMES) cruise. During this cruise NOAA's R/V OCEANOGRAPHER was used to collect biological, geological, chemical, and physical baseline data at three DOMES study sites representative of potential manganese nodule mining areas in the North Pacific. The research discussed herein was conducted in

conjunction with a series of studies planned by the US Geological Survey's Pacific Arctic Branch. As part of this effort a number of subcores were also obtained from the box cores recovered for more extensive geotechnical analysis by Lockheed Ocean Laboratory and Lehigh University. Results of laboratory tests will be available in the near future upon completion of data analysis. The study reported herein was performed as part of Lockheed's Independent Research Program on deep sea sediments.

BACKGROUND

Growing interest in the development of deep seabed nodule resources has focused attention on the need for reliable geotechnical sediment data for proper analysis of mining equipment-seafloor interactions. Presently, geotechnical information available for sediment in the major nodule areas of the North Central Pacific Ocean is very limited. Furthermore, effective use of what data are available is often prohibited due to lack of information provided regarding a) locations of core samples analyzed, b) specific sediment depths examined, c) classification of sediments tested, d) physical conditions of cores examined and e) testing equipment and procedures used for obtaining measurements.

One of the geotechnical parameters most important for assessing the performance of mining equipment interacting with the seafloor is the vane shear strength of the sediment. Obtaining reliable sediment vane shear strength information from cores analyzed in shore laboratories is very difficult since significant physical and chemical changes can occur in these cores due to their handling, shipping, and storage. For these reasons, measurement of this parameter at sea is essential whenever the accuracy of the data is of great importance.

Only a very small amount of shipboard vane shear information for nodule area sediments has been published. Studies which have reported some of these results include: Craig 1975, Kögler 1974, Hagerty 1974, Hartman et al. 1973, Keller and Bennett 1973, and Koecker 1974. Recently an extensive quantity of shipboard vane shear measurements were obtained on the April 1975 DOMES cruise (personal communication DOMES Program Office). Also during the April 1975 R/V TOMMY THOMPSON cruise hand-held vane

shear strength measurements were made on a small number of calcareous sediment box cores collected by USC (results to be published by Lockheed).

STUDY OBJECTIVES

The principal objectives of Lockheed's at-sea geotechnical investigations are to:

- (1) Assess the vane shear strength characteristics of nodule area sediments;
- (2) Assess the areal and vertical variability of the vane shear strength property.

Results of the above will be discussed in this report. In addition, other efforts presently in progress are to:

- (3) Investigate potential relationships between the vane shear strength property and the local and regional topography of nodule areas;
- (4) Assess possible degradation in subcores for geotechnical analysis due to subcoring, handling, and storage through comparisons of shipboard and laboratory vane shear measurements will be available in future reports.

Ultimate benefits from the above investigations include (1) better definition of the strength characteristics of deep ocean sediments and their relationship to depositional and erosional processes, and also to biological and chemical processes, (2) better use and interpretation of existing sediment and bathymetric information for nodule areas, (3) design of more efficient and statistically representative sediment survey programs in the nodule areas, and (4) availability of sediment strength data necessary for preliminary assessment of anticipated sediment response under a variety of dynamic and static loading conditions.

METHODS

Description of At-Sea Sampling Programs

Locations of the DOMES study sites occupied during this cruise are given in Figure 1. Within Sites A and B five stations were randomly selected for box coring. Within Site C, two of the five stations previously sampled on the April 1975 DOMES cruise were reoccupied for additional box coring purposes. In general, at each of the stations occupied four or more large box cores (20 x 20 x 24 in) were collected. Figure 1 illustrates the relative location of the stations within each site and the number of box cores collected at each station, maximum distance between cores within a station varied from approximately 2-8 nm. Coring efforts at Site A and B stations were directed at sampling sediments from various topographic features such as abyssal hills, slopes, and basins. An example of the coring locations and bathymetry at a typical station is shown in Figure 2.

The nested type of sediment sampling program undertaken on this cruise, using multiple box cores per station and multiple stations per site, is ideally suited for providing answers to the study objectives. Until the recent DOMES cruises insufficient deep sea sediment data were available for comprehensive statistical analysis.

Vane Shear Test Equipment and Procedures

A hand-held vane shear device, fabricated at Lockheed, was utilized to measure the sediment strength. The device consists of a snap-on torque wrench (0-192 in-oz torque range attached to a 28 in long stainless steel, sleeved shaft with a vane blade. One of two sizes of vanes was used for testing, depending on the stiffness of the sediment. Softer sediment cores were usually tested with either a 1 in or 1-1/2 in (height and diameter) vane, while stiffer sediment cores were always tested with the 1 in vane, so as not to exceed the range of the torque meter. A vane rotation of approximately 3 rpm was found optimum to use in order to minimize ship's motion effects during testing.

Testing of each box core consisted of making three separate vane shaft insertions and, on each insertion, measuring the original and remolded vane shear strength at successive 3 in depth intervals through the length of the core.

Vane shear measurements were conducted on 51 of the 61 box cores recovered. Table 1 lists the coordinates and water depths of the box cores tested. Box cores excluded from testing were either saved for analysis by other DOMES principal investigators or found unsuitable for testing due to insufficient material recovered or badly disturbed sediment.

Data Reduction and Statistical Analysis

Analysis of vane shear results included; 1) computing mean and standard deviation values for replicate measurements made on each individual box core at each of the test depths, 2) computing mean standard deviation values at each test depth for all box cores tested from each site and 3) statistically examining the areal variability of the sediment strengths at each test depth through the use of nested analysis of variance methods (Krumbein and Graybill, 1965). This statistical technique has been found to be particularly useful for partitioning the total sediment strength variability measured into the following sampling levels: between sites, between stations within each site, between cores within a station, and between replicate measurements within individual cores (Simpson 1974). Due to the limited number of box cores tested from Site C, the nested analysis of variance method was applied only to Site A and B data.

RESULTS

Physical Characteristics of Sediments Sampled

Table 2 presents some background information regarding the physical characteristics of the sediment samples tested. In general, box cores from Sites A and B are representative of siliceous type sediments and Site C box cores are representative of red or brown clay sediments. Water content and bulk density values presented in this table are based on preliminary results of tests conducted by Lockheed on a number of subcores taken from the box cores collected on this cruise. Initial results show that mean water content values for Site C cores are distinctly lower than those measured for Site A and B cores.

Strength Characteristics of Sediments Sampled

Table 3 presents the results of replicate vane shear strength tests performed on box cores from Station 47 (Site A). The bathymetry of the seafloor area sampled and the relative locations of the box cores tested was presented in Figure 2. With the exception of two unusually high strength cores recovered at this station, results in Table 3 illustrate some of the more significant sediment strength trends present within individual box cores and stations from the DOMES sites.

Table 4 presents the average sediment strength (original and remolded) profiles and standard deviations for all vane shear measurements made within each of the three DOMES study sites. Analysis of the areal variability for both original and remolded vane shear strength values for Sites A and B are given in Tables 5 and 6. For purposes of brevity only the components of variance in percent have been selected from the nested analysis of variance results to be included in Table 6. These results indicate the relative amount of variability present at each level of sampling and testing and identify at which stage of the sampling and testing program the greatest uncertainty exists.

DISCUSSION

Analysis of the strength data combined with visual inspection of the sediment in the box cores tested indicates the following:

1. Replicate vane shear measurements (original and remolded) were found to be very consistent, particularly in the 6-12 in test depth interval. Larger differences noted in tests performed near the surface and the base of the cores, though still relatively minor when compared to the mean shear strengths at each depth, were anticipated since in these sections of the box core the sediment is most susceptible to disturbance during core recovery and removal of the box from the coring unit. Test results near the sediment surface can also be expected to show larger differences since the

sediment strength changes most significantly in the 0-6 in depth interval. Also measurement errors are more likely to be introduced during the test at the 3 in depth by minor tilting of the vane shaft.

Results in Table 3, for example, show that excluding cores 12 and 13, standard deviations for the majority of replicate tests are below 0.2 psi for the original strength and below 0.1 psi for the remolded strength. Very similar results were noted in almost all cores tested from the three sites. In general, the average standard deviations for replicate tests (not presented in this report) are below 0.15 psi and 0.05 psi for all test depths for the original and remolded strengths, respectively. Comparing these values with the average shear strengths for each test depth (Table 4) shows that the variability of replicate tests is relatively minor. Analysis of variance results presented in Table 5 also confirmed this trend by showing that in all cores from Sites A and B; the percent variability contributed by differences between replicate tests results is less than that contributed by differences between cores from the same station. The importance of establishing the variability between replicate strength measurements is that it provides a good estimate of the inherent or natural variability of the strength parameter and the precision of the test method used. Results from the hand-held vane tests thus suggest that a) the sediment is quite uniform in a lateral direction within an individual box core, b) with the exception of the disturbed sediment layer near the surface and base of the cores, the quality of the sediment samples recovered by this method appears to be very good, and c) the hand-held vane shear testing method can provide repeatable results.

2. Original vane shear strength values for individual box cores show the largest increases in strength occur within the first 6 in sediment depth interval, thereafter values remain nearly constant or increase only by a small percent. Excluding results for the few box cores which showed very high strengths (6 cores out of 51 tested), strength values ranged from approximately 0.20 psi at a 3 in depth to 2.0 psi at a 12 in depth. However, average strength profiles computed for all vane measurements at each Site (Table 4), more precisely demonstrate that the original strengths increase from about 0.5 psi to 1.1 psi within the 3-6 in depth interval and thereafter remain nearly constant (Site C cores) or increase up to approximately 1.4 psi (Sites A and B cores) within the rest of the test depths.

One trend observed in almost all strength profiles for individual box cores was a noticeable strength decrease at the last sediment depth tested (usually 15 or 18 in). This decrease is directly attributed to the sediment disturbance discussed in item 1.

3. In regard to the high sediment strength cores recovered, results for Station 47 clearly demonstrate that significant strength differ-

ences can occur between cores less than 2-4 miles apart. However, less than 12% of all cores tested exhibited such high strength values. Also these cores were restricted to only 4 out of the 10 stations occupied at Sites A and B. Thus it appears that occurrence of high strength seafloor areas in these sites is more the exception than the rule. Vane shear strength for these cores in the 3-12 in test depth interval ranged from approximately 2.0 - 3.8 psi and from about 0.4 - 1.0 psi for the original and remolded strengths respectively.

It is interesting to note that the physical appearance of these cores was quite different from most of the other cores recovered. The sediment in these cores was not only very stiff but also had a very dark brown or greyish brown color and was highly mottled as opposed to the lighter chocolate brown color observed in most of the other cores. These box cores also had only a very thin layer (0.5 in or less) or no layer at all of the very soft sediment generally present at the surface of most box cores.

4. Analysis of remolded vane shear strength values showed that, at all test depths, they are significantly lower than the original strengths measured. Excluding the high strength cores discussed above, remolded strength values for most cores ranged from 0.10 - 0.30 psi between the 3-18 in test depth interval. The average remolded strength profiles in Table 4 confirm this trend and also show that the greatest increases in the remolded strength occur within the first 6 in of sediment.

5. Sensitivity values (ratio of original strength to remolded strength) computed for all cores indicated that sediments from Sites A and B have lower sensitivity values than sediments from Site C. For example, at a 3 in depth average sensitivities for Sites A and B are 3.4 and 4.2 respectively and 5.4 and 6.3 at a 15 in depth. Average sensitivity values Site C cores, however, are 6.7 at a 3 in depth and 6.4 at a 15 in depth.

6. Comparison of average vane shear strength values computed for each site (Table 4) demonstrated some interesting trends. First, if all cores tested from each site are considered, both the original and remolded strengths increase as one progresses from Site C (red clay) to Site B to Site A (siliceous type sediments). However if one excludes the high strength cores encountered at Sites A and B, recomputed mean strength values (original) for all three Sites agree remarkably closely in the first 9 inches of depth, thereafter Sites B and A have slightly higher strength values. For example, recomputed average and standard deviation values for Site A and B at 3 in depth are 0.53 ± 0.22 and 0.52 ± 0.13 , respectively, which are very similar to Site C values of 0.56 ± 0.17 . Thus it appears that the vane shear strength differences between sediments from these three sites are very minor. This finding was also confirmed by the nested

analysis of variance (Table 5). Which is discussed in greater detail in Item 7.

Second, examination of the standard deviations for the average strength profiles from Sites A, B, and C showed that in general, the variability of measurements at all test depths decreases as one progress from Sites C to Site A. These results suggest that the sediment at Sites A and B is less uniform or homogeneous than that at Site C.

7. Analysis of the lateral variability for all vane strength measurements from Sites A and B (Tables 5 and 6) demonstrated that the largest percent of the variability measured is contributed by differences between box cores from the same station. The next largest percent is contributed by differences between replicate measurements within individual box cores, and surprisingly enough differences between measurements from different stations or different sites account for the least percent of the variability.

In examining the results in Table 5, readers should note that the components of variance provide relative estimates of the variability encountered at each sampling level and at each test depth. The absolute magnitude of the variance is dependent on the total variance measured at each test depth. Since the total variability measured decreases with test depth (note profiles in Table 4) high percent components of variance for the lower test depths may represent lower absolute variances than those occurring in the first 2 or 3 test depths.

CONCLUSIONS

Results from this study have provided for the first time a more complete and accurate description of the strength characteristics of surficial deep sea sediments in prospective manganese nodule mining areas. The nested type of sediment sampling program undertaken on this cruise also allowed conducting a more comprehensive statistical analysis of the lateral variability of vane shear strengths within the nodule areas. The hand-held vane shear test method was found to be extremely well suited for rapid at-sea strength analysis of box cores and capable of providing reasonably accurate estimates of the sediment strength parameter. However, it is recommended that replicate testing of box cores be continued with a stabilizing device added to minimize variability possibly introduced by the testing technique.

Test results demonstrated that the most significant vane shear strength differences occur within relatively small seafloor areas (10 x 10 nm or less). This variability is presently believed to be related to the local topographic and/or sediment erosional and depositional changes within individual stations. Shear strength profiles of cores from all three

sites were found to agree very closely, particularly between cores from Sites A and B. Initial results indicate the need for a more concentrated sampling effort within individual stations, using a nested sampling program, in order to improve the reliability of the sediment strength predictions, and better define the relationships between the sediment strength and physical properties and the major topographic features. Also more extensive studies should be conducted to assess the differences between shipboard and laboratory strength results.

McGraw-Hill, 1965.

Roecker, K., Vane Shear Strength Measurements on Leg 27 Sediment, from Initial Report Deep Sea Drilling Project Vol. XXVII, Paul P. Robinson and Hans M. Bolli Eds., U.S. Gov't office, Washington, p. 425-432, 1974.

Simpson, F., Statistical analysis of marine sediment properties from San Diego Trough, ONR Contract No. N00014-73-C-0204, April 1974.

ACKNOWLEDGEMENTS

The author would like to express his appreciation to the DOMES Program Office, in particular Messrs. John Padan and Barrett Erickson, and to Dr. Jim Bischoff from the USGS Pacific Arctic Branch department for their assistance and cooperation in making this study possible. Thanks are also extended to Mr. Davey Banning (University of Washington) for all his help during at-sea testing of the box cores, and to Ms. Pamela Price (Lockheed Ocean Laboratory) for her invaluable assistance in the reduction and analysis of the data and preparation of this report.

REFERENCES

- Craig, James D., The Distribution of Ferromanganese Nodule Deposits in the North Equatorial Pacific, Master Thesis, University of Hawaii, 1975.
- Hagerty, Royal, Usefulness of Spade Cores for Geotechnical Studies and Some Results from the Northeast Pacific from Deep Sea Sediments, Anton Inderbitzen Ed., Plenum Press, New York, 1974.
- Hartman, M., F.-C. Kögler, P. Muller, and E. Suess, Preliminary Results of Geochemical and Soilmechanical Investigations on Pacific Ocean Sediments, from Papers on the Origin and Distribution of Manganese Nodules in the Pacific and Prospects for Exploration, Maury Morgenstein Ed., Honolulu, Hawaii, 1973.
- Keller, G. H. and R. H. Bennett, Sediments mass physical properties--Pansma Basin and northeastern equatorial Pacific from Initial Report Deep Sea Drilling Project Vol. XVI, T. van Andel Ed., U.S. Gov't Printing Office, Washington, p. 499-512, 1973.
- Kögler, F. C., Sediment-physical properties of three deep-sea cores from the Central Pacific Ocean, Meestechnik 5(6): 199-201, 1974.
- Krumbein, W. C. and Franklin A. Graybill, An Introduction to Statistical Models in Geology,

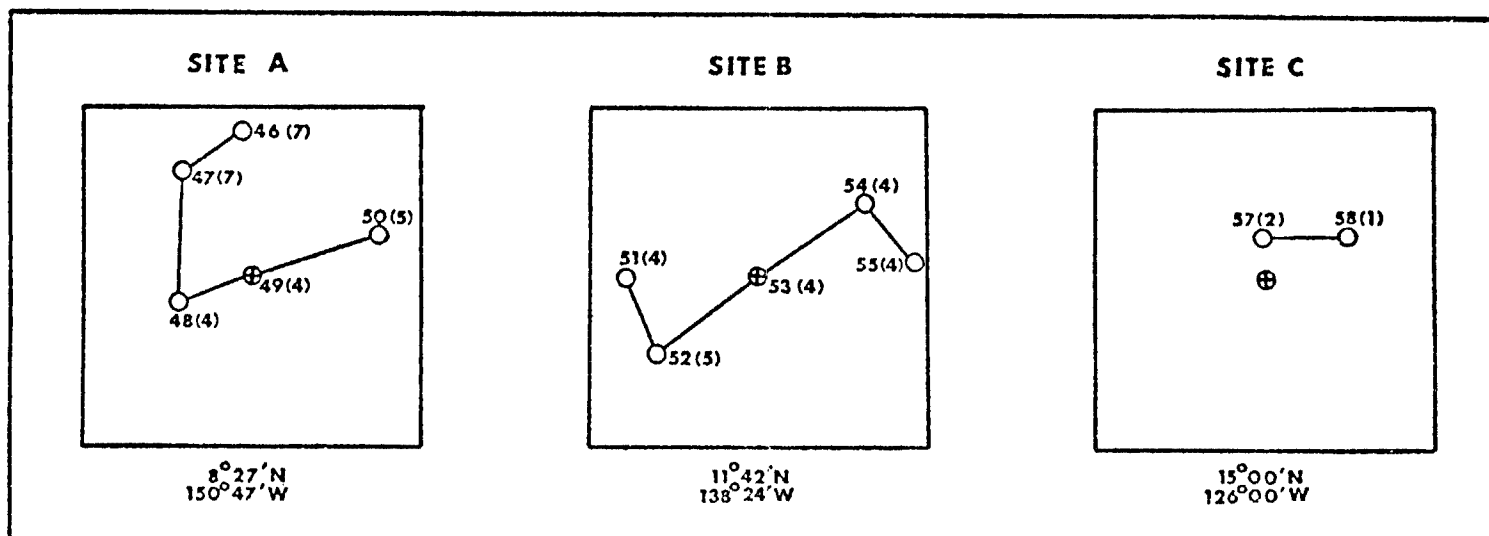


Figure 1. Locations of box core stations occupied during DOMES cruise RP-8-OC-75. DOMES sites are defined as 2° latitude rectangles and are accompanied by coordinates of their center points. Stations numbers 46-58 are followed by the number of box cores tested (in parentheses).

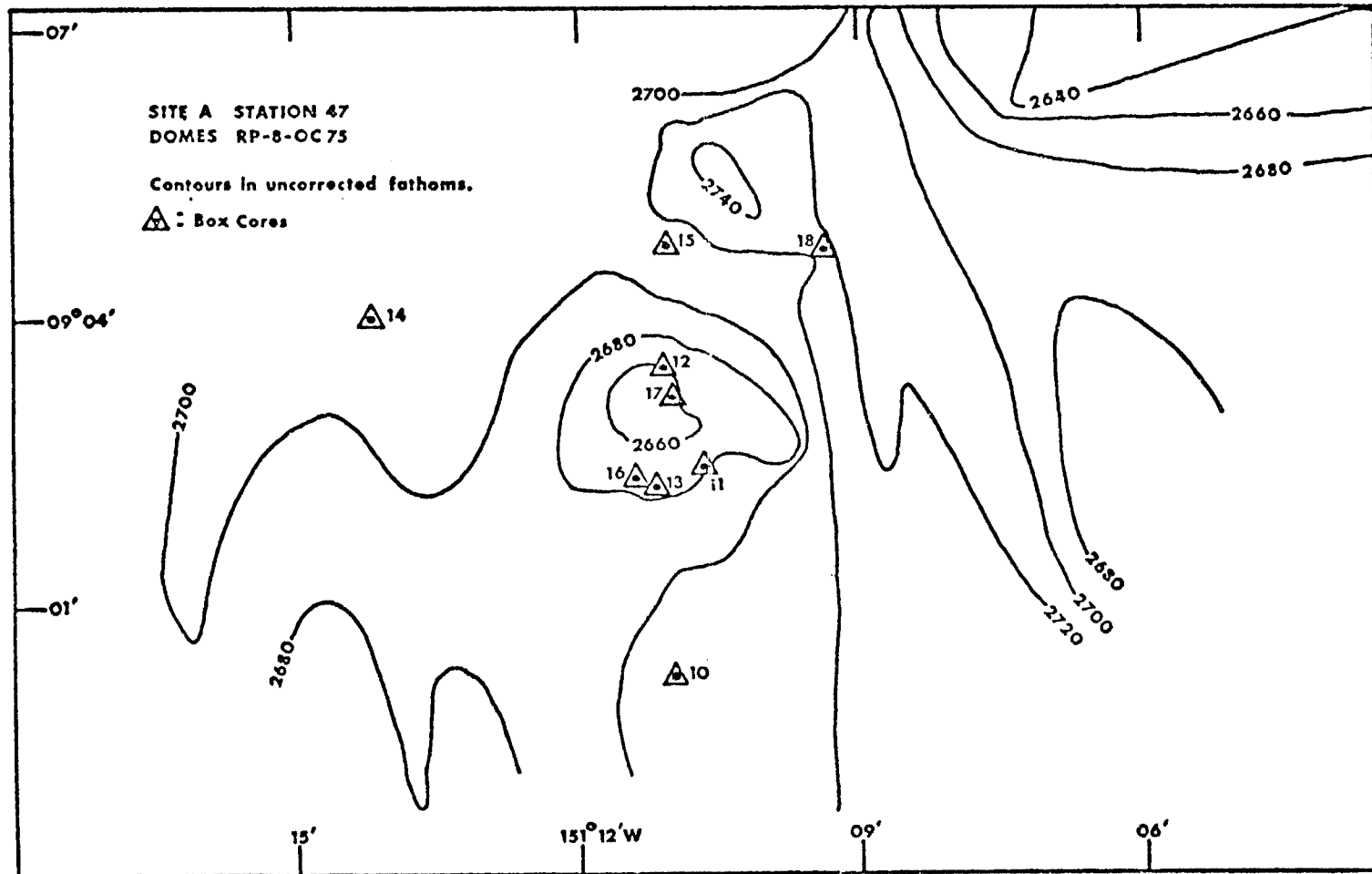


Figure 2. Bathymetry and lateral distance between box cores for a typical station occupied.

Table 1.
LOCATIONS AND WATER DEPTH OF BOX CORES TESTED WITH
HAND-HELD VANE SHEAR DEVICE

Site	Station Number	Box Core Number	Location		Water Depth (fathoms)	
A	46	1	9°20.7'N	150°50.7'W	2739	
	46	2	9°21.3'N	150°49.5'W	2755	
	46	4	9°23.8'N	150°52.8'W	2736	
	46	5	9°21.3'N	150°51.4'W	2708	
	46	6	9°24.0'N	150°49.9'W	2774	
	46	7	9°19.6'N	150°50.7'W	2715	
	46	9	9°20.0'N	150°48.4'W	2570	
	47	10	9°00.3'N	151°10.9'N	2711	
	47	11	9°02.5'N	151°10.6'W	2682	
	47	12	9°03.5'N	151°11.1'W	2658	
	47	13	9°02.3'N	151°11.2'W	2675	
	47	14	9°04.0'N	151°14.2'W	2712	
	47	15	9°04.8'N	151°11.1'W	2715	
	47	18	9°04.8'N	151°09.4'W	2722	
	48	19	8°16.5'N	151°07.3'W	2677	
	48	20	8°14.3'N	151°14.3'W	1989	
	48	22	8°16.0'N	151°11.3'W	2716	
	48	23	8°18.1'N	151°09.5'W	2730	
	49	24	8°27.5'N	150°46.7'W	2669	
	49	25	8°28.5'N	150°44.5'W	2657	
	49	26	8°27.4'N	150°50.2'W	2639	
	49	27	8°30.2'N	150°47.8'W	2675	
	50	28	8°41.7'N	150°18.7'W	1989	
	50	29	8°43.8'N	150°18.7'W	2672	
	50	30	8°41.1'N	150°15.1'W	2617	
	50	31	8°41.4'N	150°15.0'W	2638	
	50	32	8°43.1'N	150°14.1'W	2628	
	B	51	33	11°41.6'N	139°11.0'W	2592
		51	34	11°42.4'N	139°10.8'W	2615
		51	35	11°43.1'N	139°08.9'W	2609
		51	36	11°43.7'N	139°08.2'W	2609
		52	37	11°13.7'N	139°09.9'W	2588
52		38	11°14.9'N	139°05.4'W	2619	
52		40	11°16.3'N	139°04.2'W	2581	
52		41	11°13.5'N	139°07.7'W	2576	
52		42	11°15.5'N	139°03.3'W	2587	
53		43	11°42.2'N	138°23.4'W	2653	
53		44	11°43.3'N	138°22.4'W	2655	
53		45	11°43.9'N	138°22.2'W	2647	
53		46	11°44.3'N	138°21.2'W	2618	
54		47	12°10.4'N	137°44.1'W	2618	
54		48	12°11.0'N	137°41.0'W	2618	
54		51	12°08.9'N	137°44.6'W	2620	
54		52	12°09.6'N	137°42.4'W	2630	
55		53	11°48.6'N	137°28.3'W	1989	
55		54	11°50.8'N	137°26.7'W	2566	
55		55	11°48.2'N	137°26.3'W	2578	
55	56	11°48.6'N	137°24.3'W	1989		
C	57	57	15°17.8'N	125°55.3'W	1989	
	57	59	15°20.4'N	125°54.1'W	2458	
	58	60	15°17.8'N	125°28.4'W	2328	

Table 2.
PRELIMINARY DESCRIPTION OF SELECTED PHYSICAL PROPERTIES OF SEDIMENTS SAMPLED

Site	Bottom Sediment (1)	Mean Water Content % dry wt. (2)	Mean Bulk Density (g/cm ³) (3)
A	Siliceous ooze	320/291	1.25/1.25
B	Mixed, patchy siliceous ooze and red clay	264/252	1.26/1.27
C	Red clay	203/160	1.33/1.38

(1) DOMES Technical Plan - Phase I

(2) Lockheed derived, 3 inch test depth value/15 inch test depth value

(3) Lockheed derived, 6 inch test depth value/12 inch test depth value

Table 3.
 MEAN AND STANDARD DEVIATIONS VALUES FOR REPLICATE VANE SHEAR TESTS CONDUCTED ON STATION 47 (SITE A) BOX CORES

Box Core	Sediment Depth											
	3 in		6 in		9 in		12 in		15 in		18 in	
	Vo	Vr	Vo	Vr	Vo	Vr	Vo	Vr	Vo	Vr	Vo	Vr
10	.32 ± .15	.11 ± .01	.72 ± .00	.20 ± .07	1.08 ± .12	.24 ± .00	1.12 ± .18	.20 ± .07	1.28 ± .14	.17 ± .06	1.12 ± .07	.20 ± .07
11	.35 ± .03	.15 ± .02	.69 ± .05	.20 ± .02	.83 ± .05	.20 ± .02	.88 ± .06	.14 ± .02	.97 ± .05	.22 ± .02	.84 ± .00	.21 ± .00
12	2.04 ± .32	.44 ± .07	3.16 ± .18	.56 ± .14	3.72 ± .43	.60 ± .00	3.24 ± .43	.48 ± .12				
13	2.72 ± .66	.44 ± .14	3.80 ± .39	.64 ± .07	3.80 ± .91	.56 ± .18						
14	.30 ± .07	.14 ± .03	.84 ± .17	.17 ± .06	.95 ± .24	.23 ± .03	.96 ± .00	.18 ± .07	.90 ± .12	.20 ± .06	.72 ± .17	.24 ± .00
15	1.40 ± .07	.36 ± .00	1.46 ± .09	.28 ± .07	1.31 ± .12	.24 ± .00	1.36 ± .14	.24 ± .00	1.12 ± .07	.20 ± .07		
18	.64 ± .18	.20 ± .07	.88 ± .00	.20 ± .07	.84 ± .00	.20 ± .07	1.12 ± .14	.18 ± .06	1.34 ± .12	.20 ± .07	1.26 ± .27	.26 ± .09

Vo = original vane shear strength (psi)
 Vr = remolded vane shear strength (psi)

Table 4.
VANE SHEAR STRENGTH MEANS, STANDARD DEVIATIONS, AND COEFFICIENTS OF VARIATION FOR SITES A, B, AND C

Test Depth (in)		Site A*				Site B*				Site C*			
		\bar{x}	s	cv	n	\bar{x}	s	cv	n	\bar{x}	s	cv	n
3	Vo	.92	.94	1.02	83	.56	.38	.68	63	.56	.17	.30	9
	Vr	.26	.22	.85	83	.14	.08	.57	62	.08	.03	.38	9
6	Vo	1.27	.86	.68	83	1.09	.56	.51	63	.94	.05	.05	9
	Vr	.32	.22	.69	82	.21	.10	.48	63	.18	.05	.28	9
9	Vo	1.24	.81	.65	74	1.20	.53	.44	62	.98	.14	.14	9
	Vr	.26	.12	.46	74	.23	.10	.43	62	.15	.04	.27	9
12	Vo	1.37	.48	.35	72	1.22	.37	.30	59	1.00	.23	.23	9
	Vr	.26	.10	.38	72	.22	.10	.45	59	.14	.06	.36	9
15	Vo	1.37	.34	.25	69	1.30	.25	.19	53	1.10	.27	.25	9
	Vr	.26	.10	.38	69	.21	.05	.24	53	.20	.08	.40	9
18	Vo	1.20	.26	.22	46	1.26	.30	.24	38	1.09	.04	.04	3
	Vr	.27	.10	.37	46	.24	.06	.25	38	.25	.03	.12	3
		Site A**				Site B**							
		\bar{x}	s	cv	n	\bar{x}	s	cv	n				
3	Vo	.53	.22	.42	69	.52	.13	.25	57				
	Vr	.22	.19	.86	69	.25	.06	.24	56				
6	Vo	.92	.25	.27	69	.94	.19	.20	57				
	Vr	.21	.13	.62	68	.19	.05	.26	57				
9	Vo	1.01	.24	.24	68	1.06	.22	.21	57				
	Vr	.23	.06	.28	68	.20	.06	.28	57				
12	Vo	1.28	.28	.22	69	1.17	.27	.23	56				
	Vr	.25	.09	.36	69	.20	.07	.33	56				
15	Vo	1.37	.34	.25	69	1.30	.25	.19	53				
	Vr	.26	.10	.38	69	.21	.05	.24	53				
18	Vo	1.20	.26	.22	46	1.26	.30	.24	38				
	Vr	.27	.10	.37	46	.24	.06	.25	38				

Vo = original vane shear strength (psi)

Vr = remolded vane shear strength (psi)

\bar{x} = sample mean

s = standard deviation

cv = coefficient of variation

n = number of measurements

* = values computed from all core data

** = recomputed values excluding high strength cores. Note, Site C values remain unchanged.

TABLE 5.
ANALYSIS OF THE VARIABILITY IN VANE SHEAR STRENGTH MEASUREMENTS FROM SITES A AND B

Test Depth (in)	Source of Variability (sampling level)	Components of Variance in Percent	
		Vo	Vr
3	between sites	3.1	11.4
	between stations	7.5	19.3
	between cores	72.1	53.8
	between replicates	17.3	15.5
6	between sites	1.1	5.4
	between stations	4.2	33.0
	between cores	89.2	49.3
	between replicates	5.5	12.3
9	between sites	0	0
	between stations	7.1	10.1
	between cores	81.4	71.5
	between replicates	11.5	18.3
12	between sites	8.0	3.9
	between stations	0	0
	between cores	79.2	13.0
	between replicates	12.8	83.1
15	between sites	0.3	0
	between stations	7.1	1.0
	between cores	50.8	5.5
	between replicates	41.8	93.5
18	between sites	0	0
	between stations	24.7	55.6
	between cores	30.3	9.9
	between replicates	45.0	34.5

Vo = original vane shear strength
Vr = remolded vane shear strength

TABLE 6
LATERAL VARIABILITY OF VANE SHEAR STRENGTHS FOR
SEDIMENTS FROM SITES A AND B (ALL TEST DEPTHS)

Approximate Lateral Distance Between Measurements	Average Percent Variability Measured	
	(Original)	(Remolded)
6 - 14 in	22.3	42.9
2 - 8 nm	67.2	33.8
30 - 100 nm	8.4	19.8
700 - 900 nm	2.1	3.5

Micropaleontological Dating of Sediments
of DOMES PROJECT Box Cores, Test Area "C",
Tropical Pacific Ocean.

F. Theyer
Hawaii Institute of Geophysics
University of Hawaii
Honolulu, Hawaii 96822

MATERIALS AND METHODS

The sediment samples used in this study were taken from 10 box cores (Table 1), collected during Cruise RP-6-OC-75 of the DOMES field-program in the northcentral Pacific "C" test-site (between approximately 14-16°N and 125-127°W; see Table 1 for core and station data and page 4 for coordinates and additional station data), and which ranged in length from less than 20 to just over 40 cm. For all practical purposes, the cores can be thought of having collected horizontally undisturbed representations of the first 20 and 40 cm of the ocean floor, without significant distortion to the sediment surface.

The cores were sampled throughout at 2-cm intervals in the hope of obtaining a very detailed representation of the stratigraphy of the test-site's uppermost sediments. Smear-slides were prepared of each sampled interval to have a record of the sediment constituents and to search for diatoms and nanofossils that could help in the dating. Standard micropaleontological techniques of foraminiferal and radiolarian research were used (washing through 62-micron screens, boiling in H₂O₂,

etc.) to prepare the samples for the biostratigraphic work. It was realized immediately that only siliceous fossils, especially radiolarians, would be likely to be found due to the depth and location of the cores. The dried residues revealed that even radiolarians were very poorly represented or totally absent in many samples. Consequently, the ages that were determined (Table 1) are of generalized nature since assignment to the tropical radiolarian zones of the Quaternary (Nigrini, 1971) and the definition of the Quaternary radiolarian datum levels of Johnson and Knoll (1975) was not possible due to the lack of the specific taxa.

Glass micro-slides were prepared from the residues of all the samples and the work is based on these. To define the percentage of older, reworked zonal fossils within the total population, counts were made of all radiolarians contained in a specific area of the micro-slide using settings of the microscope's stage as reference points.

DISCUSSION OF RESULTS

Table 1 gives a summary of the findings. The ages are all based on 2-cm intervals taken throughout each core, even though in Table 1 similar horizons within each core were lumped together. It is immediately apparent that the upper 10 to 20 cm of the cores, and therefore presumably of the test site as a whole, are generally of Quaternary age (Holocene-Pleistocene; 0-1.8 mybp), and that at least in cores 30, 51, and 52 this age

Table 1

Biostratigraphic Ages of DOMES Box Cores from Area "C"
(Cruise RP-6-OC-75)

<i>Depth Interval (cm)</i>	<i>Age</i>	<i>Percentage of Older Zonal Fossils</i>
<u>Box Core 27, Station 20, 4672 m</u>		
0- 6	Quaternary	0%
6- 8	Barren of fossils	
8-12	Quaternary	0%
12-14	Barren of fossils	
14-16	Quaternary	0%
16-18	Barren of fossils	
<u>Box Core 29, Station 24B, 4468 m</u>		
0-16	Quaternary	Traces of Early Quaternary
<u>Box Core 30, Station 23B, 4667 m</u>		
0-18	Late Quaternary	1-20% Early Quaternary; traces of Early Miocene
18-26	Quaternary	0%
26-30	Late Quaternary	10% Early Quaternary
30-44	Quaternary	0%
<u>Box Core 36, Station 18, 4339 m</u>		
0-10	Quaternary	0%
10-16	Barren of fossils	
<u>Box Core 37, Station 18B, 4406 m</u>		
0-10	Quaternary	0%
10-20	Barren of fossils	
<u>Box Core 49 Station 16B, 4552 m</u>		
0-16	Quaternary	0%
16-20	Barren of fossils	
<u>Box Core 50, Station 15B, 4552 m</u>		
0-40	Quaternary, with barren layer at 26-30 cm	0%

Table 1 (cont'd.)

<i>Depth Interval (cm)</i>	<i>Age</i>	<i>Percentage of Older Zonal Fossils</i>
	<u>Box Core 51, Station 25, 45 61 m</u>	
0-14	Late Quaternary	Traces of Early Quaternary
14-27	Barren of fossils	
	<u>Box Core 52, Station 27, 4406 m</u>	
0-16	Late Quaternary	Traces of Early Quaternary
16-20	Barren of fossils	
	<u>Box Core 53, Station 11, 4585 m</u>	
0-14	Quaternary	0%
14-41	Barren of fossils	

can even be restricted to less than about 2×10^5 yr (Late Quaternary), since there Buccinosphaera invaginata Haeckel occurs, a species that may have appeared in the Pacific at this stratigraphic level (Johnson and Knoll, 1975).

A review of the percentage of reworked radiolarians (Table 1) discloses that only box core 30 has a significant amount of Early Quaternary (and a negligible amount of Early Miocene fossils) in what most likely is a Late Quaternary core throughout. Neither these, however, nor the other reworked specimens which are occasionally encountered in these cores are likely to be the result of local erosion and redeposition. The fauna is simply too meager to allow any meaningful analysis and the few available data do not follow a specific trend.

Thus, it is also highly speculative to try to estimate a general sediment-accumulation rate for this area from the lengths and ages of the present cores, although minimum rates can be given. Taking core 20 as an example, and assuming that it contains a continuous Late Quaternary sequence that begins with a Holocene top [assumptions which are not too far-fetched, since the layers between 18-26 cm and 30-44 cm (Table 1) are dated as "Quaternary" rather than more specifically "Late Quaternary" only because of the absence of B. invaginata], a minimum sedimentation-accumulation rate of about $0.1 \text{ cm}/10^3 \text{ yr}$ is derived. This figure is near the lowest range of the normal sediment-accumulation rates that can be expected to occur in this area. It may not necessarily bear any relation to reality,

however, since it is a theoretical minimum and typical rates in the deep central Pacific are generally 3 to 5 times higher (Theyer and Hammond, 1974). It is also possible that core 30 may represent an atypical situation and therefore it may be argued that the barren sediment layers, which almost systematically begin at about 10-20 cm in many cores (36, 37, 43, 51, 52, and 53), may conceivably constitute the top of older sediments. This interpretation would require the area's surface sedimentary facies to be composed by a very thin veneer of Quaternary sediments (rarely exceeding 20 cm) which covers older, barren sediments lying underneath. This view is consistent with color and sediment-character changes occurring in the cores described elsewhere in these reports. It is not consistent, however, with the alternation of Quaternary and barren layers observed in cores 27, 30, and 50. They suggest that in this area the barren layers simply are part of a continuous Quaternary sedimentary sequence in which, due to greater solution and/or lesser productivity, fossils are absent. This interpretation is favored here and it also agrees with the already meager assemblages that characterize even the samples containing radiolarians.

To confirm either one of the above hypothesis requires piston cores in which the stratigraphy of the upper 10 m or so of the area's sediments can be studied.

ACKNOWLEDGMENTS

Supported by USGS contract Number 14-08-0001-15277.

HIG Contrib. Number 000.

REFERENCES

- Johnson, D. A., and Knoll, A. H., 1975, Absolute ages of Quaternary radiolarian datum levels in the equatorial Pacific, *Quatern. Res.*, v. 5, p. 99-110.
- Nigrini, C. A., 1971, Radiolarian zones in the Quaternary of the equatorial Pacific Ocean, in: *The Micropaleontology of Oceans* (Funnell, B.M., and Riedel, W.R. eds.), p. 443-461, Cambridge Univ. Press.
- Theyer, F., and Hammond, S. R., 1974, Paleomagnetic polarity sequence and radiolarian zones, Brunhes to polarity Epoch 20, *Earth Planet. Sci. Lett.*, v. 22, 307-319.

Chemical Composition of Marine Sediments
of DOMES Site C

James L. Bischoff
and
David Z. Piper

U.S. Geological Survey
Menlo Park, California

Introduction

The study of the chemical composition of DOMES Site C sediment was undertaken in order to establish important baseline parameters in the overall characterization of the sediment. Such general characterization and information concerning heterogeneity and local variation of this and related parameters such as mineralogy, sediment age, and pore water chemistry, are essential in formulating predictive models concerning environmental perturbations caused by resuspension of sediments during deep sea mining.

We report here the major elements Si, Al, Fe, Mg, Ca, Na, K, Ti, P, Mn, organic C, and carbonate and minor elements B, Ba, Be, Cd, Co, Cr, Cu, Mo, Ni, Pb, Sc, Sr, U, V, and Zn for 42 separate samples. This represents the most complete set of elements analyzed on any single sample from the sea floor to date, and from the largest number and most detailed set of samples from a comparable area on the sea floor.

Sampling

Splits were taken of sediment samples from which pore water samples had been taken on board, and which were used for most of the related sediment studies (see other reports this volume).

Although much of the pore water was extracted by squeezing, the remaining sediment cakes still contained approximately 50

percent pore water with contained sea salts. The samples were dried at 110°C prior to analysis.

Analytical techniques

The major elements Si, Al, Fe, Mg, Ca, Na, K, Ti, and P were analyzed by X-ray fluorescence spectroscopy after fusion with lithium tetraborate. Concentrations were determined by comparison with appropriate sediment and rock standards and computer correction for matrix effects. CO₂, as released from solid carbonates, was measured gasometrically after acidification on a LECO Corp. CO₂ analyzer, and organic C was estimated by difference after analyzing total CO₂ released by combustion on the same instrument. Precision based on replicate analyses is estimated to be 1 percent (as 1 sigma), or less, of the amount reported for the major elements.

Ni and Cu were analyzed by atomic absorption spectroscopy after complete sample dissolution, with estimated precision better than 3 percent as 1 sigma.

The remaining elements were analyzed by optical emission spectroscopy standardized against appropriate sediment and rock standards. Precision is estimated to be on the order of 15% as one sigma.

Data and Discussion

Results are presented in Table 1, and averages in Table 2 compared with the composition of average Pacific pelagic clay taken from a combination of sources in the literature. Compiling a meaningful average from the literature is often difficult because the various investigators have used a variety of drying temperatures and other pretreatments, many of which are unspecified. Never-the-less, the averaged composition of DOMES Site C sediment is very close to such an averaged Pacific clay (Table 2). The small differences that are apparent for the majors, can be accounted for by differing salt contents and differing drying temperatures. For example, the summation of our samples averages 87.88% with the remainder due to structural water and other volatiles which would be selectively and continuously lost upon heating to 1000⁰C. The 12.12% difference from 100% this represents is about the quantity typical of such ignition losses for similar marine sediment dried at 110⁰C.

The relative Ca enrichment displayed by the Site C sediment is due, in part, to relatively higher concentrations of biogenic CaCO₃, an expected result since DOMES Site C is located closer to the high productivity zone along the equator than the average Pacific pelagic clay. However, CaO exceeds CO₂ on a molar basis by 45%, leaving a remainder of 1.17% CaO. As pelagic clay minerals do not contain significant Ca, the excess must represent

unaltered volcanic debris.

Na is likewise relatively enriched in Site C sediments, due in part to salts remaining from the pore water. Assuming 50% pore water on an average, pore water contributed Na_2O should approximate 1.9% of the dry sediment, leaving an additional 1% (or 34% of the total Na) unaccounted for. Additional Na is contained on exchange sites on clay surfaces. Average exchange capacity for these sediments is 60 meq/100g, with 40% of the sites occupied by Na (Bischoff and Rosenbauer, this volume). This represents an additional 0.74% Na_2O , leaving a remainder of 0.26% Na_2O . This remainder is likely due to the volcanic debris, whose presence is indicated by the excess Ca.

The amount of volcanic debris, therefore, can be calculated on the basis of the unaccounted for Na and Ca. Average oceanic tholeiite basalt contains 11.1 to 11.3% CaO and 2.3-2.7% Na_2O (Engel, et al. 1965). Therefore, based on the excess CaO in the Site C sediments of 1.17% we estimate that the sediments contain between 10.3 to 10.5% volcanic debris. A similar calculation using the excess Na_2O of 0.26% yields an estimated 9.6 to 11.3% volcanic debris, in excellent agreement with CaO estimate. This conclusion is supported by the petrographic observation that volcanic glass is ubiquitous in the sediments, and constitutes a major component in some samples (Hein et al, this volume).

Other major components remain relatively unchanged by salt, biogenic carbonate, and volcanic debris, and closely reflect average Pacific pelagic clay composition. One approach to make the comparison more exact is to compare ratios of elements. Al is the element commonly used as the basis for such comparison, owing to its limited variability in lithogenic material of terrigenous origin. Comparison of the remaining major elements by this technique (Table 3) shows the near identity of the DOMES Site C sediments with average Pacific pelagic clay.

The average minor element composition in general compares closely with average Pacific pelagic clay (Table 2). Exceptions to this are relative enrichments in Site C sediments for Ba (by a factor of 10), Cu and Ni (by a factor of two). Ba is generally considered associated with biogenic debris, and, therefore, would be expected to follow the Ca enrichment previously noted. Cu and Ni enrichments reflect above average content of micro-nodules in the sediment, and possibly the occurrence of hydrothermal metalliferous mud, both of which are enriched in Fe, Cu and Ni.

Metalliferous sediment of supposed hydrothermal origin was found in the lower portion of core 18B-37, intervals 8 and 9 and in lesser amounts in nearby core 18A-36, intervals 6-8. This material is characterized by low Al_2O_3 and high Fe_2O_3 , MnO, and SiO_2 (Table 1), and is described in more detail in a separate chapter (Bischoff and Rosenbauer, this volume).

In contrast, samples 18A-36 interval 1-4 are characterized by high MnO, reflected by dramatic enrichments of Cu, Ni and Co. That Fe_2O_3 is less than MnO, and $\text{SiO}_2:\text{Al}_2\text{O}_3$ ratio differs little from average Pelagic clay, leads to the conclusion that a large portion of these adjacent samples contain fragments of manganese nodules, or perhaps micronodules. Assuming an average MnO content of nodules in this area of 32% (see Piper, this volume) we estimate that interval 1, 3, and 4 contain 44, 17, and 20% respectively of nodule debris. Similar estimates based on an average Ni content of 1.2% for nodules results in estimated nodule contents of 45, 14, and 17% respectively for the three samples, all in excellent agreement. Such high contents of nodule debris or micronodules were not indicated by the petrographic description of splits of these sediments (Hein et al., this volume), and the discrepancy is puzzling.

Another anomaly associated with this core is the high CaCO_3 content of intervals 6 and 8 where it accounts for 30 and 47% of the sediment respectively. This is the only core which displays significant CaCO_3 content, and as it is the shallowest of the cores studied (4340 meters), it may represent the only station close enough to the calcite compensation depth to have preserved significant CaCO_3 .

Summary

With the exception of 3 samples that appear to contain a large fraction of micronodules or nodule fragments, the elemental composition of sediment from Site C varies over a rather limited range. The average for all samples also agrees extremely closely with that of sediment analyses reported in the literature and based on analyses of samples from throughout the Pacific. Thus, these sediments would appear to have no unusual or unique characteristics compared to pelagic sediments from other basins in the Pacific.

Acknowledgements: Sediment analyses were performed by the Chemical Analytical Laboratory, U.S.G.S., Menlo Park, Ca.

Table 1

Major and minor element composition, in weight per cent and ppm respectively, of sedimentary core samples from Site C. Major metal analyses were determined by X-ray fluorescence; Organic C and CO₂ gasometrically with a Leco analyser; Ni and Cu by atomic absorption; and the other minor elements by optical emission spectrophotometry. Summation less than 100% represents contained water and other volatiles not analyzed. Sample heading (e.g. 16B-49-1) lists station number, core number, and interval. See Table 3. Bischoff (this volume) to convert interval to depth, in centimeters, within the box core. Core locations are given in Table 1, Bischoff (this volume).

Major Components	16B-49 1	16B-49 2	16B-49 3	16B-49 4	16B-49 5	16B-49 6	16B-49 7	16B-49 8	16B-49 9	16B-49 10
SiO ₂	51.31	52.58	52.02	52.47	52.50	52.38	51.02	51.17	50.62	50.67
Al ₂ O ₃	15.35	15.70	15.37	15.59	15.29	15.11	14.99	14.92	14.75	14.65
Fe ₂ O ₃	7.35	7.43	7.31	7.32	7.25	7.18	7.19	7.16	7.18	7.17
MgO	3.21	3.28	3.17	3.21	3.24	3.23	3.02	2.98	3.08	3.06
CaO	1.46	1.39	1.35	1.33	1.37	1.37	1.35	1.37	1.34	1.37
Na ₂ O	2.92	2.84	2.96	3.08	3.14	3.23	2.88	2.94	2.98	2.69
K ₂ O	3.30	3.37	3.33	3.39	3.39	3.38	3.36	3.36	3.33	3.34
TiO ₂	.77	.78	.77	.77	.75	.74	.73	.72	.72	.72
P ₂ O ₅	.43	.46	.42	.41	.42	.43	.45	.45	.44	.39
MnO	.82	.83	.80	.89	1.05	1.24	1.34	1.15	1.31	1.41
Org. C	.31	.31	.23	.23	.18	.14	.15	.12	.12	.13
CO ₂	<u>.18</u>	<u>.18</u>	<u>.18</u>	<u>.15</u>	<u>.11</u>	<u>.11</u>	<u>.07</u>	<u>.11</u>	<u>.07</u>	<u>.04</u>
Total	87.41	89.15	87.91	88.84	88.69	88.54	86.55	86.45	85.94	85.64

Minor Components

B	150	150	150	150	150	150	150	150	150	150
Ba	3000	3000	3000	3000	3000	3000	5000	3000	5000	5000
Be	3	3	3	3	5	3	5	5	5	5
Cd	<D									
Co	100	100	150	150	150	150	150	150	150	150
Cr	50	50	70	70	70	50	70	50	50	50
Cu	950	500	460	500	570	690	680	660	690	680
Mo	10	10	10	20	20	20	30	30	30	30
Ni	160	140	260	300	350	380	450	360	380	430
Pb	70	70	100	100	100	100	100	70	100	100
Sc	20	20	20	20	20	20	20	20	20	20
Sr	300	300	300	300	300	300	300	300	300	300
U	<D									
V	100	100	100	100	100	100	100	100	100	100
Zn	150	150	150	150	150	150	200	200	200	200

Major Components	18A-36 1	18A-36 3	18A-36 4	18A-36 6	18A-36 8	18B-37 1	18B-37 2	18B-37 3	18B-37 4	18B-37 5
SiO ₂	36.37	45.17	43.23	37.69	25.95	51.95	51.70	51.47	52.05	52.24
Al ₂ O ₃	9.98	12.57	12.07	7.97	4.64	14.78	14.79	15.11	15.38	15.59
Fe ₂ O ₃	8.15	7.85	7.91	8.02	7.28	7.67	7.76	7.20	7.78	7.55
MgO	3.62	3.32	3.33	3.28	3.09	3.31	3.68	3.25	3.53	3.38
CaO	3.13	4.09	4.48	18.0	27.0	1.49	1.58	1.47	1.46	1.45
Na ₂ O	2.78	2.83	2.81	2.71	2.08	3.04	2.86	2.86	2.81	2.96
K ₂ O	2.31	2.83	2.72	2.12	1.51	3.21	3.23	3.27	3.35	3.39
TiO ₂	.64	.65	.65	.37	.22	.74	.75	.75	.75	.76
P ₂ O ₅	.52	.56	.52	.60	.56	.44	.49	.42	.50	.45
MnO	14.28	5.46	6.27	1.21	1.20	1.08	.95	.93	.87	.79
Org. C	.22	.30	.30	.26	.12	.41	.36	.34	.18	.14
CO ₂	<u>1.32</u>	<u>2.16</u>	<u>2.38</u>	<u>12.68</u>	<u>20.19</u>	<u>.18</u>	<u>.22</u>	<u>.22</u>	<u>.18</u>	<u>.15</u>
Total	83.32	87.79	86.67	94.91	93.84	88.30	88.37	87.29	88.84	88.85

Minor Components	18A-36 1	18A-36 3	18A-36 4	18A-36 6	18A-36 8	18B-37 1	18B-37 2	18B-37 3	18B-37 4	18B-37 5
B	150	150	150	100	70	150	150	150	150	150
Ba	3000	3000	3000	5000	3000	3000	5000	3000	5000	3000
Be	2	2	2	1.5	1	1.5	3	1.5	3	2
Cd	<D									
Co	700	300	500	50	30	100	100	100	100	100
Cr	50	50	50	30	10	50	70	50	50	50
Cu	4600	8500	1000	620	310	530	450	700	380	700
Mo	500	70	100	30	30	10	10	10	10	15
Ni	5400	1700	2000	60	20	330	310	500	150	300
Pb	300	150	150	70	70	70	70	70	70	70
Sc	15	20	20	15	10	15	20	15	20	15
Sr	700	700	700	700	1000	300	700	300	700	300
U	<D									
V	150	100	100	70	70	100	100	100	100	100
Zn	500	300	300	150	150	200	150	200	150	200

Major Components	18B-37 6	18B-37 7	18B-37 8	18B-37 9	20-27 1	20-27 2	20-27 3	20-27 4	20-27 5	20-27 6
SiO ₂	51.88	49.49	46.57	47.34	52.31	52.33	52.00	48.46	52.14	52.43
Al ₂ O ₃	14.95	13.01	9.43	10.12	15.73	15.68	15.64	14.76	16.04	16.18
Fe ₃ O ₄	7.81	9.21	12.03	11.56	7.38	7.43	7.43	7.86	7.51	7.48
MgO	3.45	3.51	4.32	3.96	3.12	3.15	3.10	3.13	3.12	3.15
CaO	1.55	1.63	1.76	1.74	1.27	1.26	1.27	1.31	1.27	1.27
Na ₂ O	2.86	3.40	4.15	3.50	2.46	2.51	2.71	2.33	2.31	2.70
K ₂ O	3.33	3.09	2.61	2.71	3.33	3.34	3.35	3.18	3.43	3.43
TiO ₂	.74	.65	.45	.50	.79	.80	.80	.80	.80	.79
P ₂ O ₅	.55	.50	.65	.54	.27	.26	.26	.25	.25	.27
MnO	.72	1.45	2.16	2.31	.81	.79	.78	4.54	.77	.84
Org. C	.13	.15	.15	.12	.40	.35	.31	.21	.23	.16
CO ₂	<u>.18</u>	<u>.18</u>	<u><.01</u>	<u>.18</u>	<u>.15</u>	<u>.22</u>	<u>.22</u>	<u>.26</u>	<u>.15</u>	<u>.11</u>
Total	88.15	86.27	84.20	84.58	88.02	88.12	87.87	87.09	88.02	88.81

Minor Components

B	150	150	100	150	150	150	150	150	150	150
Ba	5000	3000	7000	3000	3000	3000	3000	3000	3000	3000
Be	3	2	1.5	2	5	5	5	5	5	5
Cd	∅	∅	∅	∅	∅	∅	∅	∅	∅	∅
Co	100	100	50	70	150	150	100	300	100	100
Cr	30	50	30	20	70	70	70	70	70	70
Cu	510	1000	720	1000	370	360	360	1140	360	380
Mo	10	20	50	70	10	10	10	50	15	15
Ni	90	500	250	500	230	230	220	1500	240	260
Pb	50	70	70	70	70	70	70	200	70	70
Sc	20	15	15	10	20	20	20	20	20	20
Sr	700	300	700	300	300	300	300	300	300	300
U	∅	∅	∅	∅	∅	∅	∅	∅	∅	∅
V	100	100	100	100	100	100	100	100	100	100
Zn	150	200	200	200	150	150	150	150	150	150

Major Components	20-27 7	20-27 8	24B-29 1a	24B-29 3a	24B-29 5a	24B-29 6a	24B-29 8a	24B-29 1b	24B-29 3b	24B-29 5b
SiO ₂	51.17	50.82	54.58	53.56	52.99	53.53	52.83	55.76	52.65	52.61
Al ₂ O ₃	15.67	15.50	14.97	15.00	15.20	15.47	15.49	14.65	14.70	14.48
Fe ₂ O ₃	7.41	7.39	7.01	7.07	7.17	7.27	7.37	6.27	7.00	6.85
MgO	3.07	3.04	3.11	3.11	3.13	3.13	3.18	2.78	3.01	2.97
CaO	1.26	1.30	1.31	1.48	1.34	1.17	1.13	1.47	1.70	1.93
Na ₂ O	2.66	2.69	3.09	2.94	3.05	2.98	2.88	3.72	3.04	3.04
K ₂ O	3.36	3.37	3.14	3.18	3.28	3.31	3.30	3.02	3.18	3.20
TiO ₂	.79	.79	.73	.74	.75	.76	.76	.68	.73	.71
P ₂ O ₅	.25	.38	.32	.29	.28	.28	.29	.28	.28	.26
MnO	.77	.75	.68	.55	.48	.37	.55	.62	.52	.50
Org.C	.20	.18	.43	.35	.25	.25	.31	.42	.32	.27
CO ₂	<u>.15</u>	<u>.15</u>	<u>.29</u>	<u>.37</u>	<u>.33</u>	<u>.18</u>	<u>.18</u>	<u>.29</u>	<u>.66</u>	<u>.81</u>
Total	86.76	86.36	89.66	88.64	88.25	88.70	88.27	89.96	87.79	87.63

Minor Components	20-27 7	20-27 8	24B-29 1a	24B-29 3a	24B-29 5a	24B-29 6a	24B-29 8a	24B-29 1b	24B-29 3b	24B-29 5b
B	150	150	150	150	200	150	150	150	200	200
Ba	3000	3000	3000	3000	5000	5000	5000	3000	3000	5000
Be	5	5	3	3	3	3	5	3	3	3
Cd	<D	<D	<D	<D	<D	<D	<D	<D	<D	<D
Co	100	100	70	70	100	100	100	100	100	100
Cr	70	70	50	50	70	70	70	50	50	70
Cu	360	370	390	350	350	330	390	380	350	330
Mo	15	15	10	10	10	10	15	7	10	7
Ni	230	250	240	160	140	90	170	210	170	150
Pb	70	70	70	70	70	70	70	70	70	70
Sc	20	20	20	20	20	20	20	20	20	30
Sr	300	300	300	300	300	300	300	300	300	500
U	<D	<D	<D	<D	<D	<D	<D	<D	<D	<D
V	100	100	100	100	100	100	100	100	100	100
Zn	150	150	150	150	150	150	150	200	150	150

24B-29 7b	24B-29 9b
52.06	52.73
14.58	15.36
7.22	7.33
3.05	3.05
1.47	1.13
2.85	2.74
3.24	3.26
.74	.75
.27	.21
.47	.77
.25	.22
<u>.37</u>	<u>.11</u>
86.57	87.66

150	150
3000	5000
5	5
< D	< D
100	100
70	70
400	500
10	15
130	200
70	70
20	20
500	500
< D	< D
100	100
150	100

Table 2

Comparison of average sediment composition from Site C (Table 1) and average of values for Pacific pelagic sediment reported in the literature. Concentrations of SiO_2 , Al_2O_3 , Fe_2O_3 , MgO , CaO , Na_2O , K_2O , MnO , B, Ba, Cr, and V are from Landergren (1964); Co, Cu, Ni, and Sc from Krishnaswami (1976); Mo and Pb from Cronan (1969); Sr from Goldberg and Arrhenius (1958); P_2O_5 from El Wakeel and Riley (1961); Zn from Burnett (1971); Organic C from Lisitzin (1972); Be, Cd, and U from Turekian and Wedepohl (1961).

Table 2

Major components	Domes Site C sediments Average 42 Analyses from Table 1	Average Pacific Pelagic clay
SiO ₂	50.11	56.5
Al ₂ O ₃	14.22	15.6
Fe ₂ O ₃	7.64	8.2
MgO	3.24	3.4
CaO	2.59	0.86
Na ₂ O	2.91	1.7
K ₂ O	3.15	2.5
TiO ₂	0.71	0.64
P ₂ O ₅	0.39	0.16
MnO	1.57	2.55
Org. C	0.24	(0.1 to 0.5)
CO ₂	1.11	-
<u>total</u>	<u>87.88</u>	<u>92.36</u>
<u>Minor components</u> <u>parts per million</u>		
B	149	300
Ba	3670	390
Be	3.4	2.6
Cd	<7	0.4
Co	139	87
Cr	56	49
Cu	830	338
Mo	33	18
Ni	480	224
Pb	87	68
Sc	19	23
Sr	407	710
U	<100	1
V	100	110
Zn	177	154

Table 3

Comparison of major metal oxide: Al_2O_3 ratios for sediment from Site C (Table 1) with literature values. For source of the latter data see Table 2.

	Average of DOMES Site C	Average Pacific pelagic clay
SiO_2/Al_2O_3	3.52	3.62
Fe_2O_3/Al_2O_3	.53	.53
MnO/Al_2O_3	.11	.16
MgO/Al_2O_3	.23	.22
TiO_2/Al_2O_3	.049	.041
K_2O/Al_2O_3	.22	.16

References

- Burnett, W.C., 1971, Trace element Variations in some Central Pacific and Hawaiian Sediments, M.S. thesis, Geology Dept., Univ. of Hawaii
- Cronan, D.S., 1969, Average abundances of Mn, Fe, Ni, Co, Cu, Pb, Mo, V, Cr, Ti, and P in Pacific pelagic clays, *Geochem. Cosmochim. Acta*, v. 33; p. 1562-1565
- El Wakeel, S.K. and Riley, 1961, Chemical and mineralogical studies of deep-sea sediments, *Geochem. Cosmochim. Acta*, v. 25; p. 110-147
- Engel, A.E.J., Engle, C.G., and Havens, R.G., 1965, Chemical Characteristics of Oceanic Basalts and the Upper Mantle, *Geological Society of America Bull.*, v. 76; p.719-733
- Goldberg, E.D. and Arrhenius, G.O.S., 1958, Chemistry of Pacific Pelagic Sediments, *Geochim. of Cosmochim. Acta*, v. 13; p. 153-212
- Krishnaswami, S., 1976, Authigenic transition elements in Pacific pelagic sediments, *Geochim. Cosmochim. Acta.*, v. 40; p. 425-434
- Landergren, S., 1964, On the Geochemistry of Deep-Sea Sediments, *Reports of the Swedish Deep-Sea Expedition*, v.X; Special Investigations, No. 5, p. 61-148
- Lisitzin, A.P., 1972, Sedimentation in the World Ocean, *Soc. con. Paleon. Mineral. Spec. Pub.* 17
- Turekian, K.K. and Wedepohl, K.H., 1961, Distribution of the elements in some major units of the Earth's crust, *Geol. Soc. Am. Bull.*, v. 72; p. 175-192

INTERSTITIAL WATER CHEMISTRY IN DOMES
SITE C SEDIMENTS

Edward Callender
US. Geological Survey
Reston, Virginia

James L. Bischoff
U.S. Geological Survey
Menlo Park, California

Introduction

Studies of interstitial water chemistry were carried out as part of the general characterization of the geological baseline in DOMES site C. Interstitial water, or pore waters, are the medium through which diagenetic changes in the sediment take place. In-as-much as these interstitial waters represent a minor reservoir of chemical components in the sediments, small changes occurring in the solids result in large changes in interstitial water chemistry. Therefore, the interstitial water chemistry is a sensitive indicator of the chemical stability of the sediments with respect to sea water.

Previous work

The data concerning pore water chemistry of pelagic sediment interstitial water are few and of variable analytical quality. Presley, et al. (1967) conducted analyses for Fe, Mn, Ni, Co on pore fluids extracted from red-brown clay in the vicinity of the East Pacific Rise. While the concentration of Fe was very low (2 to 8 $\mu\text{g/l}$), the concentration of Mn was very high (5000 to 6000 $\mu\text{g/l}$). Cobalt and nickel (4.5 $\mu\text{g/l}$ and 14 $\mu\text{g/l}$ respectively) were enriched 100 times and 10 times respectively over bottom sea water concentrations. Presley and Kaplan (1970) analyzed the transition metal chemistry of pore waters squeezed from Deep Sea Drilling Project cores of pelagic calcareous and siliceous oozes. The Mn concentrations of these interstitial fluids ranged

between 70 and 150 $\mu\text{g/l}$. Bischoff and Sayles (1972) studied the pore fluid chemistry of recent deepsea sediments in the vicinity of the equatorial East Pacific Rise. While Cl, SO_4 , Mg, Ca, and K displayed little variation from bottom water concentrations, dissolved Mn and SiO_2 displayed marked enrichments. These sediments, with entrapped pore waters, are considered to be mildly reducing, hence the marked enrichment of interstitial Mn (approximately 100 $\mu\text{g/l}$) relative to oxidized bottom water (0.2 $\mu\text{g/l}$). Recent trace element analyses of the upper 1.5 meters of equatorial Pacific Ocean sediment (10° to 20°S , 80° to 150°W) by Michard, et al. (1974) have demonstrated that while sediment underlying manganese nodules exhibit pore water Mn concentrations of 5 $\mu\text{g/l}$ or less, surface sediments associated with nodules commonly exhibit Mn concentrations in the range of 50 to 150 $\mu\text{g/l}$.

Raab (1972) analyzed the trace element composition (Fe, Mn, Cu, Ni) of northeast equatorial Pacific Ocean sediment pore waters that had been extracted from cores stored at 22°C , and compared these with cores stored and squeezed at 4°C . The Mn concentrations of the warm (22°C) interstitial fluids were at least ten times higher than those of cold (4°C) pore waters which in turn were ten times higher than Mn concentrations reported in the present study. In contrast, the Cu concentrations of warm pore waters were enriched by only a factor of two relative to cold pore waters which were enriched two to four times relative to the Cu concentrations of interstitial fluids

analyzed in the present study. Hartmann and Müller (1974) analyzed the dissolved Mn, Cu, and organic carbon in pore waters extracted from a 5-meter core consisting predominantly of red clay and siliceous ooze. Both Mn and Cu concentrations (5 µg/l) varied little throughout the length of the core except in the vicinity of the 1-meter depth where Mn and Cu increased sharply to 25 and 15 µg/l respectively.

Alkalinity and nutrient analyses of pelagic sediment pore fluids generally show slight enrichment over bottom water concentrations. Hartmann and Müller (1974) and Hartmann, et al. (1974) show a slight alkalinity depletion in shallow sediment pore waters. On the other hand, ammonia concentrations exhibit marked enrichments relative to bottom water. Similarly, pore water SiO₂ concentrations increase almost exponentially from the water-sediment interface down to a depth of 3 to 4 meters. This observation is similar to that of Hurd (1973) who showed that most of the interstitial SiO₂ increase occurred within the upper one-half meter of sediment.

Sampling

Because many of the important components of the interstitial waters are labile, that is readily altered during sample handling and storage, samples must be processed at sea.

Sediments for pore water studies were sampled from box cores taken at 5 stations during the May 1975 cruise of the R/V

Oceanographer to DOMES Site C (station 16B, 18A, 18B, 20 and 24B). Cores were sampled using cylindrical plastic core tubes (6.7 cm i.d.) which sampled an entire vertical column through the box core. One to three of such "subcores" were taken from each of the box cores for pore water studies, and additional ones collected for archiving. Triplicate subcores from 16B-49, and duplicates from 18B-37, 20-27 and 24B-29 were taken to determine within core variation of pore water chemistry.

Sediment Extrusion and Pore Water Extraction

Pore water sampling was performed with a system (designed and constructed by Carl Bowser of the University of Wisconsin) specially designed to eliminate atmospheric contact with sediment, allow handling of sediment at or near in situ temperatures, and to have a minimum of handling prior to analysis. The system consists of a core extruder-thermostating device, separate squeezer bodies for each interval sampled, and an air-ram actuated squeezer press.

A core which has been kept cold (5°C) in the walk-in refrigerator was opened at the bottom and an "o"-ring sealed piston was inserted at the base. A jacket that would contain cooling liquid (anti-freeze-water mixture) was slid over the core and the entire core plus cooling jacket was placed on the extruding stand. The coolant was circulated around the core for at least 30 minutes or until a steady temperature of 3°C was reached. A base plate, through which pressurized sea water

(30psi) can move against the piston in the core, and an overlying slide assembly, for cutting off sections of the core, are rigidly attached to the core tube in the extruding assembly. The lucite slide and cutoff assembly consists of a grooved slide mounted on a lucite plate and is used to hold the inverted sediment squeezer over the core tube. After the sediment section (2cm thick) is cut off, the squeezer can be slid from a position directly over the core tube to directly over the piston which inserts into the squeezer assembly cylinder. A 2-mm thick cutoff slide is mounted into the lucite base plate for the purpose of cutting off the sediment section once it is extruded into the squeezer assembly. In operation, a precooled squeezer assembly is inverted directly over the core tube, nitrogen purged for 5 minutes, and then the core hydraulically extruded directly into the squeezer. The cutoff slide is pushed in through the sediment to isolate the core section and the main slide is pulled over so that the squeezer assembly is directly over the awaiting piston. The complete squeezer assembly with its sediment section (2cm thick) is stored in a refrigerated container preparatory to squeezing.

The complete squeezing assembly was placed in a pressurizing system that consists of 10.2 cm diameter air rams driven by compressed air. Three of these pressurizing systems were mounted side by side in the walk-in refrigerator (5°C) and the sediment was subjected to pressures no greater than 150 psi (generally well below 100 psi). Expressed pore fluid, which

first passed through Whatman No. 41 filter paper and a nucleopore 0.2 μ m-filter, was collected into a 20- and then a 5 cc disposable syringe via small volume liquid chromatographic tubing and sample valves. The resultant sediment "cake" was stored in plastic bags for future geochemical analyses.

Analysis

Sediment pore waters were collected for a variety of ship-board and laboratory analyses. The water contained in the 5 cc syringe was used for pH and alkalinity measurements. Due to the "degassing" problem when water samples are warmed to ambient temperatures not higher than 10^oC sample containers for both pH and alkalinity were "bathed" in a water bath fed by ice water. All samples, standards, reagents, and pH buffers were kept cold in a refrigerator. The pH measurements were conducted on 1 ml of sample placed in a micro-polystyrene cup into which a Markson combination pH electrode (pencil model) was inserted. Generally 5 minutes was sufficient to record a stable pH reading where the drift was less than 0.01 pH unit per minute. For titration alkalinity, 1 ml of sample was transferred to a 6ml capacity polystyrene vial along with 2 ml of 0.530M NaCl to minimize changes in liquid junction potential during the titration. A miniature stirring bar was placed in the vial and the combination semi-micro pH electrode was placed in the solution after calibration with pH 7.48 and 4.00 buffers (5^oC). Stirring commenced, an initial pH and potential was measured, and 0.01N

HCl was dispensed quickly (using a micrometer burette, 2.0 ml capacity) until the bicarbonate end point (+157mv) was approached. After that, the acid was dispensed in 0.02 ml increments and the resultant potential recorded. At least 12 points were measured beyond the equivalence point. The titration vessel was cooled to at least 10°C (usually lower) by ice water. In essence, the above potentiometric titration is the Gran titration and the bicarbonate endpoint was determined using a Gran Function.

Generally between 10 and 15 mls of pore water were recovered in the 20-cc syringe. If possible, 10 ml was placed in an acid-washed, distilled-water rinsed linear polyethylene bottle and 100µl of GN HCl was added to preserve the water sample for further shore analysis. Additionally, 5 ml pore water, aliquots from 18B-36 and 37, and 24B-29 were placed in linear polyethylene bottles and frozen for future nutrient analysis (PO_4^{-3} , SiO_2 , NH_4^+).

Laboratory Analyses

Major cation analyses (Ca, Mg, Na, K) were conducted on HCl-preserved samples stored in pre-cleaned linear polyethylene bottles. The analytical technique used was that of flame atomic absorption spectrophotometry. Nutrients (NH_4^+ , PO_4^{-3} , SiO_2) were analyzed by automated spectrophotometric techniques (Technicon Autoanalyzer) utilizing unacidified interstitial fluid samples

that were preserved frozen prior to analysis. $\text{SO}_4^{=}$ was analyzed radiochemically after precipitation with Ba^{133} .

Trace element analyses were conducted on HCl- preserved interstitial fluid samples. Analyses for total dissolved Mn and Cu were accomplished using a flameless atomic absorption technique that employs a heated graphite atomizer. Instrumentation consisted of a Perkin-Elmer 503 Atomic Absorption Spectrophotometer with an HGA-2100 Heated Graphite Atomizer and a D_2 -Arc Background Corrector. Interstitial fluid samples with admixed ammonium nitrate (to reduce smoke interference by volatilization of major sea salts at lower temperatures) were injected directly into the graphite atomizer. The practical detection limit for Mn is $0.5\mu\text{g}/\text{l}$ with a precision of $\pm 10\%$; the detection limit for Cu is $1\mu\text{g}/\text{l}$ with a precision of $\pm 20\%$. The quoted precision for Cu analyses is based upon replicate analyses of samples conducted during a period of 3 to 6 days.

Data

Results are tabulated in Table 1, and averaged in Table 2. The averages differ very little from bottom water chemistry, indicating that the sediments are not rapidly undergoing diagenesis. NH_3 is the only significant exception to this generality and suggests a certain amount of bacterial activity in the sediment.

Variation of components within samples of the same core, and between subcores of the same core are seen to be as great

as between cores. Therefore, pore water chemistry is not a function of sediment type.

Mn and Cu values are significantly greater than bottom water levels, each averaging approximately 10 ppb, but are still insignificant in terms of environmental implications. Replicate analyses over a period of time showed the Cu values but not the Mn, to increase with time suggesting contamination of the acidified aliquot by the polyethylene bottles. The reported Cu concentrations, therefore, may simply express the level of contamination, and serve only to indicate maximum possible Cu levels in-situ. Mn appears to be free of such contamination.

- Bischoff, J.L. and F.L. Sayles, 1972, Pore fluid and mineralogical studies of recent marine sediments: Bauer Depression region of East Pacific Rise; Jour. Sed. Petrol., v. 42, 711-724
- Hartmann, M., Kögler, F.C., Müller, P., and E. Suess, 1973, Preliminary results of geochemical and soil mechanical investigations on Pacific Ocean Sediments: In The Origin and Dis-
- Hartmann, M. and P. Müller, 1974, Geochemische Untersuchungen an Sedimenten und Porenwassern: Meernstachnik, v. 5, 201-202
- Hurd, D.C., 1973, Interactions of biogenic apal, sediment and sea-water in the Central Equatorial Pacific: Geochim. Cosmochim. Acta, v. 37
- Michard, G., Griman, D., and D. Lavergne, 1974, Concentrations de manganese dissous dans les eaux interstitielles des sediments du Pacifique Equatorial: Comtes rend. t. 278, series D, 3157-3160
- Presley, B.J., Brooks, R.R., and I.R. Kaplan, 1970, Manganese and related elements in the interstitial water of marine sediments: Science, v. 158, 906-989
- Presley, B.J., and I.R. Kaplan, 1970, Interstitial water chemistry: Deep Sea Drilling Project leg 7. Initial Reports Deep Sea Drilling Project, v. 7, 883-887
- Raab, W., 1972, Physical and chemical features of Pacific deep sea manganese nodules and their implications to the genesis of nodules in Ferromanganese Deposits on the Ocean Floor, D. R. Horn, ed., 293 p.

Table 1
Chemistry of Interstitial water from DOMES Site C sediments. Ca, Mg, Na, K, and SO₄ concentrations in ppm, alkalinity in m eq/l, Mn and Cu in ppb, SiO₂, PO₄⁻³ and NH₄⁺ in µg atm/l. NA indicates not analyzed.

Box Core Station No.	Interval cm	Ca	Mg	Na	K	SO ₄	Alkalinity	pH	Mn	Cu	SiO ₂	PO ₄ ⁻³	NH ₄ ⁺	
16B-49 Subcore I	0-2	398	1290	10,720	359	NA	2.02	7.19	12	11	NA	NA	NA	
	2-4	382	1290	10,460	366	"	2.41	7.46	6	5	"	"	"	
	4-6	377	1050	10,340	362	"	2.06	7.20	7	4	"	"	"	
	8-10	402	1130	10,720	372	"	2.46	7.25	13	8	"	"	"	
	12-14	415	1250	10,960	388	"	2.31	7.13	6	NA	"	"	"	
	16-18	382	1130	10,340	355	"	2.35	7.14	9	9	"	"	"	
	20-22	NA	NA	NA	NA	"	2.24	7.35	25	7	"	"	"	
	24-26	384	1170	10,090	359	"	2.42	7.18	112	23	"	"	"	
	28-30	372	1250	10,720	354	"	2.48	7.64	14	7	"	"	"	
	16B-49 Subcore III	0-2	407	1325	10,420	363	"	2.31	7.93	9	11	"	"	"
2-4		407	1285	10,820	396	"	2.22	7.61	10	8	"	"	"	
4-6		398	1285	10,690	380	"	2.50	7.73	4	6	"	"	"	
8-10		392	1245	10,060	357	"	2.34	7.51	7	7	"	"	"	
12-14		401	1270	10,310	374	"	2.80	7.56	9	7	"	"	"	
16-18		NA	NA	NA	NA	"	2.37	7.36	10	19	"	"	"	
20-22		NA	NA	NA	NA	"	NA	NA	22	11	"	"	"	
24-26		NA	NA	NA	NA	"	NA	NA	11	19	"	"	"	
28-30		NA	NA	NA	NA	"	NA	NA	45	33	"	"	"	
16B-49 Subcore IV		2-4	412	1280	10,440	378	"	2.34	7.53	13	15	"	"	"
	6-8	418	1330	10,820	390	"	2.42	7.58	5	8	"	"	"	
	10-12	424	1355	11,090	402	"	NA	7.48	7	7	"	"	"	
	14-16	401	1280	10,570	373	"	2.30	7.32	5	9	"	"	"	
	18-20	NA	NA	NA	NA	"	2.29	7.32	NA	NA	"	"	"	
	22-24	394	1280	10,570	376	2520	NA	7.52	8	12	"	"	"	
	26-28	NA	NA	NA	NA	NA	NA	NA	NA	NA	"	"	"	
	30-32	382	1245	10,060	349	2422	1.90	7.35	12	13	"	"	"	
	34-36	385	1250	10,180	358	2383	NA	7.50	12	11	"	"	"	
	18B-37 Subcore I	2-4	415	1290	10,810	371	2659	2.42	7.71	4	7	NA	NA	NA
4-6		435	1330	10,930	377	2631	NA	7.52	3	5	"	"	"	
6-8		419	1295	10,680	372	2548	2.37	7.46	3	8	"	"	"	
10-12		412	1285	10,680	359	-	NA	7.30	10	19	"	"	"	
14-16		390	1205	NA	373	2518	2.27	7.44	4	10	"	"	"	
18-20		453	1290	10,930	377	2395	NA	7.46	10	14	"	"	"	
22-24		407	1260	10,280	367	2535	NA	7.72	7	6	"	"	"	
26-28		423	1330	10,810	382	2522	NA	7.88	3	5	"	"	"	
30-32		398	1300	10,420	409	2519	2.51	7.79	4	2	"	"	"	
18B-37 Subcore II		0-2.2	423	1375	11,380	398	NA	2.44	7.83	8	14	158	2.26	6.43
		2.2-4.2	420	1305	11,000	376	"	2.06	7.30	12	6	203	2.29	5.50
		6.2-8.2	NA	NA	NA	NA	"	2.17	7.45	7	5	238	2.45	5.43
		10.2-12.2	412	1270	10,250	366	"	2.31	7.35	7	17	NA	NA	NA
		14.2-16.2	419	1350	10,810	377	"	2.27	7.21	6	7	213	2.45	5.21
		18.2-20.2	419	1160	10,420	363	"	2.10	7.17	4	5	183	2.81	3.86
	22.2-24.2	NA	NA	NA	NA	"	2.22	7.17	10	9	217	2.94	4.57	
	26.2-28.2	NA	NA	NA	NA	"	2.64	7.40	5	9	217	2.20	5.93	
30.2-32.2	NA	NA	NA	NA	"	2.39	7.34	5	7	213	2.16	8.43		
18A-36 Subcore III	0-2.7	413	1280	10,630	371	"	NA	7.10	9	36	137	2.00	14.79	
	2.7-4.7	427	1285	10,180	377	"	"	6.68	4	-	170	1.94	7.71	
	4.7-6.7	404	1285	10,630	359	"	"	6.89	28	14	120	2.03	13.64	
	6.7-8.7	444	1265	10,380	369	"	"	7.34	3	5	NA	NA	NA	
	8.7-10.7	404	1270	10,630	363	"	"	7.11	5	5	192	1.91	7.43	
	10.7-12.7	413	1300	10,750	379	"	"	7.54	2	4	165	2.20	5.36	
	12.7-14.7	413	1280	10,750	374	"	"	7.25	4	3	NA	NA	NA	
	14.7-16.7	413	1290	10,500	374	"	"	6.87	10	8	NA	NA	NA	

Box Core Station No.	Interval cm	Ca	Mg	Na	K	SO ₄	Alkalinity	pH	Mn	Cu	SiO ₂	PO ₄ ⁻³	NH ₄ ⁺
20-27	2.0-4.0	417	1285	11,210	377	NA	NA	7.73	46	62	NA	NA	NA
Subcore I	4.2-6.3	408	1275	11,090	368	"	2.79	7.86	40	34	"	"	"
	6.3-8.5	428	1350	11,470	357	"	2.70	7.75	18	32	"	"	"
	8.5-10.7	420	1275	10,840	366	"	2.54	7.68	14	6	"	"	"
	10.7-12.9	422	1305	11,090	367	"	NA	7.62	11	12	"	"	"
	12.9-17.9	459	1375	11,590	364	"	2.63	7.64	19	58	"	"	"
	17.9-22.9	424	1325	11,210	357	"	NA	7.71	5	24	"	"	"
	22.9-27.9	435	1355	11,340	348	"	2.10	NA	7	7	"	"	"
20-27	2.0-4.3	418	1315	11,090	357	"	2.48	7.61	7	20	"	"	"
Subcore II	4.3-6.5	408	1320	10,970	393	"	2.41	7.66	5	14	"	"	"
	6.5-8.5	409	1275	10,550	388	"	2.56	7.70	6	10	"	"	"
	10.5-12.5	409	1270	10,550	392	"	2.40	7.59	9	25	"	"	"
	14.5-16.5	433	1280	10,670	398	"	NA	7.46	7	9	"	"	"
	18.5-20.5	448	1340	11,290	412	"	NA	7.61	10	19	"	"	"
	22.5-24.5	389	1265	10,420	384	"	NA	7.31	4	50	"	"	"
	26.5-28.5	405	1250	10,300	384	"	NA	7.30	13	9	"	"	"
Box Core Station No.	Interval cm	Ca	Mg	Na	K	SO ₄	Alkalinity	pH	Mn	Cu	SiO ₂	PO ₄ ⁻³	NH ₄ ⁺
24B-29	0-2	452	1295	10,670	403	2551	2.70	7.72	6	5	NA	NA	NA
Subcore I	2-4	430	1315	10,920	402	2487	2.68	7.67	4	3	173	2.81	3.7
	4-6	428	1280	10,800	372	2528	2.38	7.40	5	19	172	2.45	4.4
	6-8	435	1300	10,800	384	2489	2.62	7.34	6	18	165	2.58	3.7
	8-10	445	1350	11,290	378	2530	2.60	7.47	6	2	167	2.65	3.3
	12-14	420	1320	11,020	366	2543	2.37	7.18	4	2	242	2.67	3.7
	16-18	445	1335	11,020	374	2520	2.30	7.21	6	3	NA	NA	NA
	20-22	430	1355	11,520	383	2500	2.33	7.09	4	NA	NA	NA	NA
24B-29	0-1.6	420	1290	10,630	374	NA	2.48	7.62	6	20	243	3.04	10.1
Subcore V	1.6-3.6	427	1300	10,890	390	"	2.49	7.65	4	6	187	2.62	6
	3.6-5.6	438	1280	11,140	409	"	2.53	7.75	2	4	NA	NA	NA
	5.6-7.6	434	1280	11,020	371	"	2.62	7.58	4	5	NA	NA	NA
	7.6-9.6	454	1350	11,400	387	"	2.59	7.42	8	12	222	2.52	7.4
	9.6-11.6	424	1260	10,500	359	"	NA	NA	6	6	NA	NA	NA
	11.6-13.6	430	1265	10,630	379	"	2.65	7.65	7	20	NA	NA	NA
	13.6-15.7	434	1300	10,880	387	"	2.76	7.64	5	21	NA	NA	NA
	15.7-17.7	413	1260	10,750	383	"	2.48	7.46	5	19	NA	NA	NA

Table 2
Average pore water chemistry of DOMES, Site C, box cores compared to bottom water.

	Pore Water	Bottom Water*
Ca (ppm)	416	409
Mg "	1,283	1,281
Na "	10,754	10,671
K "	376	396
SO ₄ "	2,516	2,687
AlK (meq/l)	2.41	--
pH	7.46	7.80
SiO ₂ (µg atm/l)	190	138
PO ₄ ⁻³ " "	2.42	2.4
NH ₄ ⁺ " "	6.50	0.5

*Bottom water SiO₂, PO₄⁻³, NH₄⁺, data from DOMES Site C Preliminary Report by Richards, et al. Conservative components computed from salinity of 34.69‰ given by Wooster and Volkmann (1960). pH from Park (1966).

RECENT METALLIFEROUS SEDIMENT IN THE NORTH PACIFIC MANGANESE NODULE AREA¹

James L. Bischoff
and
Robert J. Rosenbauer
U.S. Geological Survey
Menlo Park, California

ABSTRACT

Quaternary sediments cored in the NE Pacific nodule area [DOMES Site C] contain a significant amount of hydrothermal metalliferous mud. Water content, color, mineralogy, and chemical composition are analogous to metalliferous sediments of the subequatorial East Pacific Rise.

Correction for contribution of pelagic clay indicates the metalliferous fraction to be about 40 per cent of the sediment. SiO_2 and Mg are major components in the corrected composition, as they are for other metalliferous sediments similarly corrected from a variety of East Pacific Rise and DSDP metalliferous sediments. A correlation between Mg and SiO_2 for these corrected sediments indicates a hydrothermal origin for a significant portion of the SiO_2 .

Results from DSDP in the nodule area suggest that metalliferous globules are a ubiquitous minor component of the Clipperton Oceanic Formation, which underlies much of the Pacific ferromanganese nodule belt. This indicates that hydrothermal activity is not confined to spreading centers.

¹Publication authorized by the Director, U.S. Geological Survey.

I. INTRODUCTION

Metalliferous sediments on the sea floor are commonly believed to be related to hydrothermal activity associated with crustal spreading centers. Extensive deposits of such sediments are accumulating in the subequatorial East Pacific Rise and adjacent Bauer Depression, and have been studied in detail by several investigators (1-6 and references therein). Similar, but not identical, sediments have been found immediately overlying the basalt basement in many DSDP (Deep Sea Drilling Project) sites of the East Pacific. Ages range from Late Eocene to Late Miocene (7-9 and references therein) and the deposits are given the stratigraphic designation of the Line Island formation (10). These sediments are also inferred to have formed at the spreading center.

We report here the occurrence of analogous metalliferous sediment from the North Pacific manganese nodule belt, at a site 2400 km removed from the East Pacific Rise, the nearest zone of sea floor spreading.

2. OCCURRENCE AND SAMPLING

As part of the National Oceanic and Atmospheric Administration's Deep Ocean Mining Environmental Study (DOMES), box coring was carried out during May 1975 on the R/V Oceanographer, in the area for which Deep-sea Ventures Corporation filed a formal mining claim with the U.S. State

Department (11). Box cores 30 to 40 cm long and 50 cm on a side were recovered from 12 stations randomly located in a 2-degree square centered at 14° N 126° W (Site C) and were studied in the laboratory (Fig. 1).

Sediments sampled by the box cores are generally typical for this region, which is located on the boundary between the siliceous ooze and red clay belts (12). Sediment types range from light-to-dusky-brown siliceous ooze to dark-brown clay with minor and varying proportions of siliceous debris and volcanic glass, and with ubiquitous globules of red-brown semi-opaque oxides (or "RSO's" as used by DSDP, 13).

Supporting information in this area is provided by DSDP holes 159 and 160 (Fig. 1) approximately 300 km to the south. The general lithology of the uppermost unit described for these holes by van Andel et al. (14) coincides exactly with that of our box cores. They also noted that RSO's are a minor component of the clay-rich beds. Their biostratigraphic data indicate the top ten meters of this unit in both holes is Quaternary. The unit is as old as lower Miocene at the base about 20 to 30 meters below the sediment-water interface. This lithology has been designated as Clipperton Oceanic Formation by Cook (10), a diachronous unit ranging in age from recent to possibly late Eocene. Synthesis of all DSDP data for the Central Equatorial Pacific (15) indicate the entire region represented by DOMES Site C is characterized by continuous sedimentation over the last 5 million years.

3. CORE 18B: Descriptive Details

A 36 cm box core taken at station 18B (Fig. 1), contained in its lowermost 16 cm a bed of relatively pure metalliferous sediment, distinctive by its dark chocolate-brown color which contrasted with the yellowish-brown color of the top 20 cm. Ferromanganese nodules covered approximately 25 per cent of the surface, displaying a bimodal size distribution with mean diameters of 1 and 3.5 cm.

The metalliferous zone is characterized by an anomalously high water content (80 per cent as opposed to 50 per cent for the overlying siliceous clay), and upon dispersion in water the metalliferous component settled very quickly in the form of globules averaging approximately 100 μm diameter. These globules are composed of a mixture of semi-opaque reddish-yellow aggregates and detrital clay minerals of low refractive index, along with minor amounts of radiolarian debris, volcanic glass, and micronodules. The globules were disaggregated by ultrasound and the larger fragments of glass, micronodules, and biogenic debris were separated by selective settling.

Age-diagnostic microfossils were found only in the top four centimeters of the core, and are of Pleistocene to recent age (F. Theyer, personal communication, 1975). Pore water chemistry was that of normal pelagic clay, that is, little different from normal seawater. This lack of distinctive pore water chemistry also characterizes metalliferous sediments of the East Pacific Rise (16, 17).

An X-ray diffraction scan of the metalliferous sediment suggests a predominance of amorphous material with weak peaks for smectite and subordinate amounts of illite, kaolinite and chlorite.

4. CHEMICAL COMPOSITION

Chemical analysis of major components was carried out for the metalliferous sediment and a sample of a "typical" red clay (core 20) collected nearby in Site C, using atomic absorption and X-ray fluorescence spectroscopy (Table 1). The sample from core 20 is representative of the 39 samples from the other cores taken from Site C for which such chemical analyses were performed.

Compared with core 20 and with average pelagic clay, the metalliferous sediment is particularly enriched in Fe, Mn, Cu, and Ni, and depleted (by a factor of two) in Al. These characteristics are typical of East Pacific Rise metalliferous sediments and their DSDP counterparts.

5. DISCUSSION

5.1. Comparison of Elemental Ratios

Strict comparison of absolute percentage of any given chemical component with those of previous studies is made imprecise because of lack of uniformity in drying temperatures, completeness of list of elements, presence or absence of interstitial salts, and dilution by biogenous and terrigenous components. Because of these problems, comparisons are usually made on the basis of elemental ratios.

Bostrom (2) conceived of constructing a plot of Fe/Ti versus $Al/(Al + Fe + Mn)$ to show mixing relations between metalliferous

sediment and terrigenous matter of basaltic debris. Sediment from core 18B is seen to fall exactly on the mixing curve between average terrigenous material (TM) and the pure metalliferous sediment (EPR) (Fig. 2) and at a point that suggests the metalliferous contribution is approximately 40 percent. In contrast, sediment from core 20 plots close to TM. A similar approach is that of a triangular diagram of Fe-Mn-Al employed by Dymond et al. (18). Again, sediment from 18B plots well within the field of metalliferous sediments (Fig. 3) from the Bauer Depression, and that from 20 within the field of Pacific pelagic sediment. Still another approach is to compare Fe/Mn and Cu + Ni (Fig. 4). In this plot the metalliferous sediments group rather closely in the center of the field and include in their spread core 18B. Pelagic sediments, on the other hand, are characterized by a Fe/Mn ratio similar to that of the metalliferous sediments but have a lower content of Cu + Ni by a factor of ten. DOMES core 20 is clearly related to the pelagic sediments. Pacific ferromanganese nodules constitute a distinct group in both Figures 3 and 4.

5.2. Correction for Pelagic Clay Contribution

Another approach is to subtract the pelagic clay content and compare the resulting composition with similarly corrected analyses from the Bauer Depression and Basal DSDP cores.

First, we assume that the sediments are a mixture of metalliferous sediment and normal pelagic clay including calcium carbonate and interstitial salts. No correction is made for the contribution of siliceous ooze, which we assume affects only the silica content. The silica fraction also has contributions from terrigenous and metalliferous sediment.

Secondly, we assume all aluminum to be terrigenous, that is, contributed solely by the pelagic clay component. Then, using the major oxide/alumina ratio for average Pacific pelagic clay (Table 1), the pelagic clay fraction for each oxide is calculated from the alumina content and subtracted. Third, all CaO and Na₂O is assumed to represent CaCO₃ and interstitial salts, and is also subtracted. The remainder is then normalized to 100 per cent (Table 2).

Results indicate that the metalliferous component of 18B accounts for 43 per cent of the sediment, and has as its major components Si, Fe, Mn, and, somewhat surprisingly, Mg. The corrected analysis for sediment from core 20 resulted in complete removal of all oxide components, indicating the sample is 100 % pelagic clay.

Comparison with a similarly corrected Bauer Depression composite shows a remarkable similarity (Table 2). The metalliferous component in this case is 61 per cent and Si, Fe, and Mg predominate in the same proportions.

Corrected analyses of metalliferous sediment from basal DSDP, presumably analogous with metalliferous sediment forming at the ridge crest, show somewhat of a contrast. These sediments are also dominated by Fe and Mn but are relatively low in Si and Mg.

5.3. Role of Silica

Silica is the most important component in 18B and Bauer Depression sediments, exceeding both Fe and Mn. However, only minor amounts of biogenic silica were apparent under the microscope. Heath and Dymond (6) noted that silica content was very low in metalliferous sediment

from the crest of the East Pacific Rise, but increased markedly eastward into the Bauer Depression. They concluded that the excess silica was biogenic debris that had quickly reacted with hydrothermal ferric hydroxide to form nontronite. However, as Sayles et al. (1975) pointed out, there is no direct evidence of such diagenesis. No partially altered biogenic debris has been observed, and pore water chemistry is unaltered.

What about a hydrothermal source for the silica? Silica is readily mobilized from rocks in contact with hot aqueous solutions. If, as many currently believe, the metal-bearing hydrothermal fluid were seawater which had interacted with sea-floor basalts, then silica should be a major dissolved component of the fluid. Experimental studies at 200°C indicate dissolved silica of 1000 ppm and 50 to 10 ppm for Fe and Mn (19).

Regardless of the origin of the fluid, dissolved silica must be a major dissolved component, since the hydrothermal fluid would have to be intimately associated with solid silicates before discharging on the sea floor.

During discharge, dissolved silica will be either precipitated as amorphous silica because of cooling (saturation approximately 80 ppm) or will react with seawater magnesium to form a silicate such as sepiolite (saturation approximately 40 ppm), or diluted below saturation with respect to either of these phases by rapid mixing with bottom waters. Which of these happens depends on the ratio of hydrothermal fluid to seawater during the precipitation. This implies that metalliferous sediments on the crest of the East Pacific Rise precipitate under conditions

of large seawater dilution, whereby silica is quickly diluted below saturation, and, in contrast, that the Bauer Depression sediment and DOMES 18B are precipitated under conditions of less complete mixing and dilution, to account for their Si enrichment.

When excess dissolved silica is added to seawater to the point of precipitation under laboratory conditions, seawater magnesium is partially removed and incorporated in the precipitate. The precipitate, therefore, although usually X-ray amorphous, is a mixture of hydrated silica and hydrated magnesium silicate.

If the silica in the Bauer Depression and DOMES 18B sediment is predominantly of hydrothermal origin, then we might test for this by looking for a correlation between Si and Mg in such sediments after corrections have been made for terrigenous matter.

A plot of Si versus Mg for individual analyses of metalliferous sediments from the East Pacific Rise region as well as the DSDP basal unit (restricted to samples for which sufficient elements are reported to allow subtraction of a pelagic clay component as above) shows a definite relationship between the two elements (Fig. 5). The trend is above the sepiolite ratio, suggesting that both magnesium silicate and amorphous silica are precipitated together as a result of both mixing and cooling.

We conclude that much, if not all, silica in these corrected analyses is of hydrothermal origin, and that crestal metalliferous sediments precipitate under different conditions of discharge and mixing of the hydrothermal fluid and cold seawater than those of the Bauer Depression.

This conclusion differs from that of Heath and Dymond (6) who view the Bauer Depression sediment as a peripheral accumulation from hydrothermal activity on the crest of the East Pacific Rise. In support of their view is the findings of Dymond and Veeh (20), that metal accumulation rates are an order of magnitude greater on the rise crest than in the Bauer Depression. Further, it could be argued that the Mg-Si relationship shown in Fig. 5 simply reflects diagenesis between biogenic silica, metalliferous sediment and pore water Mg. From this viewpoint the lack of observed pore water depletion in Mg would be because diagenesis is taking place more slowly than ionic diffusion of Mg from bottom waters into the sediment.

We would point out, however, that while metal accumulation rates in the Bauer Depression are lower than the EPR crest, the sea floor located between the crest and Bauer Depression is accumulating heavy metals at a rate even lower than the Bauer Depression by an order of magnitude (20). Therefore, accumulation rates do not necessarily preclude local hydrothermal activity in the Bauer Depression.

5.4. Mid-plate Hydrothermal Activity

Station 18B apparently represents a local enrichment of metalliferous sediment, which may be accumulating over a wider area. As mentioned earlier, RSO's are a ubiquitous minor component of the Clipperton Oceanic Formation (14) within which core 18B was taken. This unit is time-transgressive, but is locally of Quaternary age, and apparently is actively accumulating between longitude 120° and 130° W and north of latitude 10° N. This constitutes the northeast quadrant of the North Pacific nodule belt (10 and 15). This implies that metal-

liferous sediments are presently accumulating throughout this quadrant, and are not a relic of an earlier time when the local sea floor was close to a zone of sea-floor spreading.

Active mid-plate volcanism may occur on a small scale and locally throughout the Pacific plate. There is evidence of active local volcanoes in addition to the Hawaiian volcanoes on the sea floor of the north Pacific (21). Such local activity should generate the same hydrothermal circulation of seawater envisaged for active spreading centers, and similar metallogenesis might not be unexpected. Station 18B may be in the vicinity of such local volcanism.

The question naturally arises as to the possible relation between the metalliferous sediment and the associated ferromanganese nodules, and at this point there is no obvious answer. The nodules are relatively enriched in Mn, Cu, and Ni and the possibility that these elements might have their origin with the underlying metalliferous sediments seems to be precluded by pore water data. Neither gradients nor abnormally high concentrations of these elements are found. On the other hand, it can be speculated that both have as their ultimate source the same hydrothermal fluid, with separation taking place because of kinetic differences in oxidation and precipitation of Fe and Mn. By this view, the hydrothermal fluid might precipitate a small amount of Mn, Cu, and Ni near the vent along with most of its Fe, and the remainder of these elements may then be dispersed into the water masses to come out at much slower rates and over wider area as nodules and as the hydrogenous component of marine sediments.

SUMMARY AND CONCLUSIONS

6.1. Metalliferous sediment is a major fraction of sediments at station 18B, DOMES Site C, on the basis of close similarity to Bauer Depression sediments in terms of physical properties, water content, mineralogy and bulk chemical composition. The similarity is emphasized when both are corrected for terrigenous impurities.

6.2. Magnesium and silica are variable but important hydrothermal components of metalliferous sediments in general, as indicated by large remainders of these elements and their covariance after pelagic components are subtracted. Some of the silica may be biogenic, but evidence suggests it is minor.

6.3. Accumulation of metalliferous sediment may be widespread throughout the northeast quadrant of the Pacific ferromanganese nodule belt on the basis of ubiquitous occurrence of RSO's throughout the Clipperton Oceanic Formation, of which station 18B represents a local concentration and enrichment.

References

- 1 K. Bostrom and M.N.A. Peterson, Precipitates from hydrothermal exhalations of the East Pacific Rise, *Econ. Geol.* 61 (1966) 1258-1265
- 2 K. Bostrom, The origin and fate of ferromanganoan active ridge sediments, *Stockholm Contr. Geol.* 27:2 (1973) 149-243
- 3 E.J. Dasch, J.R. Dymond, and G.R. Heath, Isotopic analysis of metalliferous sediment from the East Pacific Rise, *Earth and Planet. Sci. Letter* 13 (1971)
- 4 F.L. Sayles and J.L. Bischoff, Ferromanganoan sediments in the Equatorial East Pacific, *Earth and Planet. Sci. Letters* 19 (1973) 330-336
- 5 F.L. Sayles, T.L. Ku, and P.C. Bowker, Chemistry of ferromanganoan sediment of the Bauer Deep, *Bull. Geol. Soc. Amer.* 86 (1975) 1423-1431
- 6 G.R. Heath and J. Dymond, Genesis and diagenesis of metalliferous sediments from the East Pacific Rise, Bauer Deep and Central Basin *Bull. Geol. Soc. Amer.* (in press)
- 7 C.C. von der Borch and R.W. Rex, Amorphous iron oxide precipitates in sediments cored during Leg 5, Deep Sea Drilling Project, Initial Reports of the Deep Sea Drilling Project 5 (1970) 541-544
- 8 D.S. Cronan, T.H. van Andel, G.R. Heath, M.G. Dinkelman, R.H. Bennett, D. Burkey, S. Charleston, H. Kaneps, K.S. Rudolfo, and R.S. Yeats, Iron rich basal sediments from the Eastern Equatorial Pacific: Leg 16, Deep Sea Drilling Project, *Sci.* 175 (1972) 61-63
- 9 J. Dymond, J.B. Corliss, G.R. Heath, C.W. Field, E.J. Dasch, and H. Veeh, Origin of metalliferous sediments from the Pacific Ocean, *Bull. Geol. Soc. Amer.* 84 (1973) 3355-3372
- 10 H.E. Cook, North American stratigraphic principles as applied to deep sea sediment, *Amer. Assoc. Petrol. Geol. Bull.* 59 (1975) 817-837
- 11 J.E. Flipse, Letter to Henry A. Kissinger, Secretary of State; President, Deepsea Ventures Corp., Nov. 14, 1974
- 12 J.Z. Frazer, D.L. Hawkins, L. Hydock, W.L. Crocker, M. Schoenbechler, D.A. Newhouse, and T.E. Chase, Surface sediments and topography of the North Pacific, Geologic Data Center, Scripps Inst. Oceanography, IMR Tech. Report Series TR 29
- 13 The Shipboard Scientific Party, Site 319 Report, Initial Reports of the Deep Sea Drilling Project Vol. XXXIV, U.S. Govt. Printing Office 1973

- 14 Tj. H. van Andel, G.R. Heath, R.H. Bennett, J.D. Bukry, S. Charleston, D.S. Cronan, M.G. Dinkleman, A.G. Kaneps, K.S. Rodolfo, and R.S. Yeats, Shipboard Site Report, Site 159, Initial Reports of the Deep Sea Drilling Project, Vol. XVI, U.S. Govt. Printing Office 1972
- 15 Tj. H. van Andel, G.R. Heath, and T.C. Moore, Cenozoic History and paleoceanography of the Central Equatorial Pacific Ocean, Geol. Soc. Amer. Mem 143 (1975) 134
- 16 J.L. Bischoff and F.L. Sayles, Pore fluid and mineralogical studies of recent marine sediments: Bauer Depression Region of East Pacific Rise, Jour. Sed. Petrol. 42 (1973) 711-724
- 17 S. Brady and J.M. Gieskes, Interstitial water studies, Leg 34, Initial Reports of the Deep Sea Drilling Project Vol. XXXIV, 625-628 U.S. Govt. Printing Office 1976
- 18 J. Dymond, J.B. Corliss, and R. Stillinger, Chemical composition and metal accumulation rates of metalliferous sediments from Site 319, 320, 321, Initial Reports of the Deep Sea Drilling Project Vol. XXXIV, 575-588 U.S. Govt. Printing Office
- 19 J.L. Bischoff and F.W. Dickson, Sea water-basalt interaction at 200⁰C and 500 bars: Implications for origin of sea floor heavy metal deposits and regulation of sea water chemistry, Earth and Planet. Sci. Letters 25 (1975) 395-397
- 20 J. Dymond and H.H. Veeh, Metal accumulation rates in the Southeast Pacific and the origin of metalliferous sediments, Earth and Planet. Sci. Letter, 28 (1975) 13-22
- 21 B.P. Luyendyk, Origin and history of Abyssal Hills in the NE Pacific Ocean, Bull. Geol. Soc. Amer. 81 (1970) 2237-2260
- 22 S. Landergren, On the geochemistry of deep-sea sediments, Reports of the Swedish Deep-Sea Expedition, Vol. X, Special Investigations, No. 5 (1964) 61-148
- 23 E.D. Goldberg and G.O.S. Arrhenius, Chemistry of Pacific pelagic sediments, Geochem. et Cosmochim. Acta 13 (1958) 153-212
- 24 N.M. Strakhov, Types of manganese accumulation in present day basins: their significance in understanding of manganese mineralization, Int. Geol. Rev. 8 (1966) 1172-1196
- 25 J.L. Mero, The mineral resources of the sea, Elsevier, N.Y. (1965) 312
- 26 R. Chester, Elemental geochemistry of marine sediments, In: Riley and Skirrow, Eds., Chemical Oceanography 2 (1965) 23-80
- 27 E. Bonatti and O. Joensuu, Deep sea iron deposit from the South Pacific, Sci. 154 (1966) 643-645

TABLE 1
Chemical composition of sediment from stations 18B and 20, Pacific pelagic clay, and metalliferous sediment from Bauer Depression, and basal DSDP.

	DOMES ¹ Station 18B (34-36 cm)	DOMES ¹ Station 20 (13-18 cm)	Bauer Depression ² Metalliferous Sediment	Basal DSDP ³ Metalliferous Sediment	Pacific ⁴ Pelagic Clay
SiO ₂	49.95	52.43	44.08	17.27	54.9
Al ₂ O ₃	8.77	16.18	4.42	5.99	16.6
Fe ₂ O ₃	13.00	7.48	19.27	38.61	7.7
MnO	5.58	0.84	4.77	6.24	1.68
MgO	4.25	3.15	3.84	1.79	3.4
CaO	2.32	1.27	1.70	-	0.72
TiO ₂	0.50	0.79	0.10	-	0.78
Na ₂ O	0.74	2.70	0.99	-	1.3
K ₂ O	2.33	3.43	0.96	-	2.7
CuO	0.16	0.07	0.12	0.15	0.09
NiO	0.08	0.03	0.12	0.06	0.026
Ignition Loss (1000°C)	11.74	10.10	-	-	-
Total	99.96	98.74	80.37 ⁵	70.11 ⁵	89.89 ⁵

Notes:

1. Samples dried at 110°C.
2. Average of 8 air dried analyses reported by Sayles and Bischoff (4).
3. Average of 6 samples (DSDP sites 37-39) reported by Dymond et al (9).
4. Si, Al, Fe, Mn, Mg, Ca, Ti, Na, K, and Ni from Landergren (22).
Cu from Goldberg and Arrhenius (23).
5. Summation less than 100 per cent due to missing components or lack of ignition loss data.

TABLE 2

Corrected composition of metalliferous sediment from 18B, Bauer Depression and basal sediments, DSDP. Terrigenous material, CaCO_3 and interstitial salts have been subtracted from analyses listed in Table 2, and remainder normalized to 100 %

	<u>DOMES Station 18B (34-36 cm)</u>	<u>Bauer Depression Metalliferous Sediment</u>	<u>Basal DSDP Metalliferous Sediment</u>
SiO_2	54.92	54.21	0
Al_2O_3	0	0	0
Fe_2O_3	23.34	31.65	84.90
MnO	12.28	7.94	13.36
MgO	6.40	5.38	1.32
CaO	0	0	0
TiO_2	0.23	0	0
Na_2O	0	0	0
K_2O	2.35	0.42	0
CuO	0.29	0.18	0.28
NiO	0.17	0.20	0.12
Total	<u>100.00</u>	<u>100.00</u>	<u>100.00</u>

Figure Captions

Figure 1.

Location of stations 18B and 20 DOMES Site C, and DSDP holes 159 and 160. (18B: $15^{\circ} 12.2'N$, $126^{\circ} 58.6'W$, 4295 m. 20: $15^{\circ} 59.3'N$, $126^{\circ} 11.6'W$, 4702 m.)

Figure 2.

Fe/Ti versus Al/(Al + Fe + Mn) (after Bostrom, reference 2) showing compositional relationship of sediment from 18B and 20 to terrigenous matter (TM), basaltic debris (B) and metalliferous sediment from East Pacific Rise (EPR).

Figure 3.

Al-Fe-Mn triangular diagram (after Dymond et al., reference 18) relating sediment composition of 18B and 20 to Pacific pelagic sediments, Nazca plate nodules, and metalliferous sediments of the Bauer Depression and East Pacific Rise.

Figure 4.

Fe/Mn versus Cu + Ni showing compositional relationship between sediment from 18B and 20 to Pacific nodules, pelagic sediments, and metalliferous sediments.

Figure 5.

Relationship between silica and magnesium for Pacific metalliferous sediments corrected for terrigenous matter, calcium carbonate, and interstitial salt.

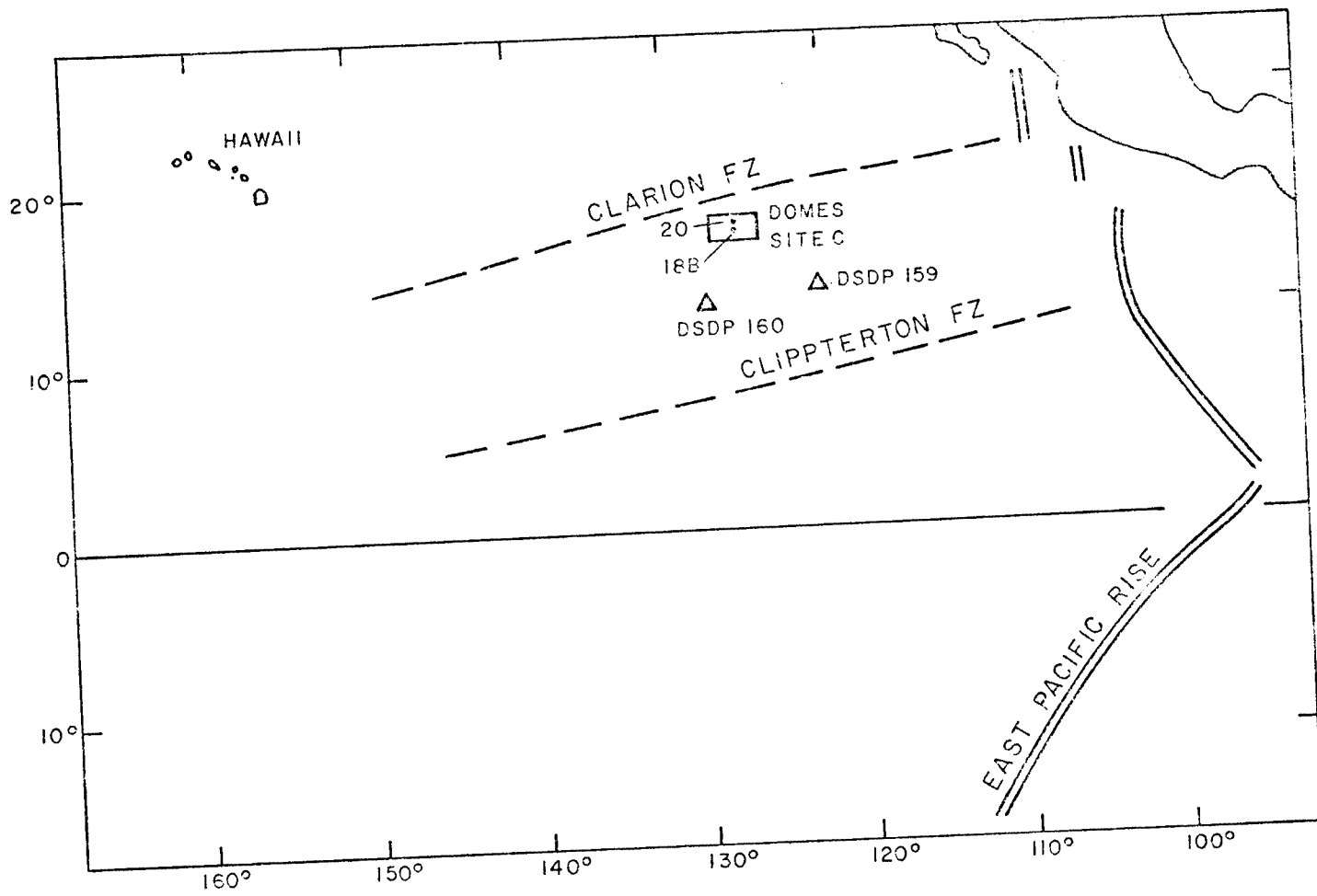


Figure 1

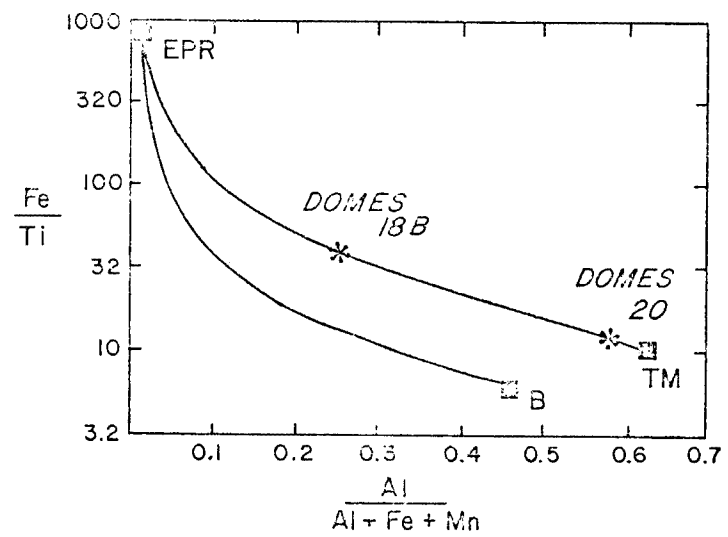


Figure 2

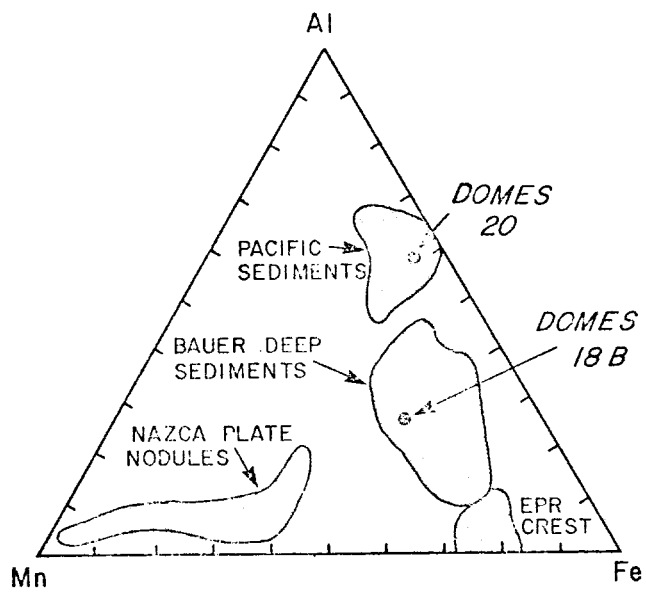


Figure 3

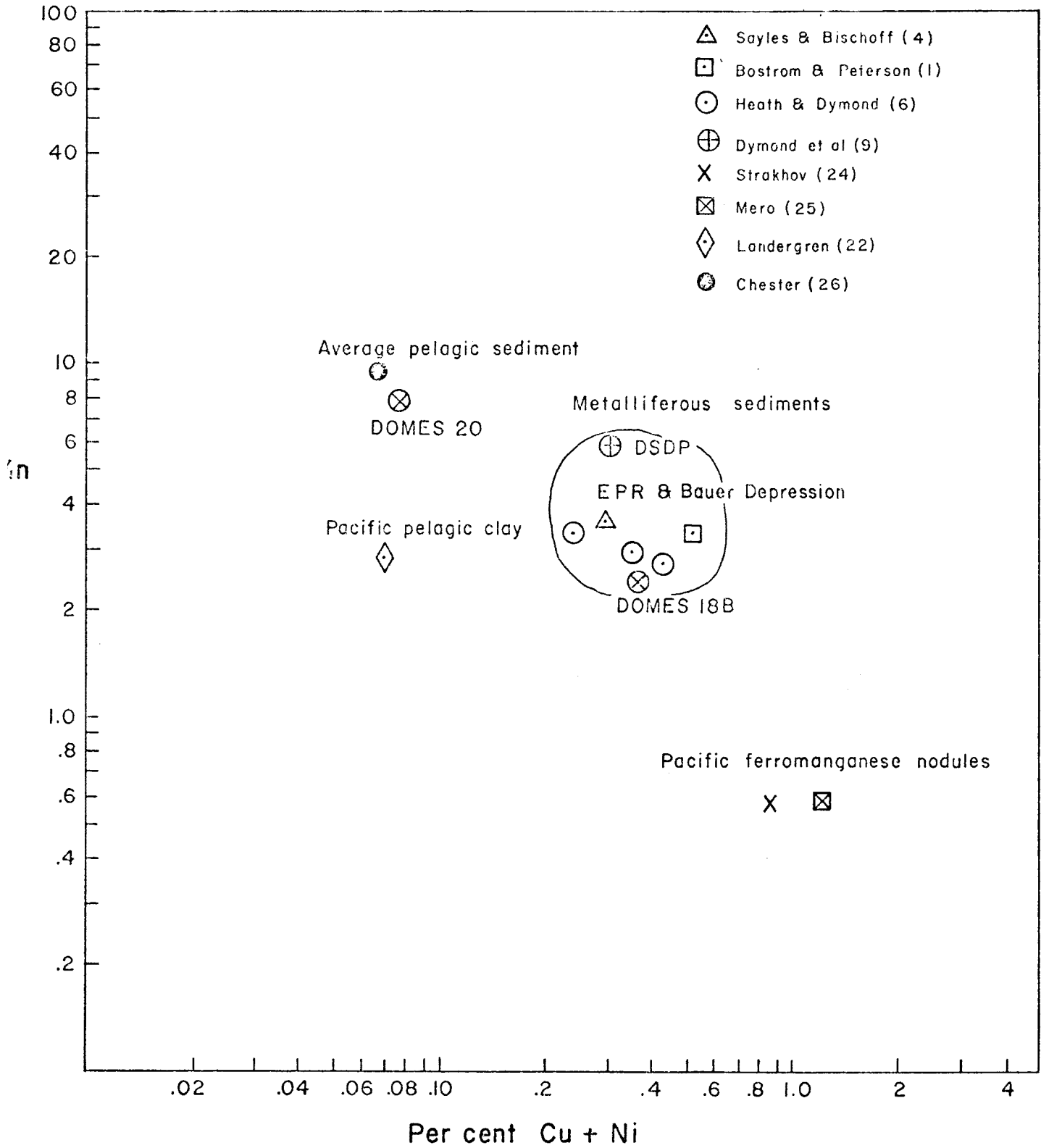


Figure 4

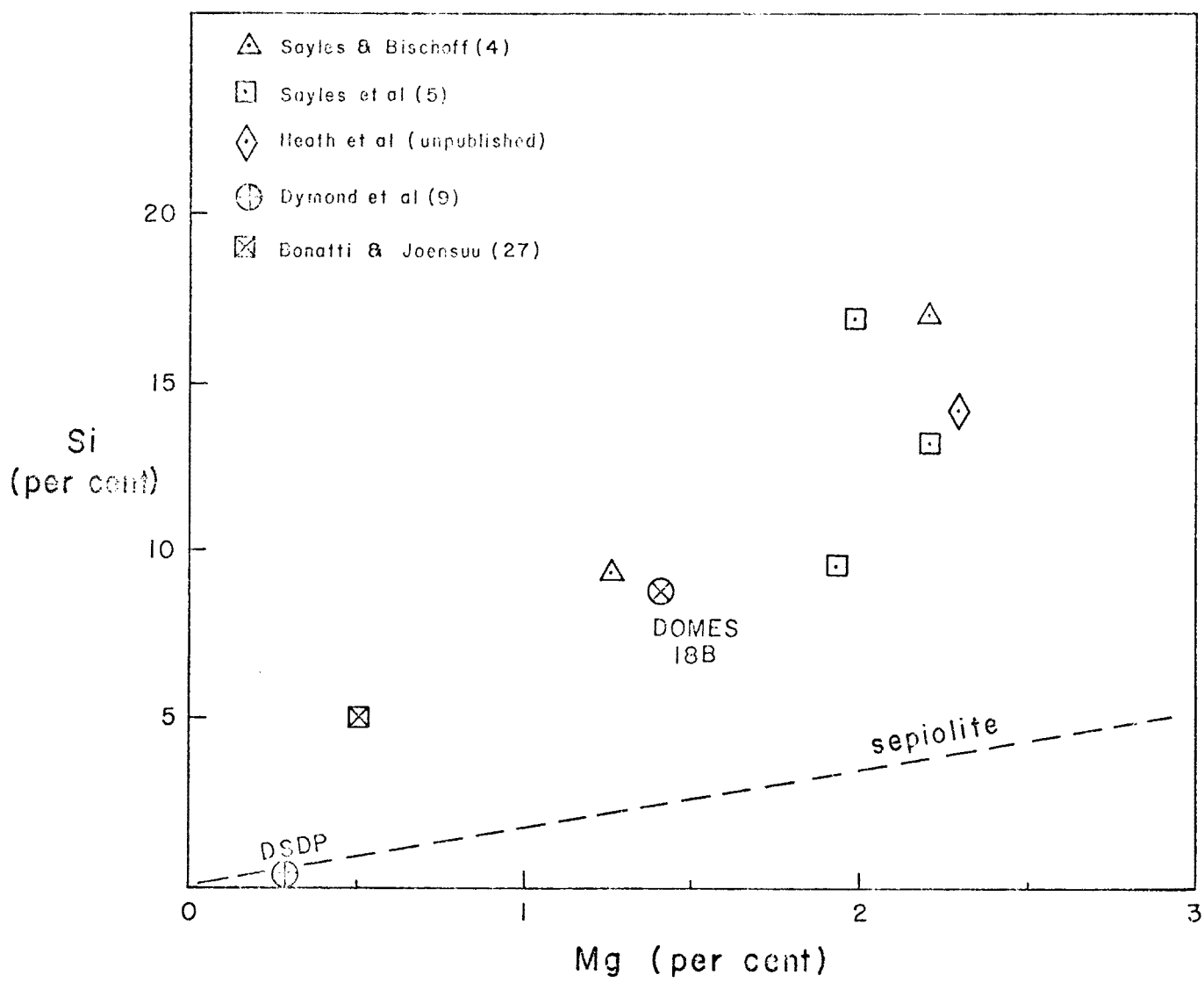


Figure 5

MICROFEATURES OF TYPICAL MANGANESE NODULES FROM

SIX BOX CORES FROM NOAA CRUISE RP6-OC-75

by R. K. Sorem and D. L. Banning, Washington State University
Pullman, Washington

INTRODUCTION

In 1975 Washington State University was contracted by the U. S. Geological Survey to conduct a study of manganese nodules collected during cruises of the DOMES project of NOAA. The nodule research was to be restricted to problems related to DOMES objectives and was not to include a study of problems of nodule distribution and origin. The project was to be coordinated with mineralogical and chemical investigations carried out simultaneously in Geological Survey laboratories.

In July 1975 R. K. Sorem and D. L. Banning sampled 8 subcores (20 x 30 cm in horizontal cross-section) of bottom sediment taken earlier by U.S.G.S. personnel from 50 x 50 cm box cores on board OSS Oceanographer. The subcores had been kept in cold storage at the University of Washington following completion of Leg 2 of NOAA cruise RP6-OC-75. In October and November, 1975, Sorem and Banning took part in Leg 3 of NOAA cruise RP8-OC-75 and sampled 62 large box cores on board ship.

This report concerns only the RP6-OC-75 samples. The RP8-OC-75 samples will be described in a later report.

GENERAL

When exploitation of marine manganese nodule deposits is well under way, millions of tons of nodules will be lifted to the surface annually. While there is little doubt that there will be widespread disturbance of the bottom mud during dredging, little is known of the effects on the nodules of collection and transportation. Since they are by far the most metal-rich objects to be raised through the water column, they should be closely studied so that predictions of some sort can be made regarding contributions they might make to the degradation, both chemical and physical, of the environment.

Manganese nodules are known to be very porous and fragile, but few data are available which will allow prediction of nodule behavior during mining. We can only say that probably much breakage will occur when they are dredged in large quantities. In this report we present data which will provide a better understanding of typical nodules from the study area, and we predict the manner in which nodules of this type will react to the agitation produced by dredging.

The body of the report describes the nature of the major types of surface features of nodules and includes numerous illustrations of typical nodules. To provide a wider coverage of nodule types in the collection, and to record some of the gross physical data on the nodules, an illustrated Appendix is also included.

Parts of the nodules described in this report, as well as others, have been supplied to the U. S. Geological Survey for mineralogical and chemical research. This chapter describes only the work done at W.S.U., however.

SCOPE OF THE PROJECT

Special emphasis was placed upon the study of the outer "crustal zone" of the nodules, for this outer few millimeters of most nodules will probably be more severely affected by mining than the inner parts. Less study was given the many internal fractures so common in Pacific Ocean deep sea nodules, although it is along these fractures that nodules commonly break, inevitably exposing the clay and metal oxide filling to sea water. These fractures are illustrated in the Appendix in nodule sections. The sections also reveal features like gross layering, mineralogical relationships, and general nodule variability in the area under study.

The basic approach was to examine thoroughly the large and small external and internal features of selected manganese nodules. The fundamental steps were binocular microscope study of exteriors, preparation of high-quality polished cross-sections of whole nodules, and study of sections with the ore microscope. A small amount of time was devoted to X-ray diffraction and macroprobe analysis to verify optical findings.

PROCEDURE

Collection data for the six box cores from which samples were obtained are summarized in Table 1. In addition to NOAA station numbers, location, and depth, the W.S.U. locality number and nodule numbers are given.

Table 1

<u>W.S.U. Locality and Nodule Numbers</u>	<u>NOAA Station</u>	<u>Latitude</u>	<u>Longitude</u>	<u>Depth (m)</u>
NP 59-1 to 40	11	16° 0.7' N	126°46.3' W	4603
NP 60-1 to 16	15B	15°45.7' N	126° 0.4' W	4552
NP 60A-1 to 10	15B	15°45.7' N	126° 0.4' W	4552
NP 61-1 to 20	16B	15°46.7' N	126°11.2' W	4552
NP 61A-1 to 12	16B	15°46.7' N	126°11.2' W	4552
NP 62-1 to 3	23B	14°45.9' N	125°58.6' W	4667
NP 63-1 to 14	25	14°14.1' N	124°58.7' W	4561
NP 64-1 to 14	27	16° 0.05' N	124°59.6' W	4406
				*Est.

The subcores removed from the original box cores were given the same number as the original core. This number is the same as the station number. At stations 15B and 16B, two subcores were taken and were labelled box 1 and box 2 in each instance. The physical condition of the subcores when they were opened for sampling ranged from good to poor, with respect to apparent degree of surface disturbance, as shown in figures 1 and 2.

After the tops of the subcores were photographed, about one-half of the nodules exposed at the surface were removed. The remainder were left for the use of U.S.G.S. personnel. All nodules which appeared to have been undisturbed were packed for shipment with the original orientation (top vs. bottom) preserved. A few nodules were removed with bottom sediment intact by coring with short plastic tubes (see Appendix). The original location of each nodule removed was marked on overlays of Polaroid photographs of the subcores at the time of removal. After nodule removal, subcore tops were again photographed (figure 3).

In the laboratory at Pullman, all nodules except those cored with sediment intact were washed with a squeeze bottle to expose most of the nodule surface. Washings from the nodules were saved for later study. After washing, the nodules were air-dried at about 20° C for one week or more. All nodules were then examined by use of a binocular microscope, and 30 were selected from the original collection of 129 nodules for detailed study. At least two nodules were studied from each subcore. Distribution of nodules studied is shown in Table 2.

Table 2

<u>W.S.U.</u> <u>Locality</u>	<u>NOAA</u> <u>Station</u>	<u>Nodules</u> <u>Collected</u>	<u>Nodules Studied</u> <u>in Detail</u>
NP 59	11	40	4
NP 60	15B	16	3
NP 60A	15B	10	4
NP 61	16B	20	5
NP 61A	16B	12	4
NP 62	23B	3	2
NP 63	25	14	3

Each of the 30 nodules selected as representative was examined by use of a Wild M-7 binocular microscope at magnifications up to 100x. External features were photographed on 35 mm film. After this study, one or more small chips were removed from the outer surface of each nodule and filed for later SEM and X-ray diffraction work. Each nodule was then cast in cold-setting resin, sawed, and polished for use with the ore microscope. One-half of each nodule was left untouched by resin, if possible, and sent to the U.S.G.S. for their use.

All polished sections were photographed with vertical illumination as an aid to further microscope study. Each polished section was examined by use of a Leitz Ortholux ore microscope, with special emphasis on the textures and mineralogy of the crustal zone. Mineralogy determined by use of polarized light was verified by X-ray diffraction analysis of microsamples, using gelatin fiber mounts, 57.3 mm diameter Debye-Scherrer

cameras, and Fe $K\alpha$ radiation. In addition, several semi-quantitative chemical analyses were made by use of a Philips X-ray macroprobe. Both polished nodule sections and compressed powder samples were used in the macroprobe work.

RESULTS

Surface Textures.

The external morphology of a manganese nodule is here defined as the general outward shape of the object, and the much smaller structures superimposed on the outer surface are called textural features. Although morphology is the basis for a broad classification of manganese nodules, a discussion of this topic is beyond the scope of this report. A general idea of the variety of nodule morphologies in the collection under study may be gained by examining the subcore surface shown in figure 4.

Surface textural features were considered to be of prime importance in this investigation because they are generally fragile and probably will be greatly abraded when nodules are agitated en masse during mining. Furthermore, like the internal parts of nodules, they are metal-rich and have a very high porosity. It might therefore be suspected that the outer parts of nodules will contribute much fine-grained material to the sea water during mining, and that these finer may be sources of chemical pollution due to partial dissolution. It has been shown by Rancitelli and Robertson (IDOE Phase I Report, 1973) that some dissolution of Fe, Co, and Zn is to be expected, and some removal of Cu, Ni, Hg, and Cd may occur. Quantitative data based upon projected mining conditions are sorely lacking, however, and much more experimental work is needed. In addition, sea water and nodule fines should be sampled in the area of a large scale mining test, and analyses of water, fines, and mined nodules should be compared and evaluated.

The interpretation of any empirical studies of the types mentioned would be difficult, however, unless base line nodule data were available. Part of the necessary data on surface textures and internal features is included in this section.

Close megascopic examination generally reveals tiny black or gray rounded forms covering external nodule surfaces. They are commonly called botryoids in allusion to the similarity to the appearance of a bunch of grapes, but microbotryoid is more appropriate for the minute features under discussion, most of which are smaller than 0.2 mm. In the collection under study, two different types of microbotryoid may be distinguished easily by external form. The characteristic features of each are best seen with the binocular microscope. "Hemispherical" microbotryoids appear like so many rounded domes, some elongate, covering the nodule surface. In contrast, "dendritic" microbotryoids are very irregular in detail, have a large height to width ratio, and resemble branching shrubs or trees in a general way (figures 5, 6, 7). Both types show a glistening black finely irregular surface at high magnification

Manganese nodules in this collection rarely show only one of these surface textures. As is the case with most Pacific Ocean deep sea nodules, both are usually found on a single nodule, commonly on opposite sides. For example, an asymmetrical nodule (discoid or ellipsoidal) generally shows a top surface covered with hemispherical microbotryoids and a bottom surface studded with dendritic forms. The most elongate dendritic forms are commonly around the equatorial zone (the level of the sediment-water interface). The net effect of these features is to produce nodules which feel smooth (hemispherical texture) or gritty (dendritic) to the hand. Low and high magnification photographs of the top and bottom of a nodule from station 23B are shown in figures 7 and 8. In comparing these photographs and those in figures 5 and 6, note that all low-power photographs have the same magnification (16x on original manuscript), as do the high magnification pictures (84x).

It is important to recognize the significance of the basic physical nature of the two types of textural features in terms of the inherent resistance of the forms to breakage. Hemispherical forms are relatively durable when a nodule is handled or allowed to roll about in a specimen tray. In contrast, dendritic forms under the same conditions are very friable and are easily broken off or reduced to powder. The difference is not particularly evident in the photographs of the top and bottom of the nodule shown in figure 9, but the fragile nature of the bottom dendritic texture is emphasized when broken dendrites are viewed from the side, as in figure 10. As discussed later in this report, these differences in strength are of prime importance in determining the chemical character of the bulk of the fines which can be expected to result during dredging of nodules.

Internal Features

The study of internal features of nodules concentrated chiefly on the mineralogy and microstructure of the surface features already described. Although the magnification is different from that of the binocular microscope photographs, the cross-sections of the hemispherical forms and the dendritic forms (figure 11) clearly correlate with the surface features of the same nodule (figure 9) and the dendrites shown in figure 10. Obviously, the internal structure of these features is very different, and the ore microscope reveals much more structural detail than does the binocular. Dendrites clearly have the less massive structure.

Another advantage of the ore microscope which is not readily apparent is that mineralogical differences between the two features can be recognized readily, particularly if polarized light is used. The oxides which make up the hemispherical features are thus found to be isotropic and consist largely of amorphous iron-rich compounds, whereas the dendritic forms are chiefly anisotropic oxides which have the properties of the manganese minerals todorokite and birnessite in cryptocrystalline intergrowths. It should be emphasized, however, that in neither type of feature is the oxide pure, and thin layers of one oxide in the other are common.

The determination of mineralogy by optical methods is especially important in this kind of a nodule investigation, for recognition of the minerals and their distribution is tantamount to determining the general distribution of chemical elements in nodules. It is well established that Cu and Ni are concentrated with manganese in the crystalline oxides in marine nodules, and macroprobe analyses on polished section NP 59-23 verified this association (see section on Fines Produced by Abrasion). It is reasonable to conclude, therefore, that dendritic microbotryoids, the most fragile structures on the surface of the nodules under study, are composed largely of oxides rich in manganese, copper, and nickel.

Mineralogy

An exhaustive mineralogical study was not within the scope of the project, but 16 microsamples representing 8 nodules were analyzed by X-ray powder camera diffraction methods. Most of the samples gave patterns showing todorokite the chief mineral. Birnessite was found to be a minor component in 8 samples, judging from the intensity of the line at about 7 Å. In one sample, amorphous oxides alone were detected. Several of the other samples produced both amorphous scattering and lines from the crystalline oxides.

The samples analyzed were removed from small pieces of the top and bottom of each of the 8 nodules. The prevalence of crystalline oxides in the samples from the upper surface of nodules was unexpected because many polished sections show abundant amorphous oxides at the top. The results illustrate the intimate association of very fine-grained oxides of different types in nodules, the optical detection of which requires careful study at high magnifications with the ore microscope. The samples described above were prepared with the aid of only a low-power binocular microscope.

Fines Produced by Abrasion

The foregoing data on the nodule collection under study lead to the conclusion that nodules of the types represented, when abraded by each other during dredging, would probably yield abundant fines and to a much lesser degree angular nodule fragments. It would be logical to expect, furthermore, that the fines would consist predominantly of broken dendritic microbotryoids, and that therefore the fines would have a chemical composition not unlike that of the crystalline oxides found in most nodules.

In an effort to explore these problems of nodule abrasion in a preliminary way, an experiment was conducted with a collection of wet nodules which had been stored in sea water in a plastic bag for nearly a year. Although not from the DOMES cruise collection, the nodules were dredged in the same general region (latitude $14^{\circ}53'$ N, longitude $124^{\circ}26'$ W) and at a similar depth (4352 m) by Deepsea Ventures in June 1975. The bag was agitated gently perhaps a dozen times prior to May 1976, when it was opened for sampling. At that time a random sample of fines was collected from the bottom of the bag by use of a pipet. Care was taken not to crush the particles when they were sampled, and screening was not attempted because of their low strength. After the wet fines were deposited in two Petri dishes, however, they were 'panned' to separate sizes in a rough way before they were allowed to dry at room temperature.

After the fines were dry, small random samples were taken for X-ray diffraction and X-ray macroprobe analysis. The diffraction patterns of the three samples taken as representative of fine, medium, and coarse particles showed virtually pure todorokite. Macroprobe semi-quantitative analyses of the same three types of material, as described below, gave results compatible with this identification. The macroprobe samples were larger (20 mg vs. less than 1 mg), however, and contained admixed Fe-rich oxides.

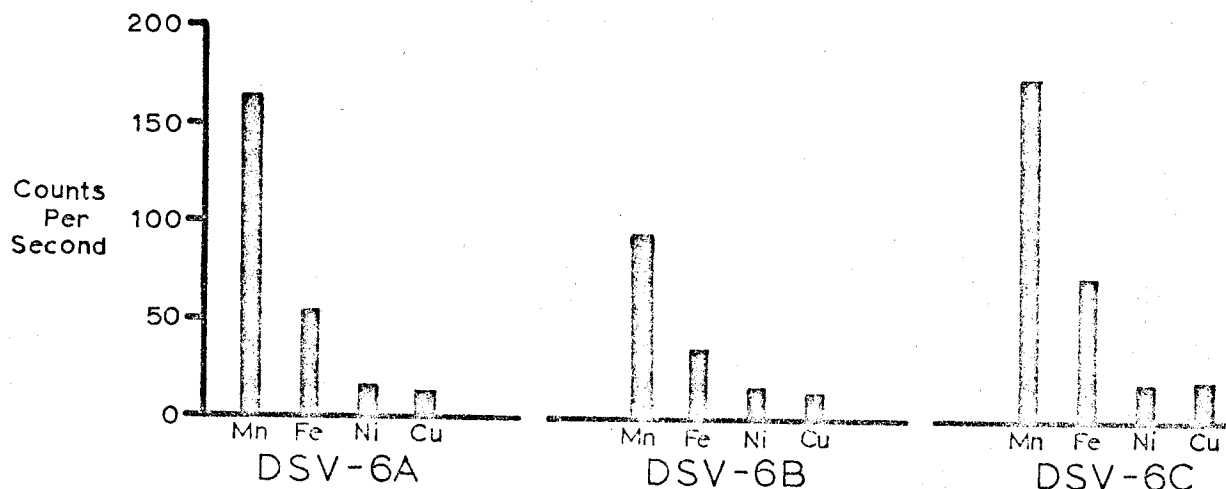
The samples were prepared for macroprobe analysis by grinding to about 200 mesh in a mullite mortar. Three 4.5 mm holes were drilled in a plastic block, and each powdered sample was packed into a hole with a small amount of liquid plastic binder. When the samples were hard, the surface was ground flat, rough polished, and placed in the spectrograph. Count rates were then recorded for Mn, Fe, Ni, and Cu for each sample, with the tube power constant. Count ratios were then calculated for Fe/Mn, Ni/Mn, and Cu/Mn. Count rates and count ratios are shown in Table 3.

Table 3 shows that Mn is the chief component, Fe next most abundant, and Ni and Cu less and approximately equal. Concentrations cannot be given because no standard was employed. The count ratios show, however, that metal concentrations in all three samples are very similar; the differences are attributed to inhomogeneity of the powdered samples. The effects of enhancement and absorption on the ratio results are considered negligible because of the small range in composition of samples.

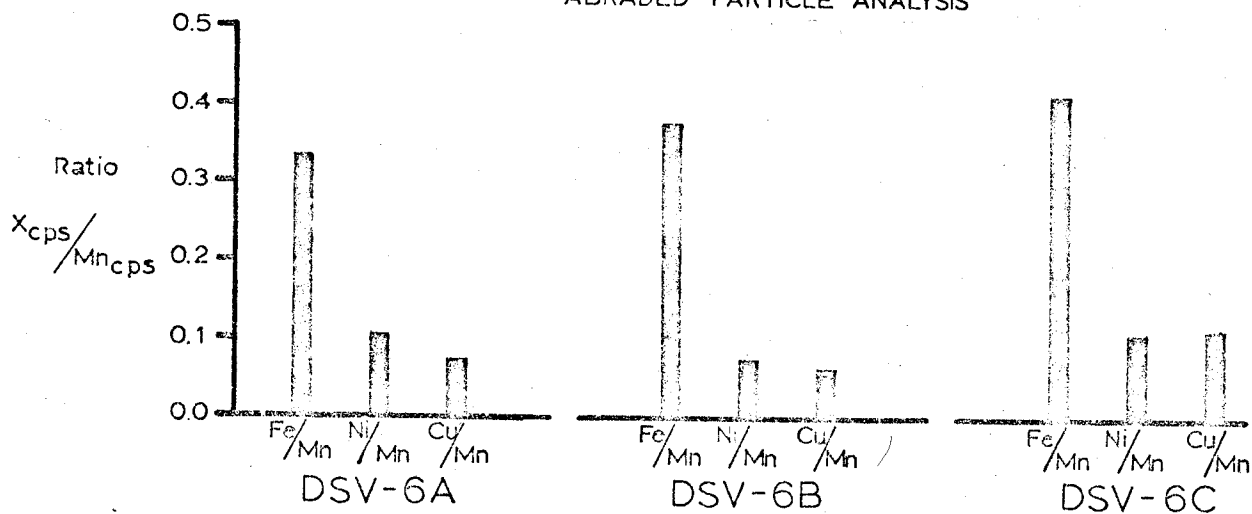
To compare the metal ratios in the fines with those of crystalline oxides in nodules, a polished section of a small nodule from the same Deepsea Ventures dredge haul was analyzed. An area consisting of anisotropic oxides was selected under the ore microscope and centered in the macroprobe. Count rates were determined in the same manner as that used for the powdered fines, and count ratios were calculated. The results, shown in Table 3 are very similar to those for the fines. For comparison, a nodule from the DOMES collection (NP 59-23) was similarly studied. The anisotropic oxides from NP 59-23 also showed metal count ratios closely approximating those of the fines. It seems reasonable to state, therefore, that the fines under study have a composition much like that of the crystalline oxides of nodules in the RP6-OC-75 cruise region.

These data do not reveal, however, whether or not the metal ratios of whole nodules differ from those of the fines, and for that reason, a powdered representative split of an analyzed bulk sample of nodules

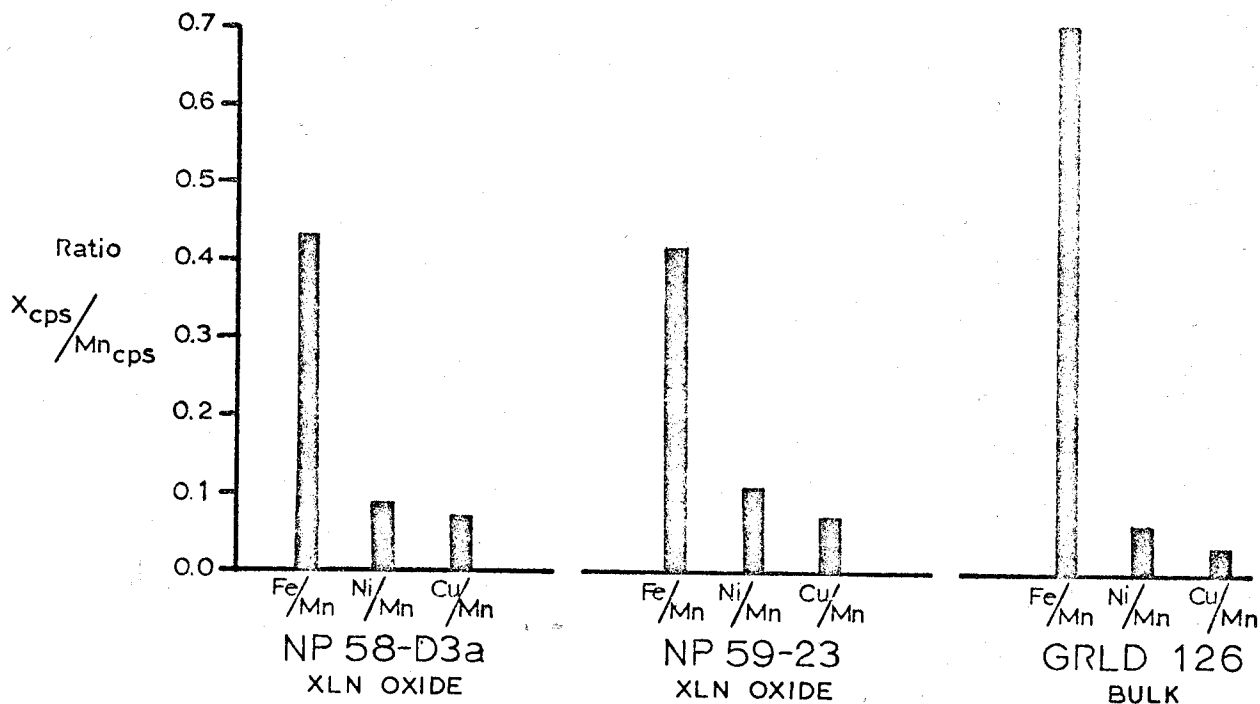
METAL RATIOS IN NODULE MATERIALS



ABRADED PARTICLE ANALYSIS



ABRADED PARTICLE RATIO



NODULE RATIO

was also analyzed. The bulk sample was GRLD 126, prepared, analyzed, and distributed by Kennecott Exploration in 1973 for use in inter-laboratory calibration in connection with the IDOE Seabed Assessment Program. The results of macroprobe analysis of this sample are also presented in Table 3. It can be seen that the Fe/Mn ratio is higher than that of the fines, and that the Ni/Mn and Cu/Mn ratios are lower. This is taken to support the observation that the fines consist chiefly of crystalline oxides, so that the result of random abrasion of nodules is to produce a concentrate of fines which by comparison with whole nodules are richer in Mn, Ni, and Cu and poorer in Fe.

Additional experiments with nodules and associated fines are to be carried out in the future. The work will include quantitative analyses of sufficient scope to test the validity of the count rate ratio method described above, and it will be broadened to include analyses for other elements (e.g. Zn and Co) and size distribution studies of the fines.

SUMMARY

The examination of 129 manganese nodules from 6 box cores obtained on DOMES cruise RP6-OC-75, and the detailed study of 30 nodules selected as representative of the group, reveal that abrasion of this type of nodules in sea water produces fine-grained debris rich in Mn, Ni, and Cu. Furthermore, Fe content of the fines is lower than that of whole nodules, with the result that the fines constitute a metal concentrate with respect to Mn, Ni, and Cu compared to the nodules which yield them. The reasons for this selective concentration are found in the microstructures on nodule external surfaces. Most nodules are encrusted partly with smooth iron-rich microbotryoids on one side (top) and finely irregular Mn-rich dendritic microbotryoids on the other (bottom) and on the sides. The Mn-rich structures are far more delicate than the Fe-rich forms, and during abrasion of whole nodules they are removed at a much faster rate than the latter.

Pollution danger from the fines produced by nodule abrasion cannot be evaluated from the data at hand. Quantitative analyses of representative fines are needed, as are size distribution studies. In addition, tests should be made of the areal dispersion of the fines in sea water, and dissolution experiments on fines of different sizes should be carried out. Until the completion of these and other tests, there is no way to know whether the production of nodule fines during deep sea mining will be harmful or beneficial to the environment.

ACKNOWLEDGMENTS

This work was carried out under U. S. Geological Survey Contract No. 14-08-0001-15245, and we thank the Survey for this support. In addition, we thank the assistants who helped with the laboratory research, including Clarence Johnson, Kaia Sorem, and Jeff Davis. Helpful discussions were contributed by James Bischoff and R. H. Fewkes. Barry Erickson was most helpful during the initial sampling of the subcores, and we appreciate his assistance.

Figure 1.

A. Top surface of subcore from station 11 before sampling. Scale is about 16 cm long. Except for minor slumping at the right, this subcore appears to be essentially undisturbed. Compare the surface after removal of nodules, as shown in figure 3.

B. Top surface of subcore from station 16B before sampling. Scale is about 16 cm long. This subcore also shows little disturbance. Thin coating of mud on top of some nodules is probably due to sloshing of supernatant water in original box core while on deck.

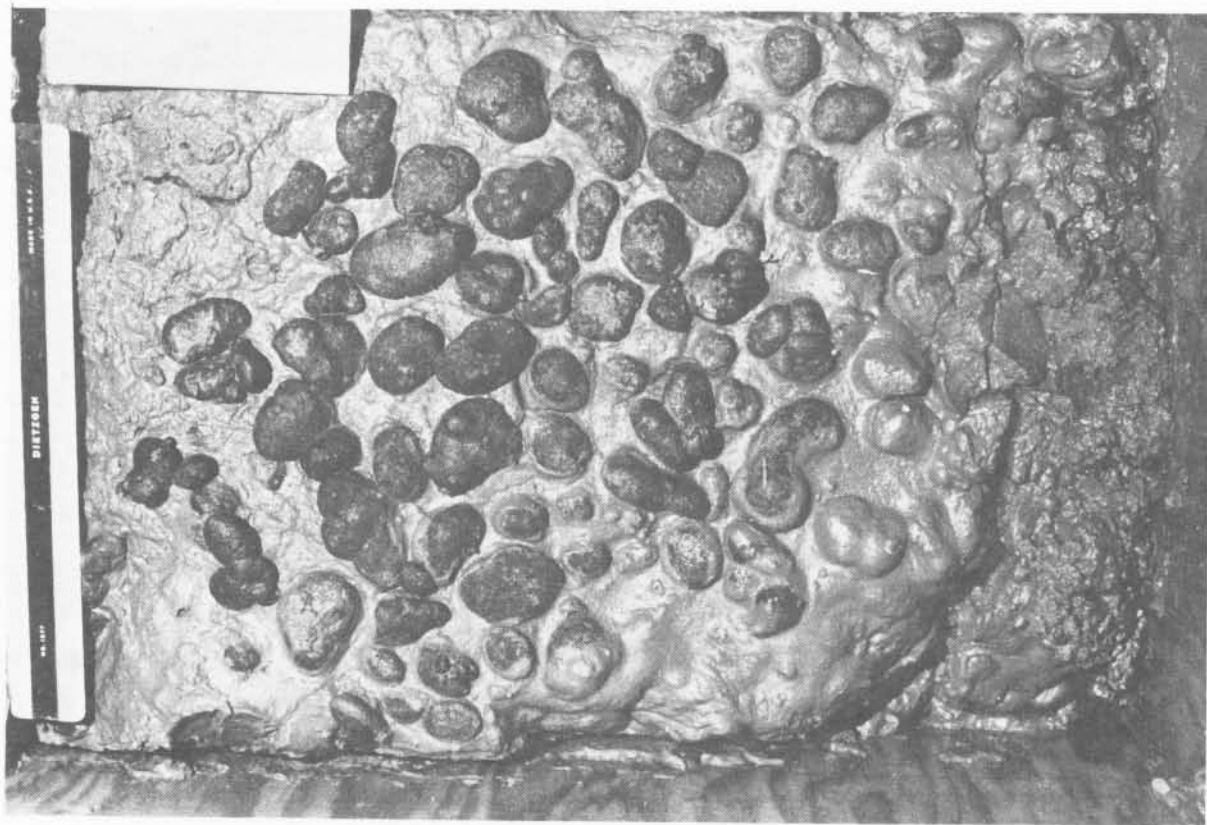


Figure 1A

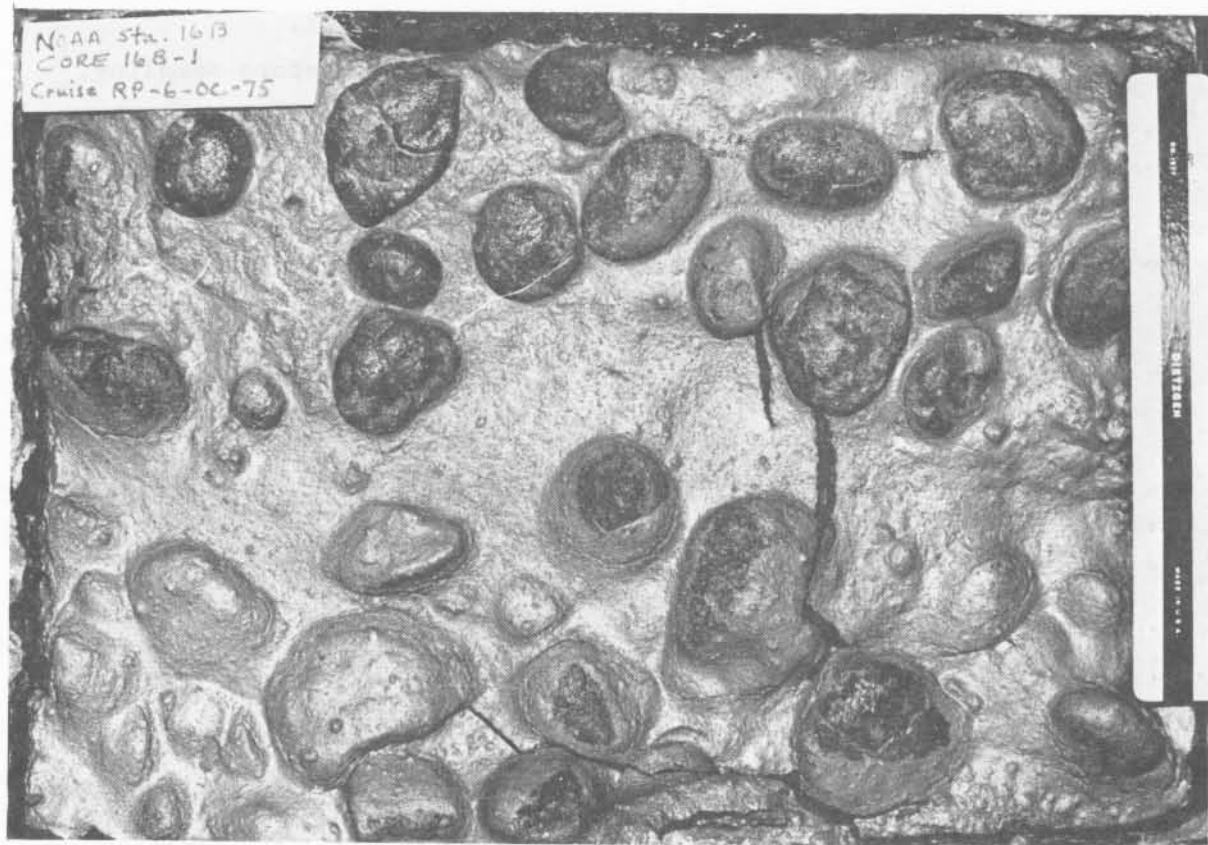


Figure 1B

Figure 2.

A. Top surface of subcore from station 23B before sampling. Disturbance of the subcore during recovery is suggested by the appearance of the mud, which appears to contain broken slabs of soft sediment and/or show indications of substantial agitation. A few nodules are buried in the mud at the right. Orientation of nodules collected from a subcore of this type is uncertain with respect to original position on the sea floor.

B. Top surface of subcore from station 27 before sampling. This subcore also appears to have suffered some disturbance, but most of the area probably contains nodules with the original orientation preserved. Nodules are found under most of the rounded mounds of mud. The mud was spread over the nodules during recovery, to judge from the general appearance.



Figure 2A



Figure 2B

Figure 3.

Top surface of subcore from station 11 after removal of nodules for W.S.U. laboratory research. Round hole marks site of nodule removed with subjacent sediment intact.

Figure 4.

Oblique view of nodules on top of station 11 subcore to illustrate variety of nodule morphology and size. Most of the nodules are sub-round and are generally discoid to ellipsoidal in shape. The largest nodule shown is about 3.5 cm long. All of the nodules show very small surface textural features, resulting in a pitted appearance at this distance.

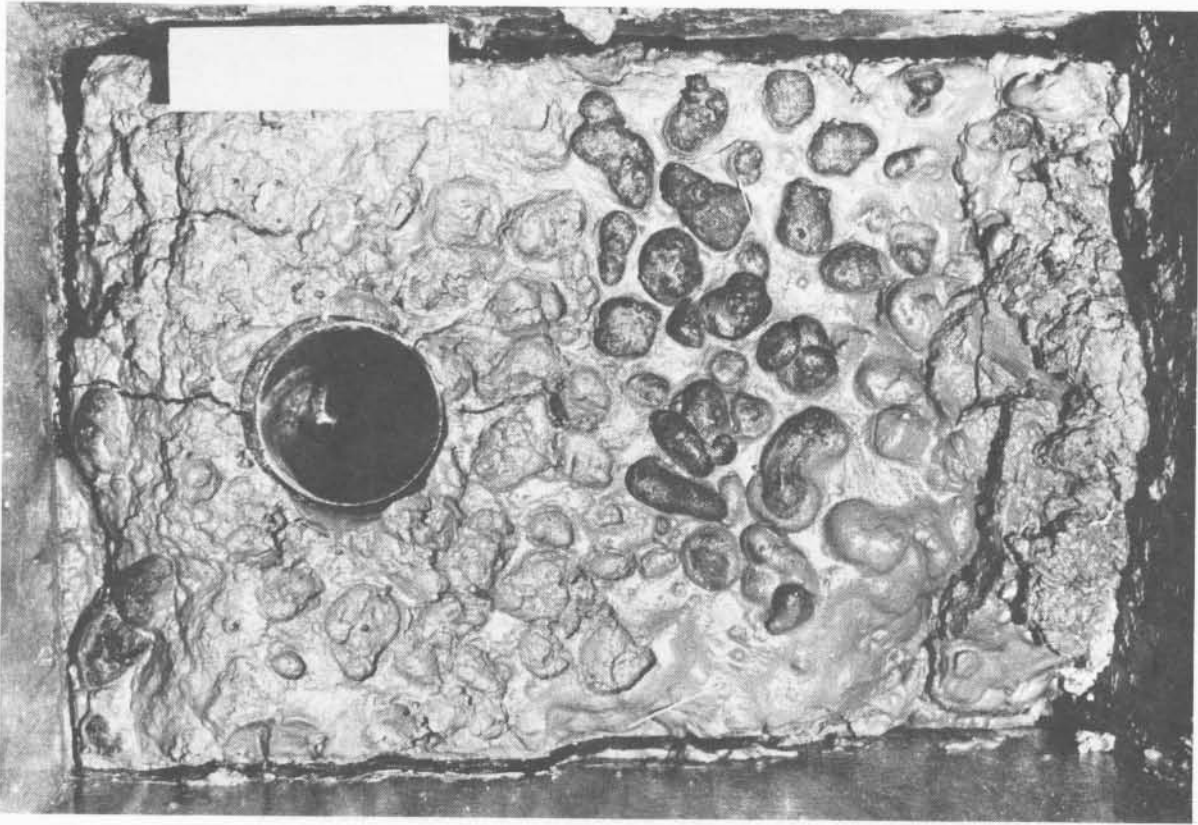


Figure 3

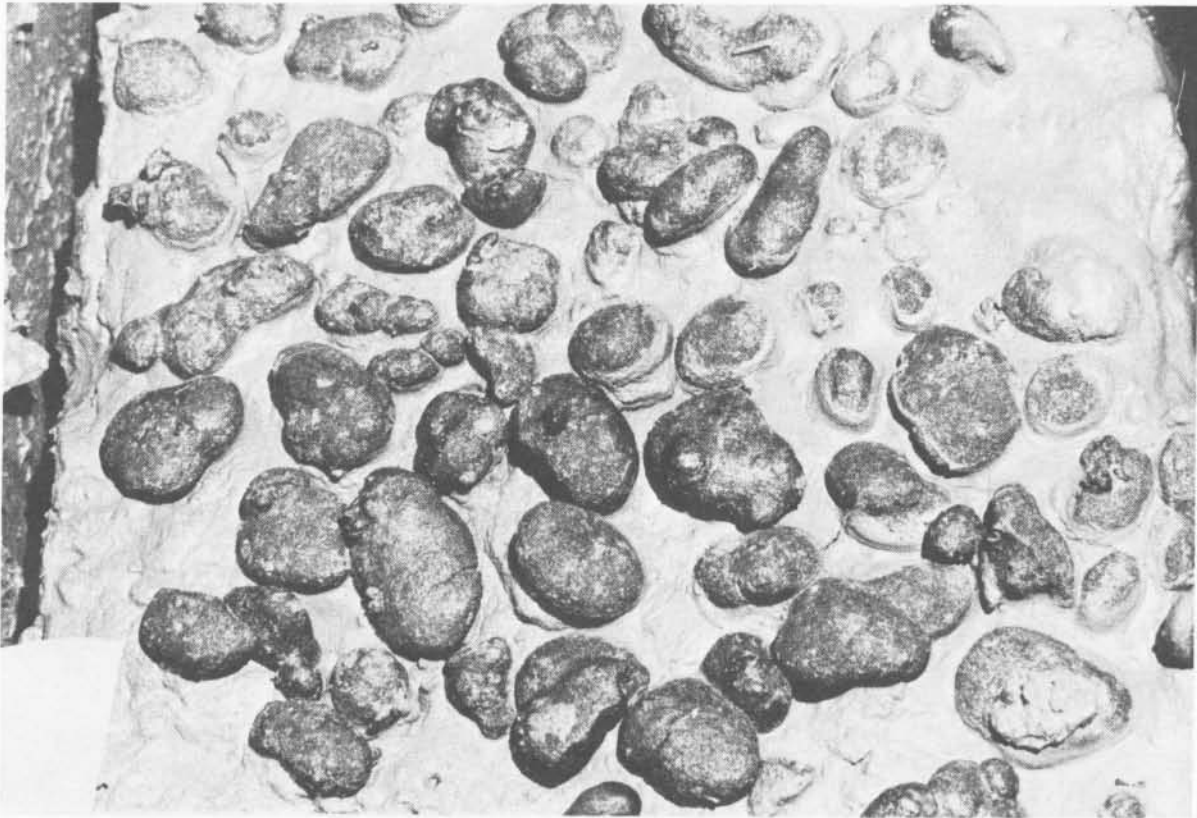


Figure 4

Figure 5.

A. Top external surface of nodule NP 64-3 (station 27). Densely packed hemispherical microbotryoids cover area. Small test of organism at right. Oblique illumination.

B. Part of the same area at higher magnification. Black oxide microbotryoids stand above interstitial clay (light gray).

Compare bottom features shown in figure 5.

See Appendix for cross-section of entire nodule.

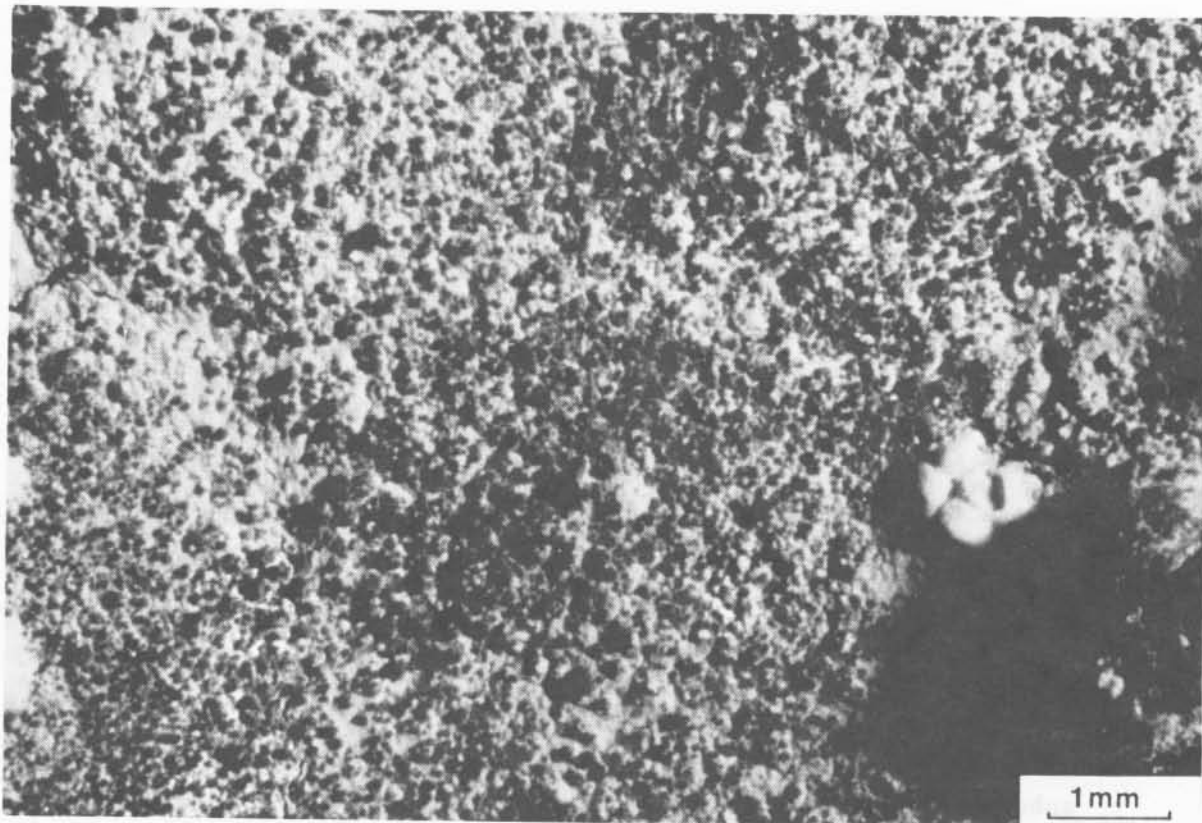


Figure 5A

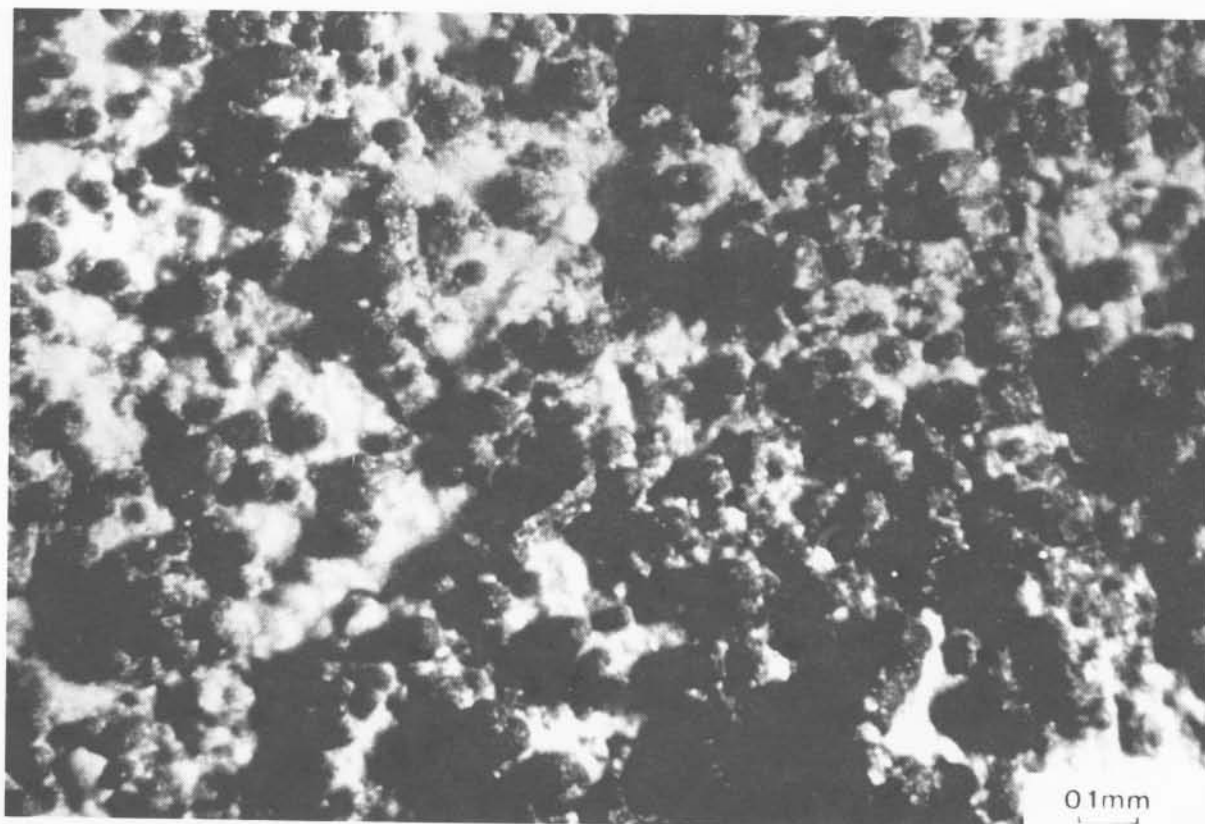


Figure 5B

Figure 6.

A. Surface features of bottom of nodule NP 64-3 (station 27). Compare figure 5A. Overall appearance is similar to top surface. Note thin fracture trending NE and white organic feature (worm tube?).

B. Part of same area as above but higher magnification view. Note very dense packing and uniformity of size of microbotryoids. Magnification is same as in figure 5B. These features are less subdued than the top features shown in figure 5 and have a rougher surface, but they are not typical dendritic microbotryoids.

See Appendix for nodule cross-section.

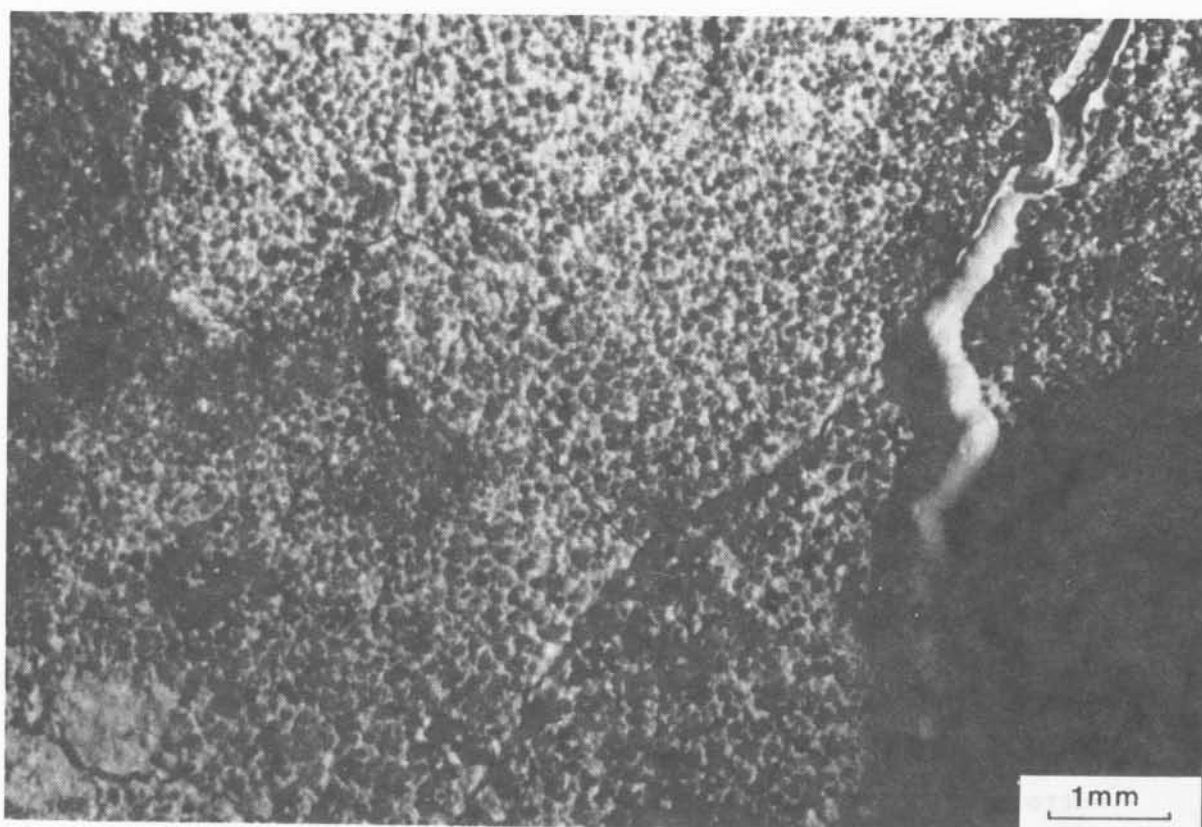


Figure 6A

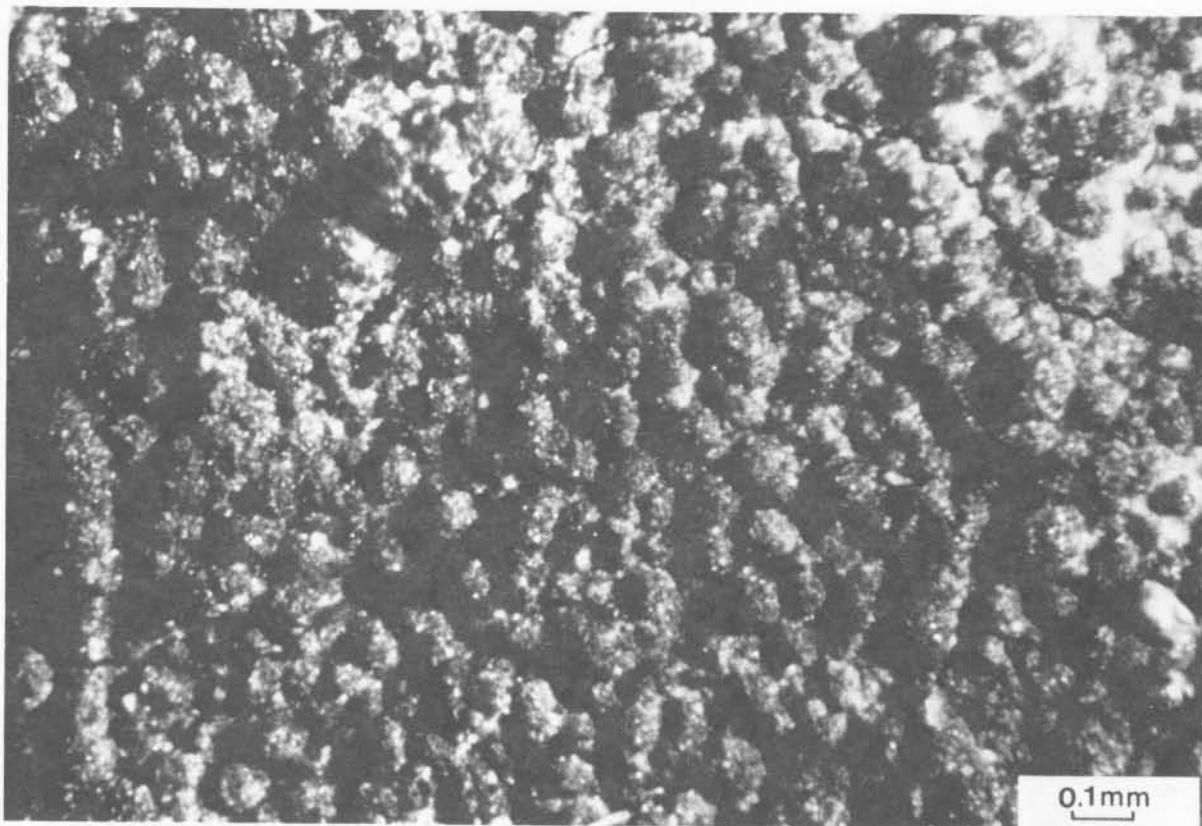


Figure 6B

Figure 7.

A. Surface features of bottom of nodule NP 62-1 (station 23B). At this low magnification, surface appears somewhat rough and has a relatively uniform texture. Note fracture (upper right) and organic structures (white).

B. Higher magnification shows dendritic form of microbotryoids in same area as above. This sort of texture is characteristic of bottom surface of many nodules, but this nodule shows the same type of feature on the top (see figure 8).

See Appendix for cross-section of whole nodule.

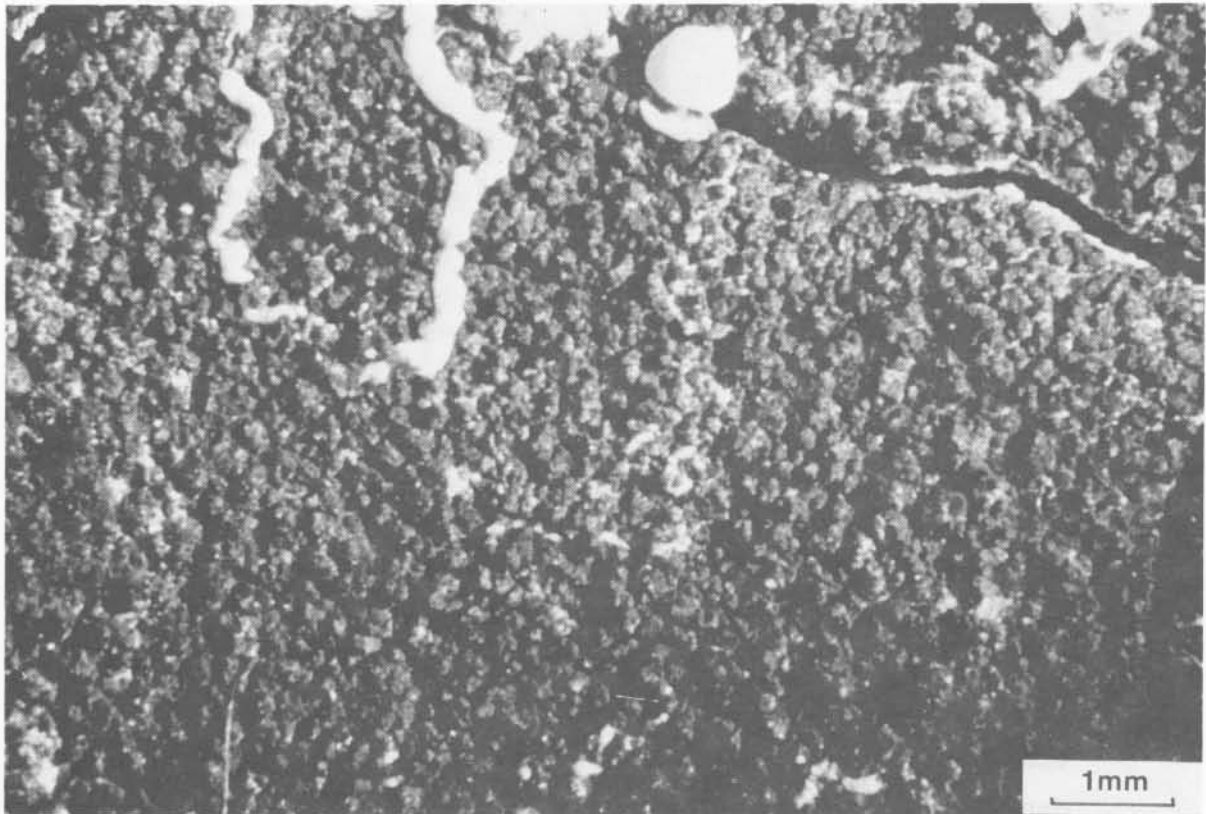


Figure 7A

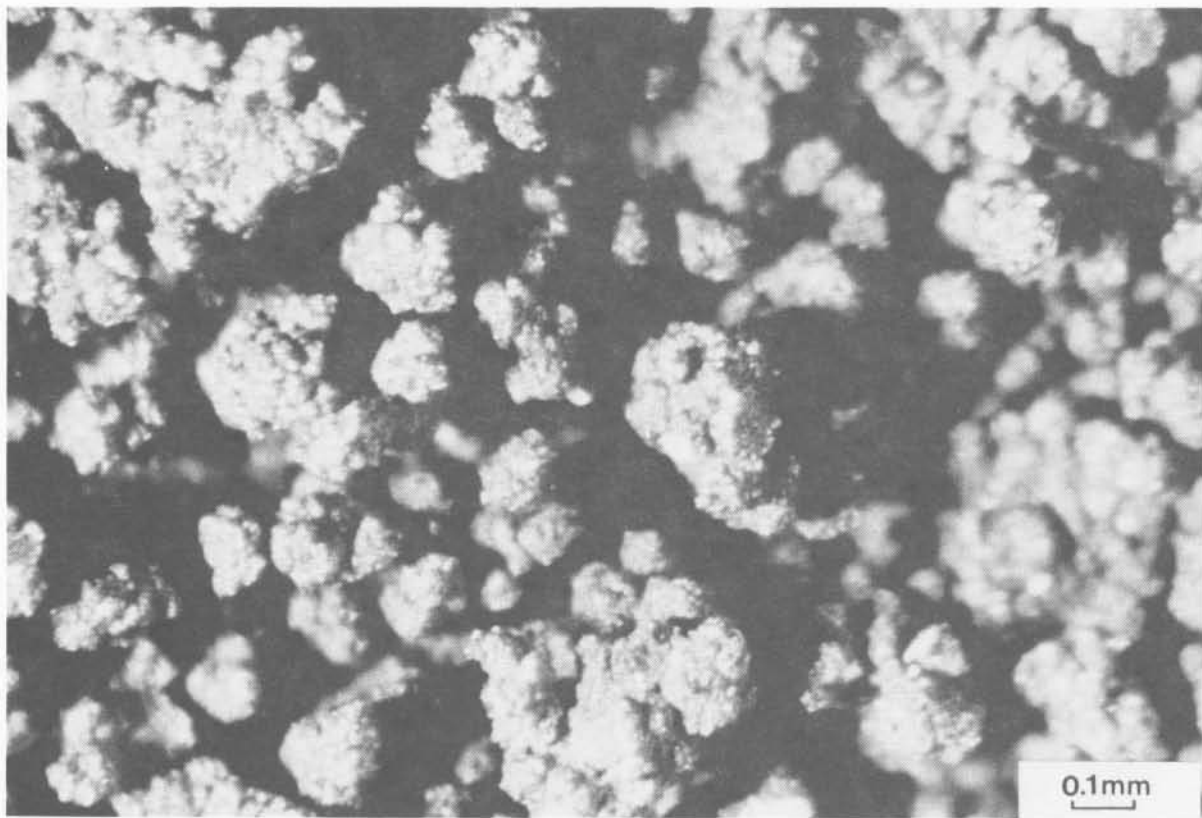


Figure 7B

Figure 8.

A. Surface textural features of top of nodule NP 62-1 (station 23B). Non-uniformity of fine features is unusual. Clay and organic material (white) are relatively abundant.

B. Typical oxide microbotryoids in area shown above as seen at higher magnification. Note greater size and relief than bottom features shown in figure 7B at same power. These dendritic forms suggest that the nodule may have been inverted during the box coring or subcoring operations. Orientation indicated here is as collected.

See Appendix for cross-section of whole nodule.

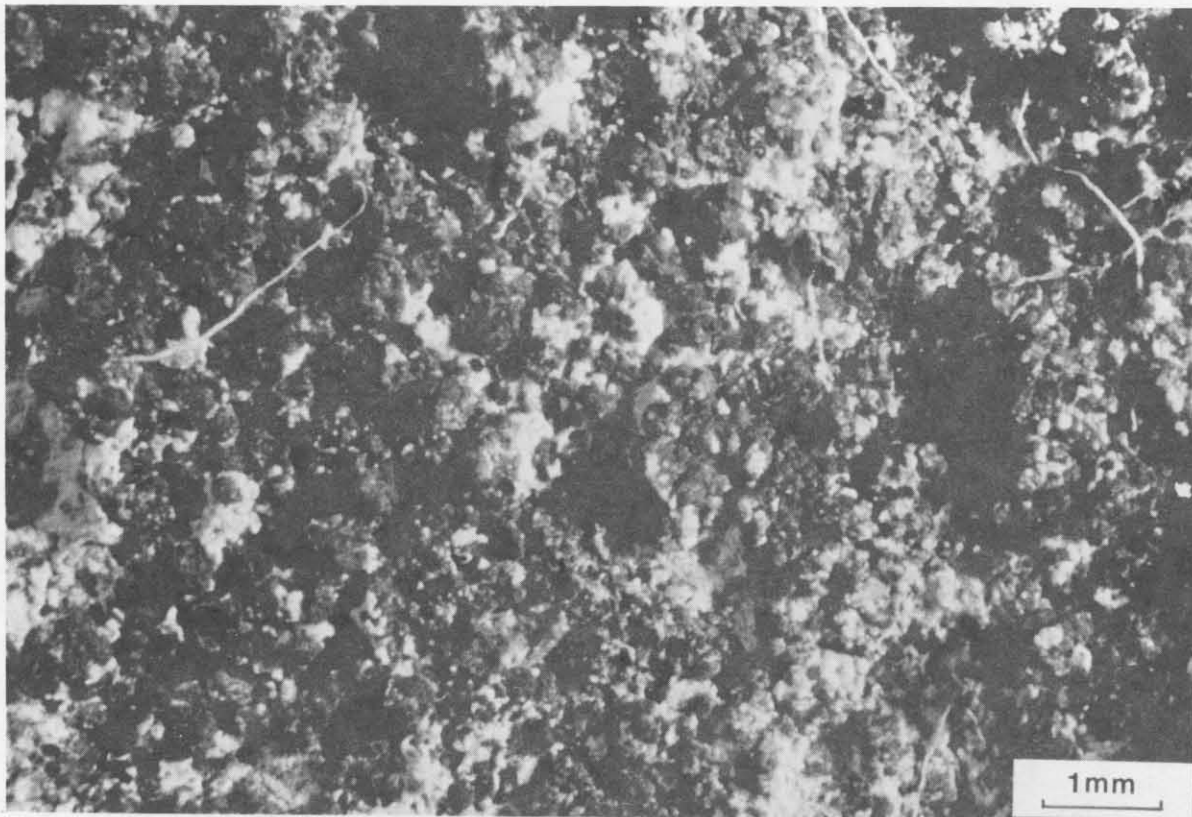


Figure 8A



Figure 8B

Figure 9.

A. Surface features of top of nodule NP 60A-10 (station 15B), at high magnification. Minute hemispherical microbotryoids are so densely packed as to leave little interstitial space. Sinuous black or gray structures (positive relief) may be oxide-coated organic features (worm-tubes?). See also figure 11A.

B. Bottom surface of same nodule at same magnification as A. Note great height to width ratio compared to forms in A (above) and finely irregular surface of the individual forms. Extreme fragility of these forms is suggested by the large amount of void space and is emphasized in the cross-sectional view of same features, shown in figure 10. See also figure 11B.

See Appendix for cross-section of whole nodule.



Figure 9A

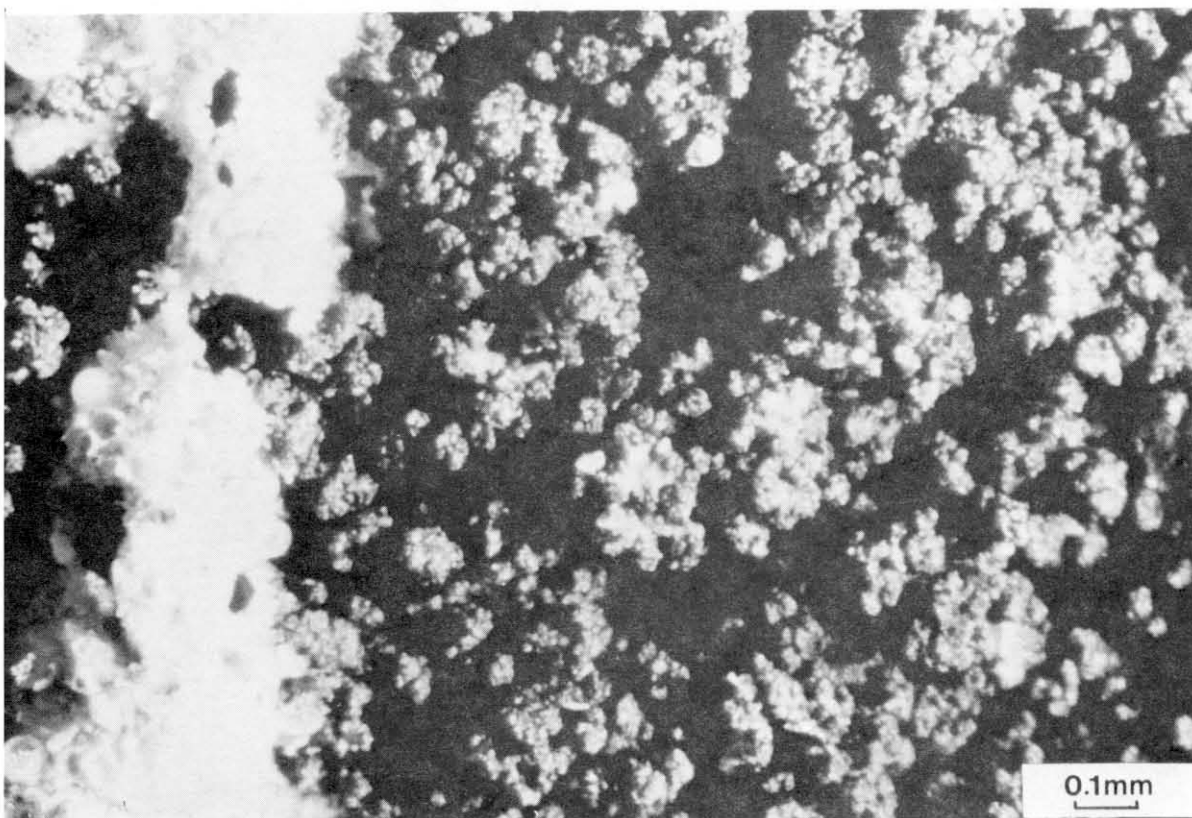


Figure 9B

Figure 10.

Side view of bottom surface features of nodule NP 60A-10 shown in figure 9B, at same magnification. Photograph is inverted for better perspective; interior of nodule is toward bottom of page. Note great porosity and delicate structure of the dendritic microbotryoids. A polished section across these forms in the same nodule is shown in figure 11B with natural orientation.

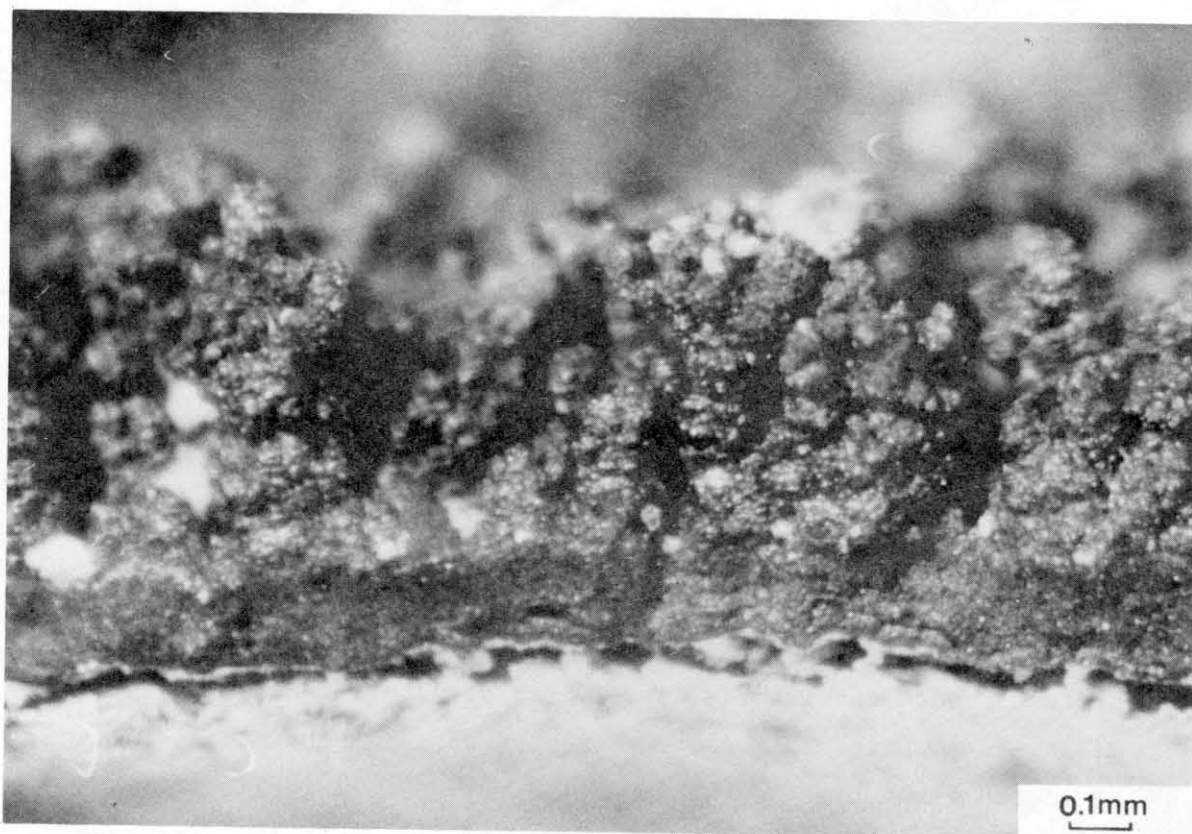


Figure 10

Figure 11.

A. Photomicrograph of part of polished section of nodule NP 60A-10. Vertical illumination. Plane-polarized light. At the top just below the plastic mounting medium (even gray) the internal structure of the hemispherical microbotryoids on the upper surface of the nodule can be seen. The layers of oxides (light gray) which form the structure are very dense and relatively uniform in character passing downward toward the center of the nodule. Optical character of these oxides is that of Fe-rich X-ray amorphous nodule material.

B. Photomicrograph of polished section of same nodule under same conditions, showing cross-section of structure at bottom surface. Note the intricately layered structure and non-uniformity of layers compared to the structures shown in A (above). This type of growth gives rise to the dendritic forms shown in figures 9A and 10. Most of the oxides shown (white and gray) are crystalline todorokite, a hydrous impure manganese oxide relatively rich in Ni and Cu.

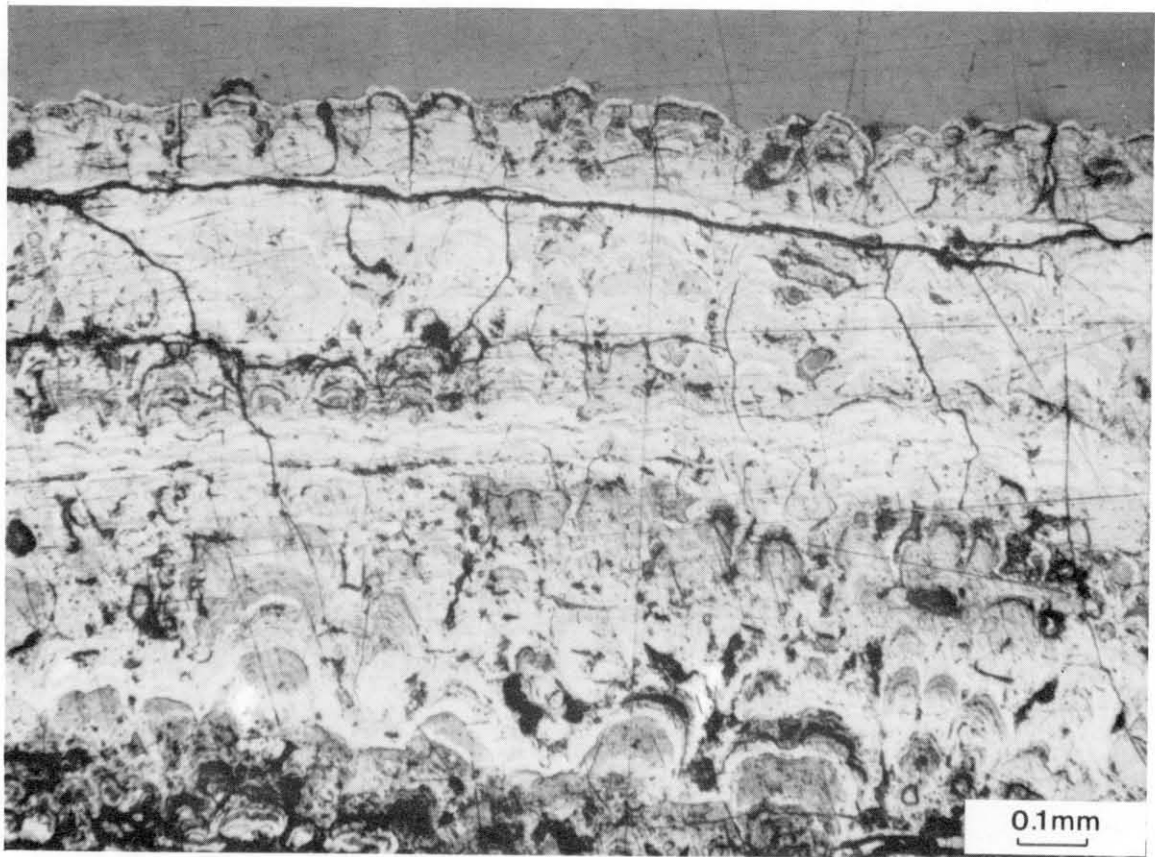


Figure 11A

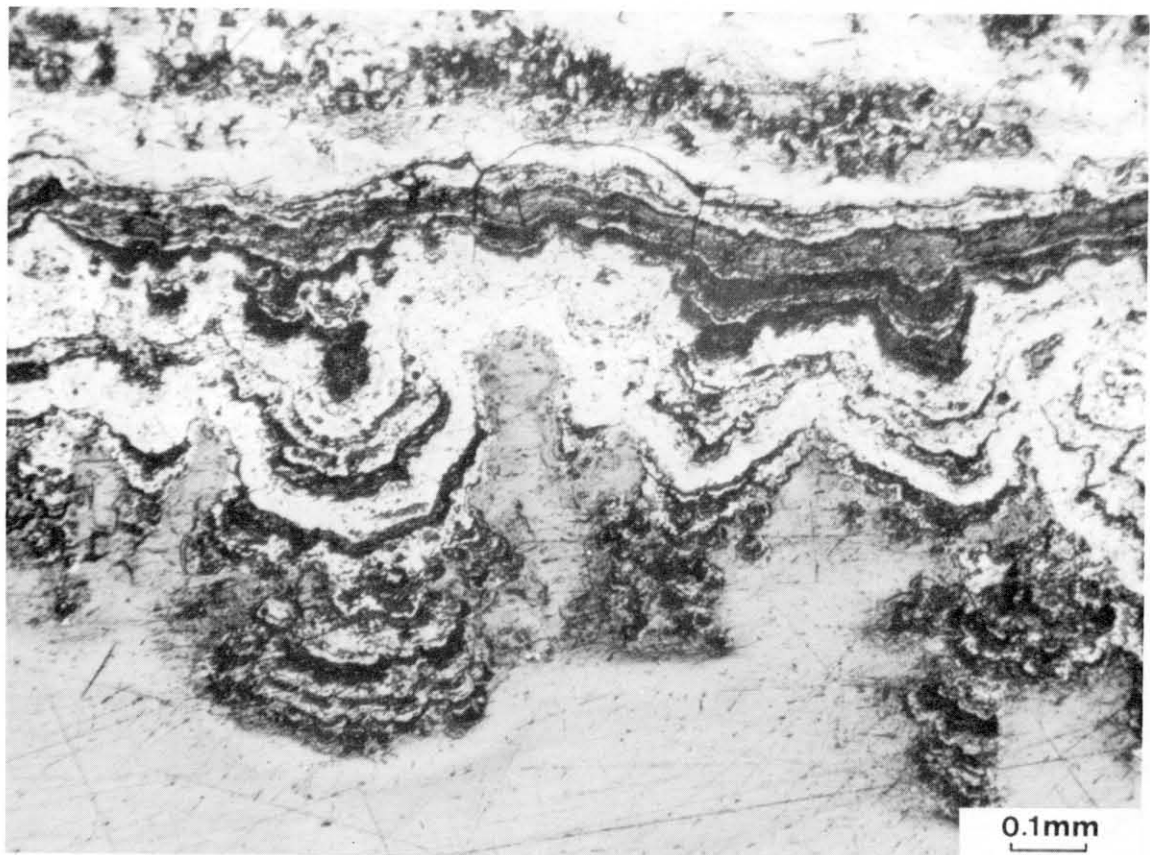


Figure 11B

APPENDIX

W. S. U. Specimen Number: NP 59-23

PHYSICAL DESCRIPTION

Dimensions (mm)

Length: 22

Width: 17

Thickness: 9

Weight dry (gm): 3.3

Morphology: Elongate discoid

Color: Dark gray

Surface texture: (see facing page) Hemispherical botryoids on both top and bottom. Relief somewhat greater on top but forms not dendritic. Along equatorial zone (not shown) small dendritic forms appear.

Polished Section: (below) Note structure of dendritic crustal zone (left and right sides), nodule fragment core, and internal fractures. Site XRF-1 is rich in Mn, Ni, and Cu. Site XRF-2 is rich in Fe and low in Mn, Ni, and Cu (ratios given in text).

COLLECTION DATA

Ship: Oceanographer

Cruise Number: RP6-OC-75

Station Number: 11

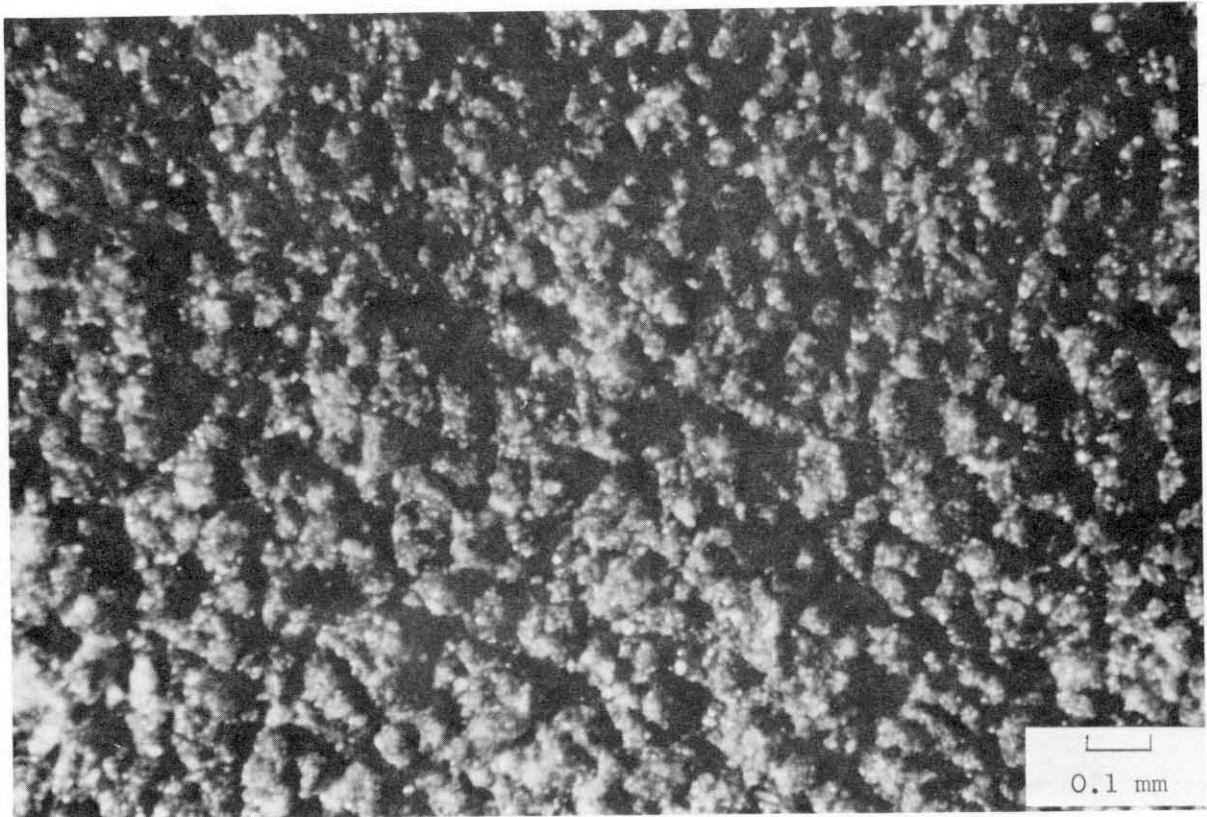
Latitude: 16°0.7'N

Longitude: 126°46.3'W

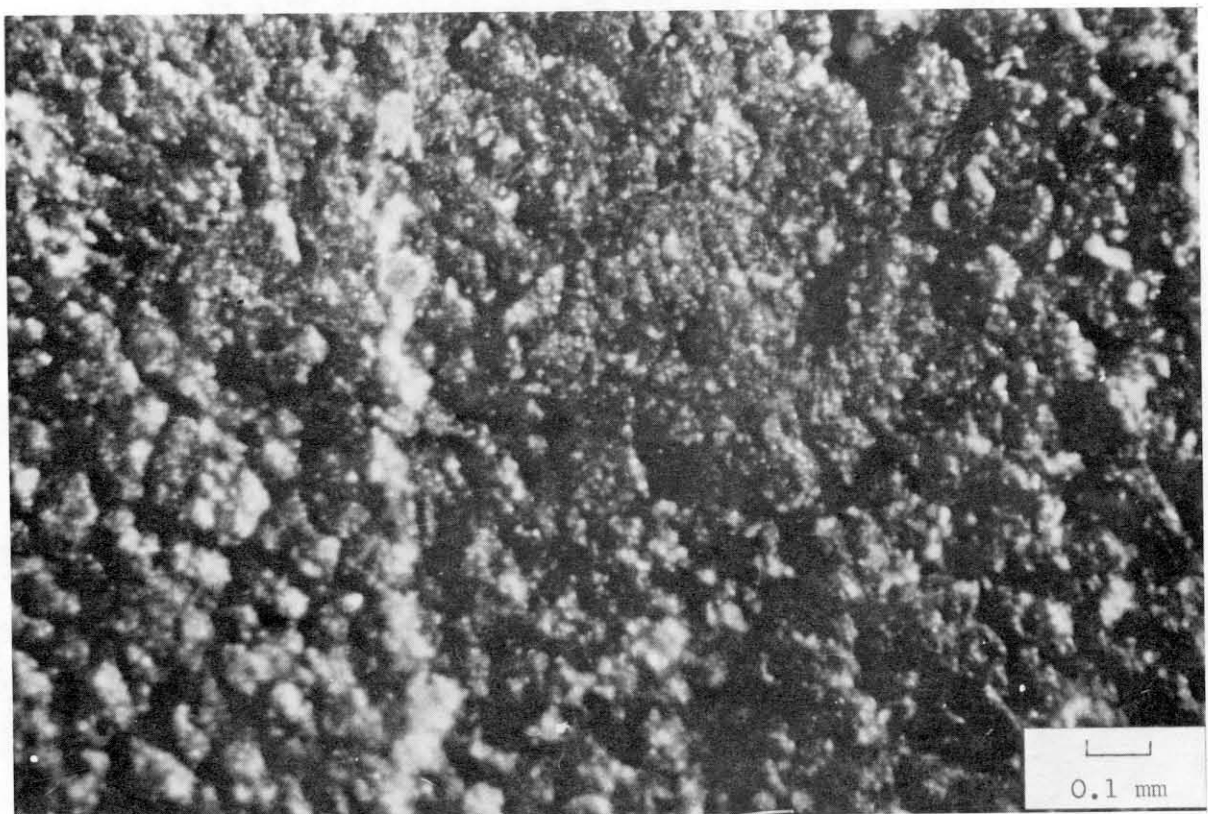
Depth (m): 4585



Polished section of Nodule NP 59-23 (Sta. 11)



Nodule NP-59-23. Surface features of top.



Nodule NP 59-23. Surface features of bottom.

W. S. U. Specimen Number: NP 59-24

PHYSICAL DESCRIPTION

Dimensions (mm)

Length: 32

Width: 19

Thickness: 9

Weight dry (gm): 6.1

Morphology: Flat ellipsoid

Color: Bottom dark gray to black. Top dark gray.

Surface Texture: Densely packed minute microbotryoids on both top and bottom (see facing page). Bottom forms somewhat dendritic.

Polished section (below): Crustal zone largely broken away from bottom during section preparation; resistant top layers intact. Core complex, includes nodule and rock fragments

COLLECTION DATA

Ship: Oceanographer

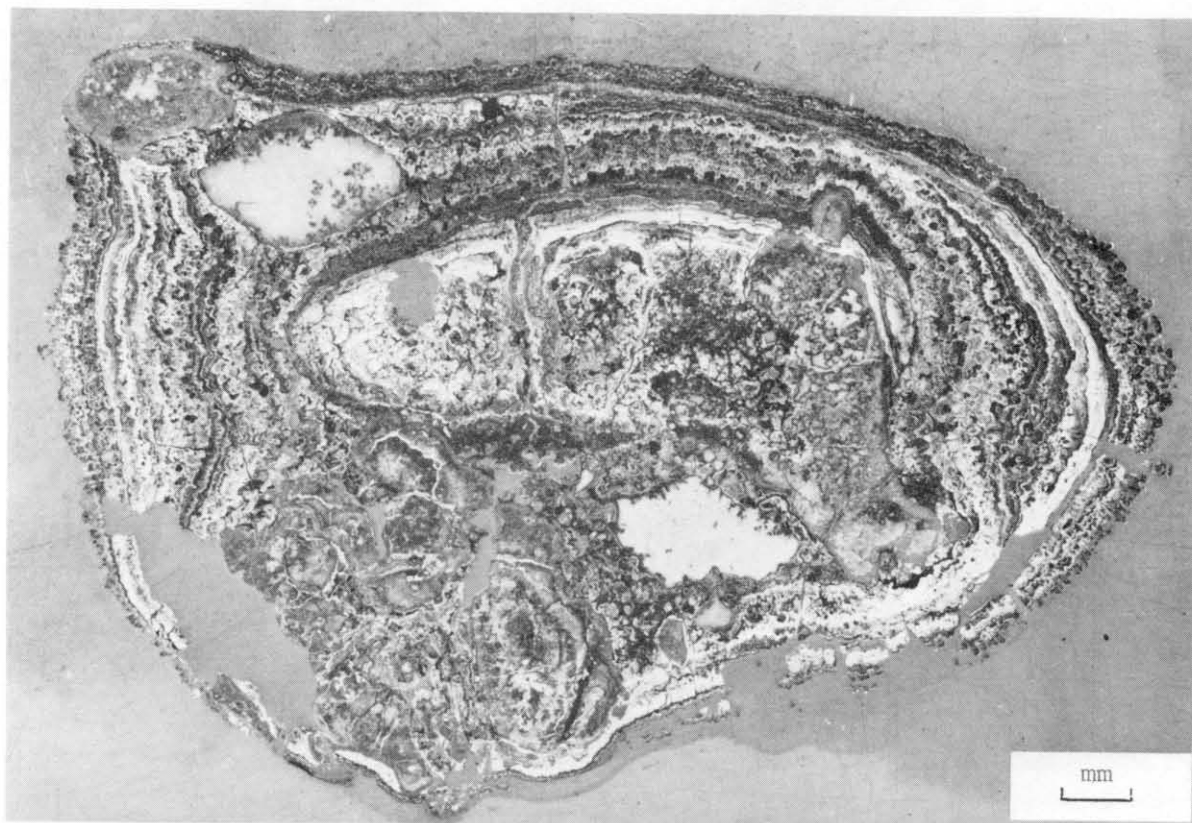
Cruise Number: RP6-OC-75

Station Number: 11

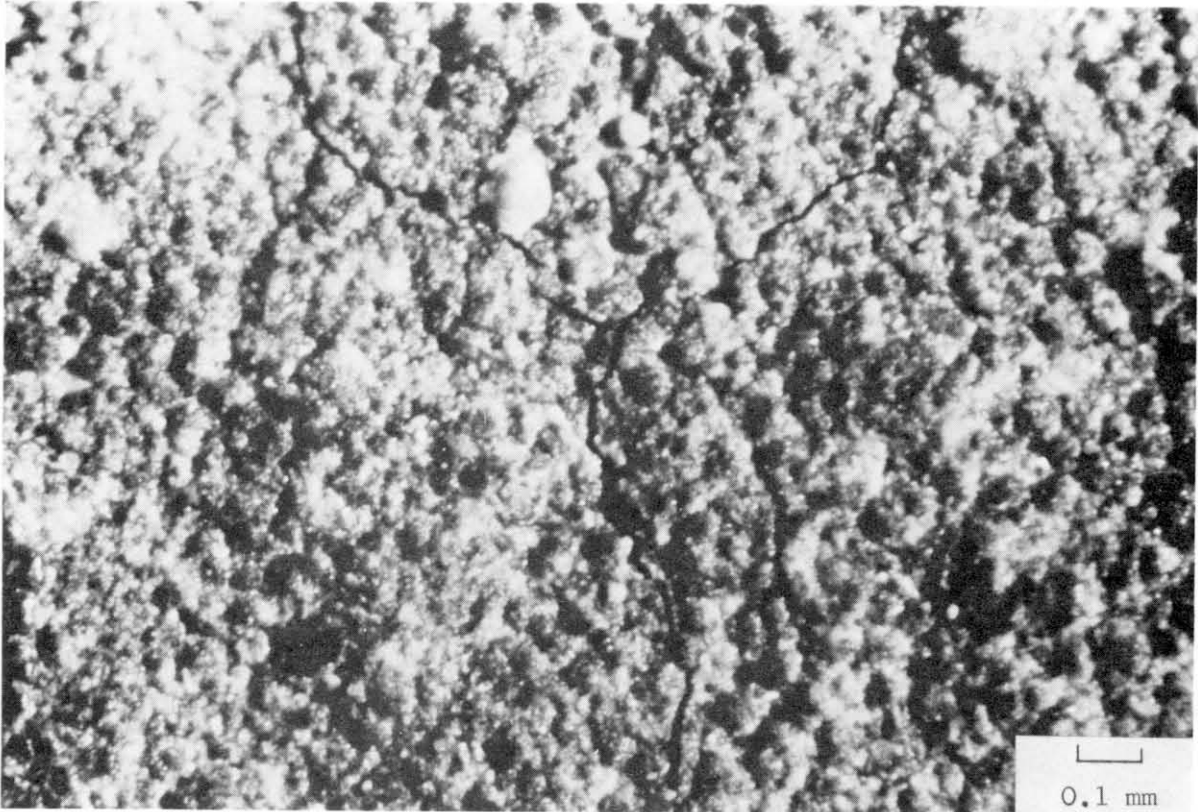
Latitude: 16°0.7' N

Longitude: 126°46.3' W

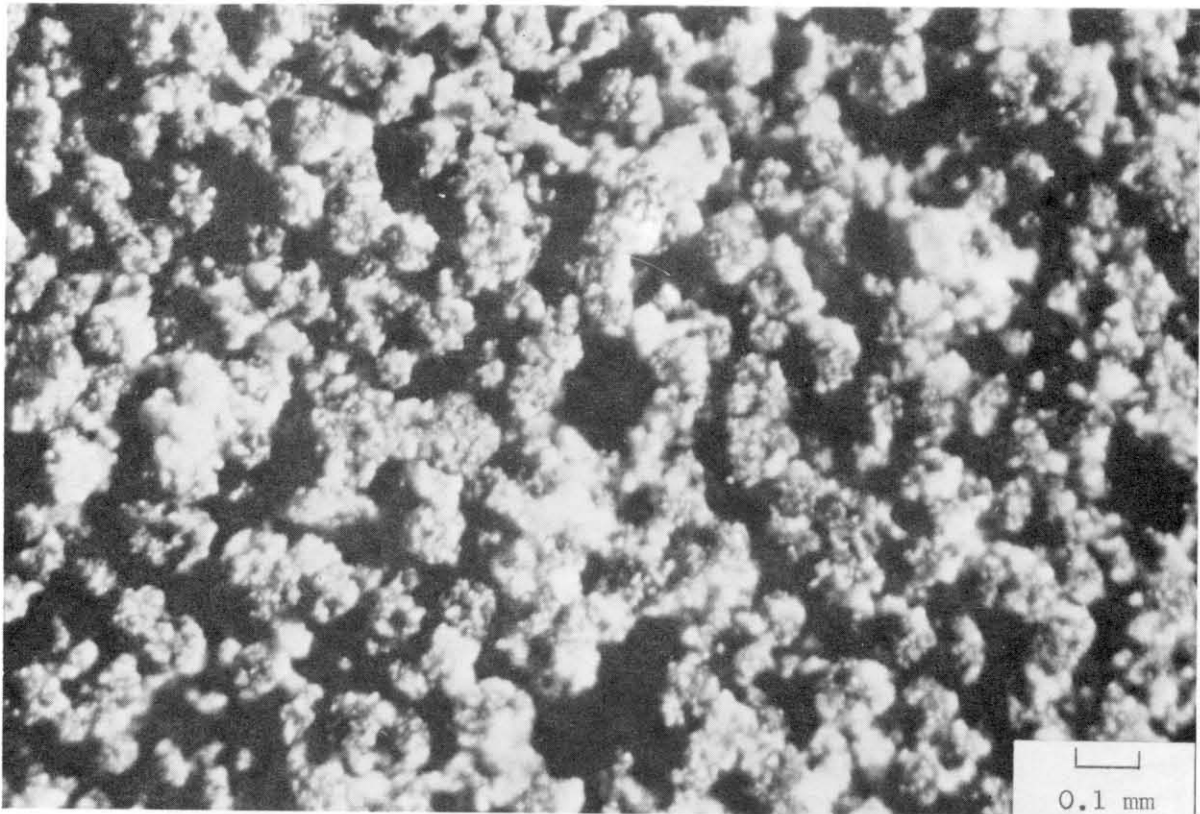
Depth (m): 4585



Polished section of Nodule NP 59-24 (Sta. 11)



Nodule NP 59-24. Surface features of top.



Nodule 59-24. Surface features of bottom.

W. S. U. Specimen Number: NP 60-3

PHYSICAL DESCRIPTION

Dimensions (mm)

Length: 46

Width: 43

Thickness: 27

Weight dry (gm): 44.5

Morphology: Irregular discoid

Color: Dark gray to black top and sides, bottom lighter color.

Surface Texture (see facing page): Top features coarser than bottom, suggesting nodule disturbance during collection.

Polished section (below): Complex growth history shown by truncated and wedging layers. Asymmetrical shape may have caused nodule to move from modern growth position during box core recovery or sampling.

COLLECTION DATA

Ship: Oceanographer

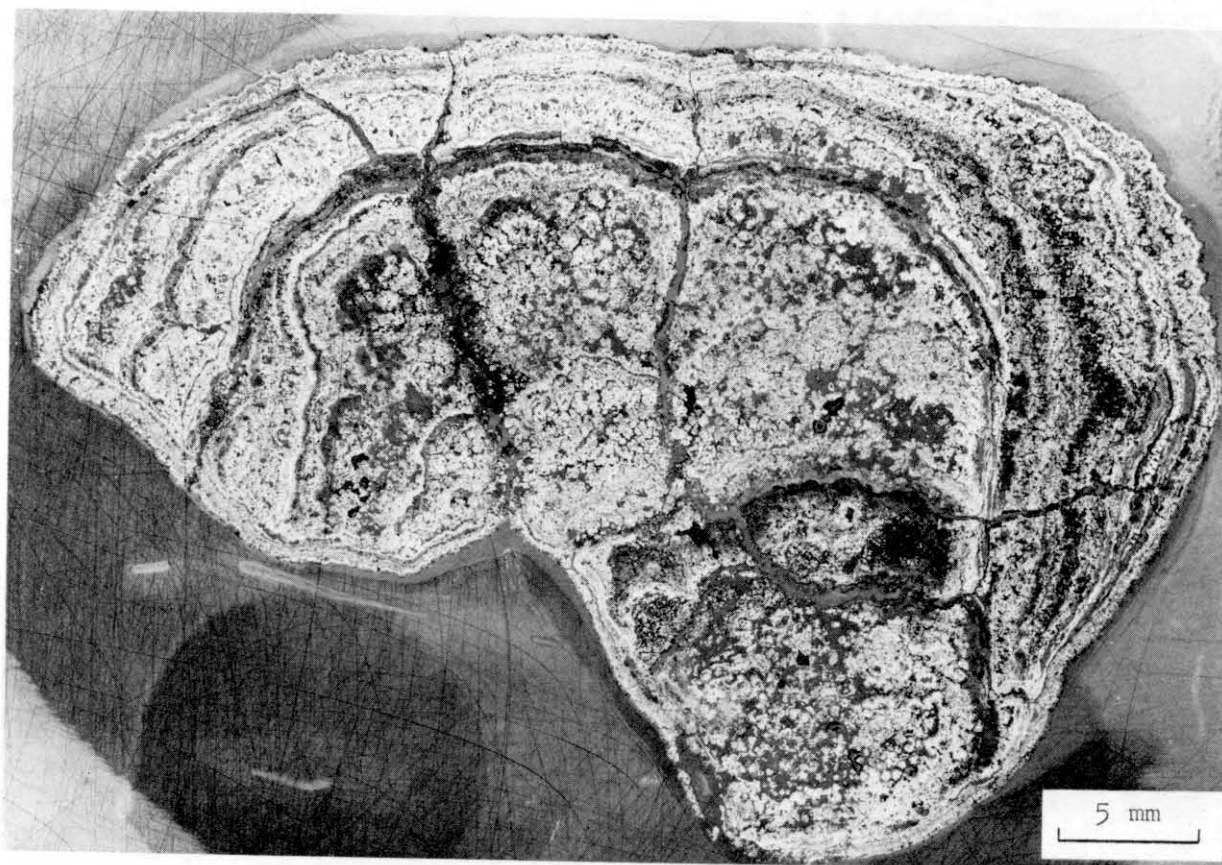
Cruise Number: RP6-OC-75

Station Number: 15B

Latitude: 15°45.7' N

Longitude: 126°0.4' W

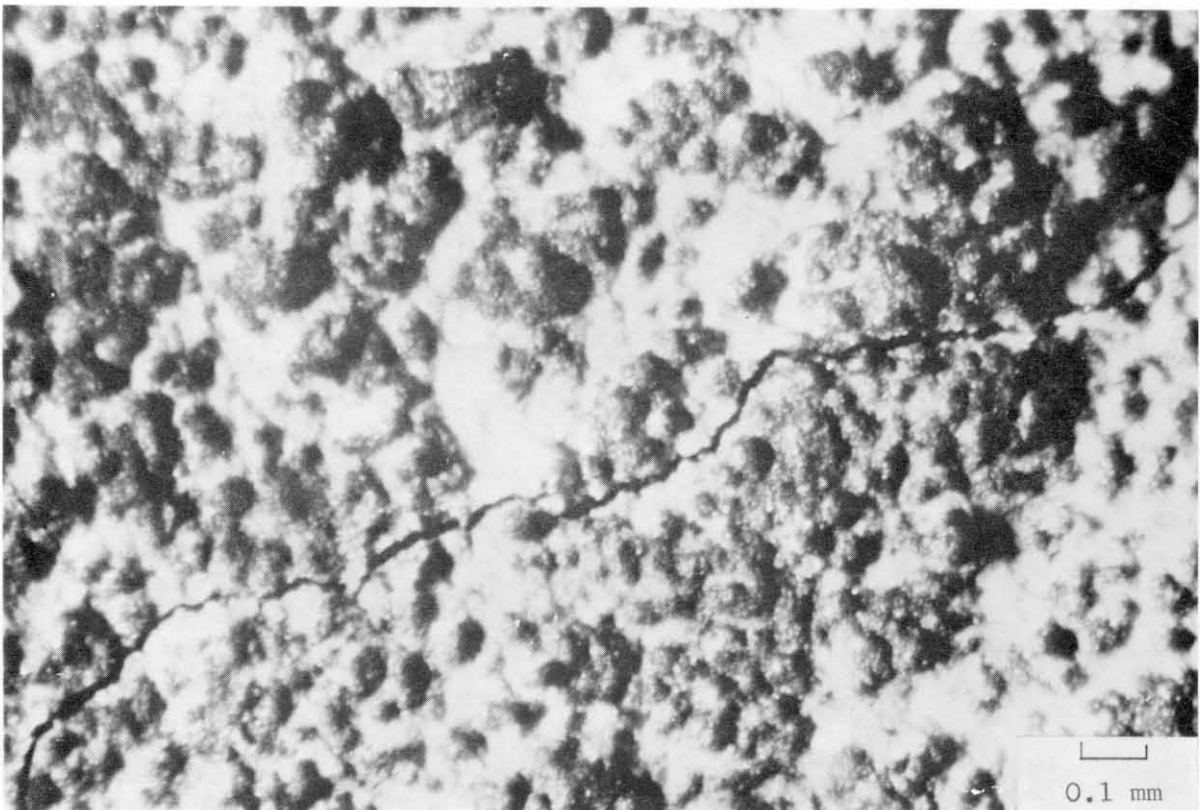
Depth (m): 4514



Polished section of Nodule NP 60-3 (Sta. 15B)



Nodule NP 60-3. Surface features of top.



Nodule NP 60-3. Surface features of bottom.

DATA SHEET

W. S. U. Specimen Number: NP 60A-1

PHYSICAL DESCRIPTION

Dimensions (mm)

Length: 48

Width: 42

Thickness: 22

Weight dry (gm): 46.9

Morphology: Discoid; bottom relatively flat, top sub-round.

Color: Top gray to black, bottom black.

Surface Texture (facing page): Closely packed hemispherical microbotryoids on top. Height slightly greater along lines of old healed fractures. Sinuous chains may be encrustations on organic forms (worm tubes?). On bottom dendritic forms predominate. Lineaments also present.

Polished Section (below): Compare dense structure of top crustal zone with porous zone at bottom. Oxide deposition in vertical crack evident.

COLLECTION DATA

Ship: Oceanographer

Cruise Number: RP6-OC-75

Station Number: 15B

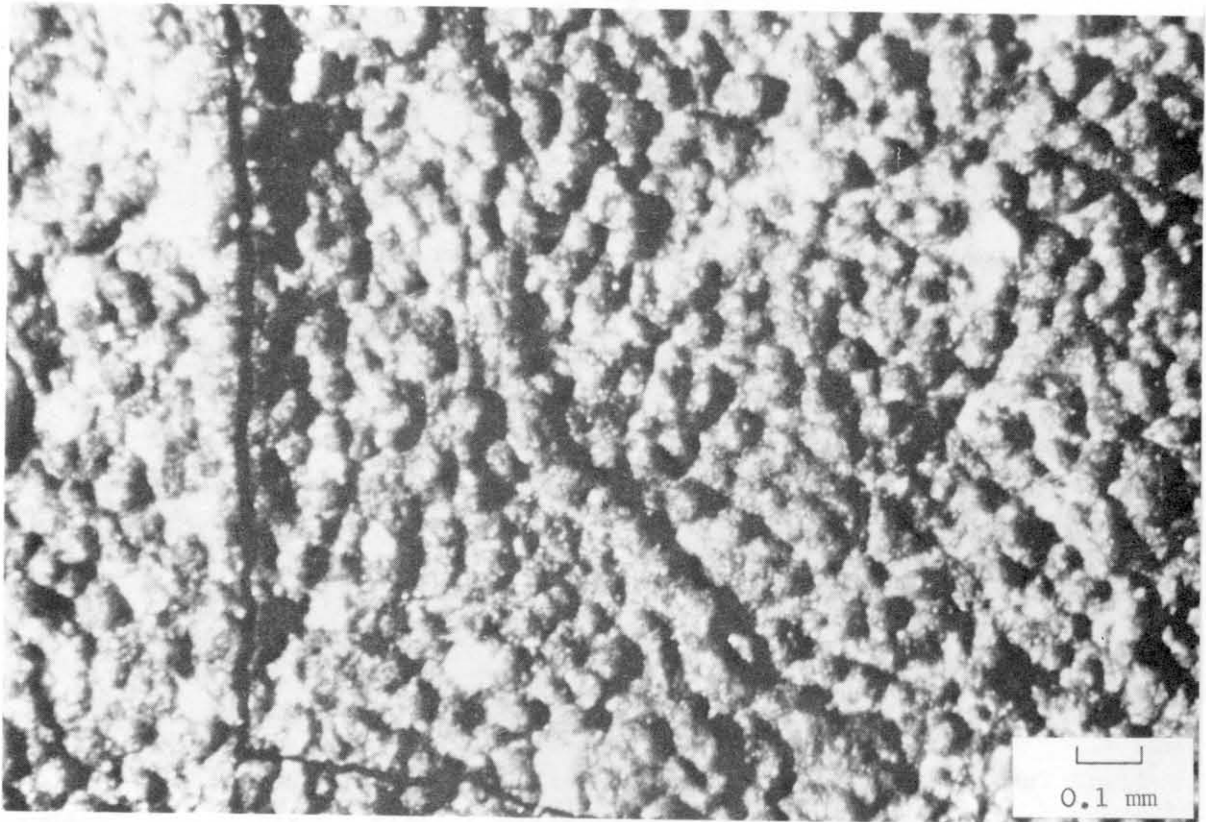
Latitude: 15°45.7' N

Longitude: 126°0.4' W

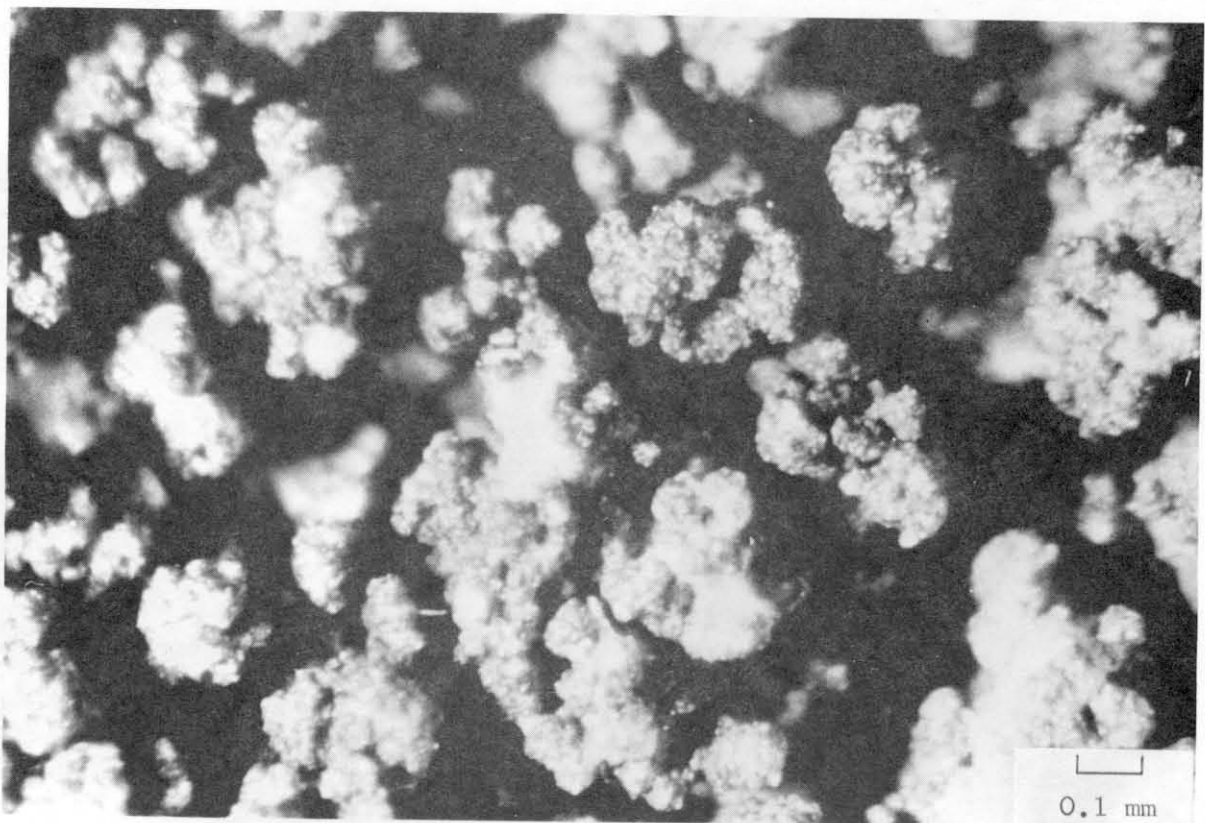
Depth (m): 4514



Polished section of nodule NP 60A-1 (Sta. 15B)



Nodule NP 60A-1. Surface features of top.



Nodule NP 60A-1. Surface features of bottom.

DATA SHEET

W. S. U. Specimen Number: NP 60A-10

PHYSICAL DESCRIPTION

Dimensions (mm)

Length: 75

Width: 50

Thickness: 29

Weight dry (gm): 123.1

Morphology: Irregular discoid

Color: Dark gray top. Bottom black.

Surface Texture: Densely packed very small hemispherical microbotryoids.

Many sinuous black "worm tubes" on top. Bottom covered with minute dendritic clusters. (See figures 9, 10, and 11.)

Polished Section (below): Structure of crustal zone at top is clearly more dense than at bottom (see also photomicrographs in figure 11). Overall nodule structure is complex but appears strong in spite of presence of several obvious old oxide- and clay-filled fractures.

COLLECTION DATA

Ship: Oceanographer

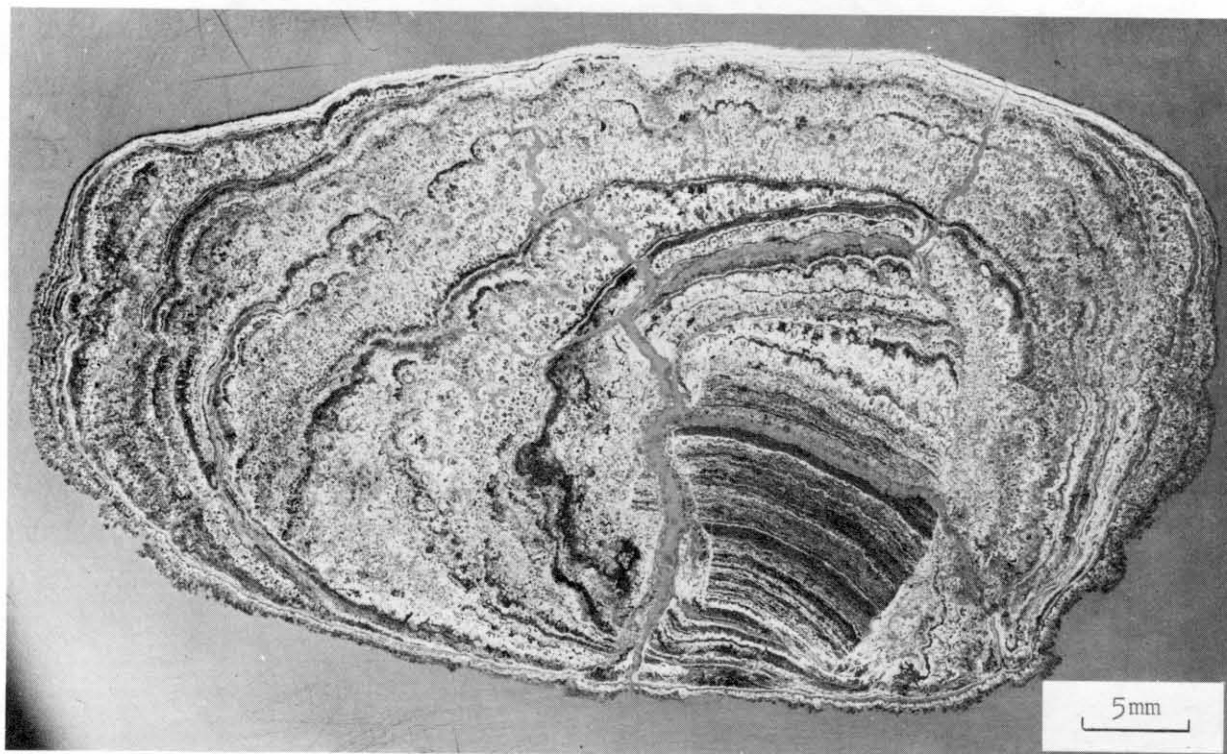
Cruise Number: RP6-OC-75

Station Number: 15B

Latitude: 15°45.7' N

Longitude: 126°0.4' W

Depth (m): 4514



Polished section of nodule NP 60A-10 (Sta. 15B)

W. S. U. Specimen Number: NP 61-1

PHYSICAL DESCRIPTION

Dimensions (mm)

Length: 26

Width: 23

Thickness: 14

Weight dry (gm): Not weighed.

Morphology: Discoid

Surface texture: Nodule studied in section only (see below).

Polished section (below): Cross-section of crustal zone shows thin relatively dense structure at top in contrast with thicker complex dendritic features along bottom. Core is old nodule fragment.

Sediment below nodule shows cracks caused by drying after collection.

COLLECTION DATA

Ship: Oceanographer

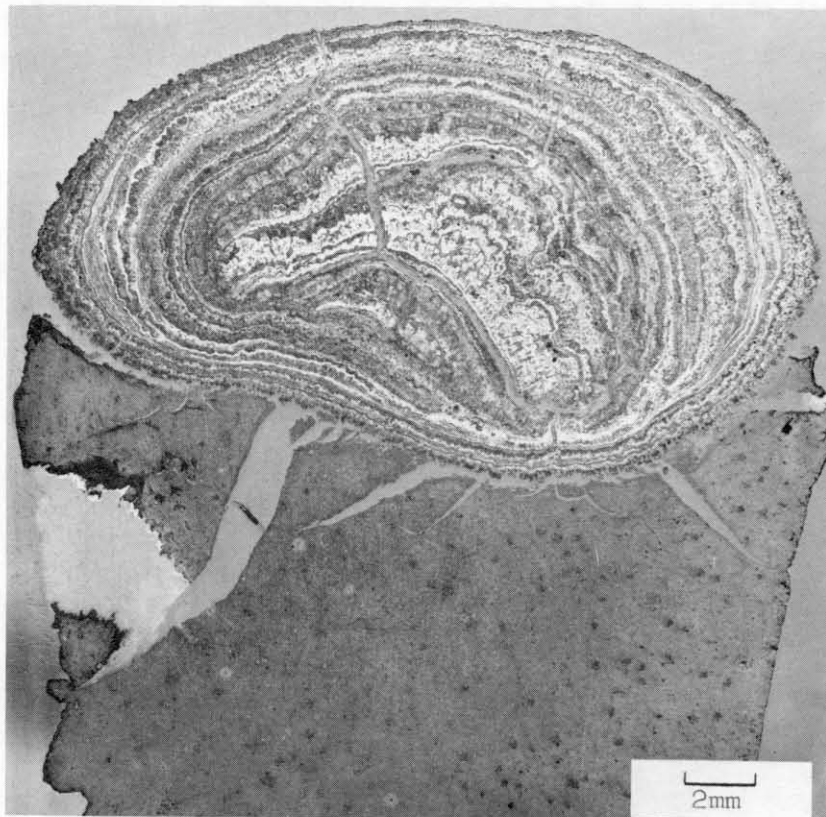
Cruise Number: RP6-OC-75

Station Number: 16B

Latitude: 15°46.7' N

Longitude: 126°11.2' W

Depth (m): ca. 4515



Polished section of nodule NP 61-1 (Sta. 16B)

W. S. U. Specimen Number: NP 61-5

PHYSICAL DESCRIPTION

Dimensions (mm)

Length: 29

Width: 18

Thickness: 14

Weight dry (gm): Not weighed.

Morphology: Elongate discoid.

Surface Texture: Nodule studied only in polished section (see below).

Polished section (below): Cross-sections of crustal zone show little difference in top and bottom surface layers. Most fragile structures (edges at 10 o'clock and 4 o'clock) probably mark sediment-water contact at time of collection. Bottom sediment intact shows **drying cracks**.

COLLECTION DATA

Ship: Oceanographer

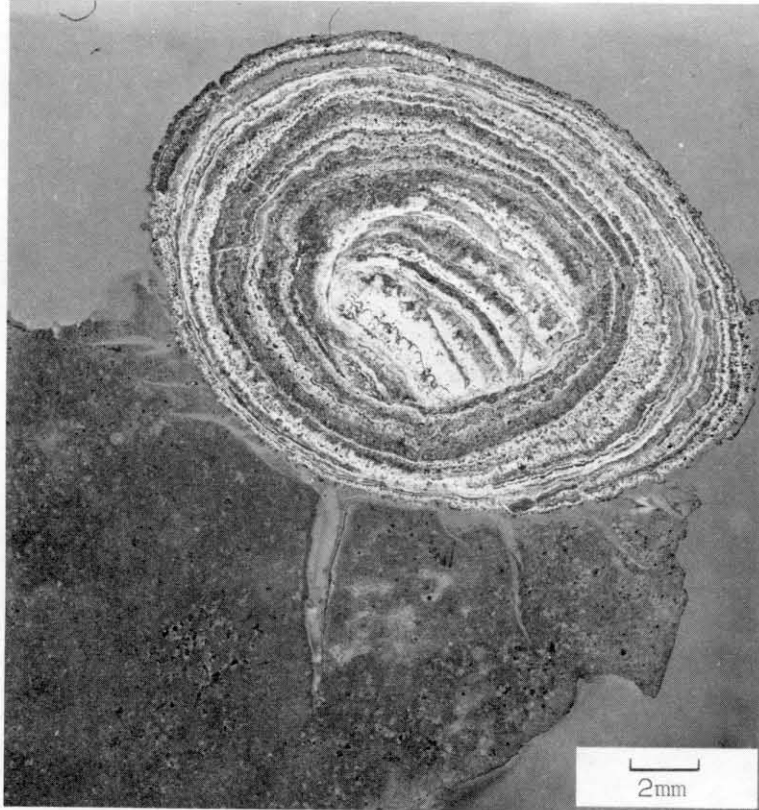
Cruise Number: RP6-OC-75

Station Number: 16B

Latitude: 15°46.7' N

Longitude: 126°11.2' W

Depth (m): ca. 4515



Polished section of nodule NP 61-5 (Sta. 16B)

W. S. U. Specimen Number: NP 61-13

PHYSICAL DESCRIPTION

Dimensions (mm)

Length: 50

Width: 36

Thickness: 25

Weight dry (gm): 45.6

Morphology: Broken discoid.

Color: Top gray to dark gray. Bottom dark gray to black.

Surface Texture: Top covered with minute hemispherical microbotryoids.

Bottom and equatorial zone have abundant dendritic forms.

Polished Section (below): Major structure is half of older nodule, with most recent oxides (crustal zone) extending over major fracture (left end), and entering fracture at top (center). Dendritic crust weak, broken.

COLLECTION DATA

Ship: Oceanographer

Cruise Number: RP6-OC-75

Station Number: 16B

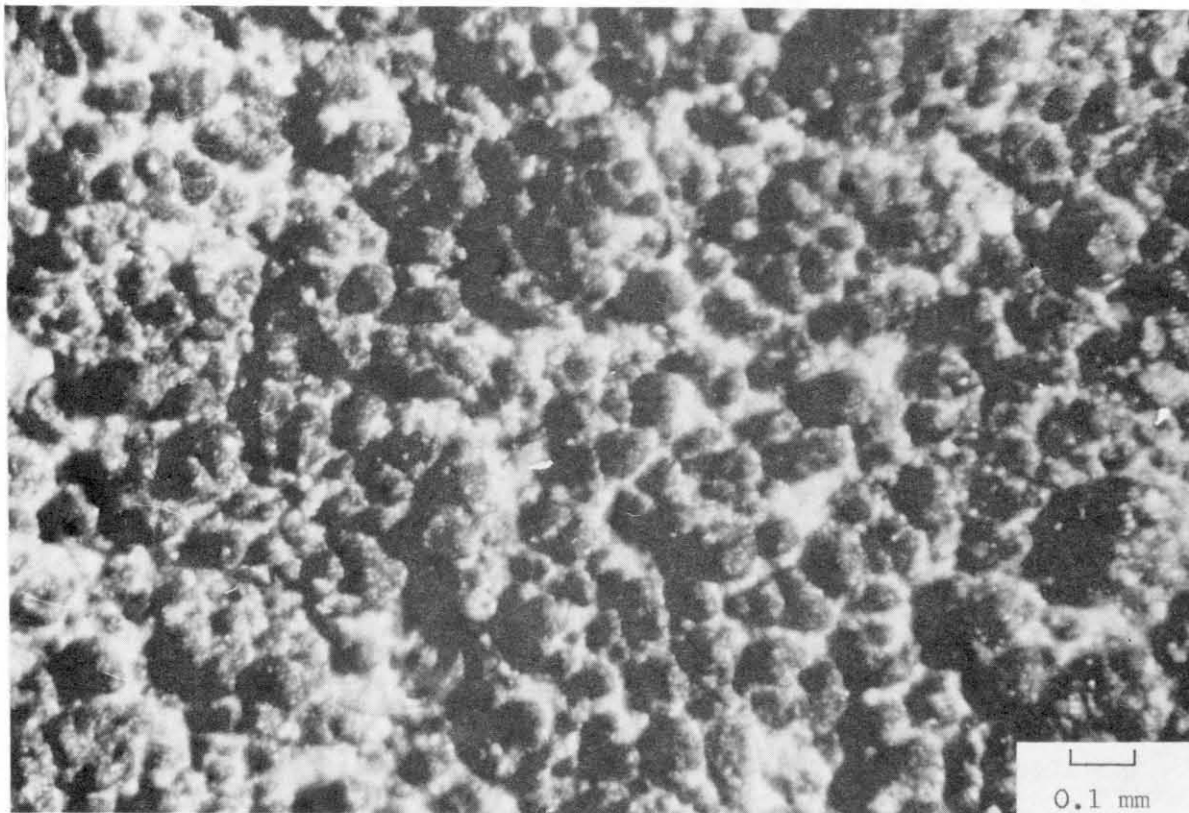
Latitude: 15°46.7' N

Longitude: 126°11.2' W

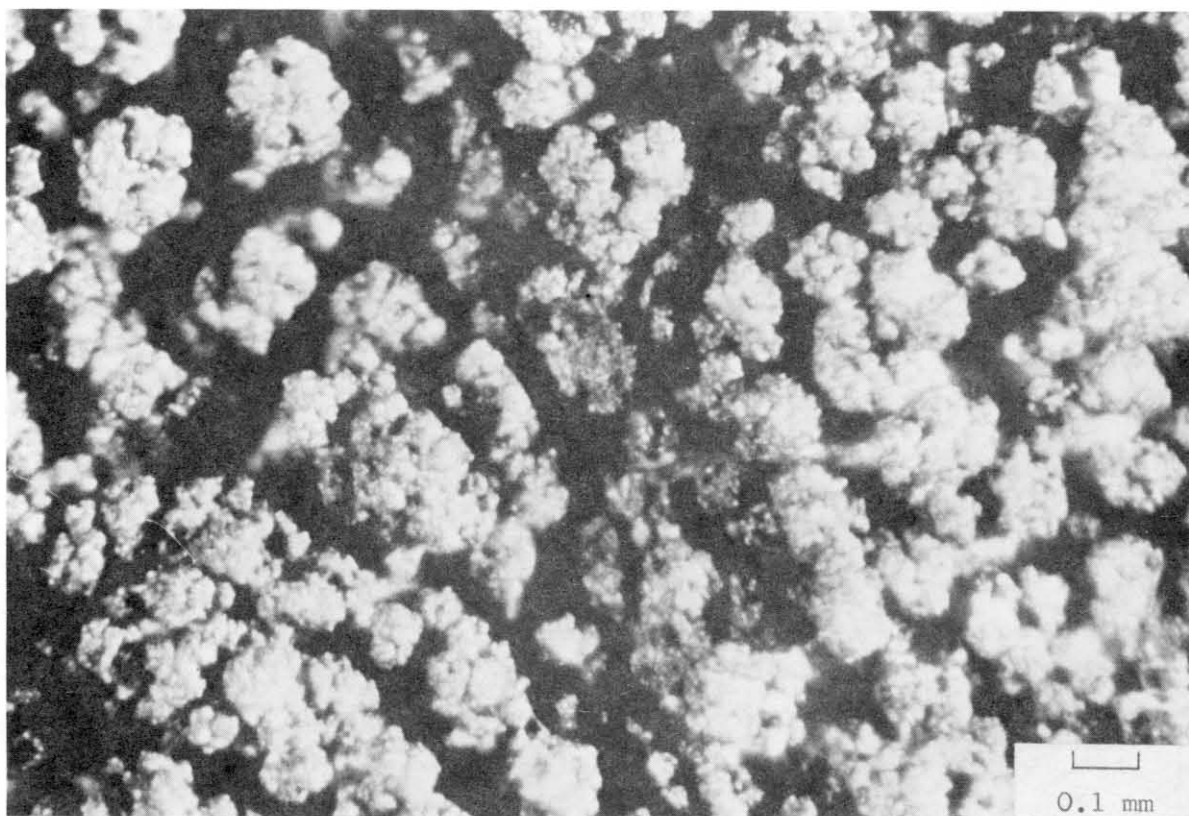
Depth (m): ca. 4515



Polished section of nodule NP 61-13 (Sta. 16B)



Nodule NP 61-13. Surface features of top.



Nodule NP 61-13. Surface features of bottom.

W. S. U. Specimen Number: NP 62-1

PHYSICAL DESCRIPTION

Dimensions (mm)

Length: 40

Width: 35

Thickness: 21

Weight dry (gm): 30.4

Morphology: Discoid

Color: Top gray to dark gray. Bottom black. (True orientation?)

Surface Texture: Both top and bottom (as collected) have dendritic-type microbotryoids, those on top somewhat larger (see figures 7 and 8). Abundant organic micro-debris on top, larger "worm tubes" on bottom. Old fractures visible on both top and bottom.

Polished Section (below): Section shows orientation when collected, but crustal zone structure (dense at bottom, dendritic at top) suggests recent overturning, perhaps during collection. Note secondary oxides and clay in fractures, and ancient nodule fragment core.

COLLECTION DATA

Ship: Oceanographer

Cruise Number: RP6-OC-75

Station Number: 23B

Latitude: 14°45.9' N

Longitude: 125°50.6 W

Depth (m): 4572



Polished section of nodule NP 62-1 (Sta. 23B)

W. S. U. Specimen Number: NP 62-2

PHYSICAL DESCRIPTION

Dimensions (mm)

Length: 17

Width: 17

Thickness: 10

Weight dry (gm): Not weighed

Morphology: Imbedded deeply in
sediment; appears discoid.

Color and Surface Texture: Obscured by sediment around and on nodule.
Nodule appears to be relatively rough on top surface.

Polished Section (below): Sediment (speckled gray) almost completely surrounds
nodule. Crustal zone structure similar at top and bottom, everywhere
typical of dendritic surface textures. No abrasion of outer surface.

COLLECTION DATA

Ship: Oceanographer

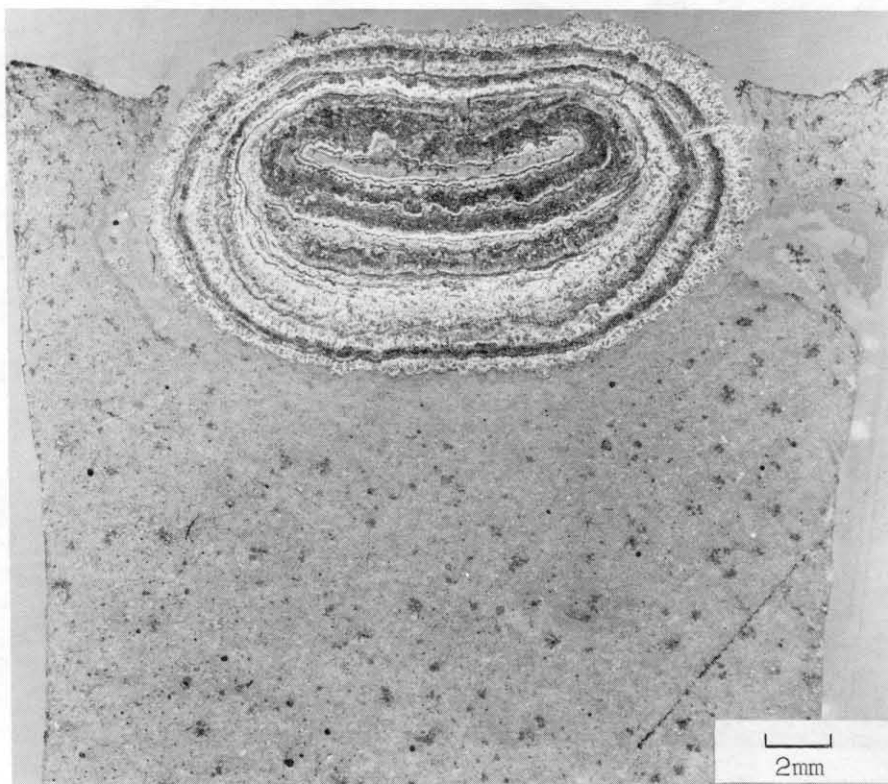
Cruise Number: RP6-OC-75

Station Number: 23B

Latitude: 14°45.9' N

Longitude: 125°50.6' W

Depth (m): 4572



Polished section of nodule NP 62-2 (Sta. 23B)

W. S. U. Specimen Number: NP 64-3

PHYSICAL DESCRIPTION

Dimensions (mm)

Length: 42

Width: 38

Thickness: 17

Weight dry (gm): 25.7

Morphology: Wedge-shaped; broken

discoid nodule? Orientation uncertain.

Color and Surface Texture: Dark gray to black. Much of nodule surface obscured by clay. Microbotryoids on top and bottom (as collected) similar in size, but bottom generally smoother (see figures 5 and 6). Dendritic forms well-developed only in equatorial zone. Note fragment core, fragments in crustal zone, and oxides and clay in fractures.

COLLECTION DATA

Ship: Oceanographer

Cruise Number: RP6-OC-75

Station Number: 27

Latitude: 12°0.29' N

Longitude: 124°59.6' W

Depth (m): 4390



Polished section of nodule NP 64-3 (Sta. 27)

Origin of the Surface Textures of Some Manganese Nodules
from the Equatorial North Pacific

C. C. Woo
U.S. Geological Survey
Menlo Park, Calif.

Manganese nodules having undisturbed orientation, collected with box-coreing during project DOMES, are the materials used for this study. They are from the North Pacific at the locations: $15^{\circ} 45.7' N$, $126^{\circ} 0.4' W$; and $16^{\circ} 0.7'$, $126^{\circ} 46.4' W$. In describing the exterior texture of the North Pacific nodule, Raab (1972) was the first to note that a gritty portion of the nodules facing the bottom sediments and the smooth one, the seawater; and also that a pisolitic or knobby texture characterizes the equatorial zone. Meyer (1973), using shape and size in conjunction of the similar surface textures, classified the North Pacific Manganese nodules into seven types. The materials here used fall in his type B and type E/S. The present study is the result of investigation of the surface textures by using the scanning electron microscope (ETEC with a non-dispersive x-ray analyzer attachment by KEVEX) for their morphological details and qualitative chemical composition and powder x-ray diffraction cameras (57 mm Gondolfi and 114 mm Phillips) for their mineralogic compositions. A model on the origin of these textures is proposed. For convenience, the nodule surfacial growth is divided into three areas; the bottom growth, the top growth, and the fracture fissure growth.

(A) The Bottom Growth

This part of the nodule feels gritty which is due to a texture that can be best described as cauliflower stalks or festoon-like (Fig. 1). The growth always occurs below the sediment burial line of the nodule. In cross-section, sediment fills the in-between spaces of the stalks or festoons.

The overall thickness of the bottom growth is thicker than the top growth, but relatively thinner in the bottom and thicker toward the periphery where a girdle of maximum thickness is present (Fig. 7). The manganese shell of the girdle is about four times as thick as in the very bottom of the bottom growth; a 5.5 cm diameter discoidal nodule is 1 mm thick and situated about 10mm below the burial line. This girdle is described as the pisolitic equatorial belt by Raab (1972) and the equatorial knobby band by Meyer (1973). This is because of the fact that the belt is also characterized by high surface relief. Throughout the nodule there are curvilinear polygonal mounds separated by shallow grooves and at the girdle these mounds and grooves become greatly accentuated and transform into knobs and deep grooves. Epifauna show a strong habitat preference to the burial line area and thus also the girdle area. The most abundant form, saccorhiza, shows preference for the grooves; and like the tests of saccorhiza, white horizontal agglutinated silica septa are also seen bridging between festoons.

(B) The Top Growth

The top growth is smooth to the touch. Under the binocular and scanning electron microscope (SEM) the texture is best described as leathery (Fig. 2). The curvilinear low relief mounds, separated by the shallow grooves, have a polished appearance at the high points. The leathery texture is actually due to grooves and mounds of a multiple order nature that the center of each smallest polygonal unit is very small smooth low knob. The grooves are healed hairline fracture fissures (Fig. 2B & C). A very fine grained thin layer of sediments is present in the surrounding area of the low knob (Fig. 2A). Under binocular some of the major hairline fissures are sealed by a reddish brown material. SEM of these revealed that

they are parallel sheets of probably smectite-illite mixed layered clay grown perpendicular to the surface of the nodule and protrude above the nodule surface in the form of a low ridge (Fig. 2C). This is contrary to the ferromanganese healed hairline fissures which are slightly depressed (Fig 2B).

(C) Fracture Fissure Growth

In the manganese nodule fractures are typical and have been described by Foster (1970), Raab (1972), and Sorem (1973). A peculiar ring-like "cell" texture is seen to occur in a band facing the top surface in front of the up-oozed clay fillings of large fractures (Fig. 4). They are in the form of vertical-wall circular rings that bridge on both walls of the fissure and are therefore mirror images of forms present on the fracture walls when they are open. Occasionally, in wide fissures, instead of circular "cells", they assume a hemispherical bubble-shell with only one side attached; these may be related to the organic originated bubbles seen on the manganese nodule described by Greenslate (1974). In general, the diameter of the "cells" is 1/2 to 2/3 of a millimeter but can be larger or smaller. A small "cell" is commonly seen enclosed essentially within a large one. The "cells" are small and more numerous in the outerzone, nearest to the nodule surface. Circular outlines of some of the outer most row of "cells" are not complete. They are horse-shoe shaped, having the open end facing the exterior of the nodule. The larger "cells" are typically the inner-most. They are circular, $1 \pm$ mm wide, several mm (2-3 mm) long and are elongated parallel to the sediment front. The cell

wall is about 10 mm thick, and can be composed entirely of black manganese material or satin white silica (x-ray, quartz).

The "cells" are also seen composed of black manganese, lined on both the inside and the outside with white cell-walls. One large irregular white "cell" is rather pearly lustered, having an organic jell-like appearance. Both sides of the cell wall are preserved, in that the structure is almost a complete sack. Inside the broken-off portion is revealed an olive brown dried substance of a once living organism. On the same specimen, inside the manganese "cell", there is a dried jell-like membrane, again suggesting an organic nature of these "cell" structures. The "cells" are in the sediment-free part of the fissure which is 70-90% sediment filled. Immediate in the sediment front, one can find limited growth of black cauliflower festoons which may partially obliterate some presumably old "cell"-like textured growths.

Mineralogy of the Nodule Surface Growths

X-ray diffraction patterns taken from the different growth areas show that the manganese on the bottom growth and black "cell" walls is todorokite and that on the top growth is birnessite. SEM pictures of the top growth (Fig. 3) show that the birnessite takes the form of thin plates. The hexagonal outline of the plate can be detected. Unlike the birnessite occurring in other nodule localities (Woo 1973 and Fewkes 1973), it is not arranged in random box-works. This birnessite is characterized by packed parallel arrays, a non-porous texture, and plates which are parallel to the surface of the nodule. A spot mode of the non-dispersive x-ray which analyzed the hexagonal plate yielded a spectrum (Fig. 3) much like that of the other parts of the top growth.

The birnessite of the nodule is a high iron-bearing manganese mineral.

Low magnification SEM photograph of the bottom growth is featureless. However the high resolution of ETEC is able to detect the very fine texture of the todorokite. In extremely high magnification, the todorokite appears to be layered growth of aggregates composed of short rod-like materials (fig. 1). The x-ray spectrums of the cauliflower textured festoons show that the todorokite is composed of very high percentage of Mn and high trace metals of Ni and Cu; relatively low in Fe and very low trace of Ti as compared with that of birnessite which is high in Fe and high in the trace metal Ti but lower in Ni and Cu. Due to the K_{α} of Fe, the trace content of Co cannot be readily resolved.

Proposed Model

Three factors are thought to control the growths:

- (1) Ferromanganese nucleation prefers a solid to have a large surface area.
- (2) Precipitation of the ferromanganese is a result of the reaction between the Mn-bearing solution from the sediments and O_2 -bearing seawater. Thus an upward diffusion of the Fe-Mn in the sediments is postulated at the interface of seawater and sediments.
- (3) The freshly precipitated ferromanganese oxide-hydroxides is present in the form of high water content jells. Ageing and crystallization of the jells yield shrinkage or

dehydration cracks. The disrupted cracked surface discourages the nucleation and the corners depress the Mn-Fe growth. The preference of microorganisms to lodge themselves in open fractures may also impede Mn growth.

From the above considerations, the surface features can be easily explained. Both the bottom growth and the top growth basically originated from the same surface, characterized by desiccation or dehydration cracks of the first, second, third ... orders. The first order cracks produce the reticular grooves and polyhedral mounds and knobs of the whole nodule. The second, third and lower order cracks produce the leathery and hairline network structure found on the top growth and the interstitial spaces between the cauliflower festoons of the bottom growth. If starting on top of the fine fractured mosaic surfaces of top growth continuous Fe-Mn nucleation vertically but not laterally the cauliflower festoons will be resulted. Therefore, the difference between the bottom and top of growths is due to the difference in the rate of growth and the direction of material transport.

The thicker bottom growth is due to its proximity to the sediment, source of the Mn. The top growth is probably the result of the diffusion of the Mn solution from sediments in the sea floor area between the nodules. The low Fe and high transitional metals in the todorokite of the bottom growths and high Fe and Ti in the birnessite of the top growth make the statement that the transitional metals are primarily associated with the Mn-bearing solution from the sediment and the higher Fe and Ti content, with the seawater an attractive theory. The precipitation of Mn on a nodule is due to the reaction of these two chemical end members.

The presence of a maximum growth girdle of the nodule well testifies that it is resulted from maximum chemical activity and coincides with the sediment-water interface Eh gradient concept of Bonatti et al (1973). The horizon of low Eh values is the optimum condition for todorokite precipitation. Since the Eh gradient is created primarily by sediment-seawater interface, genetically, the girdle may be called an interface girdle.

The manganous-bearing mineral, todorokite, characterizes both bottom growth and fracture fissure growth. It is a mineral formed within a low Eh environment. This environment lies below both the burial line and the interior of the fissure where the access of O_2 -bearing seawater is limited. On the other hand, the precipitation of birnessite, directly in contact with the seawater, occurs under a well oxygenated condition. From above, it is seen that the model also explains the mineralogical difference between the two parts of the nodule.

Raab (197) proposes that the sediment is the Mn-source, and that the Mn-bearing solution is thermally induced by deep-seated intrusions. The chemical differences of the top and bottom growths are due to leaching out the transitional metals from the top of the nodule by the constant contact of seawater. It is an attractive theory; however, it is very hard to prove that the fluctuation of first deposition and then leaching (chemical weathering) exist and that the birnessite is not a primary mineral.

Growth inside the fracture surfaces may heal the cracks which produce the hairline network of top growth. However, continuous supply of Fe-Mn from the bottom sediments and "cells" texture growth through the activities of microorganisms along the crack promote further growth and may even open

the fissures, resulting in fragmentation of the nodules. Almost all the cross-sections of the nodules show that the nuclei are composed of fragments of old generation nodules. The irregular shape of a nodule is therefore inherited from these fragments. The fragmentation or fission along fractures is one of the important methods accounting for the multiplication of nodules on the sea floor (Fig. 5).

- Bonatti, E., T. Kraemer, and H. Rydell, 1972, Classification and genesis of submarine iron-manganese deposits, p. 149-166 in D.R. Horn, Editor, Ferromanganese Deposites on the Ocean Floor, Conference, Arden House, Harriman, N.Y., 20-22 January 1972, Lamont-Doherty Geological Observatory, Columbia University and IDOE-NSF, 293 pp.
- Fewkes, R.H., 1973, External and internal features of marine manganese nodules as seen with the SEM and their implications in nodule origin, p. 21-29 in Maury Morgenstein, Editor, The Origin and Distribution of Manganese Nodules in the Pacific and Prospects for Exploration, Symposium, Honolulu, Hawaii, 23 - 25 July 1973, Valdivia Manganese Exploration Group, University of Hawaii and IDOE-NSF, 275 pp.
- Greenslate, J. 1974a, Microorganisms participate in the construction of manganese nodules, Nature, Phys. Sci., v. 249, p. 181-183.
- Meyer, K., 1973a, Surface sediment and manganese nodule facies encountered on RV Valdivia cruises 1972/73, Marine Technol., v.4, no. 6, p. 196 - 199; 1973b, p. 125 - 130 in Maury Morgenstein, Editor, The Origin and Distribution of Manganese Nodules in the Pacific and Prospects for Exploration, Symposium, Honolulu, Hawaii, 23-25 July 1973, Valdivia Manganese Exploration Group, University of Hawaii and IDOE-NSF, 175 pp.
- Raab, W., 1972, Physical and chemical features of the Pacific deep sea manganese nodules and their implications to the genesis of nodules, p. 31-50 in D.R. Horn, Editor, Ferromanganese Deposites on the Ocean Floor, Conference, Arden House, Harriman, N.Y., 20-22 January 1972, Lamont-Doherty Geological Observatory, Columbia University and IDOE-NSF, 293 pp.

Sorem, R.K., 1973, Manganese nodules as indicators of long-term variations in sea floor environment, p. 151-164 in Maury Morgenstein, Editor, The Origin and Distribution of Manganese Nodules in the Pacific and Prospects for Exploration, Symposium, Honolulu, Hawaii, 23-25 July 1973, Valdivia Manganese Group, University of Hawaii and IDOE-NSF, 175 pp.

Woo, C.C., 1973, Scanning electron micrographs of marine manganese micro-nodules, marine pebble-sized nodules, and fresh water manganese nodules, p. 165-171 in Maury Morgenstein, Editor, The Origin and Distribution of Manganese Nodules in the Pacific and Prospects for Exploration, Symposium, Honolulu, Hawaii, 23-25 July 1973, Valdivia Manganese Exploration Group, University of Hawaii and IDOE-NSF, 175 pp.

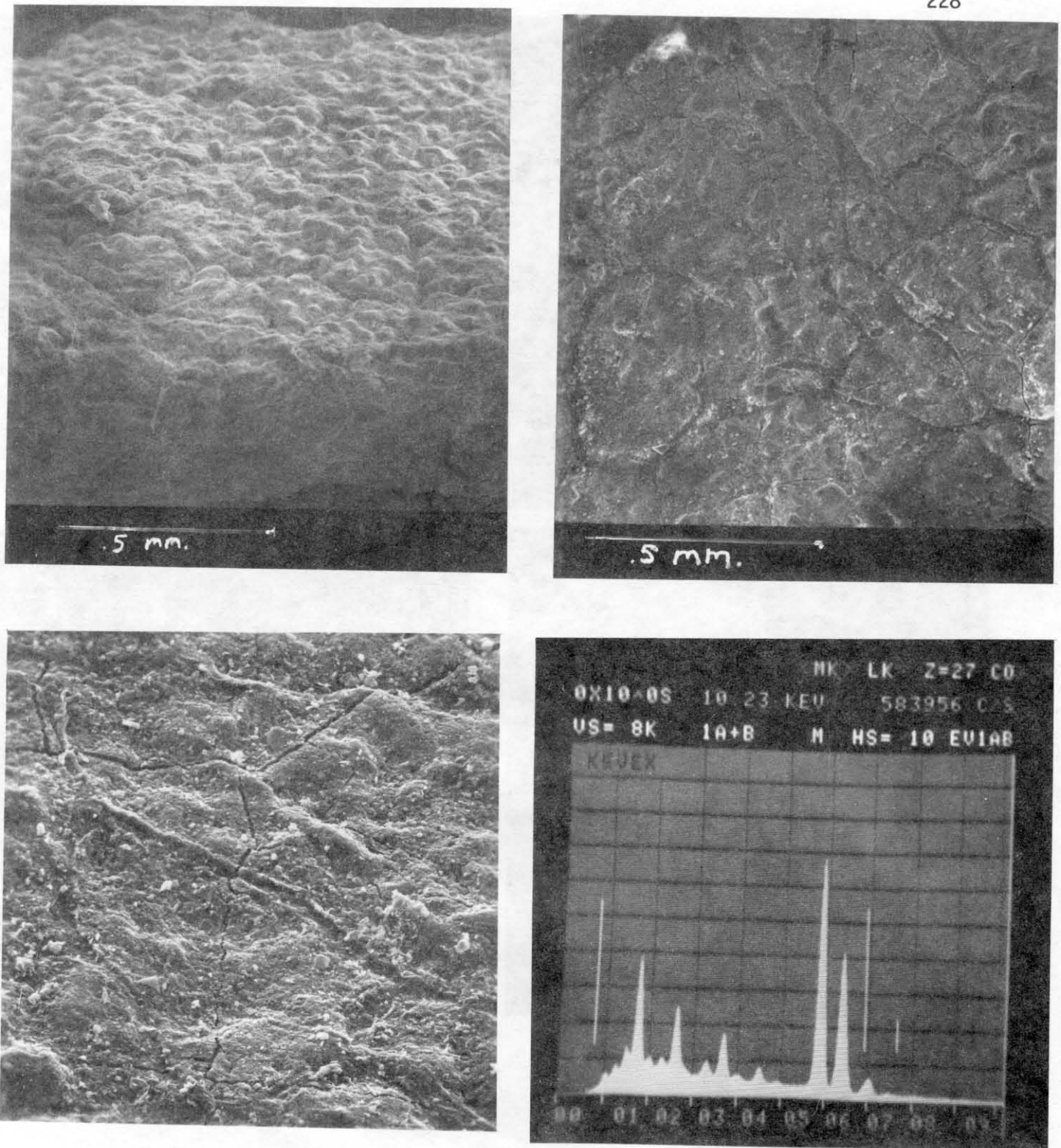


Fig. 2 Leathery texture of the top growth. A to D same as Fig. 1. (A) Oblique view to show small knobs 78X. (B) Healed hairline fractures, 85X. (C) Reddish brown clay filled hairline fractures, slightly higher relief above the surface. Black fractures caused by further dehydration shrinkage due to shelving 251X. (D) X-ray spectrum at the top of a small knob; Na, Mg, Al, (Si), P, S, (Cl), K, (Ca), Ca, (Ti), Ti, (Mn), (Fe) Mn, Fe, and Ni; the asymmetrical Fe probably indicate trace of Co.

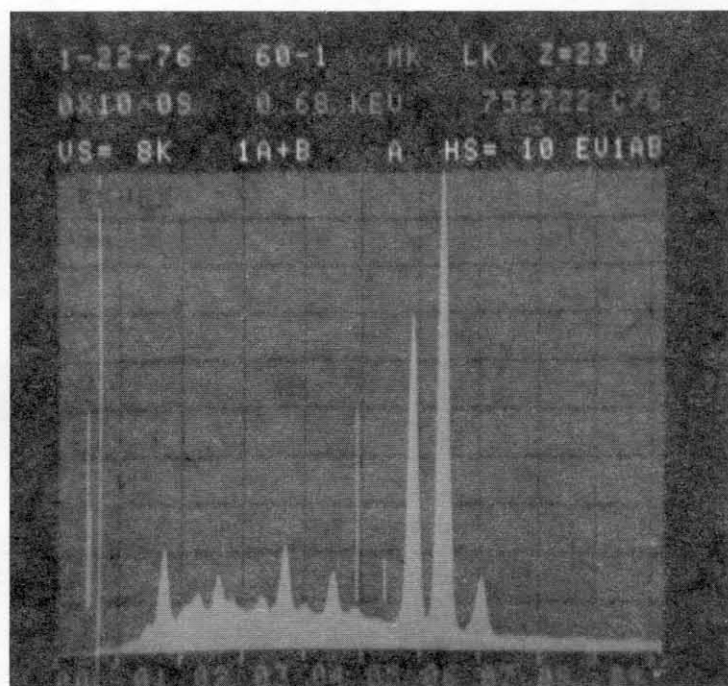
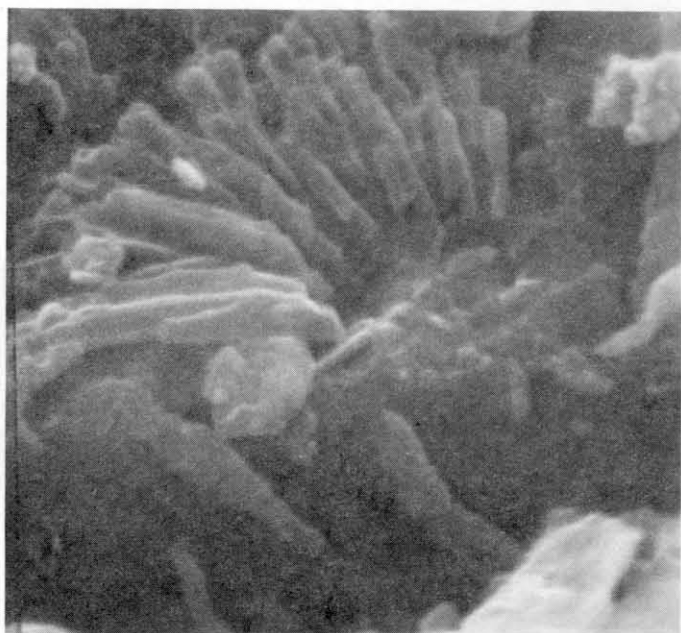
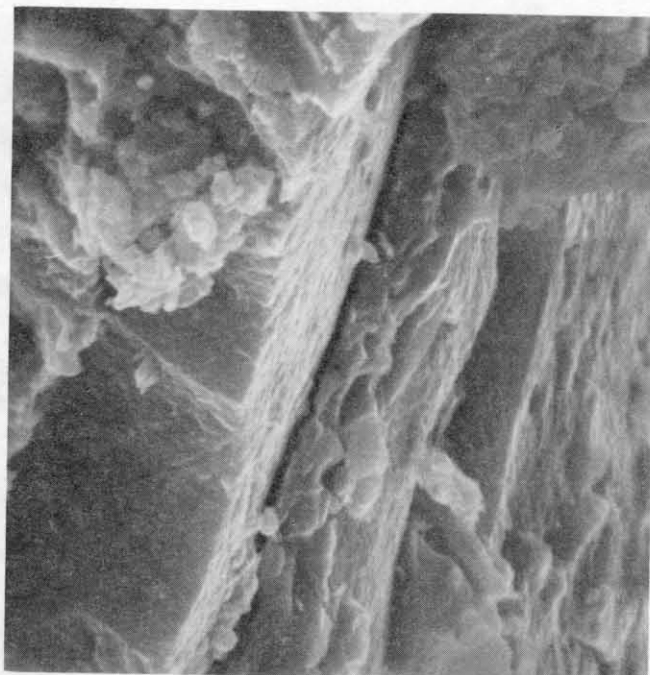
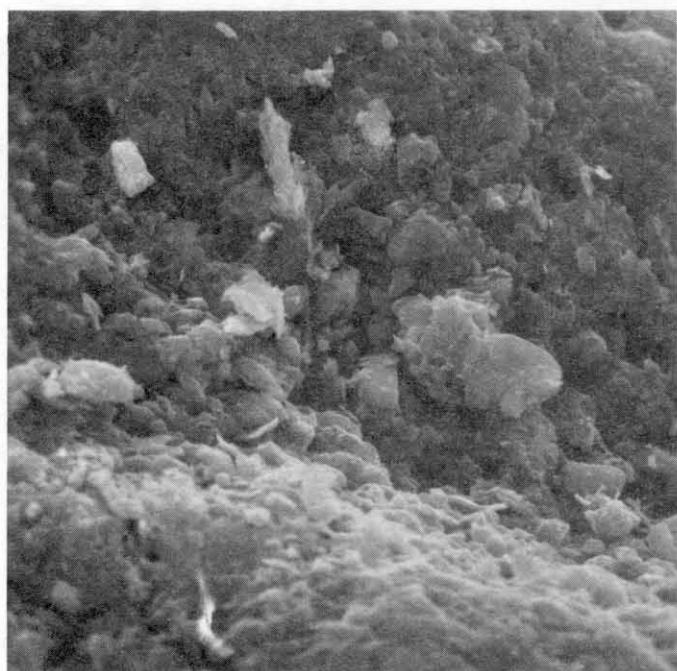


Fig. 3. Top growth (A) Sediment particles scattered around the small knob. Part of the knob is shown at the lower margin. 2,500X. (B) Birnessite sheets densely decked parallel to the surface of top growth, 4,080X. (C) Birnessite sheets, 20,080X. (D) X-ray spectrum of the left center hexagonal birnessite plate of C. Al, (Si), P, Au, (Cl), Pd, K, (Ca), Ca, (Ti), Ti, ?, (Mn), (Fe), and Fe. Au and Pd are due to coating of the specimen.

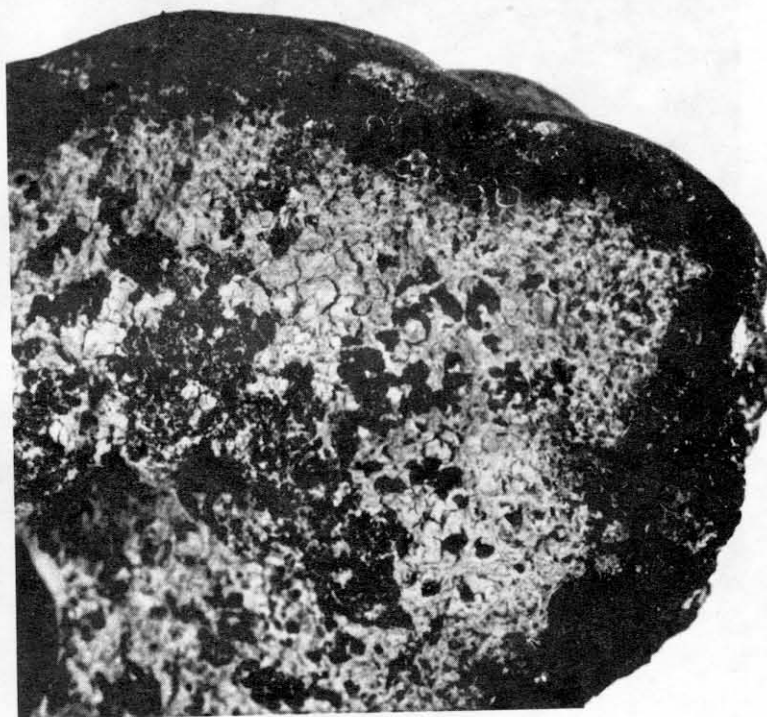
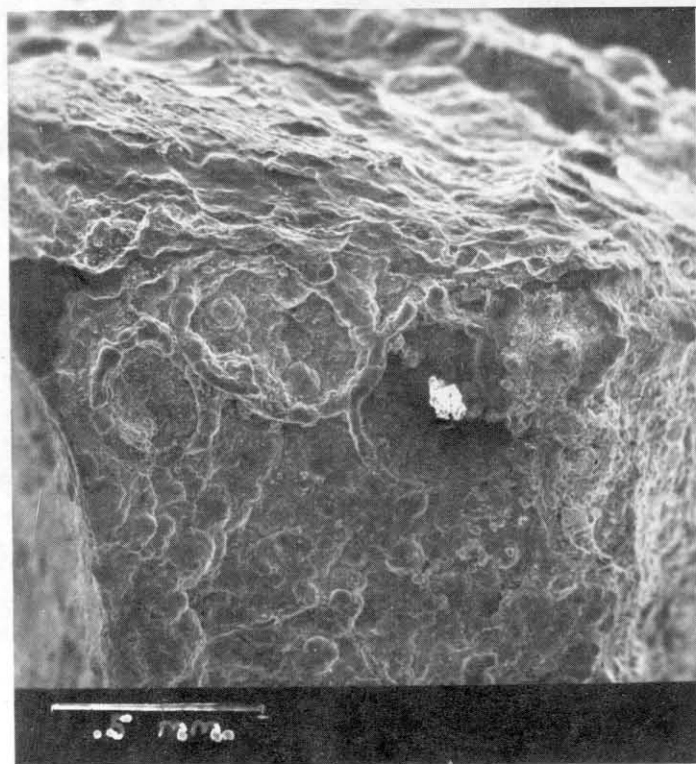
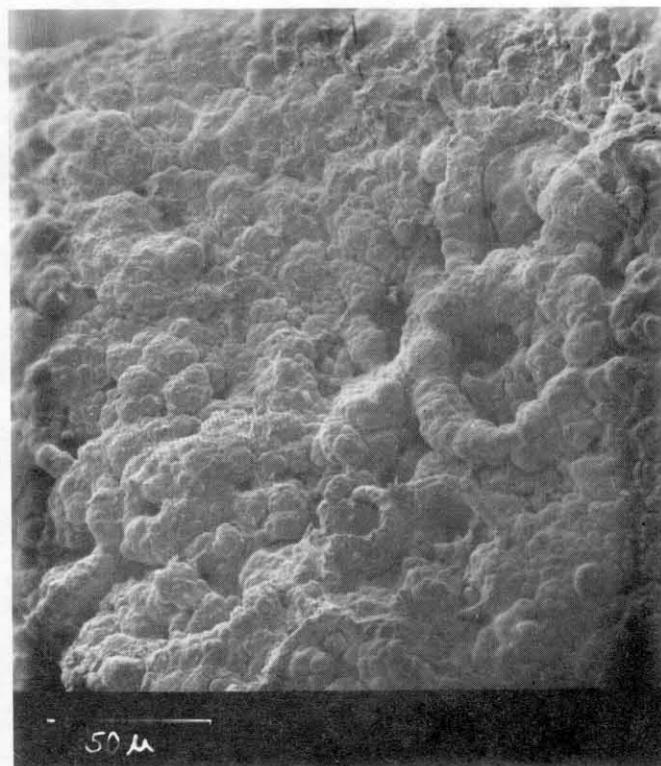
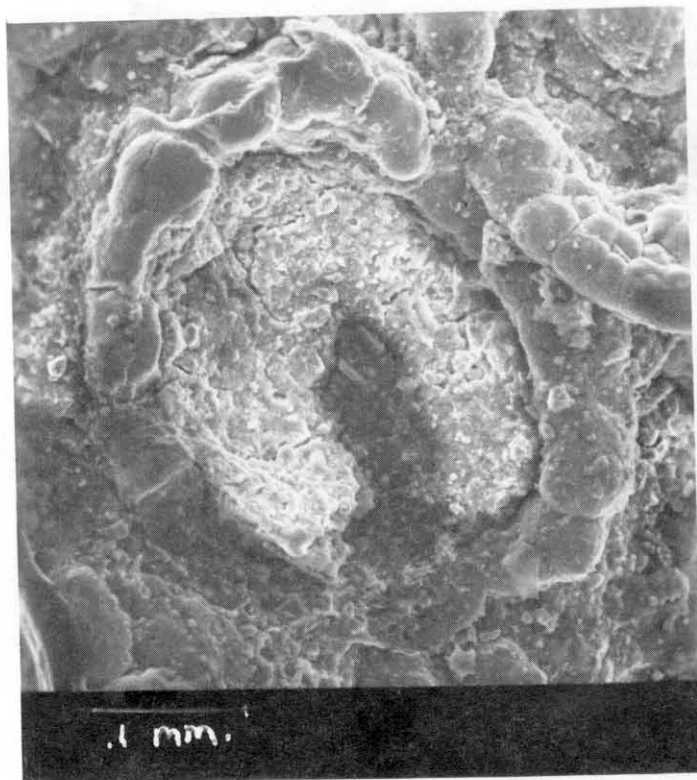


Fig. 4 "Cell" texture in fracture fissure growth, (A) 236X, (B) Old "cell", partially obliterated by cauliflower festoon bottom growth, 432X, (C) 56X low magnification of (A), (D) Photograph of fracture wall, white "cells" are composed of quartz and the black ones, of todorokite. White mass is sediment fill.

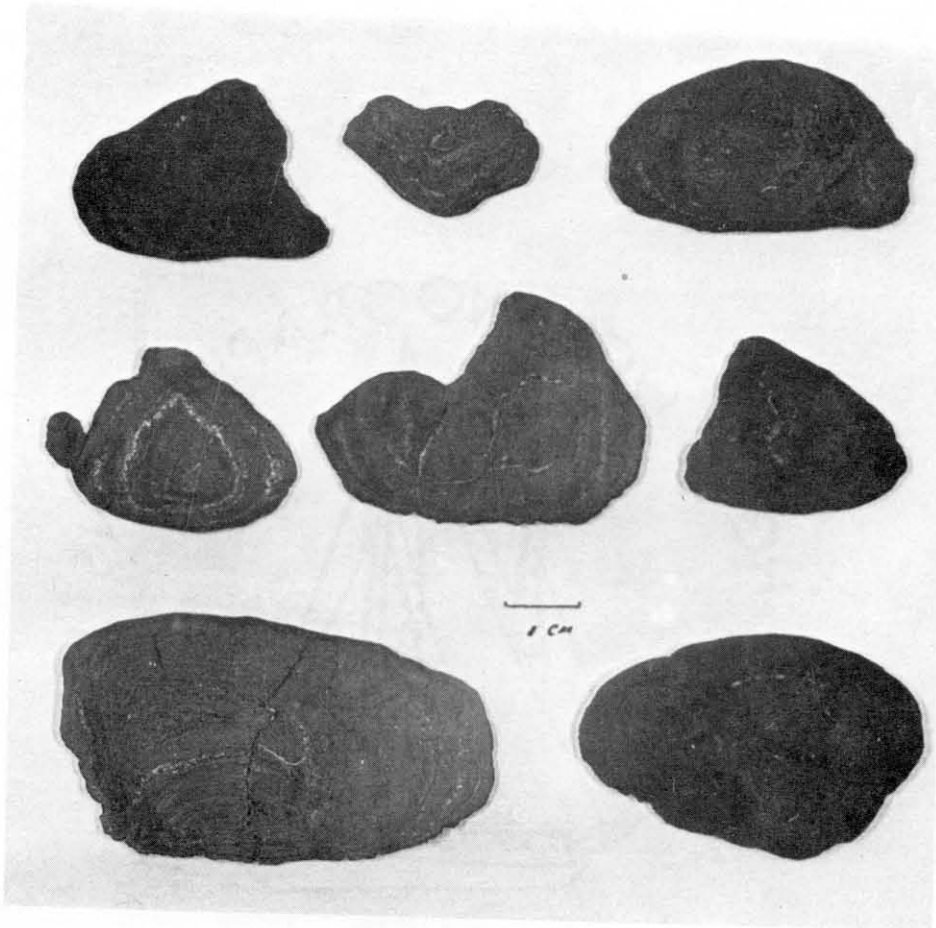


Fig. 5 Cross sections to show the broken-round shape of most of the nodules and the nuclei are fragments of old nodules.

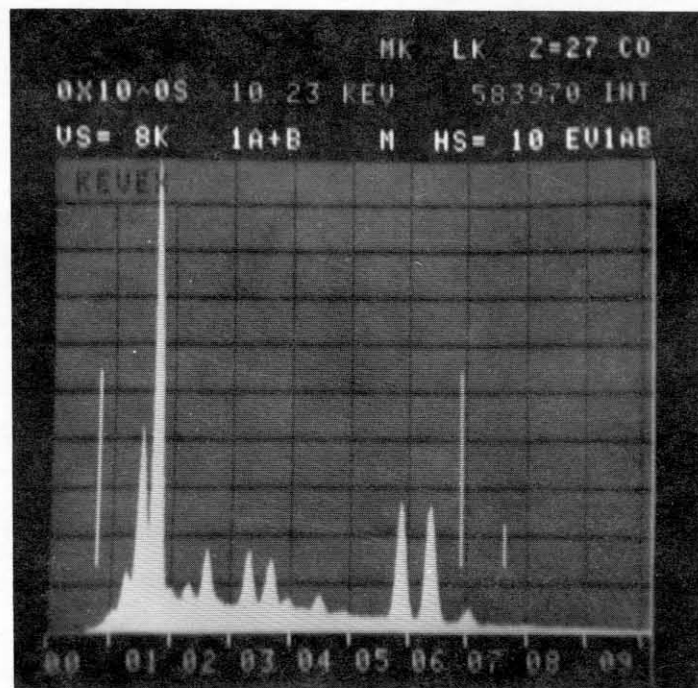


Fig. 6 X-ray spectrum of the reddish brown hairline fracture filling clay - NA, MG, (Al), (Si), P, S, (Cl), (K), (Ca), Ca, (Ti), Ti, (Mn), (Fe) Mn, and Fe

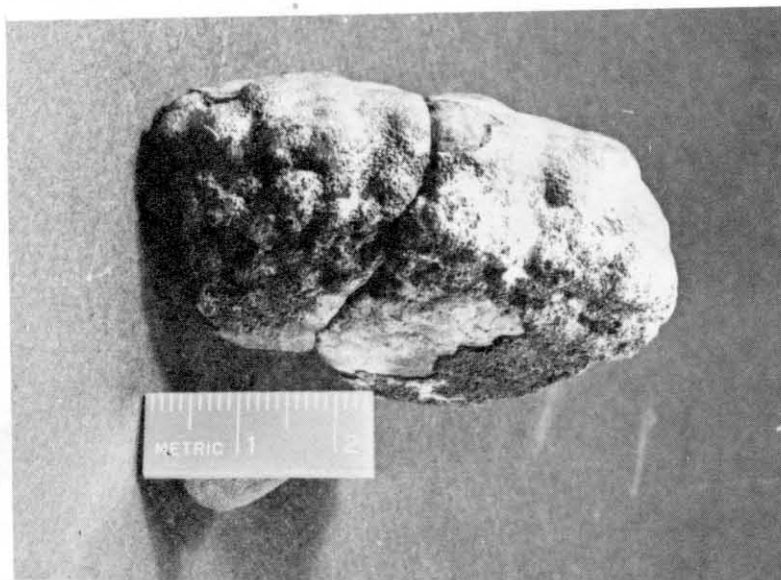


Fig. 7 Top growth, bottom growth, and interface girdle of a Mn nodule fragment. Scale in centimeters.

CHEMICAL CHANGES IN SURFACE SEA WATER CAUSED BY SUSPENSION
OF MARINE SEDIMENTS

A Preliminary Report for Domes Site C

by
James L. Bischoff
and
Robert J. Rosenbauer
U.S. Geological Survey
Menlo Park, California

Introduction

Deep Sea mining operations will stir up sediment from the ocean floor and suspend it in both the near-bottom, and at the surface or near-surface. In the latter case such suspensions may have a stimulatory or inhibitory effect on surface-dwelling organisms.

Three possible effects can be visualized. Suspended sediment, by blocking sunlight may serve to inhibit photosynthesis. Another possibility is the acceleration of respiration by providing increased particulate surface area for bacterial activity. This effect will be most critical in the oxygen minimum zone at approximately 200 meters depth, where such acceleration may even produce toxic H_2S (see preliminary report by J.J. Anderson).

The third possible effect, the subject of this report, is that the suspended sediment releases and/or takes up biologically critical dissolved components. Nutrient rich bottom waters will be brought to the surface along with sediment and nodules and the effects of this water is considered stimulatory and its effect predictable. It is the action of the sediment itself which remains less predictable.

Enrichment experiments using bottom water with and without suspended sediments have been carried out by Amos et al. (1973). They found that photosynthesis was stimulated in both sets of experiments, but stimulation was significantly greater with the suspended sediment. They suggested that the

sediments might be releasing a trace metal such as Fe having a stimulatory effect on the phytoplankton.

Robertson and Rancitelli (1973) reacted surface sea water with crushed ferromanganese nodules, and monitored dissolved Rb, V, Fe, Zn, Cs, Sb, Ag and Co. Of these, they found that only Fe displayed a measurable increase, changing from <5ppb in the original sea water to values ranging from 34 to 116ppb in the experiments. Aliquots taken for analyses were centrifuged but were not membrane-filtered, therefore leaving some doubt that the measured Fe was in true solution and not particulate.

Objectives

The purpose of this study was to assess the effect of sediment and nodule suspension on sea water chemistry in the absence of biologically mediated processes. Our experiments were designed with the following questions in mind:

- 1) Are trace metals, toxic and/or stimulatory, released by suspended sediments and nodules to levels of biological importance?
- 2) What happens to the nutrients?
- 3) What changes take place in the major dissolved components?
- 4) How does chemical interaction change with time?
- 5) How does the nature and direction of chemical reaction vary with sediment type and with different aliquots of the same sediment?

Experimental

1) Sea Water:

Surface sea water was collected at Pt. Reyes, California, was aereated and sterlized by membrane filtration (0.1 μ pore size).

2) Sediments:

Sediments were taken from 11 box cores collected at site C, 27 samples in all, and were splits of the same samples used for the collaborative study of interstitial water, sedimentology, mineralogy, biostratigraphy, and bulk chemistry (see accompanying reports, this volume). In some cases several samples were taken down a single core (16B, 18, 18B, 20, and 24B) to test within core variability, and in others a single composite sample, representing the entire core was taken (11, 15B, 23B, 25, 27). In addition, a composite of ten nodules from these same cores was also taken for resuspension experiments.

Details of the sediment types and composition are given in the accompanying reports. In general, the sediments are heterogenous, but overall fall into the category of brown siliceous mud. Typical for Pacific muds, the heavy metals are particularly enriched in these sediments, most notably for Mn, Cu and Ni. Organic carbon concentration varies between 0.1 to 0.5%, typical for sediments in these latitudes (Lisitzin 1972).

Sediment from the lower two intervals in core 18B contained a large component of hydrothermal metalliferous mud described

by Bischoff and Rosenbauer (this volume). This was an entirely unexpected occurrence, as these muds are previously known only adjacent to active spreading centers, and are believed to have precipitated from sea floor injections of hydrothermal fluids. This material is ubiquitous in most of the sediments studied from Site C, but is usually a minor or trace component.

Interstitial water was removed on board ship from each sample by squeezing at 4⁰C so that ion-exchange equilibrium was maintained, and the samples sealed in polyethelene bags and refrigerated until experiments began.

3) Experimental Technique

10 grams of the damp sediment was suspended in 100 grams of sea water in blackened polyethelene bottles by shaking on a wrist action agitator at a one second frequency. The bottles had previously been acid washed and equilibrated with sterilized sea water and drained, but not dried, prior to the experiments. Temperature was ambient, ranging between 21⁰ and 23⁰C diurnally.

10 ml. samples of the sea water were taken after gently centrifuging the bottles, into a plastic syringe and pressed through a 0.1 μ membrane filter into another syringe. Aliquots from this syringe were divided by weight for analyses of the various components.

Analysis

Major cations Mg, Ca, K were analyzed by conventional flame atomic absorption spectroscopy, standardizing against Copenhagen sea water. Cl was analyzed by automatic chloridometer (London Co.), SO_4 by radiochemical counting of a precipitate with Ba^{133} , and C_T (total dissolved CO_2 which includes $CO_3^{=}$ + HCO_3^- + H_2CO_3 and aqueous CO_2) by direct injection into an infra-red carbon analyzer (Oceanography International Corp).

The nutrients SiO_2 , NO_3^- , NO_2^- , NH_4^+ and $PO_4^{=}$ were analyzed by a Technitron autoanalyzer.

The trace metals Fe, Mn, Cu, Ni, Cr, Mn, Hg, Zn and Al were analyzed on acidified aliquots by flameless atomic absorption spectroscopy standardized against spiked Pt. Reyes sea water. Al was analyzed as a monitor to check against accidental incorporation of sediment particles in the acidified aliquot. Detection limits for these metals are as follows: Fe, Cu & Mn, Cr 5ppb, Ni and Zn 10 ppb, Hg & Al 20 ppb.

Data and Discussion

1) Pilot Experiment:

A preliminary experiment was carried out to assess rates of equilibration. For this purpose, sample 18B-37, 26-28 cm was chosen as representing an extreme case, composed of 60% red clay and 40% hydrothermal metalliferous mud. pH was monitored with time (Fig.1), and was characterized by a rapid drop from 7.9 of the starting sea water to 7.5 within 1 hour. pH then increased to 7.7 during the first two days. Subsequently, the pH remained between 7.7 and 7.8 until the end of the experiment at 33 days. This pH range compares with the shipboard measurement of pore water pH of 7.75 for this sample (Callender and Bischoff, this volume).

During this preliminary experiment water samples for complete analysis were taken at 18 days and at 33 days (Tables 1-2) with results indicating no significant change in this time interval for any component except NH_4^+ . NH_4^+ increased dramatically from 3.49, close to the pore water value, to 23.59 $\mu\text{g atm/l}$ suggestive that bacterial activity eventually becomes important in these experiments. Dissolved heavy metals remained below detection, even after 33 days.

Our interpretation of these data is that ion exchange and surface absorption re-equilibration processes control the sea water chemistry in our experimental systems and are essentially complete within the first two or three days. Afterward, the system has very little tendency to change until bacterial act-

ivity becomes important after about 10 days. The only noticeable effect of this bacterial activity, however, is the increase in NH_4^+ .

This indicated the optimum time to sample for subsequent experiments was between 6 and 10 days.

2). Chemical changes:

Based on these results the remaining samples were handled in a similar manner, but sampled once at between 6 and 11 days.

The results (Tables 3-5) indicate that direction and degree of change is similar for each sample and for each component with some minor exceptions. Variation within cores is about the same as between cores so it is possible to generalize the data in terms of individual components.

A. Major components:

As in the pilot experiment, pH decreased for all sediments, the change averaging 0.26 pH units (Table 6). The largest decrease, 0.65 units was recorded for the nodule composite.

Mg is likewise slightly depleted and K slightly enriched (Table 6). Changes in Ca and Cl are insignificant and on the order of our analytical uncertainty. SO_4 is likewise generally unchanged, except for slight systematic depletion with depth in core observed for samples from core 16B. A similar depletion is shown in the pore water from this core (Callender and Bischoff, this volume).

C_T shows a slight depletion for all samples studied (Table 6).

B. Nutrients

SiO_2 is the most dramatically changed component displaying an average enrichment by a factor of 5 (Table 6). The enrichment is more pronounced for samples higher in the cores (Table 4).

NO_3^- in general was depleted although the pattern is erratic from sample to sample. An extreme case of NO_3^- depletion is shown by samples from core 24B, where essentially 90% is removed. Unfortunately, we have no pore water analyses for NO_3^- . However, organic carbon is particularly high for sediments in this core (Bischoff and Piper, this volume), and it is possible that bacteria feeding on organic matter had depleted the O_2 and much of the NO_3^- as well. NO_3^- was likewise depleted in the nodule composite.

NO_2^- shows very little change from the starting sea water for all samples excepting those from 24B and the nodule composite, where like NO_3^- in these samples, it is almost completely depleted (Table 4).

NH_4^+ in the starting sea water was below our detection limit of $0.01\mu\text{g atm/l}$, and increased rather uniformly in all our experiments to an average of $3.44\mu\text{g atm/l}$. Pore water levels for NH_4^+ measured on board ship were also high averaging near $10\mu\text{g atm/l}$ (Callender Bischoff, this volume).

NH_4^+ enrichment in the resuspension experiments does not appear coupled with NO_3^- depletions, seemingly precluding a simple bacterial reduction of original NO_3^- in our experiments as an explanation for the NH_4^+ enrichments.

PO_4^{-3} is generally slightly depleted (Table 6), but several slight enrichments were observed (Table 4).

C. Trace metals:

In almost all samples, the trace metals Fe, Cu, Ni, Mn, Hg, Zn, Cr and Al were below detection limits in the sea water. Exceptions to this were found in only seven samples in which Fe and Al reached values of several hundred ppb (Table 5), in five of these Mn was present as well, but as less than 100 ppb, and Cu was present in only three of these, at levels of 5, 7, and 18 ppb, very close to its detection limit. Significantly, none of these included the nodule composite nor the metalliferous mud.

Fe varies with Al for these samples (Fig. 2), which leads to the conclusion that they are the result of sediment particle contamination in the acidified aliquot used for metal analysis.

Interpretation

1) Major Components and nutrients:

Direction and rapidity of observed changes, particularly for Mg and K, are analogous to those observed for the temperature of squeezing effect observed during earlier interstitial water investigations (Bischoff et al., 1970). These changes are due to redistribution of ion-exchange equilibria during the warming of a cored sediment from in-situ temperature of about 2-4°C to shipboard laboratory temperatures close to 25°C. Ion-exchange and other forms of surface adsorption equilibria are strongly effected by such a temperature change and re-equilibration is very rapid, usually being complete within hours.

A sediment particle requires hundreds to thousands of years to settle to the deep-sea floor, and during this time equilibrates its surface with essentially an infinite reservoir of sea water. After burial interstitial water is slowly expelled during compaction, and in this system, the reservoir of surface adsorbed species becomes much greater than that dissolved in the interstitial water. For example, cation exchange capacities of sediments from DOMES Site C as measured in our laboratory average close to 60 meq per 100 grams dry sediment. Na^+ accounts for approximately 40% of the exchangeable cations, so approximately 32.6 meq per 100 grams sediment are occupied by the other cations. Considering a

typical in-situ sediment to contain approximately 60% by weight interstitial water, we see that a cubic centimeter of wet sediment contains 0.13 meq of adsorbed cations and only 0.08 of dissolved cations in the interstitial water, ignoring Na in both cases. The adsorbed cations clearly represent the larger reservoir. The chemistry of the interstitial water, therefore will reflect even small changes in the distribution of the adsorbed species, and such change accounts for the earlier observed changes in interstitial water chemistry when such water was extracted at temperatures different from in-situ. This effect has also been observed for non-charged species such as SiO_2 , the concentration of which in interstitial water is strongly a function of extraction temperature (Fanning and Pilson 1971).

Extending this reasoning to the resuspension experiments, we calculate that a cubic centimeter of the sea water in our suspension experiments contains 0.9 grams of sea water and 0.1 grams of sediment; and has 0.03 meq of exchangeable cations and 1.2 meq aqueous cations. The dominate cation reservoir in this system is the sea water, but the adsorbed reservoir is by no means negligible, accounting for 20%. Changes in the distribution of species in the exchangeable reservoir due to warming is adequate to cause the slight change observed for the major cations and SiO_2 in our experiments.

Changes in NH_4^+ may also be caused by such simple surface redistribution. NH_4^+ , is one of the most strongly adsorbed cationic species, and the observation of relatively high concentration of NH_4^+ in the interstitial waters (Callender and

Bischoff, , this volume) implies even higher absorbed concentrations on the sediment particles. Resuspension of these sediments into NH_4^+ free sea water, as in our experiments, would result in release of the absorbed NH_4^+ until exchange equilibrium is established. Some NH_4^+ , particularly for the 33 day experiment, is possibly caused by bacterial activity. However, the fact the NO_3^- concentration remains unchanged, implies that such bacteria are metabolizing solid organic matter in the sediment and using O_2 . The fact that C_T did not increase in any of our experiments implies that such metabolism is very minor, and its effects are only noticeable for NH_4^+ .

2) Trace Metals:

In only 7 samples were any heavy metals detected, and in these, proportional concentrations of Al were also found (Fig. 2). Al solubility is unaffected by varying redox conditions in sea water, and at the pH of the experiments, Al should always have remained below our detection limit. Hem (1968) has shown that Al precipitates from supersaturated solution and decreases to less than 2 ppb within one day at pH between 5 and 8. Therefore, we used Al as a test for contamination by sediment particles, since the particles have comparable bulk contents of Al and Fe, and lower contents of Mn, Cu and Ni. Acidification of the contaminated aliquot would, therefore, release comparable values of Fe and Al. We conclude, therefore that the seven instances of detected heavy metals were the result of such contamination and that no heavy metals were released by the suspended sediments above our detection limits.

3) Environmental Implications:

Our experiments were designed to observe the chemical interaction between sediments and surface sea water, as might occur during surface discharge of mining wastes, at the approximate concentration of suspended solids at the point of discharge.

Under these conditions, we have no evidence to suggest that sea water chemistry will be altered in such a way it that will have any deleterious environmental effects. Changes in major components and nutrients, although detectable, remain insignificant for the variety of sediment types at DOMES Site C. No release of trace metals, toxic or stimulatory, were observed, even for hydrothermal metalliferous sediments and nodules.

The slight stimulation of productivity observed by Amos et al. 1973, is, therefore, unlikely the result of Fe release as they speculated. Based on the results of our experiments, the only suggestion we can offer is that the SiO_2 release from the sediments as such a stimulant.

4) Future Experiments:

The question of sediment-sea water interaction within the O_2 minimum zone has recently become important. The preliminary model by J. Anderson suggests that the increased surface area provided by suspended sediment as it settles through this zone may accelerate bacterial metabolism to such a degree that the water mass may go anoxic. The trace metals under these conditions may be considerably more soluble than under the oxygen rich conditions at the surface.

Experiments similar to those described in this report should be carried out, therefore, using unfiltered sea water collected from the O_2 minimum zones of the mining sites, and utilizing a completely closed experimental system.

Table 1

Major dissolved species in pilot resuspension experiment with sediment from DOMES station 18B core 37 (26.2-28.2 cm), compared with starting sea water and pore water extracted from same sample. Concentrations are in ppm except for pH.

	pH	Mg ⁺²	Ca ⁺²	K ⁺	Cl ⁻	SO ₄ ⁻²
Pt. Reyes Sea water	7.73	1235	396	382	18,540	2616
Pore Water*	7.40	1228	393	395	-	2522
Resuspension 18 days	7.83	1228	391	434	18,540	-
Resuspension 33 days	7.81	1223	390	437	18,550	2596

* Data from Callender and Bischoff (this volume)

Table 2

Dissolved nutrients in pilot resuspension experiment with sediment from DOMES station 18B core 37 (26.2-28.2 cm), compared with starting sea water and pore water extracted from same sample. Concentration for C_T in m moles/l, others in $\mu\text{g atm/l}$.

Sample	C_T	SiO_2	NO_3^-	NO_2^-	PO_4^{3-}	NH_4^+
Pt. Reyes Sea water	1.93	40	27.27	0.46	2.33	<0.01
Pore Water*	2.64	-	-	-	2.20	5.93
Resuspension 18 days	1.94	200	26.50	0.64	2.24	3.49
Resuspension 33 days	1.69	210	27.03	1.08	1.89	23.59

* Data from Callender and Bischoff (this volume)

Table 3

Major dissolved components in DOMES, Site C, resuspension experiments. Sediment was suspended in Pt. Reyes seawater at 25°C for 6-11 days. Mg⁺², Ca⁺², K⁺, Cl⁻ and SO₄⁻² in ppm, C_T in m moles/kg.

Sample	ph	Mg ⁺²	Ca ⁺²	K ⁺	Cl ⁻	SO ₄ ⁻²	C _T
Pt. Reyes Seawater	7.92	1235	396	382	18,540	2616	1.93
<u>18B-37</u>							
0-2.2 cm	7.72	1203	392	404	18,540	2644	1.72
10.2-12.2 cm	7.75	1194	399	403	18,530	2597	1.73
18.2-20.2 cm	7.82	1225	395	404	18,550	2593	1.85
26.2-28.2 cm	7.83	1228	391	434	18,540	--	1.94
30.2-32.2 cm	7.90	1230	397	405	18,530	2652	1.79
<u>16B-49</u>							
2-4 cm	7.68	1228	393	397	18,600	2514	1.73
12-14 cm	7.62	1218	393	398	18,560	2511	1.66
28-30 cm	7.61	1219	392	412	18,590	2471	1.71
<u>18A-36</u>							
2.2-4.2 cm	7.62	1216	393	398	18,610	2618	1.81
14.2-16.2 cm	7.61	1222	398	394	18,530	2614	1.79
22.2-24.2 cm	7.66	1224	390	402	18,600	2567	1.64
<u>20-27</u>							
4.2-6.3 cm	7.62	1228	394	403	18,590	2601	1.85
8.5-10.7 cm	7.61	1218	395	398	18,650	--	1.79
12.9-17.9 cm	7.61	1230	390	399	18,540	2581	1.84
<u>24B-29 (subcore 1)</u>							
2-4 cm	7.65	1217	387	400	18,580	2620	1.86
8-10 cm	7.76	1244	390	395	18,550	--	1.80
16-18 cm	7.74	1233	394	396	18,610	2581	1.77
<u>24B-29 (subcore 4)</u>							
1.6-3.6 cm	7.74	1218	392	401	18,650	--	1.80
5.6-7.6 cm	7.73	1217	390	400	18,630	--	1.82
13.6-15.7 cm	7.74	1217	395	400	18,650	--	1.83
<u>Composites</u>							
11-53	7.56	1230	390	401	18,630	2635	1.84
15B-50	7.60	1210	395	401	18,630	2660	1.77
23B-30	7.53	1238	401	397	18,550	2613	1.76
25-51	7.53	1221	394	400	18,650	2607	1.75
27-52	7.56	1227	397	397	18,550	2607	1.78
<u>Composite</u>							
Nodule	7.37	1163	398	414	18,520	2607	1.79

Table 4

Dissolved nutrients in DOMES, Site C, resuspension experiments. Sediment was suspended in Pt. Reyes seawater at 25°C for 6-11 days. All values are in $\mu\text{g atm/l}$.

Sample	SiO ₂	NO ₃ ⁻	NO ₂ ⁻	PO ₄ ⁻³	NH ₄ ⁺
Pt. Reyes Seawater	40	27.27	0.46	2.33	<0.01
<u>18B-37</u>					
0-2.2 cm	250	22.71	0.90	1.74	2.18
10.2-12.2 cm	230	15.49	0.93	1.30	2.77
18.2-20.2 cm	220	18.24	0.75	1.24	2.22
26.2-28.2 cm	200	26.50	0.64	2.24	3.49
30.2-32.2 cm	210	23.42	0.72	1.41	2.85
<u>16B-49</u>					
2-4 cm	200	22.84	1.13	2.33	3.70
12-14 cm	190	15.49	0.59	3.07	6.06
28-30 cm	200	11.16	0.84	1.91	5.56
<u>18A-36</u>					
2.2-4.2 cm	220	16.15	0.37	2.29	1.73
14.2-16.2 cm	210	12.44	1.17	1.84	1.27
22.2-24.2 cm	190	21.58	0.13	1.61	1.14
<u>20-27</u>					
4.2-6.3 cm	230	6.79	0.42	2.05	5.92
8.5-10.7 cm	230	3.31	0.53	5.04	3.63
12.9-17.9 cm	210	10.58	0.10	2.36	1.02
<u>24B-29 (subcore 1)</u>					
2-4 cm	310	24.74	0.77	1.78	2.64
8-10 cm	290	22.77	0.51	1.96	1.17
16-18 cm	290	20.60	0.60	1.71	1.44
<u>24B-29 (subcore 4)</u>					
1.6-3.6 cm	300	0.78	0.03	1.64	0.44
5.6-7.6 cm	300	0.15	<0.02	3.30	3.91
13.6-15.7 cm	280	0.07	<0.02	1.41	0.86
<u>Composites</u>					
<u>11-53</u>	220	0.10	<0.02	3.30	1.97
<u>15B-50</u>	230	0.45	<0.02	4.63	0.38
<u>23B-30</u>	270	0.59	<0.02	4.00	4.63
<u>25-51</u>	240	0.12	<0.02	4.03	2.15
<u>27-52</u>	220	6.20	<0.02	2.34	0.28
<u>Composite</u>					
Nodules	250	17.50	<0.02	1.31	5.93

Table 6

Average changes in nutrients and major element chemistry during resuspension on DOMES Site C sediments taken from Tables concentrations of Mg, Ca, K, Cl, SO₄ in ppm, C_T in m moles/l, others in ug atm/l

Species	Concentration in Pt. Reyes Seawater	Average concentration in resuspension experiments after 6-11 days (range).	Percent change
pH	7.92	7.66 (7.37-7.90)	-3.28
Mg ⁺²	1235	1220 (1163-1244)	-12.3
Ca ⁺²	396	393 (390-399)	-0.7
K ⁺	382	403 (394-434)	+5.5
Cl ⁻	18,540	18,580 (18,520-18,650)	+0.2
SO ₄ ⁻²	2616	2595 (2471-2660)	-0.8
C _T	1.93	1.78 (1.64-1.94)	-7.7
SiO ₂	38	240 (190-310)	+530 .
NO ₃ ⁻	27.27	12.88 (0.10-27.03)	-52.8
NO ₂ ⁻	0.46	0.46 (<0.02-1.17)	0.0
PO ₄ ⁻³	2.33	2.29 (1.24-5.04)	-1.7
NH ₄ ⁺	<0.01	3.44 (0.28-23.59)	----

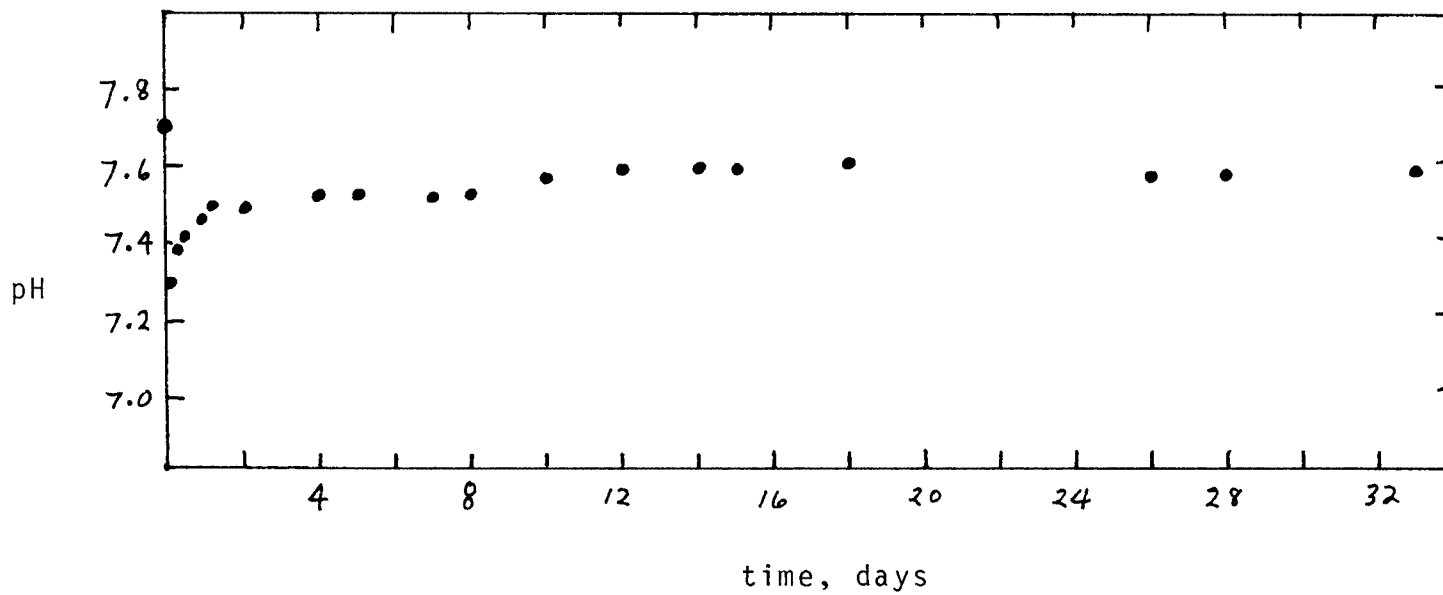


Figure 1
pH versus time for pilot experiment. 10 grams of sediment from station 18B, core 37 at 26.2 to 28.2 cm depth was suspended in 100 mls of Pt. Reyes Seawater.

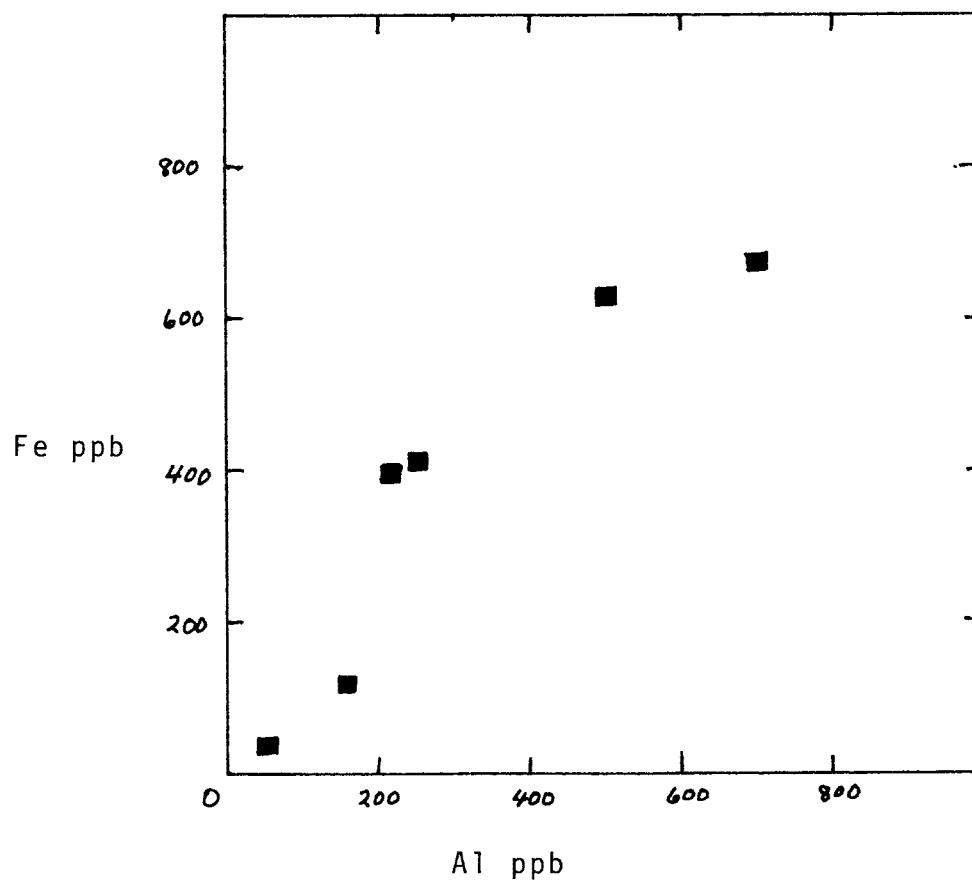


Figure 2.
Dissolved Fe vs. Al analyzed from DOMES Site C resuspension experiments. Data from Table 5.

- Amos, A.F., Garside, C., Gerard, R., Levitus, S., Malone, T. Paul, A., and Roels, O. 1973, Study of the impact of Manganese Nodule Mining on the Sea-bed and water column. Inter-University Program of Research on ferromanganese Deposits of the Ocean Floor, Phase I report, p. 221-264
- Anderson, J.J., 1976, Preliminary report: Some Potential chemical and biological impacts of a surface mining plume on the upper water column of the DOMES area, Submitted June 1976 in partial fulfillment of NOAA Contract NOAA-03-6-002-35117
- Bischoff, J.L., Greer, R.E., and Luistro, A.D., 1970, Potassium Enrichments in Interstitial waters of marine sediments: Evaluation of Temperature of Squeezing effect. *Sci.* v. 167, p. 1245-1246
- Fanning, K.A. and Pilson, M.E.Q., 1971, Interstitial Silica and pH in Marine Sediments: some effects of sampling procedures, *Sci.*, v. 173, p. 1228-1231
- Hem, J.D., 1968, Aluminum Species in Water, in: "Trace Inorganics in Water" *Advances in Chemistry Series*, no. 73, p. 98-114
- Lisitzin, A.P., 1972, Sedimentation in the World Ocean, *Soc. Econ. Paleon. Mineral. Spec. Pub.* 17
- Robertson, D.E., and Rancitelli, L.H., 1973, Trace element additions to Sea Water resulting from Contact with ferromanganese nodules particles, Inter-University Program of Research on ferromanganese Deposits of the Ocean Floor Phase I report, p. 273-278
- Wooster, W.S. and Volkmann G.H., 1960, Indications of Deep Pacific circulation from the Distribution of Properties at Five Kilometers, *Jour. of Geophys. Res.*, v. 65, no. 4, p. 1239-1249

SETTLING VELOCITIES OF THE SEDIMENT IN SEAWATER

AND X-RADIOGRAPHY OF THE BOX CORES: SITE

C PRELIMINARY DATA REPORT

by
Asbury H. Sallenger, Jr.

Gretchen Luepke

U.S. Geological Survey
Menlo Park, Calif.

METHODOLOGY

Fall Velocities

Modified pipette and hydrophotometer analyses were utilized to determine the settling velocities of the sediment. These standard methods are also used to determine the size-distribution of discrete clay and silt particles. This is accomplished by determining the fall velocity distribution of the sediment and converting to diameters, utilizing Stokes Law. The question here, however, is the fall velocity of the sediment in sea water, which may be distinctly different from the fall velocity of discrete particles due to flocculation. Flocculation is the process whereby physiochemical forces dominate a suspension of discrete particles. Many of the particles come together forming flocs, which increase the effective weight of sediment and, therefore, the fall velocity. Consequently, the methods were modified to obtain size distributions and fall velocities in sea water.

Hydrophotometer

The hydrophotometer measures percent transmission of light directed through a suspension of particles. A series of measurements are made while the particles settle, so light transmission increases with increased time. The change in transmission values can be converted to weight percents of particles by an extension of the Ben-Lambert Law:

$$\ln \frac{I_o}{I_n} = cL \frac{d_1}{d_o} K_x N_x d_x^2$$

where I_o = incident light, I_n = transmitted light, $\frac{d_1}{d_o}$ = projected particle area divided by particle diameter, c = concentration of particles, L = length of light path, K_x = apparent projected area of a particle divided by the true projected area of a particle with a diameter d_x , and N_x = number of particles with diameter d_x . The weight percents of particles can be expressed in terms of diameters with knowledge of the sampling times by an application of Stokes Law:

$$D = \frac{18 S \mu^{1/2}}{T_g (\rho_s - \rho_f)}$$

where D = particle diameter, S = sampling depth, μ = viscosity of the fluid, T = time of particle settling, g = acceleration of gravity, ρ_s particle density and ρ_f = fluid density. A more detailed description of the use and theory of the hydrophotometer is given in Jordan and others, (1971).

Modifications of the hydrophotometer to seawater and flocculation experiments are relatively straight-forward. One drawback, however, is that concentration of sediment in a hydrophotometer analysis is limited, whereas flocculation becomes more significant with increased concentration. Another problem involves the preparation of samples prior to experiments. In a standard hydrophotometer analysis, a wetting agent is routinely used to aid in dispersing the sediment. In seawater analyses where flocculation is of interest one cannot use a technique which would hinder flocculation. Consequently, the particles can be only mechanically dispersed prior to an experiment. This potential problem would apply as well to pipette analyses.

Pipette analysis is similar to the hydrophotometer in that weight percents of sediment at given levels within a suspension are derived through time. The weight percents in a pipette analysis are, however, obtained directly. The sample is dispersed in a graduated cylinder containing demineralized water and aliquots are withdrawn with a pipette at given depths through time. The aliquots are dried and the amount of sediment weighed. Applying Stokes Law, the particle-size ranges corresponding to the weight percents can be obtained. A more detailed description of the pipette technique is given in Folk (1961).

The modification of pipette analysis to seawater experiments involves in part the measurement of the weight of sediment within aliquots. Several techniques were tried. Firstly, the technique described above was used employing a correction factor for residuals (salts, etc.) in the dried aliquots. The variability of the derived correction factor, however, approached the order of magnitude of the weight of sediment. Filtering the aliquote, washing with demineralized water, and then measuring the sediment weight on the filter paper appeared to be a reliable method and was used exclusively for the data reported herein.

X-Radiography

Two-to three-centimeter vertical slabs were cut from five box cores obtained at site C. The slabs were x-rayed and analyzed for physical and biogenic structures.

Fall Velocities

Two sets of tables summarize the results of the hydrophotometer and pipette analyses. The tables list the data in terms of percentages coarser in size; diameters in the phi scale (negative log to the base 2 of the size in millimeters) and microns; settling velocities are 4^o and 20^oC; and sediment concentration. Composite samples were provided to us for analysis. The composites represent sequential combinations of samples taken at vertical intervals of a single box core with interval 1 at the top of the core.

The hydrophotometer analyses were run at sediment concentrations on the order of 10⁻⁴ g/ml, whereas the pipette analyses for the same samples had a concentration on the order of 10⁻³ g/ml. In essence, the majority of samples at low concentrations indicated a median nominal diameter between 4 and 5 μm. At higher concentrations the median nominal diameters are significantly larger, on the order of 10-15 μm, which indicates a greater degree of flocculation. The nominal diameter refers to the diameter of a quartz sphere (ρs = 2.65) with a settling velocity equivalent to that of the sediment or flocs dealt with during the experiments.

The flocculation during the relatively high-concentration pipette analyses were visually observed during the analyses. The samples were mechanically dispersed in seawater in a 10³ ml graduated cylinder. Within 15-20 minutes the majority of sediment had coalesced to form relatively large flocs which settled rapidly (see Table 2 for specific fall velocities extrapolated to 20^oC and 4^oC sea water).

As previously indicated, the majority of hydrophotometer data (Table 1) indicates median nominal diameters between 4 and 5 μm. Cores 18B intervals 8-9 and 23N intervals 1-3, however, indicate substantially larger diameters. Background data on 18B indicates that the lower portion of the core has

properties different from the upper portion. The lower portion is metaliferous (J. Bischoff, personal communication) and has unique mechanical properties. The sediment is relatively brittle and has a high water content (A. Richards, preliminary site C report). The large diameters indicated for these two samples may be in response to anomalous properties of the sediment. The ability to mechanically disperse the sediment into discrete particles in the laboratory immediately prior to the flocculation experience may also potentially be a factor.

Table 2 provides data from the pipette analyses for essentially the same samples analyzed with hydrophotometer, but at higher concentrations. Sediment concentration seems to be a sensitive, controlling variable on the sizedistribution and consequently the fall velocities. For those samples run with concentrations between 3 to 4×10^{-3} g/ml, the median nominal diameters range from 10.8 to $18.0 \mu\text{m}$; five of the six are between 10.8 and $14.6 \mu\text{m}$. Of the remaining samples those with higher concentrations than this indicate generally larger median nominal diameters, and those with lower concentration show smaller diameters. Sample 18B, intervals 8-9, again in an exception, indicating a relatively large median diameter (21 mm) even though sediment concentration is relatively low.

X-Radiography

X-radiographs of vertical slabs from box cores 11 and 16B are shown in Figure 1, and 23B, 27 and 15B are shown in Figure 2. In general the x-rays reveal evidence of bioturbation but no apparent physical structures.

Probable burrows are evident in many of the x-rays. The features appear as circles or ovals on the order of $.5 \text{ cm}$ in diameter. Cores 27 and 16B exhibit particularly good examples.

The white features at the surface of several of the cores (indicating no penetration of the x-rays) are in-place manganese nodules. The nodule 5 cm below the surface of core 16B, however, was buried during the coring process. Apparent buried micronodules are present in several of the box cores. Core 11 and 27 show particularly good examples.

DISCUSSION AND WORK IN PROGRESS

Thus far, experiments on the fall velocities of the sediment have dealt with concentrations on the order of 10^{-3} and 10^{-4} g/ml. Experiments are in progress to further define the settling velocity of the sediment in terms of significant variables. It should be realized, however, that the data on fall velocities presented herein and to be presented in the final report are subject to laboratory limitations. For example in the prototype mining area, currents and turbulence will certainly effect the residence time of particles within the photic zone. Also, filter feeding organisms tend to aggregate particles and increase settling rates (Rex and Goldberg, 1958; Manheim, Hathaway and Uchupi, 1972).

REFERENCES

- Folk, R.L., 1965, Petrology of sedimentary rocks: Hemphill's, Austin, Texas. 159 p.
- Jordan, C.F., Jr., Fryer, G.E., and Hemmen, E.H., 1971, Size analysis of silt and clay by hydrophotometer: Jour. Sed. Petrology, v. 41, n. 2, p. 489-496.
- Manheim, F.T., Hathaway, J.C., and Uchupi, E., 1972, Suspended matter in surface waters of the northern Gulf of Mexico: Limnol. & Oceanog., v. 17, n. 1, p. 17-27.
- Rex, R.W. and Goldberg, E.D., 1958, Quartz contents of pelagic sediments of the Pacific Ocean: Tellus, v. 10, p. 153-159.

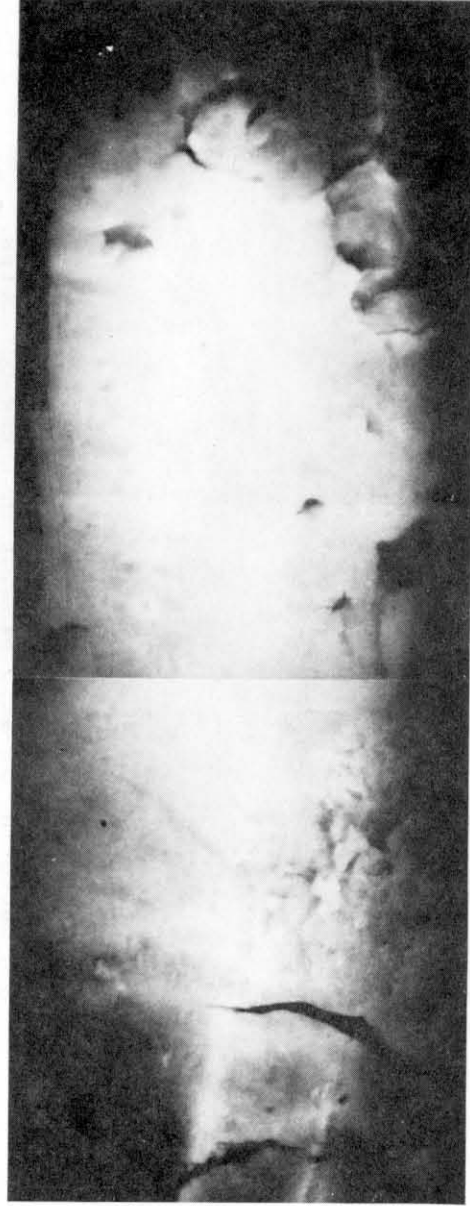
Figure 1: X-radiographs of vertical slabs from box cores 11 and 16B. Note the apparent burrows on the order of .5 cm in diameter in each of the cores. Apparent micronodules which would be indicated by small white areas are evident in box core 11.

CENTIMETERS
20
10
0



II

CENTIMETERS
20
10
0



16 B

Figure 2: X-radiographs of vertical slabs from box cores 23B, 27 and 15B. Evidence of burrowing is also present in these box cores. Evidence of buried microneodules appears in box core 27.

CENTIMETERS
20
10
0



23 B

CENTIMETERS
20
10
0



27

CENTIMETERS
20
10
0



15 B

TABLE 1

11, core 1, intervals 1-7

Analysis: hydrophotometer

Concentration: 1.35×10^{-4} g/ml

Coarser Than	Nominal Diameters		Settling Velocities	
	%	ϕ	μm	4°C (cm/sec)
25	6.95	8.1	3.44×10^{-3}	5.32×10^{-3}
50	7.85	4.3	9.89×10^{-4}	1.53×10^{-3}
75	8.0	3.9	8.03×10^{-4}	1.24×10^{-3}

11, core 1, intervals 8-14

Analysis: hydrophotometer

Concentration: 1.98×10^{-4} g/ml

Coarser Than	Nominal Diameters		Settling Velocities	
	%	ϕ	μm	4°C (cm/sec)
25	6.75	9.3	4.54×10^{-3}	7.02×10^{-3}
50	7.75	4.6	1.13×10^{-3}	1.75×10^{-3}
75	8.05	3.8	7.49×10^{-4}	1.16×10^{-3}

15B, core 1, intervals 1-6

Analysis: hydrophotometer

Concentration: 1.65×10^{-4} g/ml

Coarser Than	Diameter		Settling Velocities	
	%	ϕ	μm	4°C (cm/sec)
25	6.60	10	5.26×10^{-3}	8.13×10^{-3}
50	7.65	5	1.32×10^{-3}	2.03×10^{-3}
75	8.15	3.5	6.45×10^{-4}	9.96×10^{-4}

TABLE 1 (continued)

15B, core 1, intervals 7-13

Analysis: hydrophotometer

Concentration: 2.42×10^{-4} g/ml

Coarser Than	Diameter		Settling Velocities	
	%	ϕ	μm	4°C (cm/sec)
25	6.6	10	5.26×10^{-3}	8.13×10^{-3}
50	7.7	4.8	1.22×10^{-3}	1.88×10^{-3}
75	8.15	3.5	6.45×10^{-4}	9.96×10^{-4}

18B, core 2, subcore 2, intervals 1-5

Analysis: hydrophotometer

Coarser Than	Diameter		Settling Velocities	
	%	ϕ	μm	4°C (cm/sec)
25	6.45	11	6.89×10^{-3}	1.06×10^{-2}
50	8.0	3.9	8.03×10^{-4}	1.24×10^{-3}
75	-	-	-	-

18B, core 2, subcore 2, intervals 8-9

Analysis: hydrophotometer

Coarser Than	Diameter		Settling Velocities	
	%	ϕ	μm	4°C (cm/sec)
25	5.7	19	1.95×10^{-2}	3.01×10^{-2}
50	6.3	12.7	8.48×10^{-3}	1.31×10^{-2}
75	6.7	9.6	4.87×10^{-3}	7.52×10^{-3}

TABLE 1 (continued)

23B, core 1, intervals 1-7

Analysis: hydrophotometer

Concentration: 1.24×10^{-4} g/ml

Coarser Than	Diameter		Settling Velocities	
	%	ϕ	μm	4°C (cm/sec)
25	6.5	11	6.43×10^{-3}	9.92×10^{-3}
50	7.7	4.8	1.22×10^{-3}	1.88×10^{-3}
75	8.0	3.9	8.03×10^{-4}	1.24×10^{-3}

23B, core 1, intervals 8-15

Analysis: hydrophotometer

Concentration: 1.74×10^{-4} g/ml

Coarser Than	Diameter		Settling Velocities	
	%	ϕ	μm	4°C (cm/sec)
25	6.35	12.2	7.91×10^{-3}	1.22×10^{-2}
50	7.63	5.1	1.35×10^{-3}	2.08×10^{-3}
75	8.15	3.5	6.52×10^{-4}	1.01×10^{-3}

25, core 1, intervals 1-3

Analysis: hydrophotometer

Concentration: 1.32×10^{-4} g/ml

Coarser Than	Diameter		Settling Velocities	
	%	ϕ	μm	4°C (cm/sec)
25	4.4	47.4	1.18×10^{-1}	1.83×10^{-1}
50	5.3	25.4	3.40×10^{-2}	5.24×10^{-2}
75	6.65	9.96	5.22×10^{-3}	8.06×10^{-3}

TABLE 1 (continued)

27, core 1, intervals 1-6

Analysis: hydrophotometer

Concentration: 1.79×10^{-4} g/ml

Coarser Than	Diameter		Settling Velocities		
	%	ϕ	μm	4°C (cm/sec)	20°C (cm/sec)
25		6.95	8.1	3.44×10^{-3}	5.32×10^{-3}
50		7.75	4.6	1.13×10^{-3}	1.75×10^{-3}
75		8.25	3.3	5.68×10^{-4}	8.76×10^{-4}

27, core 1, intervals 7-12

Analysis: hydrophotometer

Concentration: 1.68×10^{-4} g/ml

Coarser Than	Diameter		Settling Velocities		
	%	ϕ	μm	4°C (cm/sec)	20°C (cm/sec)
25		7.45	5.7	1.72×10^{-3}	2.66×10^{-3}
50		7.95	4.04	8.61×10^{-4}	1.33×10^{-3}
75		8.3	3.2	5.30×10^{-4}	8.18×10^{-4}

TABLE 2

11, core 1, intervals 1-7

Analysis: pipette

Concentration: 3.82×10^{-3} g/ml

Coarser Than	Diameter		Settling Velocities	
	%	ϕ	μm	4°C (cm/sec)
25	5.3	25	3.39×10^{-2}	5.24×10^{-2}
50	6.1	14.6	1.12×10^{-2}	1.73×10^{-2}
75	6.55	10.8	6.00×10^{-3}	9.26×10^{-3}

11, core 1, intervals 8-14

Analysis: pipette

Concentration: 8.46×10^{-3} g/ml

Coarser Than	Diameter		Settling Velocities	
	%	ϕ	μm	4°C (cm/sec)
25	5.25	26	3.63×10^{-2}	5.61×10^{-2}
50	5.5	22	2.56×10^{-2}	3.97×10^{-2}
75	5.85	17	1.58×10^{-2}	2.44×10^{-2}

15B, core 1, intervals 1-6

Analysis: pipette

Concentration: 3.88×10^{-3}

Coarser Than	Diameter		Settling Velocities	
	%	ϕ	μm	4°C (cm/sec)
25	6.25	13.1	9.09×10^{-3}	1.40×10^{-2}
50	6.55	10.8	6.00×10^{-3}	9.26×10^{-3}
75	6.85	8.7	3.96×10^{-3}	6.11×10^{-3}

TABLE 2 (continued)

15B, core 1, intervals 7-13

Analysis: pipette

Concentration: 3.66×10^{-3} g/ml

Coarser Than	Diameter		Settling Velocities	
	%	ϕ	μm	4°C (cm/sec)
25	5.35	24	3.16×10^{-2}	4.89×10^{-2}
50	5.75	18	1.82×10^{-2}	2.81×10^{-2}
75	6.3	12.7	8.48×10^{-3}	1.31×10^{-2}

18B, core 2, subcore 2, intervals 1-5

Analysis: pipette

Concentration: 8.05×10^{-4} g/ml

Coarser Than	Diameter		Settling Velocities	
	%	ϕ	μm	4°C (cm/sec)
25	6.45	11.4	6.89×10^{-3}	1.06×10^{-2}
50	6.7	9.6	4.87×10^{-3}	7.52×10^{-3}
75	6.95	8.1	3.44×10^{-3}	5.32×10^{-3}

18B, core 2, subcore 2, intervals 8-9

Analysis: pipette

Concentration: 5.05×10^{-4} g/ml

Coarser Than	Diameter		Settling Velocities	
	%	ϕ	μm	4°C (cm/sec)
25	5.0	31	5.14×10^{-2}	7.94×10^{-2}
50	5.55	21	2.40×10^{-2}	3.70×10^{-2}
75	6.1	14.6	1.12×10^{-2}	1.73×10^{-2}

TABLE 2 (continued)

23B, core 1, intervals 1-7

Analysis: pipette

Concentration: 3.37×10^{-3} g/ml

Coarser Than	Diameter		Settling Velocities	
	%	ϕ	μm	4°C (cm/sec)
25	5.9	18.7	1.48×10^{-2}	2.28×10^{-2}
50	6.3	12.7	8.48×10^{-3}	1.31×10^{-2}
75	6.7	9.6	4.87×10^{-3}	7.52×10^{-3}

23B, core 1, intervals 8-15

Analysis: pipette

Concentration: 3.33×10^{-3} g/ml

Coarser Than	Diameter		Settling Velocities	
	%	ϕ	μm	4°C (cm/sec)
25	5.7	19	1.95×10^{-2}	3.01×10^{-2}
50	6.2	14	9.74×10^{-3}	1.50×10^{-2}
75	6.6	10	5.26×10^{-3}	8.13×10^{-3}

25, core 1, intervals 1-3

Analysis: pipette

Concentration: 6.1×10^{-4} g/ml

Coarser Than	Diameter		Settling Velocities	
	%	ϕ	μm	4°C (cm/sec)
25	6.45	11.4	6.89×10^{-3}	1.06×10^{-2}
50	6.75	9.3	4.54×10^{-3}	7.02×10^{-3}
75	-	-	-	-

TABLE 2 (continued)

27, core 1, intervals 1-6

Analysis: pipette

Concentration: 3.77×10^{-3} g/ml

Coarser Than	Diameter		Settling Velocities	
	%	ϕ	μm	4°C (cm/sec)
25	5.5	22	2.56×10^{-2}	3.97×10^{-2}
50	6.1	14.6	1.12×10^{-2}	1.73×10^{-2}
75	6.6	10	5.26×10^{-3}	8.13×10^{-3}